

**Development of quantum dot fluorescence sensors for detection of
targeted pesticides & polycyclic aromatic hydrocarbons**

by

Sifiso Albert Nsibande

Submitted in partial fulfilment of the requirements for the degree

Doctor of Philosophy in Chemistry

In the Faculty of Natural & Agricultural Sciences

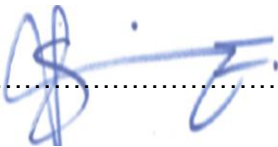
University of Pretoria

March 2020

Supervisor: Prof PBC Forbes

Declaration

I, Sifiso Albert Nsibande, declare that this thesis, which I hereby submit for the degree Doctor of Philosophy (Chemistry) at the University of Pretoria, is my own work and has not previously been submitted by me for a degree at this or any other tertiary institution.

Signature: 

Date: 31 March 2020

Acknowledgements

What an incredible journey this has been! I am excited to finally be able to document this work to serve as my small contribution to the scientific body of knowledge.

I first want to thank my supervisor and mentor, Professor Patricia Forbes, for the opportunity to do my PhD studies with her research group. Words may not adequately express my gratitude, but I thank you Prof for your wise counsel and for your patience with me while I was finding my way around this field. I deeply appreciate your support and general mentorship in shaping my career and equipping me with both scientific and professional skills. For that, I will forever be grateful.

I also want to express my gratitude to my family for all the love and support throughout this journey. *Lutsandvo lwenu ngilo belungikhutsata ngisenta lolucwaningo. Ngiyabonga kini nonkhe boGoje, boMdlanyoka boPhangelakhulu, boNdzenge loncoma. Nginyanitsandza nonkhe boPhangela.*

My colleagues became my second family during my stay at the University of Pretoria. Sharing the office and laboratory spaces with them have made this journey a pleasant experience filled with mutual respect and the drive to see each other succeed. A special thanks to ALL of you! I want to specifically thank Dr Oluwasesan Adegoke and Dr Hanieh Montaseri for their valuable technical advice and inputs as I was working on this project.

Finally, I want to thank the National Research Foundation (NRF), Water Research Commission (WRC), Photonics Initiative of South Africa (PISA) and the University of Pretoria for providing financial support for this project.

Abstract

Pesticides and polycyclic aromatic hydrocarbons (PAHs) are environmental pollutants that continue to be of great concern due to their potential toxic and human health effects. Human activities play a significant role in the release of these compounds into the environment. The occurrence of these pollutants in low concentration and the need for their continuous monitoring presents a challenge for the environmental analytical chemist. Sensitive analytical techniques that can selectively detect these compounds without being affected by the environmental matrix are required. Advances in nanotechnology have allowed for the design of sensitive and selective nanomaterials which provide alternative analytical tools for such challenges.

In this work, therefore, extensive reviews on the current application of quantum dots (QDs) and nanoparticles in designing probes for detection of pesticides and PAHs were conducted. Through these reviews, the current status on the application of QDs sensors for these compounds was assessed. Knowledge gaps were identified where it was noted that there were no QD-based sensors for atrazine and graphene quantum dots (GQD) sensors for PAHs. The reviews further assessed the advantages and challenges for coupling QDs to various analyte receptors to enhance selectivity and how these impact on the scaling of such sensors for routine applications.

QDs are highly fluorescent nanoparticles with interesting optical and structural properties that could be explored for designing sensitive fluorescence probes. Thus, QD-based fluorescence probes were designed for the detection of targeted pesticides and PAHs in water samples. Atrazine and pyrene were chosen as representative pesticide and PAH compounds, respectively. The structure and properties of the QD probes were studied using a range of techniques including fluorescence, UV-vis, Fourier transform infrared spectroscopy (FTIR), high-resolution transmission electron microscopy (HRTEM), Raman, and powered X-ray diffraction (XRD).

A quantum dot coupled to molecularly imprinted polymer (QD@MIP) sensor for atrazine detection was developed and optimized. Under optimal conditions, the sensor showed excellent sensitivity and selectivity for atrazine due to the size and shape specificity of the molecularly imprinted polymer as a receptor. The developed sensor showed excellent sensitivity and could detect atrazine down to $0.80 \times 10^{-7} \text{ mol L}^{-1}$ which is below the World Health Organization (WHO) guideline for atrazine in water ($4.6 \times 10^{-7} \text{ mol L}^{-1}$).

A GQD based sensor was also developed for the detection of PAHs in water samples. GQDs offer a safer alternative to cadmium-based QDs in designing fluorescence probes. In this work, GQDs were synthesized using bottom-up and top-down approaches and a fluorescence “turn-off-on” strategy that uses GQDs with ferric ions was developed and used for rapid detection of PAHs in water, using pyrene as a case study. The probe showed a linear response to pyrene concentration within the $2 - 10 \times 10^{-6} \text{ mol L}^{-1}$ range and was able to detect pyrene down to $0.325 \times 10^{-6} \text{ mol L}^{-1}$ and $0.242 \times 10^{-6} \text{ mol L}^{-1}$ for GO-GQDs and CA-GQDs, respectively. The potential application of the developed probe was tested using real environmental water samples spiked with known pyrene concentrations, and recoveries between 97 – 107% were obtained. This part of the thesis demonstrated, for the first time, the promising application of GQDs for environmental monitoring of PAHs in water samples.

This work demonstrated how nanotechnology advances could be harnessed and used to solve environmental challenges. The main objectives were achieved and future research recommendations to enhance the robustness of the developed sensors were proposed. These recommendations include (i) immobilizing the QD sensor materials on solid supports and investigating their re-usability, (ii) further optimization of the GQD sensor for PAHs to improve its sensitivity, (iii) exploring the possibility of using such sensors for multi-analyte detection, and lastly (iii) standardizing the QD-based sensing methods as analytical protocols that could be used in by regulators in environmental monitoring.

Research outputs

Published articles

1. S.A. Nsibande, P.B.C. Forbes, Development of a turn-on graphene quantum dot-based fluorescence probe for sensing pyrene in water in water, *RSC Advances*, 10 (2020) 12119 - 12128. DOI: <https://doi.org/10.1039/c9ra10153e>
2. S.A. Nsibande, H. Montaseri, P.B.C. Forbes, Advances in the application of nanomaterial-based sensors for detection of polycyclic aromatic hydrocarbons in aquatic systems, *TrAC Trends in Analytical Chemistry*, 115 (2019) 52 - 69.
DOI: <https://doi.org/10.1016/j.trac.2019.03.029>
3. S.A. Nsibande, P.B.C. Forbes, Development of a quantum dot molecularly imprinted polymer sensor for fluorescence detection of atrazine, *Luminescence*, 34 (2019) 1 - 9.
DOI: <http://dx.doi.org/10.1002/bio.3620>
4. S.A. Nsibande, P.B.C. Forbes, Fluorescence detection of pesticides using quantum dot materials – A review, *Analytica Chimica Acta*, 945 (2016) 9-22.
DOI: <http://dx.doi.org/10.1016/j.aca.2016.10.002>

Co-authored articles

1. O. Adegoke, H. Montaseri, S.A. Nsibande, P.B. Forbes, Alloyed quaternary/binary core/shell quantum dot-graphene oxide nanocomposite: Preparation, characterization and application as a fluorescence “switch ON” probe for environmental pollutants, *Journal of Alloys and Compounds*, 720 (2017) 70 - 78.
DOI: <https://doi.org/10.1016/j.jallcom.2017.05.242>
2. O. Adegoke, H. Montaseri, S.A. Nsibande, P.B.C. Forbes, Passivating effect of ternary alloyed AgZnSe shell layer on the structural and luminescent properties of CdS quantum dots, *Materials Science in Semiconductor Processing*, 90 (2019) 162-170.
DOI: <https://doi.org/10.1016/j.mssp.2018.10.025>

Technical reports

1. H. Montaseri, S.A. Nsibande, and P.B.C. Forbes Development of novel fluorescent sensors for the screening of emerging chemical pollutants in water - Part II, WRC Report No. K5/2752, WRC Report No. 2752/1/19, October 2019, ISBN 978-0-6392-0090-3.
2. O. Adegoke, J.M. Dabrowski, H. Montaseri, S.A. Nsibande, F. Petersen and P.B.C. Forbes. Development of novel fluorescent sensors for the screening of emerging chemical

pollutants in water – Part I, WRC Report No. 2438/1/17, November 2017, ISBN 978-1-4312-0936-1.

Conference presentations

1. Nsibande, S.A. and Forbes, P.B.C., Development of a quantum dot molecularly imprinted polymer sensor for fluorescence detection of atrazine, Nanoscience Young Researchers' Symposium, 12 November 2019, Future Africa, University of Pretoria. [**Oral presentation**] (**Won 3rd-place best PhD oral presentation*).
2. Nsibande, S.A. and Forbes, P.B.C., Development of a quantum dot fluorescence sensor for detection of atrazine, Analitika, 22 – 25 July 2018, Mookgophong, Limpopo. [**Poster**].
3. Nsibande, S.A. and Forbes, P.B.C., Development of a quantum dot molecularly imprinted polymer sensor for fluorescence detection of atrazine, 18th International Symposium on Luminescence Spectrometry, 19 – 22 June 2018, Brest, France. [**Oral presentation**].
4. Forbes, P.B.C.*, Adegoke, O., Montaseri, H. and Nsibande, S.A., Quantum dot based photonic sensor materials for emerging chemical pollutants in water, 18th International Symposium on Luminescence Spectrometry, 19 – 22 June 2018, Brest, France [***Plenary oral presentation by PBC Forbes**].
5. Nsibande, S.A. and Forbes, P.B.C., Synthesis of graphene quantum dots and their application as fluorescence sensors for polycyclic aromatic hydrocarbons, The 7th International Conference on Nanoscience and Nanotechnology in Africa. 22 – 25 April 2018, Salt Rock, Durban. [**Oral presentation**].
6. Nsibande, S.A. and Forbes, P.B.C Preparation of graphene quantum dots for fluorescence sensing of polycyclic aromatic hydrocarbon. SACI Inorganic, 25 – 29 June 2017, Hermanus, Western Cape. [**Poster**].

Table of contents

Declaration.....	ii
Acknowledgements.....	iii
Abstract.....	iv
Research outputs.....	vi
Published articles	vi
Co-authored articles	vi
Technical reports.....	vi
Conference presentations.....	vii
List of figures	x
List of tables.....	xvi
List of abbreviations	xviii
CHAPTER 1 Background.....	1
1.1 Problem statement.....	1
1.2 Aims and objectives	3
1.3 Thesis layout.....	4
1.4 References	5
CHAPTER 2 Introduction	7
2.1 Semiconductor quantum dots.....	7
2.1.1 Introduction.....	7
2.1.2 Synthesis techniques of semiconductor QDs	9
2.2 Graphene quantum dots	10
2.2.1 Introduction.....	10
2.2.2 Synthesis methods for GQDs.....	11
2.3 Characterization techniques for QDs.....	12
2.3.1 Optical characterization	12
2.3.2 Structural and morphological characterization.....	13
2.4 The principle of QD fluorescence sensing.....	14
2.5 Target compounds.....	15
2.5.1 Atrazine	15
2.5.1.1 Sources and occurrence of atrazine in the environment.....	15

2.5.1.2	Toxicity of atrazine.....	17
2.5.1.3	Legal limits for atrazine in water.....	18
2.5.2	Polycyclic aromatic compounds.....	19
2.5.2.1	Sources and occurrence of PAHs.....	19
2.5.2.2	Toxicity of PAHs.....	21
2.5.2.3	Legal limits.....	23
2.6	Conclusion.....	24
2.7	References.....	25
CHAPTER 3	Application of quantum dots for detection of pesticides – A review.....	32
	Paper.....	32
CHAPTER 4	Advances in the application of nanomaterial-based sensors for detection PAHs in aquatic systems.....	47
	Paper.....	47
CHAPTER 5	Development of a quantum dot molecularly imprinted polymer sensor for fluorescence detection of atrazine.....	66
	Paper.....	66
	Supporting information.....	76
CHAPTER 6	Development of a turn-on graphene quantum dot-based fluorescence probe for sensing of pyrene in water.....	77
	Paper.....	77
	Supplementary information.....	88
CHAPTER 7	Conclusions and future work.....	92
7.1	Conclusions.....	92
7.2	Future work.....	94
APPENDICES.....		96
	Co-authored paper 1: Fluorescence sensor for PAHs detection.....	96
	Co-authored paper 2: Synthesis & characterization of CdS/AgZnSe QDs.....	106

List of figures

Chapter 2

Figure 1 Comparison of the energy level diagram for a bulk semiconductor and its analogue atomic semiconductor with that of a quantum dot. Adapted from [6]..... 8

Figure 2 Schematic illustration of the effect of increasing QD particle size on the emission wavelength..... 8

Figure 3 (a) Schematic illustration of different pathways through which pesticides can contaminate non-targeted environmental resources and (b) the chemical structure of atrazine...15

Chapter 3:

Figure 1 (A) Fluorescence sensor for ultra-sensitive detection of glyphosate. (B) Response of the sensor to increasing glyphosate concentration 39

Figure 2 (A) Preparation of MIP-coated ZnS:Mn QDs for detection of cyphenothrin (TEOS: Tetraethoxysilane, KH550: silane coupling agent, AM: functional monomer, EGDMA: crosslinking agent). (B) (left) Fluorescence intensity of the probe decreased with increasing cyphenothrin concentration, (right) fluorescence of NIP-coated QDs with increasing cyphenothrin concentration.....40

Figure 3 (A) Schematic illustration showing the molecular imprinting process for l-cyhalothrin (LC) imprinted silica nanospheres embedded CdSe quantum dots (APTS:3-Aminopropyltriethoxy-silane, TEOS: tetraethoxysilane). (B) Schematic illustration for the molecular imprinting mechanism of LC in a silica matrix through the hydrogen bond reaction.40

Figure 4 Chemical structures of pesticides commonly targeted using QD-AChE based fluorescence biosensors..... 41

Figure 5 (a) Schematic illustration of the working principle of the AChE based biosensor for pesticide detection (SiQDs: silicon quantum dots). (b) Incubation time dependence of fluorescence intensity of SiQDs-AChE-ChO probe at different concentrations of carbaryl. (c) Inhibition efficiency (IE) vs log of carbaryl concentration under optimized conditions 42

Figure 6 (A) Schematic diagram illustrating the working principle of the CuInS₂ QD biosensor for parathion-methyl (PM) detection (Abbreviations: DMPA: di-methylthiophosphoric acid, OPH: Organophosphorus hydrolase). (B) Response of the sensor to increasing concentration of parathion-methyl (c) Plot of fluorescence intensity ratios of the CuInS₂ sensor versus the logarithm of concentration of PM. I and I₀ were the fluorescence intensity of CuInS₂ QDs complex in the presence and absence of PM, respectively43

Chapter 4:

Figure 1 Schematic illustration of the major sources of PAHs in the environment and their distribution and fate in the ecosystem.....50

Figure 2 (A) Illustration of the possible interaction of cyclodextrins with PAHs to form a complex with fluorescence quenching effect upon interaction with CdTe QDs. (B) Change in QD fluorescence intensity with change in phenanthrene concentration..... 51

Figure 3 (A) Schematic illustration of the phenanthrene detection mechanism upon interaction with GO. (B) Fluorescence response of the probe to phenanthrene. (C) Calibration curve showing a linear response of the QD-GO probe to increasing phenanthrene concentration...52

Figure 4 (A) Schematic illustration of the pyrene detection mechanism. (B) Fluorescence quenching spectra of graphene-CdTe quantum dot nanocomposites upon addition of pyrene. Experimental conditions: graphene-cadmium telluride quantum dot nanocomposites, 2.0×10^{-3} mol L⁻¹; pyrene (A – L; 0 – 2.0×10^{-6} mol L⁻¹). Inset: fluorescence of graphene–cadmium telluride quantum dot nanocomposites in the (a) absence and (b) presence of pyrene. 53

Figure 5 (A) Schematic fabrication of pyrene-imprinted polyterthiophene (poly(3T)) thin film sensor (QCM = quartz crystal microbalance; PPC = pre-polymerization complex). (B) Fluorescence spectra showing the difference between MIP and NIP after pyrene binding, (C) MIP and NIP selective binding of pyrene. The inset shows the fluorescence response as a function of pyrene concentration.54

Figure 6 Schematic illustration of SERS analysis and multiple analyte detection. SERS substrates can be modified via different strategies to facilitate adsorption of PAHs. The SERS spectrum is unique for each analyte..... 54

Figure 7 Schematic representation of the procedure for SERS detection of PAHs.58

Figure 8 (A) TEM images of single Ag@SiO₂ NPs and distribution of Ag@SiO₂ NPs in ethanol. (B) Schematic illustration of CD dimer-immobilized Ag assembly with embedded silica NPs for detection of PAHs. (C) SERS spectra of β-CD dimer@Ag@SiO₂ NPs at 1 × 10⁻² mol L⁻¹ to 1 × 10⁻⁷ mol L⁻¹. (D) Normalized SERS intensities of β-CD dimer@Ag@SiO₂ and Ag@SiO₂ with perylene at 1293 cm⁻¹.58

Figure 9 (A) Schematic illustration of nanosensor surface functionalization and pre-concentration of the targeted compounds via weak interactions. Gold Nanostructures GNSs, DSC₁₀H₂₁, 4-dodecyl benzenediazonium-tetrafluoroborate diazonium salt. (B - D) SERS detection of benzo[a]pyrene (BaP) at 0.75 mg L⁻¹, fluoranthene (FL) at 5 mg L⁻¹, and naphthalene (NAP) at 50 mg L⁻¹ (C) using gold nanostructures (GNSs) functionalized with diazonium salt (Au-Phi-C₁₀H₂₁).59

Figure 10 (A) Complex assembling of gold nanoparticles and antibody anti-benzo[a]pyrene (BaP13) using 5,5'-dithiobis(succinimidyl-2-nitrobenzoate) (DSND) as a coupling agent and Raman reporter and the interaction free antibody binding sites of the nanoprobe with grafted BaP on a gold coated quartz substrate. (B) Schematic illustration of the SERS sensing procedure for detection of BaP.60

Figure 11 (A) Schematic illustration of the synthesis of GR-PANI nanocomposite via in situ polymerization. (B) SWV responses of GR-PANI/GCE sensor for 20 – 1000 × 10⁻⁶ mol L⁻¹ anthracene. Experimental conditions: 0.1 mol L⁻¹ LiClO₄ in acetonitrile/water (80:20 v/v). (SW frequency = 5 Hz and SW amplitude = 25 mV). (C) A calibration plot of the GRPANI|GCE sensor for 0.012 – 1000 × 10⁻⁶ mol L⁻¹ anthracene.61

Figure 12 (A) Structure of generation three poly(propylene thiophenimine) dendrimer (G3PPT-co-P3HT). (B) CV voltammograms of the Au|G3PPT-co-P3HT with different phenanthrene (PHE) concentrations. (C) The calibration plot of Au|G3PPT-co-P3HT sensor for PHE.62

Figure 13 (A) Schematic illustration of a benzo[a]pyrene biosensor. (B) DPV voltammograms of guanine obtained at the DNA/hemin/nafionegraphene/GCE at different concentrations of benzo[a]pyrene biosensor (a – g; 0 – 22 × 10⁻⁸ mol L⁻¹).63

Chapter 5

Figure 1 Schematic illustration of the synthesis of hydrophobic CdSeTe/ZnS QDs through stepwise hot injection of organometallic precursors. The reaction was continuously purged

with argon while monitoring time and temperature. Water soluble QDs were obtained after ligand exchange with L-cysteine 69

Figure 2 Schematic representation of the simultaneous silica encapsulation and vinyl modification of the CdSeTe/ZnS QDs. The MPS caps on the hydroxyl groups of L-cysteine through active condensation, leaving the vinyl groups free for polymerization70

Figure 3 Powder X-ray diffraction patterns for CdSeTe QDs, CdSeTe/ZnS QDs, CdSeTe/ZnS-MPS and CdSeTe/ZnS@MIP showing the characteristic zinc-blende crystal structure which was retained after polymerization 70

Figure 4 FTIR spectra of CdSeTe QDs, CdSeTe/ZnS QDs, CdSeTe/ ZnS-MPS and CdSeTe/ZnS@MIP nanoparticles.....70

Figure 5 Transmission electron microscopy (TEM) images showing spherically shaped CdSeTe QDs (a) and CdSeTe/ZnS QDs (b) dispersed in water. The insets show statistical size distributions with Gaussian fits (black curves). The average particle size for the core was 3.1 ± 0.1 nm while the core/shell was 5.0 ± 0.5 nm. Images in (c) show the CdSeTe/ZnS@MIP material with the QDs imbedded inside the polymer's fiber-like network 71

Figure 6 Fluorescence emission spectra (solid lines) of CdSeTe QDs at 575 nm, CdSeTe/ZnS QDs at 605 nm, and CdSeTe/ ZnS@MIP at 599 nm. The excitation wavelength was 365 nm for all measurements. Absorption spectra (dotted lines) are included with the corresponding emission spectra 72

Figure 7 (a) The effect of concentration on the fluorescence intensity of the CdSeTe@MIP sensor. (b) The effect of incubation time on the quenching of sensor solution 100 μ L of 6×10^{-7} mol L⁻¹ concentration. (c) Effect of pH on the fluorescence intensity of the sensor..... 73

Figure 8 Schematic illustration of the binding of atrazine (template) carboxyl groups on methacrylic acid (MAA) through hydrogen bonding on the molecularly imprinted polymer (MIP) matrix and the specific site cavities left after removal of the template 73

Figure 9 The fluorescence spectra of L-cys-CdSeTe/ZnS@MIP in the presence of different concentrations of atrazine ($2-20 \times 10^{-7}$ mol L⁻¹). The inset shows the linear response of F_0/F versus atrazine concentration where F_0 is the fluorescence intensity of CdSeTe/ZnS@MIP without atrazine and F is the fluorescence intensity after interaction with atrazine ($n = 3$)73

Figure 10 The fluorescence spectra of L-cys-CdSeTe/ZnS@NIP in the presence of different concentrations of atrazine ($2-12 \times 10^{-7}$ mol L⁻¹). The inset shows a plot of F_0/F versus atrazine

concentration where F_0 is the fluorescence intensity of CdSeTe/ ZnS@NIP without atrazine and F is the fluorescence intensity after interaction with atrazine.....74

Figure 11 Quenching effect of (1) atrazine, (2) simazine and (3) terbuthylazine on CdSeTe/ ZnS@MIP sensor solution. A 100 μL of 6×10^{-7} mol L^{-1} for each compound was used ($n = 3$)74

Figure 12 (a) UV-visible absorption spectra of atrazine, CdSeTe/ ZnS@MIP and emission spectrum of CdSeTe/ZnS@MIP. (b) Schematic illustration of the proposed fluorescence quenching mechanism based on molecular orbital theory..... 74

Figure S1 Tauc plots used for estimating the band gap (eV) of CdSeTe QDs, CdSeTe/ZnS QDs and CdSeTe/ZnS@MIP.77

Chapter 6:

Figure 1 Schematic illustration of the synthesis of fluorescent GQDs from citric acid through pyrolysis and carbonization 80

Figure 2 Schematic illustration of the top-down preparation of GQDs through oxidation of graphene oxide 81

Figure 3 (a) TEM images of (A) CA-GQDs and (B) GO-GQDs with corresponding particle size distributions (right). The averages size for CA-GQDs was 4.8 ± 0.1 nm and 5.5 ± 0.3 nm for GO-GQDs..... 81

Figure 4 FTIR spectra of both GO-GQDs (A) and CA-GQDs (B) and their respective precursors. (C) Raman spectra of graphene oxide (GO), CA-GQDs and GO-GQDs..... 82

Figure 5 Absorption and emission spectra of GO-GQDs (A) and CA-GQDs (B). The inset shows the GQDs solution under visible light (i) and under 365 nm UV light (ii)..... 83

Figure 6 The effect of excitation wavelength on the emission spectra of (A) GO-GQDs and (C) CA-GQDs. B and D show the effect of excitation wavelength on the maximum PL intensity (PL_{max}) in each case. 84

Figure 7 The effect of successive irradiations at the excitation wavelength for GO-GQDs (A) and CA-GQDs (B). The effect of storage at 4°C on the stability of the GO-GQDs (B) and CA-GQDs (C)..... 84

Figure 8 Fluorescence detection of pyrene using CA-GQDs (A) and GO-GQDs (B). The concentration of pyrene ($2 - 10 \times 10^{-6} \text{ mol L}^{-1}$). The inset show linear response of F/F_0 versus concentration where F_0 is the fluorescence intensity GQDs- Fe^{3+} in the absence of pyrene and F is the fluorescence intensity after interactions with pyrene ($n = 3$)..... 84

Figure 9 Schematic illustration of the interaction of GQDs with Fe^{3+} which results in fluorescence quenching. Upon interaction with pyrene the fluorescence is turned on. 86

Figure S1(A) raw unfiltered GQDs after oxidation of GO. (B) Orange-yellowish GQDs solution after filtering through $0.45 \mu\text{m}$ PTFE filter, (C) pale yellow GQDs solution after filtering through a $0.22 \mu\text{m}$ PTFE filter. 89

Figure S2 Effect of filtering on the PL intensity during the purification step..... 90

Figure S3 (A) HRSEM image of graphite showing flat shiny carbon sheets staked in layers. (B) Graphene oxide sheets folded into crumpled silk waves following oxidation..... 91

List of tables

Chapter 2

Table 1 Comparison of advantages and disadvantages of the synthesis strategies for GQDs (Adapted from [27]).	12
Table 2 Physiochemical properties of atrazine (adapted from [39, 40]).	16
Table 3 Concentration ($\mu\text{g L}^{-1}$) of atrazine sampled over four seasons in drinking water in selected areas across South Africa. Average concentrations are indicated (n=3) [43].	17
Table 4 Guideline value for atrazine in drinking water [66].	19
Table 5 Natural and anthropogenic sources of polycyclic aromatic hydrocarbons (PAHs)...	19
Table 6 Chemical structures and physical properties of the 16 PAHs listed as US EPA priority pollutants [67].	21
Table 7 PAHs and their toxic equivalency factors (TEFs) expressed relative to benzo[a]pyrene [71].	22
Table 8 Water quality standards for PAHs in water [78].	24

Chapter 3

Table 1 Comparison of selected QD based pesticide sensor limits of detection (LOD) with regulatory guideline limit values and typical concentrations found in samples (nd = not detected)	33
Table 2 Quantum dots with molecular recognition elements as receptors for pesticide detection. Where possible reported LOD and linear range values were converted to Molar units for comparison purposes	37
Table 3 Summary of studies employing quantum dots with MIPs for fluorescence detection of pesticides in different media. Reported LOD and linear range values have been converted to Molar units for comparison purposes.	37
Table 4 Biosensors using quantum dots as recognition elements for fluorescence detection of pesticides in different media. Where possible the reported LOD and linear range values were converted to Molar units for comparison purposes.	38

Chapter 4

Table 1 Research studies that use nanomaterials for fluorescence (PL) detection of PAHs in water samples (note: examples based on detection in solvents have been included as they have potential application to water samples) 51

Table 2 Summary of nanomaterials using different types of affinity agents for surface-enhanced Raman scattering (SERS) detection of polycyclic aromatic hydrocarbons (PAHs) in water samples (note: studies based on detection in solvents have been included as they have potential application to water samples) 55

Table 3 Examples of research studies that use nanomaterials for electrochemical detection of PAHs in water samples (note: studies based on detection in electrolyte solution have been included as they have potential application to water samples). 60

Table 4 Summary of nanomaterial-based biosensor systems that use nanoparticles for PAH detection in water samples 63

Table 5 Examples of nano-sensors for PAH metabolites/degradation products 64

Chapter 5

Table 1 Summary of the photo physical properties CdSeTe QDs, CdSeTe/ZnS QDs and CdSeTe/ZnS@MIP 72

Table 2 Recovery tests of atrazine spiked in tap water and lake water at three different concentrations (n = 3) 75

Table 3 Comparison of the proposed CdSeTe/ZnS@MIP sensor with other reported sensor systems 75

Chapter 6

Table 1 Recovery tests of pyrene spiked lake water at three different concentrations.....86

Table S1 ICP scan results showing background elemental composition (mg L⁻¹) of the lake water sample.....92

List of abbreviations

ADI: acceptable daily intake

DWMCL: drinking water maximum contaminant level

ECP: emerging chemical pollutant

FRET: Förster resonance energy transfer

FTIR: Fourier-transform infrared

GQD: graphene quantum dot

HHOO: human health organism only values

HHWO: human health water + organism values

HOMO: highest occupied molecular orbital

HRTEM: high-resolution transmission electron microscope

LOD: limit of detection

LOQ: limit of quantitation

LUMO: lowest unoccupied molecular orbital

MCLG: maximum contaminant level goal

MIP: molecularly imprinted polymer

NIP: non-imprinted polymer

NOAEL: non-observed adverse effect level

PAH: polycyclic aromatic hydrocarbon

PL: photoluminescence

QD: quantum dot

QY: quantum yield

TEF: toxic equivalency factors

TEM: transmission electron microscope

US EPA: United States Environmental Protection Agency

UV-Vis: ultraviolet-visible

WQC: water quality criteria

XRD: X-ray diffraction

CHAPTER 1 Background

This chapter presents the problem statement which is the bases for embarking on this project. This is then followed by the research aims and objectives, and thesis layout.

1.1 Problem statement

Environmental pollution is one of the global challenges facing environmental regulators around the world as it threatens human health, aquatic life, and the general ecosystem. Human activities through industrialization and agriculture over the years have largely contributed to the release of pollutants with unintended consequences to the environment. Most of these activities are necessitated by advances in industrial development and agriculture with the aim to meet the ever-increasing population demands. It is therefore not surprising that industrialization and agriculture have become the backbone for most economies around the world. The agricultural sector, for example, is required to increase production in order to meet population demand, and to achieve this, the use of pesticides becomes necessary.

These human activities have led to the release of emerging chemical pollutants (ECPs) which are a group of chemical pollutants with no clear environmental legislative status and/or are not included in regulatory monitoring programmes [1]. The environmental fate and biological impacts of such compounds are often poorly understood [2, 3]. Some pesticides and polycyclic aromatic hydrocarbons (PAHs) form part of ECPs that are continuously released into environmental compartments by human activities. These compounds are of great environmental importance as they can have a negative impact on human health and the ecosystem in general [4]. For example, several chemical pollutants have been shown to have mutagenic and carcinogenic effects on exposed organisms, including humans [5-7].

The monitoring of ECPs in the environment is therefore very important in understanding the exposure risks that are associated with them. Current conventional chromatography-based analytical techniques are widely used as the 'gold standard' for environmental monitoring of

these compounds [8]. The challenge, however, with these techniques is the relatively high costs that are associated with them, especially where routine monitoring is required. Advances in the nanotechnology field in recent years have seen the development of highly sensitive and selective sensors that could be used in the environmental monitoring of ECPs [9]. The use of fluorescence nanomaterials based on quantum dots (QDs) in environmental sensing is a growing area of research due to their attractive properties (these are discussed in detail in Chapter 2).

This project, therefore, sought to develop QD-based fluorescence sensors or probes that could be used as alternative analytical methods for the detection of targeted pesticides and PAHs in environmental water samples.

Pesticides are widely used in agriculture for controlling pests and weeds in order to maximize production. Although these compounds are highly regulated, their extensive use can lead to non-target contamination of surrounding resources like water bodies through various pathways like spray drift, leaching and runoff. The serious potential negative effects of pesticides on the environment and human health warrants research attention on this class of compounds.

PAHs are a class of organic compounds with fused benzene rings which are equally of environmental concern because of their negative health effects. PAHs are produced from a wide variety of sources and hence they are one of the classes of pollutants which are of global concern [10, 11]. These compounds can be introduced into environmental water systems through various ways (like leaching and runoff) after wet or dry deposition from the atmosphere. Some of the sources of PAHs include industrial combustion activities, biomass burning, and vehicular emissions.

1.2 Aims and objectives

In addressing the above-stated challenge, the broad aims of this project were to develop quantum dot-based fluorescence probes and to evaluate their potential use in the detection of selected pesticides and polycyclic aromatic compounds in water samples.

The specific objectives were to:

1. Synthesize semiconductor quantum dots (QDs), through modification of existing high temperature inorganic synthetic strategies, for detection of the pesticide atrazine.
 - 1.1. Tailor the QDs towards specific recognition of targeted compounds by making use of molecularly imprinted polymers.
 - 1.2. Fully characterize the materials with techniques including TEM, XRD, UV-Vis, FTIR, and fluorescence spectrophotometry.
 - 1.3. Test the application of the developed probe in the detection of atrazine in real environmental water samples.

2. Synthesize graphene quantum dots (GQDs) for compound-class detection of polycyclic aromatic hydrocarbons (PAHs).
 - 2.1. Investigate bottom-up and top-down synthesis routes.
 - 2.2. Fully characterize the developed GQDs with techniques including TEM, Raman, UV-Vis, FTIR, and fluorescence spectrophotometry.
 - 2.3. Test the application of the developed probe in the detection of PAHs in real environmental water samples.

3. Compare the performance of these sensors to other sensing methods.

1.3 Thesis layout

Chapter 2 presents a general background to QDs, their synthesis, characterization, and the basis for their application in fluorescence sensing. It also introduces the target analytes and highlights their environmental significance. Chapters 3 and 4 review the application of fluorescence sensors for pesticide and PAH detection, respectively. In Chapters 5 and 6 the fluorescence sensors that were developed in this work are presented. Finally, an overall conclusion is presented in Chapter 7, and future work is highlighted. The chapters where the work has been published are presented in journal article format, i.e. as published.

1.4 References

- [1] M.I. Farré, S. Pérez, L. Kantiani, D. Barceló, Fate and toxicity of emerging pollutants, their metabolites and transformation products in the aquatic environment, *TrAC, Trends Anal. Chem.*, 27 (2008) 991-1007.
- [2] T.H. Hutchinson, B.P. Lyons, J.E. Thain, R.J. Law, Evaluating legacy contaminants and emerging chemicals in marine environments using adverse outcome pathways and biological effects-directed analysis, *Mar. Pollut. Bull.*, 74 (2013) 517-525.
- [3] Q. Liu, Q. Zhou, G. Jiang, Nanomaterials for analysis and monitoring of emerging chemical pollutants, *TrAC, Trends Anal. Chem.*, 58 (2014) 10-22.
- [4] M. Gavrilescu, K. Demnerova, J. Aamand, S. Agathos, F. Fava, Emerging pollutants in the environment: present and future challenges in biomonitoring, ecological risks and bioremediation, *N. Biotechnol.*, 32 (2015) 147-156.
- [5] J.A. Kapeleka, E. Sauli, P.A. Ndakidemi, Pesticide exposure and genotoxic effects as measured by DNA damage and human monitoring biomarkers, *Int. J. Environ. Res.*, (2019) 1-18.
- [6] C. Hilgert Jacobsen-Pereira, C.R. dos Santos, F. Troina Maraslis, L. Pimentel, A.J.L. Feijó, C. Iomara Silva, G.d.S. de Medeiros, R. Costa Zeferino, R. Curi Pedrosa, S. Weidner Maluf, Markers of genotoxicity and oxidative stress in farmers exposed to pesticides, *Ecotoxicol. Environ. Saf.*, 148 (2018) 177-183.
- [7] O. Idowu, K.T. Semple, K. Ramadass, W. O'Connor, P. Hansbro, P. Thavamani, Beyond the obvious: Environmental health implications of polar polycyclic aromatic hydrocarbons, *Environ. Int.*, 123 (2019) 543-557.
- [8] K.M. Dimpe, P.N. Nomngongo, Current sample preparation methodologies for analysis of emerging pollutants in different environmental matrices, *TrAC, Trends Anal. Chem.*, 82 (2016) 199-207.
- [9] R. Soni, M. Soni, D.P. Shukla, Emerging techniques and materials for water pollutants detection, in: D. Pooja, P. Kumar, P. Singh, S. Patil (Eds.) *Sensors in Water Pollutants Monitoring: Role of Material*, Springer Singapore, Singapore, 2020, pp. 277-297.
- [10] E. Manoli, C. Samara, Polycyclic aromatic hydrocarbons in natural waters: sources, occurrence and analysis, *TrAC, Trends Anal. Chem.*, 18 (1999) 417-428.

- [11] O.S.S. Sojnu, J.-Z. Wang, O.O. Sonibare, E.Y. Zeng, Polycyclic aromatic hydrocarbons in sediments and soils from oil exploration areas of the Niger Delta, Nigeria, *J. Hazard. Mater.*, 174 (2010) 641-647.

CHAPTER 2 Introduction

The first part of this chapter provides a general background to quantum dots, their properties, the different synthesis approaches, and the characterization techniques that are often used regarding these materials. Special emphasis is on the QDs that were used in this work. The last part of the chapter gives an overview of the target analytes and places their environmental significance into context.

2.1 Semiconductor quantum dots

2.1.1 Introduction

Quantum dots (QDs), are small crystalline nanoparticles whose physical size is smaller than their exciton Bohr radius. As such, the movement of excitons (electron-hole pairs) within the crystal lattices of QDs is physically confined to discrete energy levels which are analogous to those in molecules as shown in **Figure 1** QDs therefore exhibit quantum confinement effects, which is to say their optical and electronic properties are affected by their particle size as shown in **Figure 2**. This interesting feature of QDs allows for tailoring of QD-based materials with desired optical properties by simply controlling the particle size during synthesis. Other unique and attractive electronic and optical properties of QDs include high photoluminescence quantum yields, photostability, narrow emission spectra, wide and continuous UV-vis absorption and versatile surface chemistry [1]. These properties have led to their application in cells [2], as biological labels [3], in microelectronics [4] and in electrochemical [5] and optical sensing.

The most popular type of QDs is semiconductor QDs, which are often made by alloying of atoms from groups IIB and VIA elements (known as II-VI semiconductors) or atoms from groups IIIA and VA elements (known as III-V semiconductors). Examples of II-VI type QDs include ZnO, ZnS, CdS, CdSe and CdTe while the III-V type includes GaN, GaP, InP and InAs.

Other oxides like TiO_2 and WO_3 also exhibit semiconductor properties and have been used to make quantum dots.

A relatively new class of QDs are the graphene quantum dots (GQDs) which are made from carbonaceous materials and they have gained popularity due to their low toxicity. A separate discussion on GQDs is presented in **Section 2.2**.

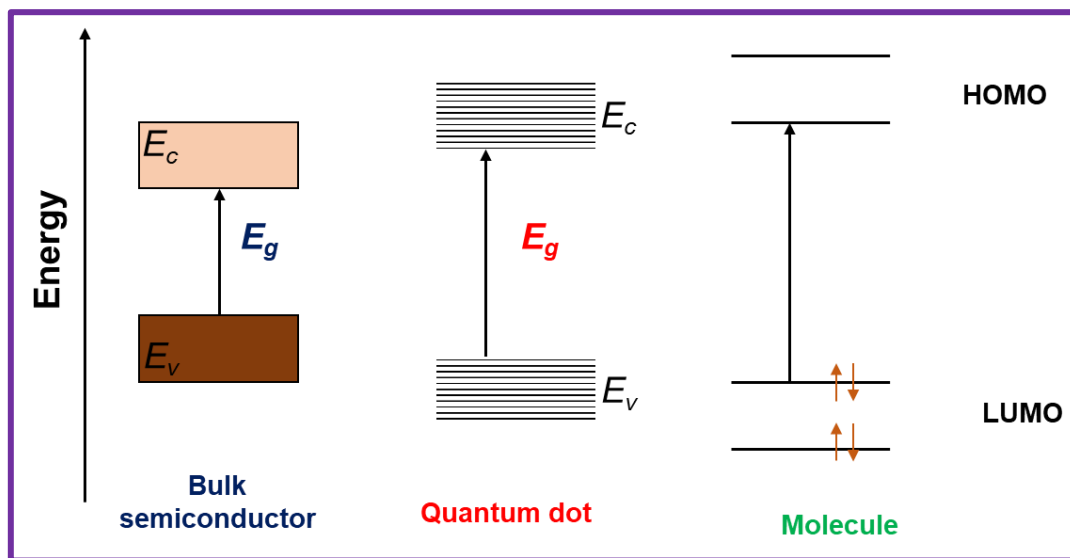


Figure 1 Comparison of the energy level diagram for a bulk semiconductor and its analogue molecular semiconductor with that of a quantum dot. (E_v = valence band; E_c = conduction band; E_g = band gap); Adapted from [6]

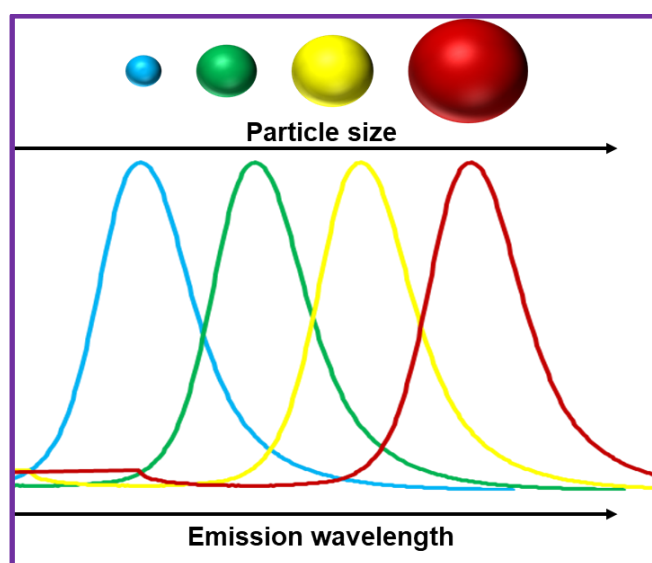


Figure 2 Schematic illustration of the effect of increasing QD particle size on the emission wavelength.

2.1.2 Synthesis techniques of semiconductor QDs

Crystalline semiconductor QDs nanoparticles can be prepared using different approaches that are well documented in literature [6-8]. The synthesis techniques can broadly be grouped into two main categories:

- (i) Colloidal chemistry or “bottom-up” approach which involves injecting precursors in hot organic solutions under vigorous stirring and allowing nucleation to occur thereby producing the QDs as colloids.
- (ii) Epitaxial growth or nanoscale patterning “top-down” approach where QDs are produced lithographically or chemically from semiconductor substrates.

Of these synthesis approaches, colloidal chemistry is the most preferred route because of its simplicity and the quality of QDs produced. Another advantage of this route is that the metal precursors can be mixed in a single flask, hence it is sometimes referred to as a “one-pot” synthesis, and reaction time and temperature variables are monitored to allow for nucleation. When this is carried out in low-temperature polar solvents like water and methanol, it is generally referred as ‘wet chemistry’ and if non-polar organic solvents like trioctylphosphine oxide (TOPO) are used it is typically referred to as ‘organometallic synthesis’. Hot organometallic synthesis is usually preferred as it yields more stable QDs with higher quantum yields. Variables like precursor concentration, temperature and reaction time can be optimized and varied in order to obtain the desired QD nanoparticles. The size of the QDs has a significant effect on their fluorescence properties and this can be easily controlled by the reaction time. The obtained QDs are hydrophobic and can be surface functionalized with the desired ligands to obtain hydrophilic particles through ligand exchange reactions [9]. Depending on the choice of ligand used, these can have stabilization effects on the QD surface and offer more functionalities which can be explored for application.

2.2 Graphene quantum dots

2.2.1 Introduction

Graphene quantum dots (GQDs) consist of small (<100 nm) crystalline sp^2 hybridized carbon lattices which are typically less than 10 carbon layers thick [10]. They have unique optical and fluorescence properties which arise from the radiative recombination of electron-hole (e-h) pairs within the sp^2 aromatic lattice. Since graphene has an infinitely large Bohr radius (distance between e-h electron and hole), when it has a finite size less than the Bohr radius, as is the case with GQDs, it exhibits quantum confinement [11, 12]. This is to say the $\pi-\pi^*$ electronic transitions within the sp^2 lattice become discrete and confined because of the size of the material. Thus, just like with semiconductor QDs, the optical properties of GQDs can be modulated by controlling the size during synthesis and the surface and edge functionalities, making them attractive for various applications.

GQDs have certain advantageous properties over semi-conductor QDs including low toxicity, excellent solubility, biocompatibility, large surface area, and better surface grafting using $\pi-\pi$ conjugation and surface groups [13-15]. The low toxicity of GQDs has allowed for their biological applications including in bioimaging, biosensing, drug delivery and in antimicrobial materials [16, 17]. Environmental application of GQDs has also been on the rise owing to their excellent optical properties and low toxicity [13, 18-20]. Most of the environmental studies, however, have been towards sensing of pollutant metal ions [21] and a few studies have been reported for detection of organic pollutants, like pentachlorophenol [22], trinitrotoluene [23] and the pesticide tributyltin [24].

Despite the attractive optical properties of GQDs, they have some drawbacks that still need to be addressed in order to extend their areas of application. For example, most of the reported GQDs emit only in the blue to yellow regions of the visible spectrum, and this can limit their application [10]. Also, reproducible synthesis of GQDs with the exact size is still a challenge due to agglomeration and formation of large sizes [25]. Lastly, the fluorescence quantum yields of most report GQDs are still relatively lower than those of semiconductor QDs [26].

While various strategies, including doping, have been proposed for producing high quantum yield GQDs, but this was beyond the scope of this thesis and was not explored.

2.2.2 Synthesis methods for GQDs

GQDs can be prepared using two approaches, namely the ‘top-down’ approach or the ‘bottom-up’ approach and these are summarized in **Table 1**. The top-down approach involves cutting of large macroscopic carbon materials (e.g. graphite, carbon fibers, graphene oxide, metal-organic frameworks, etc.) into small GQDs pieces, usually through harsh oxidation treatments. On the other hand, the bottom-up approach involves formation of GQDs from molecular or atomic carbon precursors (e.g. chlorobenzene, acetic acid, glucose, and even from PAHs) through controlled reactions to obtain desired GQD sizes [13, 19].

Table 1 Comparison of advantages and disadvantages of the synthesis strategies for GQDs (Adapted from [27]).

	Method	Advantages	Disadvantages
Top-down synthesis	Oxidative cleavage	<ul style="list-style-type: none"> • It is the most widely used method • Can achieve mass production because it is simple and effective 	<ul style="list-style-type: none"> • Uses oxidizers which may cause burning or explosions • The post-processing process to remove excess salts can be complicated
	Hydrothermal/solvothermal	<ul style="list-style-type: none"> • It is a simple and rapid method • Environmentally friendly 	<ul style="list-style-type: none"> • The carbon materials need to be treated through strong oxidation before the reactions happen
	Microwave-assisted/ultrasonic-assisted	<ul style="list-style-type: none"> • Uses shorter reaction time • Has higher product yield 	<ul style="list-style-type: none"> • High cost of the microwave/ultrasonic reactor • The volume is limited in industrial production
	Electrochemical oxidation	<ul style="list-style-type: none"> • The GQDs obtained by this method show high levels of stability • Size distribution is uniform 	<ul style="list-style-type: none"> • Pretreatment of raw materials and the purification of GQD products take a long time • Low product yield, therefore not suitable for mass production

Bottom-up synthesis	Controllable synthesis	<ul style="list-style-type: none"> The as-prepared QDs have an accurate number of carbon atoms, uniform size and shape 	<ul style="list-style-type: none"> The preparation process includes multi-step complicated chemical reactions, which are time consuming Low yield
	Carbonization from simple carbon sources	<ul style="list-style-type: none"> It is an environmentally friendly and facile method 	<ul style="list-style-type: none"> QDs with polydispersity are obtained because the size and structure are difficult to precisely control.

2.3 Characterization techniques for QDs

A variety of complementary techniques are used to characterize QDs in order to get in-depth information on their nature. In this section, a brief overview of the common techniques is given, with a focus on those used in this thesis.

2.3.1 Optical characterization

The optical properties of QDs are usually studied using UV-vis and fluorescence spectroscopy. Both techniques can be used to derive valuable information on the surface electronic ground and transition states of QDs.

UV-vis absorption spectroscopy is based on focusing incident light (with wavelengths in the UV-visible region) on the sample to induce excitation of electrons in specific orbitals (or bands), into excited states. These electronic transitions occur without significant change in the nuclei (Franck-Condon principle) [28]. This technique is therefore widely used to study the electronic states and estimate the bandgap of QDs.

The principles of fluorescence spectroscopy are best explained by studying the Jablonski electronic transition diagram [28]. Briefly, a monochromatic light beam is directed towards the sample to induce excitation of electrons from singlet ground state, S_0 , to an excited state S_n ($n>1$). The excited electrons can therefore return to the ground state, S_0 , via different processes including (a) via the lowest excited S_1 states (known as internal conversion), (b) through radiative emission of a photon (fluorescence) (c) collisional quenching or (d) via

excited triplet states with energies lower than S_1 states (inter-system crossing). In fluorescence sensing an appreciation of these transitions is essential in elucidating fluorescence sensing mechanisms.

Fluorescence and UV-vis spectroscopy are also used to derive secondary information like estimating the photoluminescence quantum yields (QY) of the QDs. The QY is the ratio of photons absorbed to photons emitted through fluorescence [29]. It is often used to indicate the quality of QDs and is largely influenced by the synthesis method. The QY can be improved through various synthetic strategies including choosing a shell material that has a wider bandgap than the core [30]. QY can be determined either through relative means with reference to a standard (e.g. Rhodamine 6G) or by absolute methods by making use of an integrating sphere.

2.3.2 Structural and morphological characterization

To study the structural composition and nature of QDs, imaging and spectroscopic techniques can be used and here a very brief summary of the commonly used techniques is provided.

Transmission electron microscopy (TEM) or high-resolution transmission microscopy (HRTEM) involves the illumination of a sample with a beam of short wavelength electrons under vacuum. Part of the beam gets transmitted through the sample and is focused onto a charge coupled device camera to obtain images that can be used to study the morphology and size distribution of QDs. HRTEM can also be used to visualize lattice fringes of nanomaterials thereby allowing for information on their phase and crystal axes to be deduced [31].

X-ray diffraction (XRD) spectroscopy involves irradiating a sample with an X-ray beam to obtain diffraction patterns which reveal information on the crystalline phases, lattice parameters, and for estimating the crystalline grain size of a sample. This technique can also be used to infer the composition of the material by making reference to standard references

(International Centre for Diffraction Data) [32]. The crystal packing in semiconductor QDs is usually either centred cubic (zinc blende) or hexagonal (wurtzite) [8].

Fourier-transform infrared (FTIR) spectroscopy is used as a powerful technique to study the surface chemistry of QDs. This technique is based on the absorption of light in the infra-red region ($4000 - 400 \text{ cm}^{-1}$) by a sample which modifies its dipole. The FTIR spectrum gives information on the nature of bonds and functional groups that are present in a sample, and standard FTIR tables are normally used to infer this information [33]. In QDs this is a useful technique to confirm any modifications of their surface chemistry.

Raman spectroscopy is widely used for characterization of nanomaterials, including QDs, to study their structure, phase, crystallinity and molecular interactions. The technique is based on the scattering of an incident monochromatic laser beam by the material at a different wavelength from that of the incident beam. The intensity and wavelength positions of the scattered light (Raman spectrum) gives fingerprint information on the collective vibrational, rotational, and other low-frequency transitions that are present in the sample [34].

2.4 The principle of QD fluorescence sensing

In order to understand how fluorescence sensing works, it is important to understand how the fluorescence emission arises. The emission is due to radiative recombination of electron-hole pairs following absorption of photons. If there are any surface defects or adsorbates (or analytes) that are present on the QD surface they introduce 'trap' states through which the excited photons may fall [6]. The lowest unoccupied molecular orbitals of the adsorbates may then interact with the trap states in a donor-acceptor fashion which then affects the radiative recombination of the photoexcited electron-hole [6, 35]. These electron transfer processes can spectroscopically be observed as fluorescence quenching [36] and it forms the basis for QD sensing.

When the interaction of analytes with QDs involves long-range dipole-dipole interactions in a donor-acceptor fashion, Förster resonance energy transfer (FRET) between the donor and

acceptor may occur [37, 38]. Such interactions may result in either fluorescence quenching or enhancement thus allowing for quantitative analyte detection. The selectivity of QD sensors can be achieved through various surface modification strategies which are discussed in Chapter 3.

2.5 Target compounds

2.5.1 Atrazine

2.5.1.1 Sources and occurrence of atrazine in the environment

Atrazine (6-chloro-4-N-ethyl-2-N-propan-2-yl-1,3,5-triazine-2,4-diamine), shown in **Figure 3**, is a widely used herbicide for controlling annual broad-leaved weeds and grasses in pre- or post-emergent crops like maize, sorghum and sugar cane. Some of the physical and chemical properties of atrazine are presented in **Table 2** Its mode of action involves inhibiting the photosynthetic electron transport of the weeds, while the target crop is tolerant to atrazine because of rapid detoxification [39].

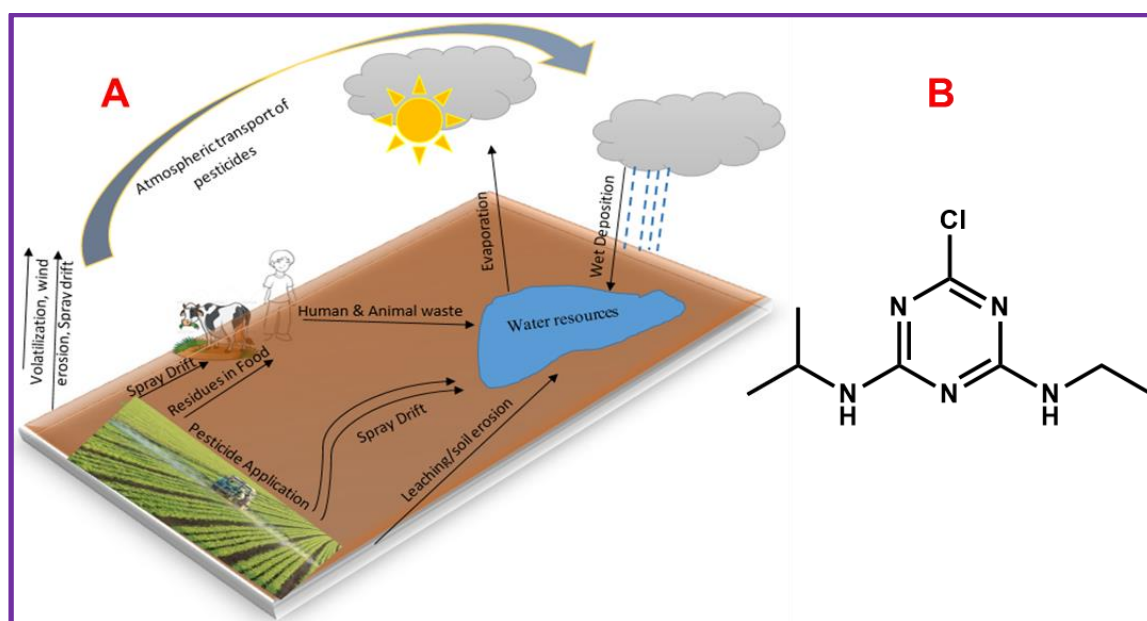


Figure 3 (a) Schematic illustration of different pathways through which pesticides can contaminate non-targeted environmental resources and (b) the chemical structure of atrazine.

Table 2 Physiochemical properties of atrazine (adapted from [39, 40]).

Property	Value
Molecular weight	215.7 g mol ⁻¹
Molecular formula	C ₈ H ₁₄ ClN ₅
Form	Colourless powder
Melting point	175.8 °C
Boiling point (at 101 kPa)	205.0 °C
Vapour pressure (at 25 °C)	3.85×10 ⁻² mPa
K _{ow} log P	2.5 (25 °C)
Henry's constant	1.5×10 ⁻⁴ Pa m ³ mol ⁻¹
Density (at 22 °C)	1.23 g cm ⁻³
Solubility: in water (at 22 °C, pH 7)	33 mg L ⁻¹
K _d	2.60
Log K _{SA}	7.18

K_{SA}: volatilization potential from soil to air

K_d : distribution coefficient from soil and soil-water partitioning

K_{ow}: octanol-water partition coefficient

Because of its high annual use in agriculture, atrazine has been one of the most frequently detected pesticides in freshwater systems in many parts of the world. For example, Gilliom [41] found that atrazine was the most frequently detected pesticide in the USA surface and groundwater systems. A similar assertion has been made for European groundwater [42]. In South Africa, atrazine has also been shown to have the largest number of seasonal occurrences [43] as shown in **Table 3**. A study by Dabrowski, et al. [44] dealing with the prioritization of pesticides that are used in South Africa, featured atrazine as the highest-ranked pesticide among 25 priority pesticides. The ranking and prioritization was based on a weighted hazard potential (WHP) – a prioritization index which is directly proportional to the

pesticide's toxicity potential (TP) and the total quantity of use. Several studies have found atrazine in South African freshwater systems [45-47] due to its high use.

Table 3 Concentration ($\mu\text{g L}^{-1}$) of atrazine sampled over four seasons in drinking water in selected areas across South Africa. Average concentrations are indicated (n=3) [43].

Sampling site	Summer	Autumn	Winter	Spring
Bloemfontein North tap	0.02	0.15	0.01	0.02
Bloemfontein South tap	0.01	0.19	0.02	0.15
Bloemfontein	0.02	0.02	0.01	0.01
Cape Town	0.00	0.00	0.00	0.00
Durban	0.02	0.02	0.00	0.01
Johannesburg	0.03	0.15	0.11	0.12
Pietermaritzburg	0.02	0.02	0.02	0.02
Port Elizabeth	0.01	0.00	0.00	0.00
Pretoria	0.04	0.16	0.00	0.01

2.5.1.2 Toxicity of atrazine

Atrazine in water systems has been reported to have harmful effects on aquatic organisms, including causing endocrine disrupting effects [48-50]. Some studies have also shown that it also has endocrine disruption effects in human cells [51, 52]. Moreover, atrazine can be quite persistent in water, as a study of Lake Superior in Canada suggested that the half-life of atrazine in lakes was over 10 years [53]. This stability can lead to prolonged negative effects on aquatic organisms.

For example, a study by Hayes, et al. [54] showed that atrazine exposure demasculinized (chemically castrated) male African clawed frogs (*Xenopus laevis*) leading to suppressed mating behaviours and reduced spermatogenesis. Studies by Santos and Martinez [55] showed that exposure to 2 – 10 $\mu\text{g L}^{-1}$ of atrazine resulted in biochemical changes and DNA damage on Neotropical fish species (*Prochilodus lineatus*). Ingestion of 100 g of atrazine by fish was observed to have catastrophic results. Such exposure may lead to coma, heart and

peripheral vessel damage, and renal failure, resulting in death [56, 57]. Other delayed, fatal consequences include leukaemia and brain cancer [58].

Exposure to atrazine has been linked to carcinogenic risks. Tumours of the reproductive organs and lymph cancer were related to atrazine exposure [57, 58]. Alarming, one study by Van Leeuwen, et al. [59] showed an association between stomach cancer and atrazine exposure in the range 50 – 649 ng L⁻¹, which is well below the maximum contaminant level (MCL) of 3 µg L⁻¹ for drinking water as set by the US EPA. Other critical effects revolve around vulnerabilities of women during pregnancy and on the foetus or infants. These effects include foetal development aberrations like growth retardation, a decrease in gestation age, and gastroschisis [60-63]. Lower birth weight was also directly associated with perinatal mortality in the USA [64].

Moderate effects of exposure to atrazine include a decrease in sperm concentration and motility, known as oligospermia [65]. Minor side effects of exposure included fatigue, dizziness, nausea, and skin irritations [56, 57].

2.5.1.3 Legal limits for atrazine in water

The World Health Organization (WHO) has derived guideline values for atrazine and its metabolites and these are shown in **Table 4**. Typical atrazine concentrations rarely exceed 2 µg L⁻¹ and are commonly well below the 0.1 µg L⁻¹ guideline limit for atrazine in drinking water. Higher concentrations can however be expected around agricultural areas where it is extensively used. The acceptable daily intake for atrazine and its chloro-s-triazine metabolites is between 0 – 0.02 mg kg⁻¹ bodyweight based on luteinizing hormone surge suppression and subsequent disruption of the oestrous cycle seen at 3.6 mg kg⁻¹ body weight per day in a 6-month study in rats [66].

Table 4 Guideline value for atrazine in drinking water [66]

Compound	Guideline Value (mg L ⁻¹)	Acceptable daily intake	Guideline value derivation
Atrazine	0.1	0–0.02 mg kg ⁻¹ body weight based on the NOAEL for atrazine of 1.8 mg kg ⁻¹ body weight per day.	Allocation to water: 20% of upper limit of ADI Bodyweight: 60 kg adult Consumption: 2 L per day

ADI = acceptable daily intake

NOAEL = non-observed adverse effect level

2.5.2 Polycyclic aromatic compounds

2.5.2.1 Sources and occurrence of PAHs

PAHs are produced from a wide variety of sources and hence they are one of the pollutant classes which are of global concern [67, 68]. **Table 5** illustrates the classification of the various sources of PAH compounds.

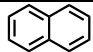
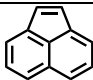
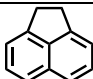
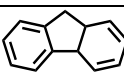
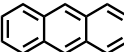
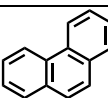
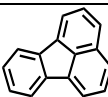
Table 5 Natural and anthropogenic sources of polycyclic aromatic hydrocarbons (PAHs).

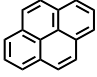
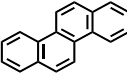
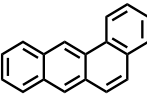
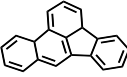
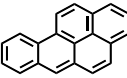
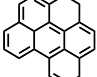
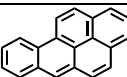
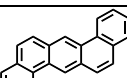
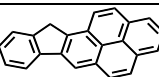
Natural sources	Anthropogenic sources
<ul style="list-style-type: none">• Vegetative Decay• Plant Synthesis• Fires• Volcanic Eruptions	<ul style="list-style-type: none">• Petroleum Spills• Pesticide Formulations• Sewage Sludge• PAH-contaminated Media• Road Dust• Vehicles (Internal combustion)• Jet Aircrafts• Incineration• Wood Burning• Cigarette Smoke• Cooking• Other Industries/Processes

PAHs can be introduced into environmental water systems through various ways after wet or dry deposition from the atmosphere after their release from sources including industrial combustion activities, biomass burning, and vehicular emissions. A comprehensive review on the occurrence and typical concentration ranges of PAHs in South African water systems was carried out by Chimuka, et al. [69] where it was shown that PAH levels in water can have seasonal variations ranging from 30.0 ng L⁻¹ in summer to as high as 60.8 L⁻¹ in winter. Clearly, these compounds occur at low concentrations in runoff and river water, but continuous exposure may pose human health effects.

Generally, PAHs have low solubility in water and typically those with higher molecular weight, like benzo[a]pyrene, have the least solubility (0.0057 mg L⁻¹ at 25 °C) while lower molecular weight naphthalene has the highest solubility (31.69 mg L⁻¹ at 25 °C) as shown in **Table 6**. Removal of PAHs in water systems can be achieved either by using traditional methods like destructive oxidation with ozone or by using adsorption technology with adsorbents like activated carbon [70].

Table 6 Chemical structures and physical properties of the 16 PAHs listed as US EPA priority pollutants [67]. (in order of increasing molecular weight)

PAH	Structure	Vapor pressure at 20 °C (Torr)	Solubility in water (mg L ⁻¹)	K _{ow}
Naphthalene		0.0492	32	2300
Acenaphthylene		10 ⁻³ – 10 ⁻²	3.93	12000
Acenaphthene		10 ⁻³ – 10 ⁻²	3.4 at 25 °C	21000
Fluorene		10 ⁻³ – 10 ⁻²	1.9	15000
Anthracene		2 × 10 ⁻⁴	0.05 – 0.07 at 25 °C	28000
Phenanthrene		6.8 × 10 ⁻⁴	1.0 – 1.3 at 25 °C	29000
Fluoranthene		10 ⁻⁶ – 10 ⁻⁴	0.26 at 25 °C	340000

Pyrene		6.9×10^{-9}	0.14 at 25 °C	2×10^5
Chrysene		$10^{-11} - 10^{-6}$	0.002 at 25 °C	4×10^5
Benzo[a]anthracene		5×10^{-9}	0.01 at 25 °C	4×10^5
Benzo[b]fluoranthene		$10^{-11} - 10^{-6}$	–	4×10^6
Benzo[a]pyrene		5×10^{-9}	0.0038 at 25 °C	1×10^6
Benzo[ghi]perylene		$\sim 10^{-10}$	0.00026 at 25 °C	1×10^7
Benzo[a]pyrene		5×10^{-9}	0.0038 at 25 °C	1×10^6
Dibenzo[a,h]anthracene		$\sim 10^{-10}$	0.0005 at 25 °C	1×10^6
Indeno[1,2,3-cd]pyrene		$\sim 10^{-10}$	–	5×10^7

2.5.2.2 Toxicity of PAHs

The exposure to various PAH compounds can lead to serious toxic effects to both humans and aquatic organisms. In order to qualitatively assess the potential health risk of each of the PAHs, a study by Nisbet and LaGoy [71] assigned toxic equivalency factors (TEFs) to each of the PAHs which are a measure of their carcinogenicity relative to that of benzo[a]pyrene (Table 7).

Table 7 PAHs and their toxic equivalency factors (TEFs) expressed relative to benzo[a]pyrene [71].

PAH compounds	TEF
Benzo[a]pyrene	1
Benzo[a]anthracene	0.1
Benzo[b]fluoranthene	0.1
Phenanthrene	0.001
Indeno[1,2,3-cd]pyrene	0.1
Anthracene	0.01

Benzo[ghi]perylene	0.01
Chrysene	0.01
Acenaphthene	0.001
Acenaphthylene	0.001
Fluoranthene	0.001
Fluorene	0.001
Pyrene	0.001
Naphthalene	0.01
Dibenzo[ah]anthracene	5

It is also important to note that PAHs rarely occur as single compound in environmental water systems. A study by Engraff, et al. [72] demonstrated the importance of considering PAH mixtures when studying their toxicity in aquatic systems. Thus, the use of single PAH compound concentrations for risk assessment purposes can lead to an underestimation of the risk since the effect of a mixture of compounds can be additive or synergistic.

The toxicity of PAHs to aquatic organisms can further be enhanced by their metabolism and photooxidation into more toxic derivative compounds. Natural UV light and other environmental factors can facilitate their derivatization [73]. PAHs can also be directly absorbed by animals through dermal contact, inhalation and injection pathways, and once in their system, they can cause adverse effects like tumours and can affect reproduction, development and immunity [73].

Ikenaka, et al. [74] conducted exposure experiments to investigate the acute toxicity of benzo[a]pyrene on Cladocera species (*Ceriodaphnia reticulata* and *Daphnia magna*) and its impact on zooplankton communities. They found the LC50 to be 4.3 and 4.7 $\mu\text{g L}^{-1}$ for *C. reticulata* and *D. magna* respectively. The study further showed that benzo[a]pyrene induced a decrease in zooplankton abundance when environmentally relevant concentrations (5 and 10 $\mu\text{g L}^{-1}$) were used with <4 days residence time.

The potential of harmful effects of PAHs on humans is equally concerning. Some studies reported that PAHs can have possible carcinogenic effects not only to aquatic animals but

also to humans [75]. PAHs can affect the hematopoietic and immune systems and can produce reproductive, neurologic, and developmental effects [76, 77].

2.5.2.3 Legal limits

Some guideline values for PAHs in water have been drafted by the US EPA [78] and these are shown in **Table 8**. For drinking water, only benzo(a)pyrene, which is a known carcinogen, has a maximum contentment level value of $<0.2 \mu\text{g L}^{-1}$ and not values have been determined for the other PAHs. There are no regulatory guideline values for PAHs in South African drinking water, and this remains a challenge for local environmental regulation.

Table 8 Water quality standards for PAHs in water [78].

Parameter ($\mu\text{g L}^{-1}$)	WQC ($\mu\text{g L}^{-1}$)		DWMCL/MCLG
	HHWO	HHOO	
Napthalene	-	-	
Fluorene	1100	5300	
Benzo(a)anthracene	0.0038	0.018	
Benzo(a) pyrene	0.0038	0.018	0.2/zero
Benzo(a) fluoranthene	0.0038	0.018	
Benzo(k) fluoranthene	0.0038	0.018	
Chrysene	0.0038	0.018	
Dibenzo(a,h) anthracene	0.0038	0.018	
Indeno(1,2,3-cd) pyrene	0.0038	0.018	
Acenaphthene	670	990	
Acenaphthylene	-	-	
Anthracene	8300	40000	
Benzo(ghi) perylene	-	-	
Fluoranthene	130	140	
Phenanthrene	-	-	
Pyrene	830	4000	

DWMCL: EPA Drinking Water MCLs/Other Standard, EPA 822-R-02-038, summer 2002

HHOO: Human Health Organism Only Values

HHWO: Human Health Water + Organism Values

MCLG: Maximum Contaminant Level Goal

WQC: EPA National Recommended Water Quality Criteria, EPA-822-R-02-047, November 2002

2.6 Conclusion

This chapter has introduced QDs and their properties that make them attractive for designing fluorescence sensors. The established synthesis and characterisation techniques for QDs have been reviewed. For semiconductor QDs, the hot organometallic synthesis method was used in this work because of its advantages in producing stable QDs. For the synthesis of graphene quantum dots, however, both bottom-up and top-down approaches were explored and compared.

The principles of the main characterization techniques that are used to study the structural and optical properties of QDs were highlighted. It is important to stress that these techniques are complementary to one another and a combination thereof is used to gain in-depth understanding of the nanomaterial being investigated.

Lastly, a brief background to the target analytes (PAHs and atrazine) was provided in order to highlight their environmental importance and relevance. From this background, it is apparent that the occurrence of these compounds in water systems is almost inevitable, especially in an agriculturally intensive country like South Africa. The lack of local regulatory guidelines clearly indicates that these are ECPs of concern that require ongoing environmental monitoring.

2.7 References

- [1] H. Kuang, Y. Zhao, W. Ma, L. Xu, L. Wang, C. Xu, Recent developments in analytical applications of quantum dots, *TrAC, Trends Anal. Chem.*, 30 (2011) 1620-1636.
- [2] A.J. Nozik, M.C. Beard, J.M. Luther, M. Law, R.J. Ellingson, J.C. Johnson, Semiconductor quantum dots and quantum dot arrays and applications of multiple exciton generation to third-generation photovoltaic solar cells, *Chem. Rev.*, 110 (2010) 6873-6890.
- [3] S. Jin, Y. Hu, Z. Gu, L. Liu, H.-C. Wu, Application of quantum dots in biological imaging, *J. Nanomater.*, 2011 (2011) 1-13.
- [4] F.D. de Menezes, A.G. Brasil Jr, W.L. Moreira, L.C. Barbosa, C.L. Cesar, R.d.C. Ferreira, P.M.A. de Farias, B.S. Santos, CdTe/CdS core shell quantum dots for photonic applications, *Microelectron. J.*, 36 (2005) 989-991.
- [5] H. Huang, J.-J. Zhu, The electrochemical applications of quantum dots, *Analyst*, 138 (2013) 5855-5865.
- [6] C.J. Murphy, J.L. Coffey, Quantum Dots: A Primer, *Appl. Spectrosc.*, 56 (2002) 16A-27A.
- [7] J. Drbohlavova, V. Adam, R. Kizek, J. Hubalek, Quantum Dots — Characterization, Preparation and Usage in Biological Systems, *Int. J. Mol. Sci.*, 10 (2009) 656-673.
- [8] D. Bera, L. Qian, T.-K. Tseng, P.H. Holloway, Quantum dots and their multimodal applications: A review, *Materials*, 3 (2010) 2260 - 2345.
- [9] F. Dubois, B. Mahler, B. Dubertret, E. Doris, C. Mioskowski, A versatile strategy for quantum dot ligand exchange, *J. Am. Chem. Soc.*, 129 (2007) 482-483.
- [10] P. Tian, L. Tang, K.S. Teng, S.P. Lau, Graphene quantum dots from chemistry to applications, *Mater. Today Chem.*, 10 (2018) 221-258.
- [11] S. Zhu, Y. Song, X. Zhao, J. Shao, J. Zhang, B. Yang, The photoluminescence mechanism in carbon dots (graphene quantum dots, carbon nanodots, and polymer dots): current state and future perspective, *Nano Research*, 8 (2015) 355-381.
- [12] L. Li, G. Wu, G. Yang, J. Peng, J. Zhao, J.-J. Zhu, Focusing on luminescent graphene quantum dots: current status and future perspectives, *Nanoscale*, 5 (2013) 4015-4039.
- [13] J. Shen, Y. Zhu, X. Yang, C. Li, Graphene quantum dots: emergent nanolights for bioimaging, sensors, catalysis and photovoltaic devices, *Chem. Commun.*, 48 (2012) 3686-3699.

- [14] Y. Chong, Y. Ma, H. Shen, X. Tu, X. Zhou, J. Xu, J. Dai, S. Fan, Z. Zhang, The in vitro and in vivo toxicity of graphene quantum dots, *Biomaterials*, 35 (2014) 5041-5048.
- [15] S. Wang, I.S. Cole, Q. Li, The toxicity of graphene quantum dots, *RSC Adv.*, 6 (2016) 89867-89878.
- [16] X.T. Zheng, A. Ananthanarayanan, K.Q. Luo, P. Chen, Glowing graphene quantum dots and carbon dots: Properties, syntheses, and biological applications, *Small*, 11 (2015) 1620-1636.
- [17] K. Li, W. Liu, Y. Ni, D. Li, D. Lin, Z. Su, G. Wei, Technical synthesis and biomedical applications of graphene quantum dots, *J. Mater. Chem. B*, 5 (2017) 4811-4826.
- [18] H. Sun, L. Wu, W. Wei, X. Qu, Recent advances in graphene quantum dots for sensing, *Mater. Today*, 16 (2013) 433-442.
- [19] S. Benítez-Martínez, M. Valcárcel, Graphene quantum dots in analytical science, *TrAC, Trends Anal. Chem.*, 72 (2015) 93-113.
- [20] L. Lin, M. Rong, F. Luo, D. Chen, Y. Wang, X. Chen, Luminescent graphene quantum dots as new fluorescent materials for environmental and biological applications, *TrAC, Trends Anal. Chem.*, 54 (2014) 83-102.
- [21] J. Ju, W. Chen, Graphene quantum dots as fluorescence probes for sensing metal ions: Synthesis and applications, *Curr. Org. Chem.*, 19 (2015) 1150-1162.
- [22] Q. Liu, K. Wang, J. Huan, G. Zhu, J. Qian, H. Mao, J. Cai, Graphene quantum dots enhanced electrochemiluminescence of cadmium sulfide nanocrystals for ultrasensitive determination of pentachlorophenol, *Analyst*, 139 (2014) 2912-2918.
- [23] L. Fan, Y. Hu, X. Wang, L. Zhang, F. Li, D. Han, Z. Li, Q. Zhang, Z. Wang, L. Niu, Fluorescence resonance energy transfer quenching at the surface of graphene quantum dots for ultrasensitive detection of TNT, *Talanta*, 101 (2012) 192-197.
- [24] E. Zor, E. Morales-Narváez, A. Zamora-Gálvez, H. Bingol, M. Ersoz, A. Merkoçi, Graphene quantum dots-based photoluminescent sensor: A multifunctional composite for pesticide detection, *ACS Appl. Mater. Interfaces*, 7 (2015) 20272-20279.
- [25] S. Campuzano, P. Yáñez-Sedeño, J.M. Pingarrón, Carbon dots and graphene quantum dots in electrochemical biosensing, *Nanomaterials*, 9 (2019) 634-652.
- [26] V.A. Chhabra, R. Kaur, N. Kumar, A. Deep, C. Rajesh, K.-H. Kim, Synthesis and spectroscopic studies of functionalized graphene quantum dots with diverse fluorescence characteristics, *RSC Adv.*, 8 (2018) 11446-11454.

- [27] W. Chen, G. Lv, W. Hu, D. Li, S. Chen, Z. Dai, Synthesis and applications of graphene quantum dots: a review, *Nanotechnology Reviews*, 2018, pp. 157.
- [28] J.R. Albani, Principles and applications of fluorescence spectroscopy, John Wiley & Sons, Garsington Road, Oxford, UK, 2008.
- [29] A.T.R. Williams, S.A. Winfield, J.N. Miller, Relative fluorescence quantum yields using a computer-controlled luminescence spectrometer, *Analyst*, 108 (1983) 1067-1071.
- [30] R. Xie, U. Kolb, J. Li, T. Basché, A. Mews, Synthesis and characterization of highly luminescent CdSe–Core CdS/Zn_{0.5}Cd_{0.5}S/ZnS multishell nanocrystals, *J. Am. Chem. Soc.*, 127 (2005) 7480-7488.
- [31] C. Rentenberger, T. Waitz, H. Karnthaler, HRTEM analysis of nanostructured alloys processed by severe plastic deformation, *Scripta Mater.*, 51 (2004) 789-794.
- [32] S. Mourdikoudis, R.M. Pallares, N.T.K. Thanh, Characterization techniques for nanoparticles: comparison and complementarity upon studying nanoparticle properties, *Nanoscale*, 10 (2018) 12871-12934.
- [33] M.A. Mohamed, J. Jaafar, A.F. Ismail, M.H.D. Othman, M.A. Rahman, Chapter 1 - Fourier Transform Infrared (FTIR) Spectroscopy, in: N. Hilal, A.F. Ismail, T. Matsuura, D. Oatley-Radcliffe (Eds.) *Membrane Characterization*, Elsevier 2017, pp. 3-29.
- [34] G. Gouadec, P. Colomban, Raman Spectroscopy of nanomaterials: How spectra relate to disorder, particle size and mechanical properties, *Prog. Cryst. Growth Charact. Mater.*, 53 (2007) 1-56.
- [35] C.J. Murphy, Peer reviewed: Optical sensing with quantum dots, *Anal. Chem.*, 74 (2002) 520 A-526 A.
- [36] R. Freeman, I. Willner, Optical molecular sensing with semiconductor quantum dots (QDs), *Chem. Soc. Rev.*, 41 (2012) 4067-4085.
- [37] A. Shamirian, A. Ghai, P. Snee, QD-based FRET probes at a glance, *Sensors*, 15 (2015) 13028-13051.
- [38] K. Chou, A. Dennis, Förster resonance energy transfer between quantum dot donors and quantum dot acceptors, *Sensors*, 15 (2015) 13288 -13325.
- [39] C. MacBean, *The Pesticide Manual*, 16th ed., British Crop Production Council, Omega Park, Alton, Hampshire, GU34 2QD, UK, 2012.

- [40] N. Ratola, V. Homem, J.A. Silva, R. Araujo, J.M. Amigo, L. Santos, A. Alves, Biomonitoring of pesticides by pine needles--chemical scoring, risk of exposure, levels and trends, *Sci. Total Environ.*, 476-477 (2014) 114-124.
- [41] R.J. Gilliom, Pesticides in US streams and groundwater, *Environ. Sci. Technol.*, 41 (2007) 3408-3414.
- [42] M. Gavrilescu, K. Demnerova, J. Aamand, S. Agathos, F. Fava, Emerging pollutants in the environment: present and future challenges in biomonitoring, ecological risks and bioremediation, *N. Biotechnol.*, 32 (2015) 147-156.
- [43] H. Patterson, Scoping study and research strategy development on currently known and emerging contaminants influencing drinking water quality, 2013, WRC Report No. 2093/1/13, W.R. Commission, Water Research Commission, <http://goo.gl/qy9R9X>.
- [44] J.M. Dabrowski, J.M. Shadung, V. Wepener, Prioritizing agricultural pesticides used in South Africa based on their environmental mobility and potential human health effects, *Environ. Int.*, 62 (2014) 31-40.
- [45] F.E. Pick, L.P. van Dyk, E. Botha, Atrazine in ground and surface water in maize production areas of the Transvaal, South Africa, *Chemosphere*, 25 (1992) 335-341.
- [46] L.H. Du Preez, P.J. Jansen van Rensburg, A.M. Jooste, J.A. Carr, J.P. Giesy, T.S. Gross, R.J. Kendall, E.E. Smith, G. Van Der Kraak, K.R. Solomon, Seasonal exposures to triazine and other pesticides in surface waters in the western Highveld corn-production region in South Africa, *Environ. Pollut.*, 135 (2005) 131-141.
- [47] J.M. Dabrowski, N. Aneck-Hahn, J. Chamier, C. De Jager, P. Forbes, B. Genthe, J.A. Meyer, R. Pieters, J. Shadung, M. Thwala, M.C. Van Zijl, Sampling and analysis of water and sediments for endocrine disrupting activity and concentrations of pesticide active ingredients, 2013, WRC Project No: K5/1956 - Deliverable 9, W.R. Commission, Water Research Commission,
- [48] G. Giusi, R. Facciolo, M. Canonaco, E. Alleva, V. Belloni, F. Dessi, D. Santucci, The endocrine disruptor atrazine accounts for a dimorphic somatostatinergic neuronal expression pattern in mice, *Toxicol. Sci.*, 89 (2006) 257-264.
- [49] T.B. Hayes, V. Houry, A. Narayan, M. Nazir, A. Park, T. Brown, L. Adame, E. Chan, D. Buchholz, T. Stueve, S. Gallipeau, Atrazine induces complete feminization and chemical castration in male African clawed frogs (*Xenopus laevis*), *Proceedings of the National Academy of Sciences of the United States of America*, 107 (2010) 4612-4617.

- [50] S. Hrouzková, E. Matisová, Endocrine disrupting pesticides, in: R.P. Soundararajan (Ed.) Pesticides—Advances in Chemical and Botanical pesticides, InTech, Croatia, 2012, pp. 99-126.
- [51] W. Fan, T. Yanase, H. Morinaga, S. Gondo, T. Okabe, M. Nomura, T. Komatsu, K. Morohashi, T. Hayes, R. Takayanagi, Atrazine-induced aromatase expression is SF-1 dependent: Implications for endocrine disruption in wildlife and reproductive cancers in humans, *Environ. Health Perspect.*, 115 (2007) 720-727.
- [52] J.T. Sanderson, W. Seinen, J.P. Giesy, M. van den Berg, 2-Chloro-s-triazine herbicides induce aromatase (CYP19) activity in H295R human adrenocortical carcinoma cells: A novel mechanism for estrogenicity, *Toxicol. Sci.*, 54 (2000) 121-127.
- [53] E.M. Thurman, A.E. Cromwell, Atmospheric transport, deposition, and fate of triazine herbicides and their metabolites in pristine areas at Isle Royale National Park, *Environ. Sci. Technol.*, 34 (2000) 3079-3085.
- [54] T.B. Hayes, V. Khoury, A. Narayan, M. Nazir, A. Park, T. Brown, L. Adame, E. Chan, D. Buchholz, T. Stueve, Atrazine induces complete feminization and chemical castration in male African clawed frogs (*Xenopus laevis*), *Proceedings of the National Academy of Sciences*, 107 (2010) 4612-4617.
- [55] T.G. Santos, C.B.R. Martinez, Atrazine promotes biochemical changes and DNA damage in a Neotropical fish species, *Chemosphere*, 89 (2012) 1118-1125.
- [56] M.J. Ellenhorn, S. Schonwald, G. Ordog, J. Wasserberger, *Ellenhorn's medical toxicology: diagnosis and treatment of human poisoning*, 2nd ed., Williams & Wilkins, Baltimore, 1997.
- [57] ATSDR, Toxicological profile for atrazine, 2003, Agency for Toxic Substances and Disease Registry, <https://www.atsdr.cdc.gov/ToxProfiles/tp153.pdf>.
- [58] E. Bingham, B. Cohrssen, C.H. Powell, *Patty's toxicology. Volume 2: toxicological issues related to metals, neurotoxicology and radiation metals and metal compounds*, John Wiley and Sons, New York, USA, 2001.
- [59] J.A. Van Leeuwen, D. Waltner-Toews, T. Abernathy, B. Smit, M. Shoukri, Associations between stomach cancer incidence and drinking water contamination with atrazine and nitrate in Ontario (Canada) agroecosystems, 1987-1991, *Int. J. Epidemiol.*, 28 (1999) 836-840.

- [60] C. Chevrier, G. Limon, C. Monfort, F. Rouget, R. Garlantézec, C. Petit, G. Durand, S. Cordier, Urinary biomarkers of prenatal atrazine exposure and adverse birth outcomes in the PELAGIE birth cohort, *Environ. Health Perspect.*, 119 (2011) 1034-1041.
- [61] R. Munger, P. Isacson, S. Hu, T. Burns, J. Hanson, C.F. Lynch, K. Cherryholmes, P. Van Dorpe, W.J. Hausler Jr, Intrauterine growth retardation in Iowa communities with herbicide-contaminated drinking water supplies, *Environ. Health Perspect.*, 105 (1997) 308-314.
- [62] H. Ochoa-Acuña, J. Frankenberger, L. Hahn, C. Carbajo, Drinking-water herbicide exposure in Indiana and prevalence of small-for-gestational-age and preterm delivery, *Environ. Health Perspect.*, 117 (2009) 1619-1624.
- [63] S.A. Waller, K. Paul, S.E. Peterson, J.E. Hitti, Agricultural-related chemical exposures, season of conception, and risk of gastroschisis in Washington State, *Am. J. Obstet. Gynecol.*, 202 (2010) 241. e241-241. e246.
- [64] N.S. Paneth, The problem of low birth weight, *The future of children*, (1995) 19-34.
- [65] S.H. Swan, Semen quality in fertile US men in relation to geographical area and pesticide exposure, *Int. J. Androl.*, 29 (2006) 62-68.
- [66] WHO, Guidelines for drinking-water quality 4th Edition, 2011, World Health Organization, http://apps.who.int/iris/bitstream/10665/44584/1/9789241548151_eng.pdf.
- [67] E. Manoli, C. Samara, Polycyclic aromatic hydrocarbons in natural waters: sources, occurrence and analysis, *TrAC, Trends Anal. Chem.*, 18 (1999) 417-428.
- [68] O.S.S. Sojinu, J.-Z. Wang, O.O. Sonibare, E.Y. Zeng, Polycyclic aromatic hydrocarbons in sediments and soils from oil exploration areas of the Niger Delta, Nigeria, *J. Hazard. Mater.*, 174 (2010) 641-647.
- [69] L. Chimuka, P. Sibiyi, R. Amdany, E. Cukrowska, P.B.C. Forbes, Status of PAHs in environmental compartments of South Africa: A country report, *Polycyclic Aromat. Compd.*, 36 (2016) 1-19.
- [70] Z.C. Zeledón-Toruño, C. Lao-Luque, F.X.C. de las Heras, M. Sole-Sardans, Removal of PAHs from water using an immature coal (leonardite), *Chemosphere*, 67 (2007) 505-512.
- [71] I.C. Nisbet, P.K. LaGoy, Toxic equivalency factors (TEFs) for polycyclic aromatic hydrocarbons (PAHs), *Regul. Toxicol. Pharm.*, 16 (1992) 290-300.

- [72] M. Engraff, C. Solere, K.E.C. Smith, P. Mayer, I. Dahllöf, Aquatic toxicity of PAHs and PAH mixtures at saturation to benthic amphipods: Linking toxic effects to chemical activity, *Aquat. Toxicol.*, 102 (2011) 142-149.
- [73] H.I. Abdel-Shafy, M.S.M. Mansour, A review on polycyclic aromatic hydrocarbons: Source, environmental impact, effect on human health and remediation, *Egypt. J. Pet.*, 25 (2016) 107-123.
- [74] Y. Ikenaka, M. Sakamoto, T. Nagata, H. Takahashi, Y. Miyabara, T. Hanazato, M. Ishizuka, T. Isobe, J.-W. Kim, K.-H. Chang, Effects of polycyclic aromatic hydrocarbons (PAHs) on an aquatic ecosystem: acute toxicity and community-level toxic impact tests of benzo[a]pyrene using lake zooplankton community, *J. Toxicol. Sci.*, 38 (2013) 131-136.
- [75] ATSDR, Case studies in environmental medicine toxicity of polycyclic aromatic hydrocarbons (PAHs), 2012, Agency for Toxic Substances and Disease Registry, <https://www.atsdr.cdc.gov/csem/pah/docs/pah.pdf>.
- [76] A. Szczeklik, J. Szczeklik, Z. Galuszka, J. Musial, E. Kolarzyk, D. Targosz, Humoral immunosuppression in men exposed to polycyclic aromatic hydrocarbons and related carcinogens in polluted environments, *Environ. Health Perspect.*, 102 (1994) 302.
- [77] X. Zhao, Effects of benzo (a) pyrene on the humoral immunity of mice exposed by single intraperitoneal injection, *Chin. J. Prev. Med.*, 24 (1990) 220-222.
- [78] USEPA, Existing water quality standards, 2010, United States Environmental Protection Agency, <https://www3.epa.gov/region1/npdes/remediation/Appendix-A.pdf>.

CHAPTER 3 Application of quantum dots for detection of pesticides – A review

This chapter presents a literature review on quantum dots and their application for detection of pesticides. The review is presented as published in Analytica Chimica Acta.

Paper

S.A. Nsibande, P.B.C. Forbes, Fluorescence detection of pesticides using quantum dot materials – A review, Analytica Chimica Acta, 945 (2016) 9-22.

DOI: <http://dx.doi.org/10.1016/j.aca.2016.10.002>



Review

Fluorescence detection of pesticides using quantum dot materials – A review



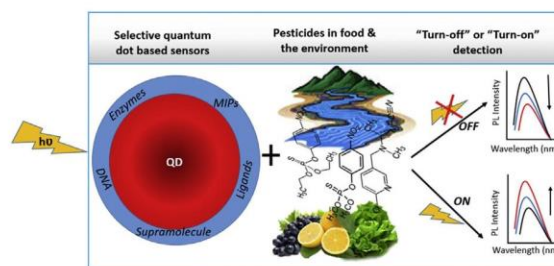
S.A. Nsibande, P.B.C. Forbes*

Department of Chemistry, Faculty of Natural and Agricultural Sciences, University of Pretoria, Lynnwood Road, Pretoria 0002, South Africa

HIGHLIGHTS

- Application of quantum dots as fluorescence probes in pesticide detection.
- Recognition elements and modification strategies towards selective pesticide detection.
- Sensitive detection below regulatory limits in various matrices.
- Challenges and possible solutions towards standardization of quantum dot based analytical methods.

GRAPHICAL ABSTRACT



ARTICLE INFO

Article history:

Received 21 June 2016
 Received in revised form
 9 September 2016
 Accepted 2 October 2016
 Available online 5 October 2016

Keywords:

Pesticides
 Quantum dots
 Sensors
 Fluorescence
 Probes

ABSTRACT

High pesticide use, especially in agriculture, can lead to environmental pollution and potentially adverse health effects. As result, pesticide residues end up in different media, including water and food products, which may serve as direct routes for human exposure. There is thus a continuous drive to develop analytical methods for screening and quantification of these compounds in the different environmental media in which they may occur. Development of quantum dot (QD) based sensors for monitoring pesticides has gained momentum in recent years. QD materials have excellent and unique optical properties and have high fluorescence quantum yields compared to other fluorophores. They have thus been used in numerous studies for the development of probes for organic pollutants. In this paper we specifically review their application as fluorescence probes for pesticide detection in different media including water and in fruits and vegetables. The low detection limits reported demonstrate the potential use of these methods as alternatives to expensive and time-consuming conventional techniques. We also highlight potential limitations that these probes may present when it comes to routine application. Finally we discuss possible future improvements to enhance the selectivity and robustness of these sensors. We note that there is still a need for researchers to develop standardized QD based sensors which could lead to their commercialization and routine application.

© 2016 Elsevier B.V. All rights reserved.

Contents

1. Introduction	10
2. QD modification strategies and their application for pesticide detection	11

* Corresponding author.

E-mail address: patricia.forbes@up.ac.za (P.B.C. Forbes).

2.1. Doped QDs for pesticide detection	11
2.2. Silica nanoparticles -modified QDs	11
2.3. QD modification with macrocyclic/supramolecular host molecules	12
2.4. QD modification with molecularly imprinted polymers (MIPs)	14
2.5. Enzyme-modified QDs (biosensors) for pesticide detection	14
2.6. Carbon quantum dots for pesticide detection	17
2.7. QD films in pesticide sensing	18
3. Concluding comments and future outlook	19
4. Future prospects	19
Acknowledgements	19
References	19

1. Introduction

Pesticides are widely used in agriculture for controlling weeds and pests so as to improve food production to meet the demands of an ever increasing population. High pesticide use however, can lead to contamination of non-target environments through runoff, leaching and spray drift [1] thereby causing negative effects on other organisms. For example, human exposure to these compounds has been linked to negative health effects like neurotoxicity, endocrine disruption, genotoxicity, mutagenicity and carcinogenesis [2].

Governments have promulgated a number of laws for regulating pesticide use and have implemented maximum tolerance residue levels in water and agricultural products [3–5]. These media can serve as direct dietary exposure routes for humans, and prolonged exposure via these routes may lead to adverse health effects – even though the pesticides might be present at low concentrations. Due to high food production demand, pesticide use is almost inevitable and despite the implemented regulations, different studies have reported the occurrence of pesticide residues in a number of agricultural products, and in some instances recommended limits have been exceeded [6,7]. For example, a study by the European Food Safety Authority [7] sampled over 80 000 different agricultural products from different countries. They found that products coming from Third World countries had a higher exceedance rate (5.7%) of the recommended limits than those from European Union countries (1.4%). While most of the samples were found to be within recommended limits, continuous exposure to these residues can pose serious public health risks. Moreover, some pesticides are widely used in agriculture yet they have no regulatory limits and new types of pesticides, whose toxic effects may be less understood, are being continuously introduced into the market. Examples of pesticide concentrations which have been found in water and food samples in various countries are provided in Table 1.

Therefore, in order for control measures to be enforced, highly sensitive, selective, and affordable analytical methods are required to monitor these compounds. Conventional analytical methods can be tedious in that they require careful sample preparation steps such as extraction, clean-up, enrichment and sometimes derivatisation in order to achieve the required sensitivity. In recent years, fluorescence sensing using quantum dot (QD) materials has been presented by different authors as a possible alternative to these conventional methods.

Quantum dots (QDs) are semiconductor crystalline nanomaterials that have unique electronic and optical properties due to quantum confinement effects [8]. They have a number of attractive properties that make them suitable as analytical sensors. Through surface modification strategies they have found various applications across disciplines. Reviews have been published on their application in solar cells [9], as biological labels [10], in

microelectronics [11] and in electrochemistry [12]. Crystalline QD nanoparticles can be prepared from group II–VI or III–V elements of the periodic table using different approaches that have been comprehensively discussed in previous reviews [8,13,14]. A different class of QDs made from carbon materials has recently emerged and is finding application in analytical sensing [15–20].

QD cores are often synthesized from heavy metals, specifically cadmium, which can potentially have toxic effects on the environment and humans. Studies have thus been done to investigate the toxicity of various QDs in different living systems like cell cultures and mice [21]. It has been shown that passivating the core with nontoxic shell layers greatly reduces leakage of cadmium, thereby reducing potential toxic effects. For example, a study by Kuzyniak et al. [22] spiked living cells with increasing concentrations of CdSe QDs and the release of cytoplasmic enzyme (LDH) was used as a measure of toxicity. Their study showed that capping the QDs with the ligand glutathione (GSH), and encapsulating with a nontoxic ZnS shell to form GSH-CdSe/ZnS nanoparticles, greatly reduced the toxicity of QDs to the living cells. This therefore has opened doors for their wide application, including the detection of pesticides.

Sensing with QDs is based on the sensitivity of their luminescence to the surface state of the nanoparticles. Thus sensing can result from interaction (chemical or physical) with the target analyte which can lead to either photoluminescence enhancement or quenching [23]. The basis of most QD sensing assemblies however, is not direct interaction with the QD surface, but rather energy flow between the QD fluorophore and analyte molecules. Förster Resonance Energy Transfer (FRET) occurs when energy absorbed by a donor (usually the QDs) is transferred to a nearby acceptor species via dipole-dipole interactions. The efficiency of this non-radiative energy transfer depends on (i) the distance between the FRET pair (donor and acceptor), (ii) special arrangement or orientations of the pair, (iii) the spectral overlap of the donor emission and acceptor absorption, and finally (iv) the fluorescence lifetime of the donor should be long enough for FRET to occur [24–26]. Evidence of FRET is seen when there is a decrease in the fluorescence and excited state lifetime of the donor while the fluorescence of the acceptor increases. Therefore QDs are suitable as sensors through the FRET mechanism because of their broad absorption spectra, high quantum yields and long fluorescence lifetimes.

Studies have shown that QD sensors can detect pesticides at concentrations far below some of the regulatory limits or guidelines, as shown in Table 1. A number of reviews have been published on sensors based on QDs and another functional nanomaterials for detecting various analytes [19,27–36], but none of these focus primarily on pesticide detection. In this paper, we seek to update the reader on current applications of QD sensors utilising fluorescence for pesticide detection in different food and water matrices. QD based electrochemical sensors are therefore outside the scope

Table 1

Comparison of selected QD based pesticide sensor limits of detection (LOD) with regulatory guideline limit values and typical concentrations found in samples (nd = not detected).

Pesticide	Matrix	Occurrence			Guideline limit		Sensing with QDs	
		Country	Concentration range ($\mu\text{g L}^{-1}$)	Study	$\mu\text{g L}^{-1}$	(mol L^{-1})	Reported LOD (mol L^{-1}) ^c	Study
Paraquat	Water	Thailand	1.5–87.0	[37]	10 ^a	38.89×10^{-9}	6.39×10^{-9}	[38]
							11.7×10^{-12}	[39]
							2×10^{-8}	[40]
Parathion	Water	India	0–2.12	[41]	50 ^a	0.172×10^{-6}	4.82×10^{-12}	[42]
							4.47×10^{-12}	[43]
							32.5×10^{-9}	[44]
							2.47×10^{-12}	[45]
							34.3×10^{-9}	[46]
Pentachlorophenol	Water	China	nd–103.70	[47]	60 ^a	0.225×10^{-6}	86×10^{-9}	[48]
							11.3×10^{-12}	[49]
Carbaryl	Water	Bangladesh	nd–0.163	[50]	90 ^a	0.447×10^{-6}	12.4×10^{-9}	[51]
Chlorpyrifos	Water	Bangladesh	nd–1.189	[50]	90 ^a	0.257×10^{-6}	17×10^{-9}	[52]
Diazinon	Water	USA	nd–0.09	[53]	20 ^a	65.7×10^{-9}	0.164×10^{-6}	[54]
Glyphosate	Water	Mexico	nd–36.7	[55]	280 ^a	1.66×10^{-6}	0.0725×10^{-9}	[56]
Carbaryl	Apples	China	0–10 $\mu\text{g g}^{-1}$	[57]	15000 ^b	74.5×10^{-3}	26.8×10^{-12}	[58]
Paraquat	Rice				50 ^b	0.198×10^{-6}	6.39×10^{-9}	[38]
Parathion-methyl	Rice				1000 ^b	3.8×10^{-6}	61.8×10^{-9}	[59]

Notes:

^a Guidelines for Canadian Drinking Water Quality [60].

^b Tolerances and exemptions for pesticide chemical residues in food in the USA [61].

^c Values that were not reported in mol L^{-1} were converted for comparison.

of this paper, but readers are referred to reviews on this topic by Dhull et al. [33] and Periasamy et al. [29] for further information. The different strategies to tailor QDs for selective detection will be discussed, as will the analytical merits and limitations of the respective sensors.

2. QD modification strategies and their application for pesticide detection

QDs are typically synthesized from organometallic precursors where the QD particle is normally protected by a capping layer of organic ligands like trioctylphosphine (TOP) or trioctylphosphine oxide (TOPO). The functional groups in these ligands allow modifications to be done in tailoring the QD for a desired application via surface chemistry, which enables the coupling of QDs to various receptors to offer selectivity towards target analytes [36,62]. Such receptors include enzymes, antibodies, nucleic acids, supramolecules, and molecularly imprinted polymers (MIPs).

In some cases the surface ligands on the QDs have been used as recognition sites for target analytes. For example Walia and Acharya [63] used glutathione coated CdS (GSH-CdS) QDs for selective detection of dicofol, a multicide related to dichlorodiphenyltrichloroethane (DDT) used for killing mites. They found the sensor to be selective towards dicofol in the presence of other pesticides (namely dimethoate, chlorpyrifos, and imidacloprid). The chloride groups in the structure of dicofol were shown to interact with the $-\text{NH}_2$ and $-\text{COOH}$ groups of glutathione ligand, leading to an increase in fluorescence of the GSH-CdS QDs to allow “turn-on” detection. Their probe was able to detect dicofol down to 55 ± 11 ppb. The drawbacks of such a sensor include potential interferences by metal ions [64,65], poor selectivity due to the reactivity of $-\text{NH}_2$ and $-\text{COOH}$ groups, low quantum yields [66], and potential toxic effects from the unprotected cadmium core.

In the following sections we review the different strategies that have been used to modify QDs for detection of different pesticides including the advantages and limitations thereof. Tables 2–4 present summaries of these studies and the detection limits that were achieved.

2.1. Doped QDs for pesticide detection

Doping involves incorporating atoms (usually transition metals like manganese, Mn^{2+}) into the lattice structure of a material to avail the desired properties. Doped quantum dots retain almost all of the properties of the un-doped QDs, and may have added advantages of longer emission lifetimes and lower cytotoxicity [67]. For example a study by Cao et al. [68] showed that the Mn^{2+} doped CuInS/ZnS QDs had extremely long radiative excited-state lifetimes (3.78 ms) compared to those which were not doped (401 ns). Similarly, Subha et al. [69] reported 0.35 ms lifetimes for Mn^{2+} doped ZnS QDs which was 4–5 orders higher than other semiconductor QDs.

A lot of studies have used ZnS: Mn^{2+} QDs to design fluorescence sensors for pesticides including pentachlorophenol [48,70], cyphenothrin [71] and acetamiprid [72]. The doped QDs may also be coupled to a recognition element like aptamers [72], enzymes [73] or molecularly imprinted polymers [48,52,54,71,74] in order to achieve selectivity towards target pesticides (discussed in sections to follow).

2.2. Silica nanoparticles -modified QDs

Functional materials based on QDs incorporated into silica (QD-Si) nanoparticles have been used to design fluorescence sensors used to detect different pesticides such as λ -cyhalothrin, methomyl, glyphosate and parathion-methyl in water by different research groups [56,75–77]. The preparation of QD-Si nanoparticles can be achieved via various strategies, where reverse microemulsion is the most commonly used approach [78–81]. Preparation of spheres doped with QDs can be achieved directly through co-condensation of the silica precursors [82] and, depending on use, the surface of the sphere can be decorated with suitable ligands or receptor molecules.

The advantage of encapsulating QDs into silica spheres is that it improves their chemical stability thereby reducing leaching and potential toxicity of the QDs. It also has been found to reduce photobleaching without affecting the photophysical properties of

Table 2

Quantum dots with molecular recognition elements as receptors for pesticide detection. Where possible reported LOD and linear range values were converted to Molar units for comparison purposes.

Quantum dot	Recognition element	Detection technique	Analyte(s)	LOD	Linear range	Matrix	Ref.
CdTe/CdS		Laser Induced Fluorescence	Mevinphos Methidathion Diazinon Phosalone	0.16 mg kg ⁻¹ 0.05 mg kg ⁻¹ 0.18 mg kg ⁻¹ 0.12 mg kg ⁻¹	0.2–28.0 mg kg ⁻¹ 0.1–20.0 mg kg ⁻¹ 0.3–18.0 mg kg ⁻¹ 0.2–30.0 mg kg ⁻¹	Tomatoes	[90]
C [4]/SiO ₂ /CdTe	Calix [4]arene	Fluorescence	Methomyl	80 nM	0.1–50 μM	Water	[76]
C [6]/SiO ₂ /CdTe	Calix [6]arene	Fluorescence	Glyphosate	0.0725 nM	1.0–25.0 nM	Water	[56]
TGA-CdTe	<i>p</i> -sulfonatocalix [4] arene	Luminescence	Fenamithion Acetamiprid	12 nM 34 nM	0–10 ⁻⁴ M 0–10 ⁻³ M	Garlic samples, Aqueous solution	[88]
ZnCdSe films	–	Fluorescence	Carbaryl	<12.4 nM	12.4–12,400 nM	Water	[51]
Graphene-CdS	–	Electrochemiluminescence	Pentachlorophenol	0.0113 nM	37 pM–1.9 μM	Tap water, River water	[49]
GSH-CdS	–	Fluorescence	Dicofol	55 ± 11 ppb	3.32–62.5 μM	Methanol	[63]
RF-CdTe@SiO ₂ -AuNPs	Trypsin/protamine	Fluorescence	Parathion-methyl	0.0684 nM	0.15–1500 nM	Tap water, milk, rice	[77]
MPA-CdTe	–	Fluorescence	Chlorpyrifos	0.1 nM	0.1–10,000 nM	Apples	[91]
TGA-CdTe/CS-AuNPs	–	Fluorescence	Glyphosate	9.8 ng kg ⁻¹	0.02–2.0 μg kg ⁻¹	Apples	[25]
CdTe/CdS	–	Fluorescence	Paraquat	6.39 nM	9.90–1500 nM	Rice, Wheat flour, Lettuce leaves, Waste water	[38]
(3-MPA)-CdSe/ZnS	–	Fluorescence	Paraquat	0.0117 nM	0.039–19 nM	Water	[39]
Double QDs (ZnCdSe and CdSe)	–	Fluorescence	Paraquat Dursban Dipterex Methyl thiophanate Cartap	20 nM	2 × 10 ⁻⁸ –5 μM 5 × 10 ⁻⁸ –3 μM 2 × 10 ⁻⁸ –5 μM 5 × 10 ⁻⁸ –5 μM 5 × 10 ⁻⁸ –5 μM	Waste water, Tea	[40]
CDs/AgNPs	–	Fluorescence	Glyphosate	12 ng mL ⁻¹	0.025–25 μg mL ⁻¹	Rice, millet, wheat flour, and maize flour	[92]

Abbreviations: GSH – Glutathione; RF – Ratiometric fluorescent; TGA – Thioglycolic acid; CDs – carbon dots.

Table 3

Summary of studies employing quantum dots with MIPs for fluorescence detection of pesticides in different media. Reported LOD and linear range values have been converted to Molar units for comparison purposes.

Quantum dot	Recognition element	Detection technique	Analyte(s)	LOD (×10 ⁻⁹ M)	Linear range (×10 ⁻⁹ M)	Matrix	Ref.
ZnS:Mn ²⁺	MIP	Fluorescence	Pentachlorophenol	86	200–3900	River water	[48]
ZnS:Mn ²⁺	MIP	Fluorescence	Diazinon	164	164–2000	Tap water	[54]
CdSe@SiO ₂ @MIP	MIP	Fluorescence	λ-cyhalothrin	80.03	100–1,000,000	Water	[75]
CdTe–SiO ₂ -MIPs	MIP	Fluorescence	Deltamethrin	31 700	1000–69,000	Fruit and vegetable samples	[86]
ZnS:Mn ²⁺	MIP	Fluorescence	Nicosulfuron	1.1	12–6000	Water	[74]
ZnS:Mn ²⁺	MIP	Fluorescence	Cyphenothrin	9.0	100–80,000	Water	[71]
ZnS:Mn ²⁺	MIP	Fluorescence	Chlorpyrifos	17	300–60,000	Water	[52]
Magnetic Silica Beads/Graphene QDs/MIP (mSGP)	MIP	Fluorescence	Tributyltin	146.7	0–48,000	Seawater	[63]
CdSe/ZnS	MIP	Fluorescence	Carbaryl	147	497–398,000	Rice, Chinese cabbage	[28]
Carbon dots	MIP	Fluorescence	Dimethoate	0.0183	0.6–34	Chinese cabbage, Broccoli, Cucumber	[95]
OVDAC/CdTe	MIP	Fluorescence	λ-cyhalothrin	30	100–16 000		[94]
CdTe	MIP	Fluorescence	Parathion	218	50–1,000,000	Water	[93]
ZnS:Mn ²⁺	MIP-Fe ₃ O ₄	Fluorescence	Pentachlorophenol	500	0–30,000	Water	[70]

Abbreviations: OVDAC - Octadecyl-4-vinylbenzyl-dimethyl-ammonium chloride.

the QDs [83,84]. The abundance of silicon on earth makes these materials affordable and thus potentially useful for preparing low-cost sensing devices. Another advantage of using silica nanoparticles is that they are chemically inert and optically transparent, making them suitable for fluorescence sensing applications in various chemical media [85]. Furthermore, the silica materials are amenable to surface modifications and this makes it possible to functionalize them with receptors like calix[n]arenes [56,76], molecularly imprinted polymers [75,86], or with graphene sheets [87] to offer selectivity towards the target pesticide analyte. Such modified QDs and their applications are discussed the following sections.

2.3. QD modification with macrocyclic/supramolecular host molecules

Guest-host interactions by means of macrocyclic molecules that have suitable cavities can also be used in conjunction with QDs as recognition elements for pesticide detection. Calix[n]arene supramolecules for example, have hydrophobic cavities which can be used as receptors for different target pesticides. It is possible to achieve some selectivity by tuning and or selecting the appropriate size of the calix[n]arene. As such they have been used to functionalize the surface of QDs in different studies to develop probes for pesticide detection. Li and Qu [76] fabricated silica spheres

Table 4

Biosensors using quantum dots as recognition elements for fluorescence detection of pesticides in different media. Where possible the reported LOD and linear range values were converted to Molar units for comparison purposes.

Quantum dot	Recognition element	Detection technique	Analyte(s)	LOD	Linear range	Matrix	Ref.
CdTe	AChE/ChOx	Fluorescence	Paraoxon Dichlorvos Parathion	0.00275 nM 0.00209 pM 4.82 pM	1 pM–1 μM	Apples	[42]
CdTe	AChE	Fluorescence	Paraoxon Parathion	10.5 pM 4.47 pM	1 pM–1 μM	Apples, Tap water, Beans	[43]
ZnSe:Mn ²⁺	ChOx-AChE-ACh	Fluorescence	Paraoxon	13.1 pM	48.4 pM–4.84 μM	Tap water, milk	[73]
CdS	AChE	Fluorescence	Paraoxon	80 pM	–	Human serum	[114]
MPA-CdTe	AChE and ChOx	Fluorescence	Paraoxon Parathion	4.30 pM 2.47 pM	10 pM–1.0 μM	Apples	[45]
CdTe (QDs/PDDA) ₃ (AChE/PDDA) ₃	AChE	Fluorescence	Paraoxon Parathion	10 μg L ⁻¹	5–100 μg L ⁻¹	Water, Apples	[46]
CdSe/ZnS and CdSe/ZnSe	AChE and ATCh	Photoluminescence	Parathion-methyl Acetamidrid	190 nM 11,200 nM	–	–	[115]
AChE -CdTe, AChE -CdSe/ZnS	AChE	Photoluminescence	Parathion-methyl Acetamidrid	1 ppb	0.05–10 ppb	–	[116]
AChE -CdSe/ZnSe/ZnS	AChE	Fluorescence	Paraoxon	2 nM	–	–	[100]
AChE-Graphene-ZnSe QDs	AChE and ACTh	Fluorescence	Parathion-methyl	190 nM	190–3800 nM	Water	[117]
MPA-CdSe/ZnSe/ZnS	AChE and ChOx	Fluorescence	Dichlorvos	4.49 nM	Two segment: 4.49–896 nM 2240–6780 nM	Apples	[118]
CdTe/CdS	AChE and ChOx	Fluorescence	Dichlorvos	4.49 nM	Two segment: 4.49–896 nM 2240–6780 nM	Apples	[118]
MPA-CdTe	AChE and ChOx	Fluorescence	Dichlorvos	4.49 nM	Two segment: 4.49–896 nM 2240–6780 nM	Apples	[118]
SiQDs-AChE-ChOx	AChE and ChOx	Photoluminescence	Carbaryl Parathion Diazinon Phorate	$7.25 \times 10^{-9} \text{ g L}^{-1}$ $3.25 \times 10^{-8} \text{ g L}^{-1}$ $6.76 \times 10^{-8} \text{ g L}^{-1}$ $1.9 \times 10^{-7} \text{ g L}^{-1}$	7.49 ng L ⁻¹ –0.749 mg L ⁻¹	Apples, Tomatoes, Cucumbers	[44]
CQDs	AChE and ChOx	Photoluminescence	Carbaryl	0.0268 nM	0.0313–31.3 nM	Apples	[58]
Q-QDs	AChE	Fluorescence	Dichlorvos	0.019 nM	0.050–100 nM	Fruit juice	[119]
TGA-CdTe	AChE	Fluorescence	Monocrotophos	32.0 nM	89.5–6090 nM	Aqueous solutions	[106]
TGA-CdSe/chitosan films	OPH	Photoluminescence	Paraoxon	1000 nM	–	–	[103]
CdSe/ZnS	OPH	Photoluminescence	Paraoxon	10 nM	Non-linear	Water	[104]
MPA-CdTe-CTAB	OPH	Fluorescence	Parathion-methyl	61.8 nM	95–11,000 nM	Tap water, rice	[59]
MPA-CuInS ₂	OPH	Fluorescence	Parathion-methyl	60 nM	100–38 000 nM	Tap water, River water, Rice, Bananas	[105]
MPA-CdTe/IgG	anti-2,4-D antibody (IgG) ELISA	Fluoroimmunoassay	2,4-dichlorophenoxy acetic acid	1.13 nM	1130–4520 nM	–	[120]
QDs 530 goat anti-mouse IgG conjugate (QDs-Ab ₂)	cFLISA ELISA	Fluorescence	Chlorpyrifos	24 nM 46 nM	43–586 nM	Drinking water	[121]
ZnS:Mn ²⁺	DNA aptamer	Fluorescence	Acetamidrid	0.7 nM	0–15 nM	Water, Cabbage leaves	[72]
CdTe-AuNPs	DNA aptamer	Fluorescence	Acetamidrid	7.29 nM	50–1000 nM	Lettuce, Pakchoi, Cauliflower, Pampfrey, Chinese cabbage, Celery	[98]
IgG-CDs	IgG	Fluorescence	Glyphosate	8 ng mL ⁻¹	0.01–80 μg mL ⁻¹	River water, soil samples	[122]
CDs-AgNPs	AChE	Fluorometric Colorimetric	Carbaryl	0.006 μg L ⁻¹ 0.007 μg L ⁻¹	1×10^{-8} – $1 \times 10^{-4} \text{ g L}^{-1}$	Tap water, apple juice	[123]
MEA-CdTe/ATP	ACP	Fluorescence	Parathion-methyl	2.2 ng mL ⁻¹	0.001–5.0 g mL ⁻¹	Water	[124]
C-dots/ZrO ₂ - GCE		Electrochemical (CV)	Methyl parathion	0.056 ng mL ⁻¹	0.2 ng mL ⁻¹ to 48 ng mL ⁻¹	Rice	[125]

Abbreviations: ATP – adenosine triphosphate, ACP – acid phosphate; MEA – cysteamine; cFLISA – competitive fluorescence-linked immunosorbent assay; CQDs – Carbon quantum dots; CTAB – Cetyltrimethylammonium bromide; ELISA – Enzyme-linked immunosorbent assay; IgG – glyphosate antibody; MPA – Mercaptopropionic acid; Q-QDs – Quaternized carbon dots; TGA – Thioglycolic acid; PDDA – poly(dimethyldiallyl ammonium chloride).

which were embedded with CdTe QDs in their core and were coated with calix [4]arene on the surface for pesticide detection. The probe showed fluorescence enhancement with increase in methomyl concentration and allowed for its detection down to 80 nM. Their probe also showed good selectivity in the presence of other pesticides, namely parathion-methyl, fenamithion, optunal, and acetamidrid.

Qu et al. [88] functionalized the surface of CdTe QDs with *p*-sulfonatocalix [4]arene to produce a fluorescent sensor for the detection of fenamithion and acetamidrid down to 12 nM and 34 nM, respectively. They found that the *p*-sulfonatocalix [4]arene offered selectivity towards acetamidrid compared to other pesticides (parathion-methyl, methomyl, fenamithion, and optunal).

Li et al. [56] used calix [6]arene to develop a fluorescence sensor for detection of the pesticide glyphosate. Here CdTe QDs embedded in silica spheres which were then functionalized with calix [6]arene were employed (Fig. 1). The probe was selective for glyphosate in the presence of other pesticides (chlorpyrifos, cyromazine, carbaryl, imidacloprid, methiocarb) and allowed for its detection down to 0.0725 nM which they found to be lower than conventional HPLC and MS techniques at that time.

Although this strategy shows promising results, the binding affinity of supramolecular host molecules can be affected by a range of factors including the binding mechanism, the medium pH, stereoelectronic effects and allosteric effects [89]. Thus a probe based on such receptors could suffer serious limitations in terms of

repeatability, making it difficult to design standard methods based on this technology.

2.4. QD modification with molecularly imprinted polymers (MIPs)

Quantum dot sensors can be modified with molecularly imprinted polymers (MIPs) as receptor or recognition elements towards target analytes. A molecularly imprinted polymer (MIP) is prepared through co-polymerization of monomers of a desired template molecule after which they are extracted to leave cavities in the polymer. Such a material is then used as an artificial receptor for that particular molecule. These materials are cheap, have high mechanical and chemical stability and can be reusable. They have found application in a number of QD based fluorescence sensors where they offer selectivity for different target pesticide analytes [48,54,63,70,71,74,75,86,93–96]. Table 3 includes a summary of pesticides that have been studied with MIP QD fluorescence based sensors.

By encoring a suitably tailored MIP on the QD surface it is possible to achieve selectivity for different target pesticides even when using the same QD materials as signal transducers. For example, recent studies by Ren and Chen [71] used MIP-coated manganese-doped ZnS QDs for selective detection of the pesticide cyphenothrin (Fig. 2). The selectivity towards cyphenothrin was attributed to the size, shape, and functionality of the template and it allowed for detection down to 9.0 nM in water. With the same QD and by simply changing the template for the MIP, other sensors were prepared for detecting the herbicide nicosulfuron in

water down to 1.1 nM [74] and the insecticide chlorpyrifos in water with limits of detection down to 17 nM [52].

MIPs can also be used as a functional coating around silica-embedded QDs in pesticide sensing. Li et al. [75] prepared CdSe QDs embedded in silica spheres which they modified with a MIP for selective trace detection of λ -cyhalothrin in water (Fig. 3). Energy transduction between the CdSe@SiO₂@MIP particles and the pesticide quenched the luminescence intensity of the chemophores linearly as described by the Stern-Volmer type equation:

$$I_{\max}/I = 1 + K_{SV}[S]$$

Where I is fluorescence intensity of CdSe@SiO₂@MIP at a given pesticide concentration and I_{\max} is the intensity in a pesticide-free solution. K_{SV} is the Stern-Volmer quenching constant and $[S]$ is the pesticide concentration. Thus the authors showed the probe could selectively detect λ -cyhalothrin down to 80.03 nM.

Ge et al. [86] modified CdTe-doped silica spheres with MIPs to form CdTe-SiO₂-MIP composites for selective detection of deltamethrin in fruit and vegetable matrices. Just like with the probe by Li et al., the fluorescence intensity of the probe was quenched with increasing deltamethrin concentration, allowing for detection down to 0.16 $\mu\text{g mL}^{-1}$.

Wei et al. [94] functionalized CdTe QDs with the polymerizable surfactant octadecyl-4-vinylbenzyl-dimethyl-ammonium chloride (OVDAC). They used the OVDAC-CdTe QDs to prepare a MIP-OVDAC-CdTe composite sensor for detection of λ -cyhalothrin, an insecticide which potentially has endocrine disrupting effects in humans. The vinyl ends of this surfactant directed the polymerization selectively to the surface of the CdTe QDs. This sensor could detect λ -cyhalothrin down to a concentration of 0.03 μM . Furthermore, they found the FL intensity of the probe was not affected by the presence of certain cations and anions (K^+ , Na^+ , Ca^{2+} , Mg^{2+} , NO_3^- and CO_3^{2-}) and was selective towards λ -cyhalothrin in the presence of analogue pyrethroids (β -cyfluthrin, fevalerate and bifenthrin). When applied to spiked real water samples, the authors reported recoveries ranging from 97.25% to 105.5% due to the sensitivity and selectivity of the MIP-OVDAC-CdTe sensor.

Studies by Wang et al. [48] and Yang et al. [70] have both used ZnS:M²⁺ QDs which were imprinted with an MIP for detection of pentachlorophenol, an organochloride pesticide that is industrially used as a wood preservative. Yang et al. [70] further modified MIP polymers by incorporating Fe₃O₄ nanoparticles to provide the MIP matrix with superparamagnetic properties to make the separation of the particles (including pentachlorophenol) easy when an external magnetic field was applied. This sensor could detect pentachlorophenol down to 0.5 μM , whilst 86 nM was the limit of detection reported by Wang et al. [48] where the polymer had no Fe₃O₄ nanoparticles. The Fe₃O₄ nanoparticles loaded MIP matrix could selectively adsorb pentachlorophenol in the presence of other aromatic compounds (2,4-dichlorophenoxy acetic acid, 2,4-dichlorophenol and phenol) and when applied to spiked real water samples high recoveries > 97% were obtained [67].

Although MIP based sensors have been successfully employed, there are still some challenges in preparation of the MIP probes, where the main challenge is extraction of template molecules from the polymers. This is often a tedious process, requiring a lot of solvents and may lead to distortion of some of the cavities. Overcoming this challenge is crucial in order to develop standardized probes and to pave the way for their commercialization.

2.5. Enzyme-modified QDs (biosensors) for pesticide detection

A biosensor can be described as a probe that consists of a signal transducer (e.g. QDs or a fluorophore) linked to a biological

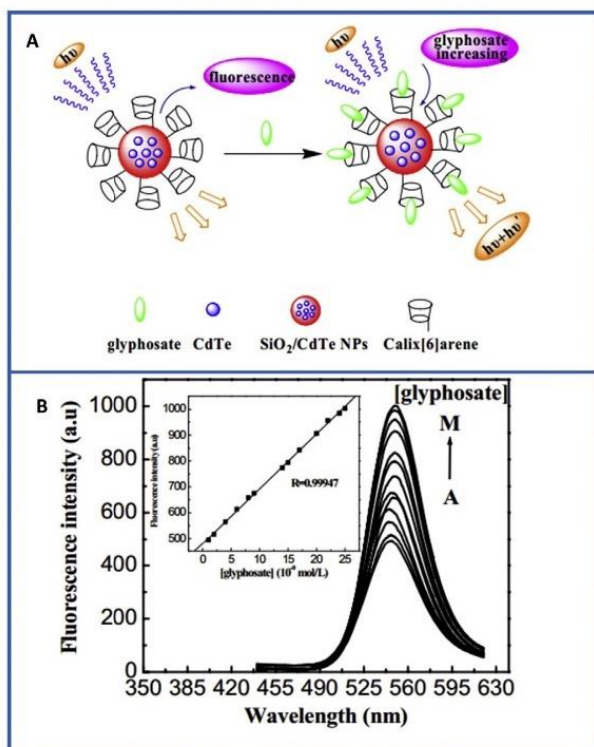


Fig. 1. (A) Fluorescence sensor for ultra-sensitive detection of glyphosate. (B) Response of the sensor to increasing glyphosate concentration (reprinted from Ref. [56] with permission from Scientific Report Publishing).

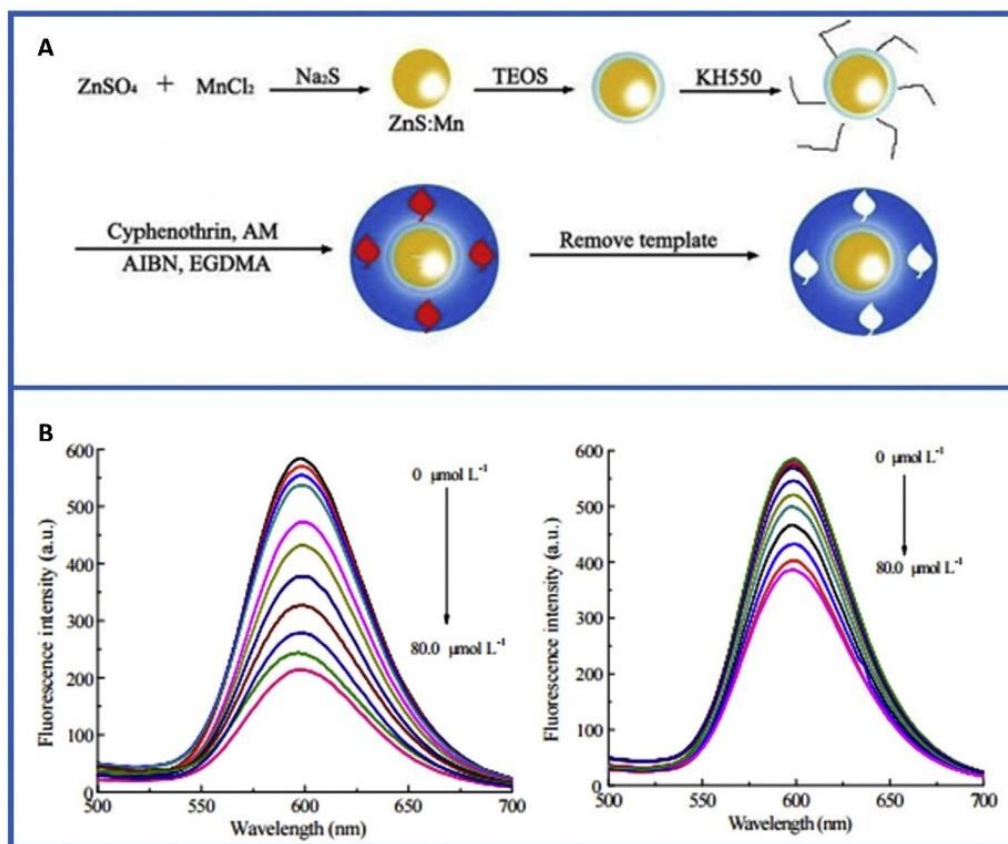


Fig. 2. (A) Preparation of MIP-coated ZnS:Mn QDs for detection of cyphenothrin (TEOS: Tetraethoxysilane, KH550: silane coupling agent, AM: functional monomer, EGDMA: cross-linking agent). (B) (left) Fluorescence intensity of the probe decreased with increasing cyphenothrin concentration, (right) fluorescence of NIP-coated QDs with increasing cyphenothrin concentration (reprinted from Ref. [71]). Copyright (2016) with permission from Elsevier.

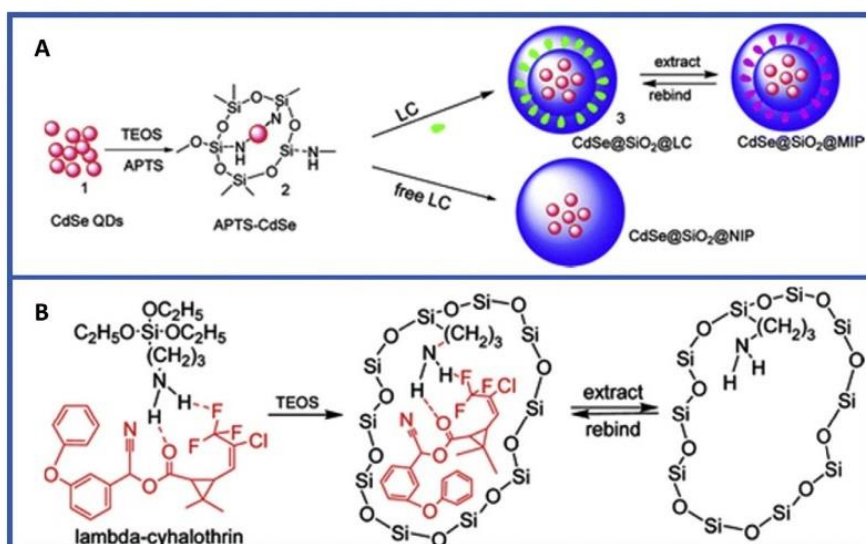


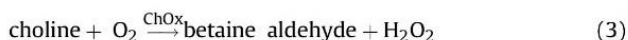
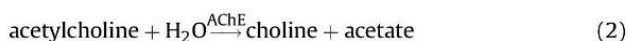
Fig. 3. (A) Schematic illustration showing the molecular imprinting process for λ -cyhalothrin (LC) imprinted silica nanospheres embedded CdSe quantum dots (APTS: 3-Aminopropyltriethoxy-silane, TEOS: tetraethoxysilane). (B) Schematic illustration for the molecular imprinting mechanism of LC in a silica matrix through the hydrogen bond reaction (reprinted with permission from Ref. [75]). Copyright (2016) American Chemical Society.

recognition element, which could be an enzyme, cell, antibody, or DNA [32,97]. For instance, DNA aptamers that selectively bind to acetamiprid have been recently used for detection of this insecticide with QDs as signal reporters [72,98]. However screening and selecting the appropriate aptamer for the target pesticide can be challenging which may limit their application as recognition elements.

QD-enzyme biosensors have been widely explored for pesticide detection, particularly for organophosphorus pesticides (OPs). Enzymes are particularly attractive as recognition elements in QD biosensors because of their specificity towards target pesticides.

One commonly used enzyme for these probes is acetylcholinesterase (AChE) – an enzyme found in nervous systems. Reviews on the use of AChE as a recognition element in different pesticide detection techniques using various types of nanomaterials have been published [29–31,33,99]. Here we focus on techniques where QDs are used as transducers for fluorescence detection.

AChE hydrolyses the neurotransmitters, acetylthiocholine and acetylcholine to thiocholine and acetylcholine respectively (Equations (1)–(2)). If the sensor is coupled with the choline oxidase (ChOx) enzyme, then choline can be oxidized to generate hydrogen peroxide (H_2O_2) (Equation (3)) which can quench the fluorescence intensity of QDs [44].



Trace amounts of OPs and carbamate type pesticides can inhibit the activity of the ChOx enzyme (the mechanism which leads to the paralysis and death of insects) leading to an increase in PL intensity of the conjugated QDs. The ability of the enzyme to recognize pesticide molecules has allowed for the development of QD based sensors for these target analytes. Like other previously discussed sensors, enzyme-based sensors can also be conjugated with other support platforms like graphene [100,101] and multi-walled carbon nanotubes [72,102] to improve their sensitivity. Typical pesticide target analytes of QD/AChE biosensors are shown in Fig. 4. The

structurally similar pesticides parathion-methyl, paraxon, and parathion have been extensively and successfully targeted using this type of sensor possibly due to similar interactions that they have with the enzyme.

A study by Yi et al. [44] for example, used silicon quantum dots (SiQDs), AChE and ChOx to fabricate a biosensor for detecting pesticides (carbaryl, parathion, diazinon, phorate) in food samples (Fig. 5). They found the inhibiting effect of these pesticides on the enzyme to be linearly proportional to the logarithm of the pesticide concentration. The accuracy of the probe was comparable to traditional HPLC methods with the added advantage of being highly sensitive, simple and rapid.

Another enzyme used in conjunction with QDs for pesticide detection is organophosphorus hydrolase (OPH) which hydrolyses a variety of OPs to produce harmless products like *p*-nitrophenol and diethyl phosphate. Depending on the type of QD, both these products can interact with the QDs causing either an increase or decrease in their fluorescence intensity thereby allowing for detection. This enzyme has been used in QD sensors for detection of the pesticides paraxon [103,104] and parathion-methyl [59,105] in matrices like river water.

Yan et al. [59] used CdTe QDs in cetyltrimethylammonium bromide (CTAB) and OPH to make a biosensor for parathion-methyl detection. Presence of the pesticide results in the quenching of the PL intensity of the QDs because *p*-nitrophenol (product of hydrolysis by OPH) is electron deficient and is therefore adsorbed on the alkyl chains of CTAB through hydrophobic interactions, thereby quenching the PL intensity of the QDs. This quenching effect was proportional to the parathion-methyl concentration in the 25–3000 ng mL⁻¹ range and allowed for detection down to 18 ng mL⁻¹ in tap water.

In a different study Yan et al. [105] made a biosensor consisting of CuInS₂ QDs, lead ions (Pb²⁺) and the OPH enzyme which was also used for detecting parathion-methyl. The fluorescence intensity of the probe was quenched by Pb²⁺ ions. Instead of *p*-nitrophenol, this probe made use of the other OPA hydrolysis product, dimethylthiophosphoric acid, which bonded to Pb²⁺ ions resulting in an increase in PL intensity with pesticide concentration (Fig. 6).

Despite the high sensitivity and selectivity of biosensors, they still have some serious limitations that can hinder their use and large scale production. Firstly, the biological recognition

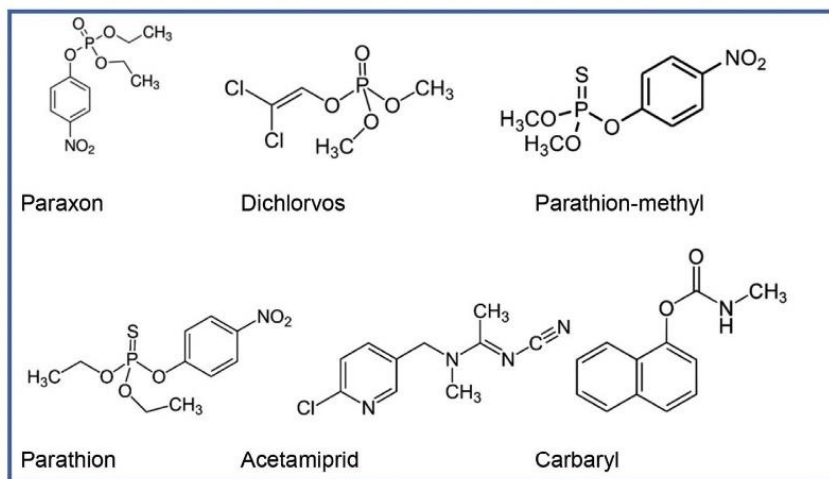


Fig. 4. Chemical structures of pesticides commonly targeted using QD-AChE based fluorescence biosensors.

elements in these sensors (enzymes, nucleic acids, etc.) have poor stability which is dependent on temperature and pH conditions. Secondly, the production, isolation and purification of these elements can be tedious, time-consuming, and costly. Thirdly, the inhibition of enzyme based sensors by pesticides is hardly reversible, and this presents a challenge when one wants to design reusable sensing devices. The one study by Sun et al. [106] which claims a reusable AChE enzyme biosensor by using oxime compounds showed that only 83% of the sensors' original activity could be regenerated. The reduction in activity after attempting to regenerate the sensor could affect sensitivity and reproducibility in subsequent applications.

2.6. Carbon quantum dots for pesticide detection

Carbon quantum dots are a class of fluorescent nanoparticles

that include graphene quantum dots (GQDs), polymer dots, and carbon nanodots and have found a number of applications in fluorescence sensing [16,17,107–109]. These types of QDs offer unique fluorescence properties and have the advantage of low toxicity and excellent biocompatibility compared to semiconductor QDs [110]. Carbon quantum dots are an emerging alternative to semi-conductor sensors and some authors have used them in designing pesticide probes. Nan et al. [100] used graphene quantum dots (GQDs) in conjunction with the AChE enzyme for sensitive detection of paraxon, a highly toxic organophosphate pesticide, down to 0.2 nM. Liu et al. [49] used GQDs linked to CdS QDs to form GQDs-CdS nanocrystals for detection of pentachlorophenol, an organochlorine pesticide, in water samples. The GQDs were used as signal amplification material thus low detection limits (3 pg mL^{-1}) were obtained. In recent studies, carbon dots have also been used for detection of pesticides like parathion-methyl [111],

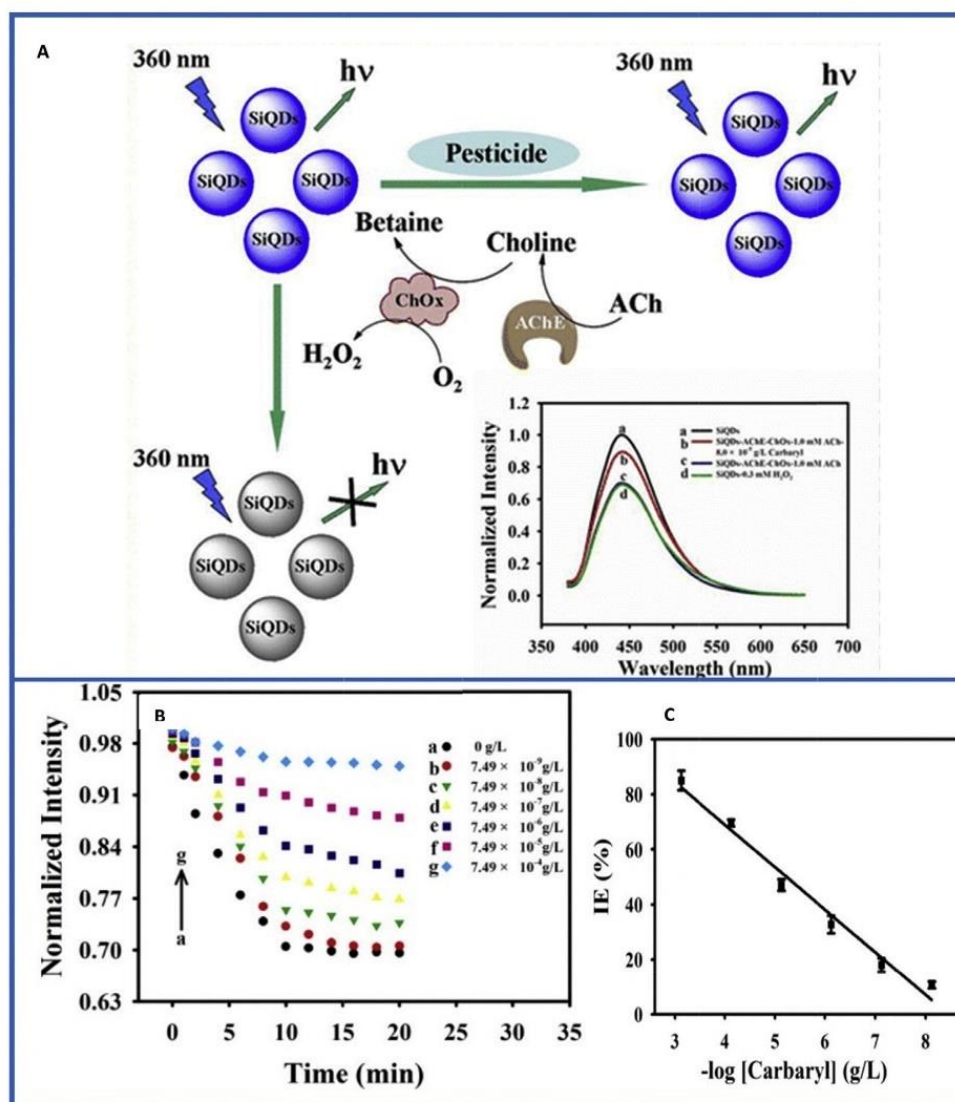


Fig. 5. (a) Schematic illustration of the working principle of the AChE based biosensor for pesticide detection (SiQDs: silicon quantum dots). (b) Incubation time dependence of fluorescence intensity of SiQDs-AChE-ChO probe at different concentrations of carbaryl. (c) Inhibition efficiency (IE) vs log of carbaryl concentration under optimized conditions (Reprinted with permission from Ref. [44]. Copyright (2016) American Chemical Society).

dimethoate [95] dichlorvos and carbaryl [58] at low detection limits (Table 4). Like other quantum dots, these can also be used with enzymes or MIPs to achieve selectivity for target pesticides. A disadvantage of carbon dots is their poor quantum yields compared to semi-conductor QDs. However, current research is showing that it is possible to produce high quantum yield carbon dots through, for example, co-doping the carbon dots with nitrogen and sulphur atoms [58,108,112,113].

2.7. QD films in pesticide sensing

Most of the sensing systems discussed so far have been based on solution-based probes which, although they have been successfully employed, they still have some serious limitations. Firstly, the analyte cannot be recovered from the solution, meaning the solution sensor can only be used once before being disposed. This can lead to environmental contamination and can raise the costs for their routine application. Secondly, it is rather difficult to handle or store these solutions because they can degrade with time and become unstable. Thus this can complicate their use in designing portable

sensor devices.

A possible solution to some of these challenges could be the incorporation of the QD sensors into solid materials. Films can offer some advantages over solution-based probes including good stability, portability, tunable shape and size, real-time detection, and extensive suitability in gas/vapour sensing [126]. Different materials can be used as substrates for assembling QD films including silicone, polydimethylsiloxane (PDMS) and glass.

Some work has been done on preparing QD-enzyme films for the detection of organophosphorus pesticides [42,43,46,103,106,127,128]. For example, the study by Zheng et al. [43] used acetylcholinesterase (AChE) and choline oxidase (ChOx) enzymes as recognition elements and CdTe QDs as transducers to design CdTe/ChOx/AChE multilayer films. They showed that these films could detect paraoxon, dichlorvos and parathion in apples through inhibition of the enzymes and subsequent fluorescence quenching of the QDs.

While these films show promising results, constructing them with biological recognition elements (enzymes) remains a concern regarding stability considerations and – by extension – when

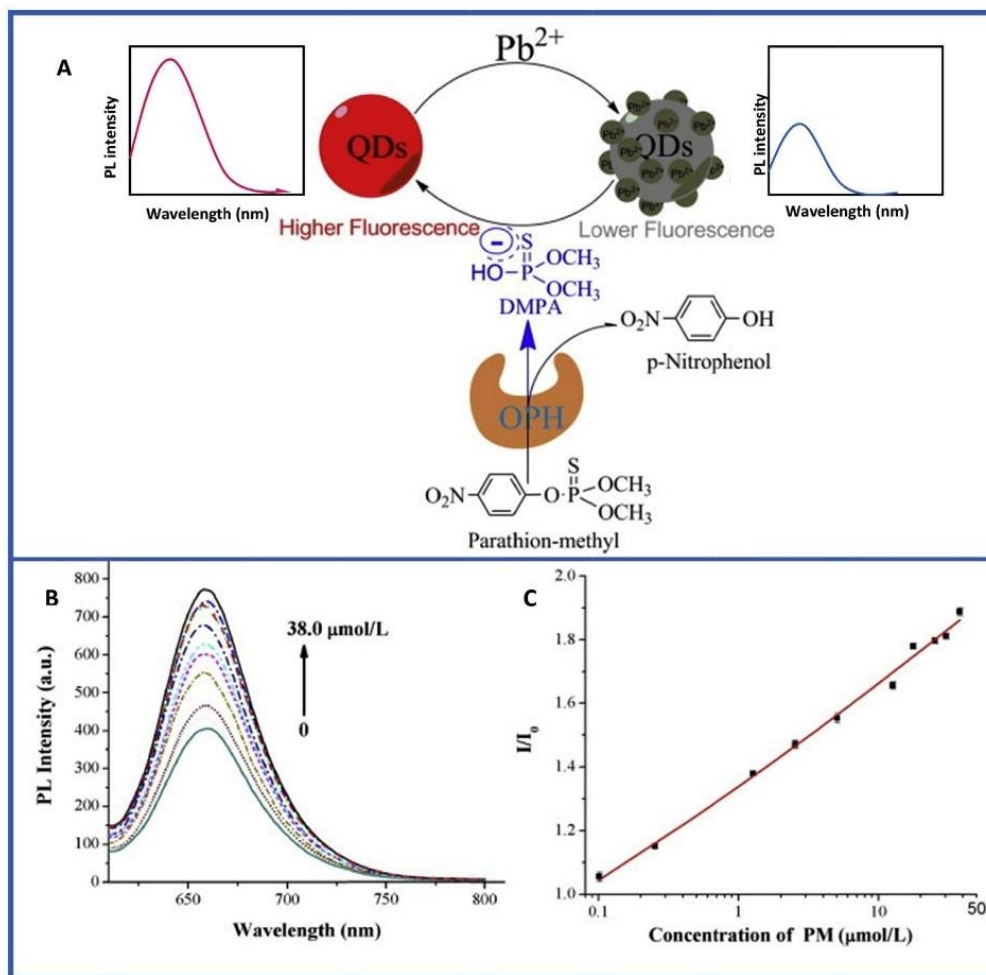


Fig. 6. (A) Schematic diagram illustrating the working principle of the CuInS₂ QD biosensor for parathion-methyl (PM) detection (Abbreviations: DMPA: di-methylthiophosphoric acid, OPH: Organophosphorus hydrolase). (B) Response of the sensor to increasing concentration of parathion-methyl (c) Plot of fluorescence intensity ratios of the CuInS₂ sensor versus the logarithm of concentration of PM. I and I₀ were the fluorescence intensity of CuInS₂ QDs complex in the presence and absence of PM, respectively (reprinted from Ref. [105], Copyright (2016), with permission from Elsevier).

designing reusable devices. Future work is expected to focus on using these films with artificial analyte receptors, like MIPs, which can overcome some of the challenges that come with biological enzymes.

3. Concluding comments and future outlook

The reviewed literature shows that quantum dot-based fluorescence sensors can offer excellent and potentially superior sensitivity compared to most conventional analytical techniques for detecting pesticide concentrations at or below legislative limits in environmental matrices. Efforts to improve the analytical performance of these sensors include coupling them to recognition elements like enzymes, MIPs, or specially crafted supramolecules which offer selectivity towards targeted pesticides. Although these sensors are simple to prepare, show great analytical performance, and are cost-effective, there are some serious limitations that still have to be overcome in order to develop standardized methods that could lead to their commercialization. For instance, enzyme-based QD sensors are limited by slow enzyme reactions which are temperature and pH dependent. In MIP sensors, the polymer could be irregular and the template molecules could be permanently trapped leading to poor adsorption kinetics for target molecules. Host-molecule based sensors may also be prone to matrix interferences with other molecules that can have interactions with their cavities. Thus there is still a need for further research to improve the analytical robustness and selectivity of QD based fluorescence sensors towards target pesticide analytes in real samples where matrix interferences could play a major role.

4. Future prospects

- Most of the fluorescence sensors for pesticide applications have focused on organophosphate pesticides (OPs) because of their inhibiting effects on most enzymes that are incorporated in biosensors. Limited research has focused on organochlorine pesticides (OCs), like atrazine and terbutylazine, which are both widely used in agriculture. These two pesticides have been identified as contaminants of emerging concern (CECs) in water systems [129] hence they should be included as targets for future QD based fluorescence sensor development. Other pesticides, like glyphosate, are not routinely analyzed in laboratories because of difficulties arising from their chemical instabilities. Thus it is anticipated that further research in terms of the development of QD based fluorescence sensors for this pesticide will be conducted.
- The use of aptamers in biosensors is emerging, and could become the focus of future biosensor research. However, there are some challenges such as isolating the right aptamer for a particular target analyte, which have to be addressed. The stability of aptamer based probes also has to be improved to allow for them to be easily stored.
- Future research is expected to also seek for less toxic QDs as alternatives to the widely used cadmium based QDs, but which retain the excellent optical properties thereof. The emergence of carbon quantum dots is promising in this regard.
- MIPs have a number of advantages as artificial receptors in QD sensors. However some improvements are still needed regarding their synthesis and in the extraction of template molecules. Further, they can be incorporated onto or into solid supports or thin films in designing stable sensor devices.
- Finally, designing reusable devices is expected to be a significant future focus, where green chemistry approaches which also have economic advantages are to be considered. The solution based probes which have currently been developed can only be

used once, which can lead to the generation of potentially toxic waste. Research on the immobilization of QD nanoparticles onto solid surfaces to allow for the development of solid reusable devices which can be more readily standardized and commercialized is thus of importance.

Acknowledgements

Funding from the Water Research Commission (WRC) (Grant K5/2438/1), the Photonics Initiative of South Africa (Grant PISA-15-DIR-06) and the National Research Foundation of South Africa (postgraduate student bursary (SN) and funding grants 90720 and 93394 (PF)) is gratefully acknowledged.

References

- [1] R. Schulz, Comparison of spray drift- and runoff-related input of azinphos-methyl and endosulfan from fruit orchards into the Lourens River, South Africa, *Chemosphere* 45 (2001) 543–551.
- [2] W.H. Hallenbeck, K.M. Cunningham-Burns, *Pesticides and Human Health*, Springer New York, New York, USA, 2012.
- [3] USEPA, (US Environmental Protection Agency), *Setting Tolerances for Pesticide Residues in Foods*, 2016.
- [4] NPIC, (National Pesticide Information Center), *International Pesticide Regulations*, 2016.
- [5] WHO, *Guidelines for Drinking-water Quality 4th Edition*, 2011. Retrieved from, http://apps.who.int/iris/bitstream/10665/44584/1/9789241548151_eng.pdf.
- [6] Defra, (Department for Environment Food and Rural Affairs), *Pesticide Residues in Food: Results of Monitoring Programme Food and Farming Industry Environmental Quality – Expert Committee on Pesticide Residues in Food (PRiF): Annual Report for 2015, 2016*. United Kingdom. Retrieved from, <https://www.gov.uk/government/publications/expert-committee-on-pesticide-residues-in-food-prif-annual-report-for-2015>.
- [7] EFSA, European Food Safety Authority, *The 2013 European Union report on pesticide residues in food*, *EFSA J.* 13 (2015) 4038.
- [8] C.J. Murphy, J.L. Coffey, *Quantum dots: a primer*, *Appl. Spectrosc.* 56 (2002) 16A–27A.
- [9] A.J. Nozik, M.C. Beard, J.M. Luther, M. Law, R.J. Ellingson, J.C. Johnson, Semiconductor quantum dots and quantum dot arrays and applications of multiple exciton generation to third-generation photovoltaic solar cells, *Chem. Rev.* 110 (2010) 6873–6890.
- [10] S. Jin, Y. Hu, Z. Gu, L. Liu, H.-C. Wu, Application of quantum dots in biological imaging, *J. Nanomater.* 2011 (2011) 13.
- [11] F.D. de Menezes, A.G. Brasil Jr., W.L. Moreira, L.C. Barbosa, C.L. Cesar, R.d.C. Ferreira, P.M.A. de Farias, B.S. Santos, CdTe/CdS core shell quantum dots for photonic applications, *Microelectron. J.* 36 (2005) 989–991.
- [12] H. Huang, J.-J. Zhu, The electrochemical applications of quantum dots, *Analyst* 138 (2013) 5855–5865.
- [13] J. Drbohlavova, V. Adam, R. Kizek, J. Hubalek, Quantum dots — characterization, preparation and usage in biological systems, *Int. J. Mol. Sci.* 10 (2009) 656–673.
- [14] D. Bera, L. Qian, T.-K. Tseng, P.H. Holloway, Quantum dots and their multimodal applications: a review, *Materials* 3 (2010) 2260–2345.
- [15] X. Du, D. Jiang, Q. Liu, G. Zhu, H. Mao, K. Wang, Fabrication of graphene oxide decorated with nitrogen-doped graphene quantum dots and its enhanced electrochemiluminescence for ultrasensitive detection of pentachlorophenol, *Analyst* 140 (2015) 1253–1259.
- [16] Y. Dong, J. Cai, Y. Chi, Carbon based dots and their luminescent properties and analytical applications, in: N. Yang, X. Jiang, D.-W. Pang (Eds.), *Carbon Nanoparticles and Nanostructures*, Springer International Publishing, Cham, 2016, pp. 161–238.
- [17] D. Kong, F. Yan, D. Shi, Q. Ye, Z. Han, L. Chen, L. Wang, Carbon dots: synthetic methods and applications as fluorescent probes for the detection of metal ions, inorganic anions and organic molecules, *J. Iran. Chem. Soc.* 12 (2015) 1841–1857.
- [18] J. Shen, Y. Zhu, X. Yang, C. Li, Graphene quantum dots: emergent nanolights for bioimaging, sensors, catalysis and photovoltaic devices, *Chem. Commun.* 48 (2012) 3686–3699.
- [19] L. Lin, M. Rong, F. Luo, D. Chen, Y. Wang, X. Chen, Luminescent graphene quantum dots as new fluorescent materials for environmental and biological applications, *TrAC Trends Anal. Chem.* 54 (2014) 83–102.
- [20] S. Benítez-Martínez, M. Valcárcel, Graphene quantum dots in analytical science, *TrAC Trends Anal. Chem.* 72 (2015) 93–113.
- [21] A. Valizadeh, H. Mikaeili, M. Samiei, S. Farkhani, N. Zarghami, M. Kouhi, A. Akbarzadeh, S. Davaran, Quantum dots: synthesis, bioapplications, and toxicity, *Nanoscale Res. Lett.* 7 (2012) 480.
- [22] W. Kuzyniak, O. Adegoke, K. Sekhosana, S. D'Souza, S.C. Tshangana, B. Hoffmann, E.A. Ermilov, T. Nyokong, M. Höpfer, Synthesis and characterization of quantum dots designed for biomedical use, *Int. J. Pharm.* 466

- (2014) 382–389.
- [23] C.J. Murphy, Peer reviewed: optical sensing with quantum dots, *Anal. Chem.* 74 (2002) 520A–526A.
- [24] K. Chou, A. Dennis, Förster resonance energy transfer between quantum dot donors and quantum dot acceptors, *Sensors* 15 (2015) 13288–13325.
- [25] J. Guo, Y. Zhang, Y. Luo, F. Shen, C. Sun, Efficient fluorescence resonance energy transfer between oppositely charged CdTe quantum dots and gold nanoparticles for turn-on fluorescence detection of glyphosate, *Talanta* 125 (2014) 385–392.
- [26] L. Yang, B. Chen, S. Luo, J. Li, R. Liu, Q. Cai, Sensitive detection of polycyclic aromatic hydrocarbons using CdTe quantum dot-modified TiO₂ nanotube array through fluorescence resonance energy transfer, *Environ. Sci. Technol.* 44 (2010) 7884–7889.
- [27] L. Cui, X.-P. He, G.-R. Chen, Recent progress in quantum dot based sensors, *RSC Adv.* 5 (2015) 26644–26653.
- [28] W. Zhang, A. Asiri, D. Liu, D. Du, Y. Lin, Nanomaterial-based biosensors for environmental and biological monitoring of organophosphorus pesticides and nerve agents, *TrAC Trends Anal. Chem.* 54 (2014) 1–10.
- [29] A.P. Periasamy, Y. Umasankar, S.-M. Chen, Nanomaterials - acetylcholinesterase enzyme matrices for organophosphorus pesticides electrochemical sensors: a review, *Sensors* 9 (2009) 4034.
- [30] C.S. Pundir, N. Chauhan, Acetylcholinesterase inhibition-based biosensors for pesticide determination: a review, *Anal. Biochem.* 429 (2012) 19–31.
- [31] E.J. Llorent-Martínez, P. Ortega-Barrales, M.L. Fernández-de Córdoba, A. Ruiz-Medina, Trends in flow-based analytical methods applied to pesticide detection: a review, *Anal. Chim. Acta* 684 (2011) 30–39.
- [32] P. Kumar, K.-H. Kim, A. Deep, Recent advancements in sensing techniques based on functional materials for organophosphate pesticides, *Biosens. Bioelectron.* 70 (2015) 469–481.
- [33] V. Dhull, A. Gahlaut, N. Dilbaghi, V. Hooda, Acetylcholinesterase biosensors for electrochemical detection of organophosphorus compounds: a review, *Biochem. Res. Int.* 2013 (2013) 18.
- [34] G. Aragay, F. Pino, A. Merkoçi, Nanomaterials for sensing and destroying pesticides, *Chem. Rev.* 112 (2012) 5317–5338.
- [35] R. Buiculescu, M. Hatzimarinaki, N.A. Chaniotakis, Biosilicated CdSe/ZnS quantum dots as photoluminescent transducers for acetylcholinesterase-based biosensors, *Anal. Bioanal. Chem.* 398 (2010) 3015–3021.
- [36] W. Kong, X. Yang, M. Yang, H. Zhou, Z. Ouyang, M. Zhao, Photoluminescent nanosensors capped with quantum dots for high-throughput determination of trace contaminants: strategies for enhancing analytical performance, *TrAC Trends Anal. Chem.* 78 (2016) 36–47.
- [37] W. Amondham, P. Parkpian, C. Polprasert, R. DeLaune, A. Jugsujinda, Paraquat adsorption, degradation, and remobilization in tropical soils of Thailand, *J. Environ. Sci. Health Part B* 41 (2006) 485–507.
- [38] Q.-Q. Bian, Y.-F. Liu, J.-S. Yu, CdTe/CdS semiconductor quantum dots as a highly sensitive sensor for pesticide paraquat, *Chem. J. Chin. U* 6 (2010) 015.
- [39] G.M. Durán, A.M. Contento, A. Ríos, Use of CdSe/ZnS quantum dots for sensitive detection and quantification of paraquat in water samples, *Anal. Chim. Acta* 801 (2013) 84–90.
- [40] Y. Fan, L. Liu, D. Sun, H. Lan, H. Fu, T. Yang, Y. She, C. Ni, “Turn-off” fluorescent data array sensor based on double quantum dots coupled with chemometrics for highly sensitive and selective detection of multicomponent pesticides, *Anal. Chim. Acta* 916 (2016) 84–91.
- [41] Mamta, R.J. Rao, K.A. Wani, Monitoring of organochlorine and organophosphorus pesticide residues in water during different seasons of Tighra reservoir Gwalior, Madhya Pradesh, India, *Environ. Monit. Assess.* 187 (2015) 1–14.
- [42] Z. Zheng, X. Li, Z. Dai, S. Liu, Z. Tang, Detection of mixed organophosphorus pesticides in real samples using quantum dots/bi-enzyme assembly multilayers, *J. Mater. Chem.* 21 (2011) 16955–16962.
- [43] Z. Zheng, Y. Zhou, X. Li, S. Liu, Z. Tang, Highly-sensitive organophosphorus pesticide biosensors based on nanostructured films of acetylcholinesterase and CdTe quantum dots, *Biosens. Bioelectron.* 26 (2011) 3081–3085.
- [44] Y. Yi, G. Zhu, C. Liu, Y. Huang, Y. Zhang, H. Li, J. Zhao, S. Yao, A label-free silicon quantum dots-based photoluminescence sensor for ultrasensitive detection of pesticides, *Anal. Chem.* 85 (2013) 11464–11470.
- [45] G. Xue, Z. Yue, Z. Bing, T. Yiwei, L. Xiuying, L. Jianrong, Highly-sensitive organophosphorus pesticide biosensors based on CdTe quantum dots and bi-enzyme immobilized eggshell membranes, *Analyst* 141 (2016) 1105–1111.
- [46] E. Luan, Z. Zheng, X. Li, H. Gu, S. Liu, Inkjet-assisted layer-by-layer printing of quantum dot/enzyme microarrays for highly sensitive detection of organophosphorus pesticides, *Anal. Chim. Acta* 916 (2016) 77–83.
- [47] W. Zheng, H. Yu, X. Wang, W. Qu, Systematic review of pentachlorophenol occurrence in the environment and in humans in China: not a negligible health risk due to the re-emergence of schistosomiasis, *Environ. Int.* 42 (2012) 105–116.
- [48] H.-F. Wang, Y. He, T.-R. Ji, X.-P. Yan, Surface molecular imprinting on Mn-Doped ZnS quantum dots for Room-temperature photoluminescence optosensing of pentachlorophenol in water, *Anal. Chem.* 81 (2009) 1615–1621.
- [49] Q. Liu, K. Wang, J. Huan, G. Zhu, J. Qian, H. Mao, J. Cai, Graphene quantum dots enhanced electrochemiluminescence of cadmium sulfide nanocrystals for ultrasensitive determination of pentachlorophenol, *Analyst* 139 (2014) 2912–2918.
- [50] A.Z. Chowdhury, S.A. Jahan, M.N. Islam, M. Moniruzzaman, M.K. Alam, M.A. Zaman, N. Karim, S.H. Gan, Occurrence of organophosphorus and carbamate pesticide residues in surface water samples from the Rangpur district of Bangladesh, *Bull. Environ. Contam. Toxicol.* 89 (2012) 202–207.
- [51] N.A. Bakar, M.M. Salleh, A.A. Umar, M. Yahaya, The detection of pesticides in water using ZnCdSe quantum dot films, *Adv. Nat. Sci. Nanosci. Nanotechnol.* 2 (2011) 025011.
- [52] X. Ren, H. Liu, L. Chen, Fluorescent detection of chlorpyrifos using Mn (II)-doped ZnS quantum dots coated with a molecularly imprinted polymer, *Microchim. Acta* 182 (2015) 193–200.
- [53] H. Wijnja, J.J. Doherty, S.A. Safie, Changes in pesticide occurrence in suburban surface waters in Massachusetts, USA, 1999–2010, *Bull. Environ. Contam. Toxicol.* 93 (2014) 228–232.
- [54] Y. Zhao, Y. Ma, H. Li, L. Wang, Composite QDs@MIP nanospheres for specific recognition and direct fluorescent quantification of pesticides in aqueous media, *Anal. Chem.* 84 (2012) 386–395.
- [55] J. Ruiz-Toledo, R. Castro, N. Rivero-Pérez, R. Bello-Mendoza, D. Sánchez, Occurrence of glyphosate in water bodies derived from intensive agriculture in a tropical region of southern Mexico, *Bull. Environ. Contam. Toxicol.* 93 (2014) 289–293.
- [56] T. Li, Y. Zhou, J. Sun, K. Wu, Ultrasensitive detection of glyphosate using CdTe quantum dots in sol-gel-derived silica spheres coated with calix [6] arene as fluorescent probes, *Am. J. Anal. Chem.* 3 (2012) 12–18.
- [57] Y. Fan, K. Lai, B.A. Rasco, Y. Huang, Determination of carbaryl pesticide in Fuji apples using surface-enhanced Raman spectroscopy coupled with multivariate analysis, *LWT Food Sci. Technol.* 60 (2015) 352–357.
- [58] H. Li, C. Sun, R. Vijayaraghavan, F. Zhou, X. Zhang, D.R. MacFarlane, Long lifetime photoluminescence in N, S co-doped carbon quantum dots from an ionic liquid and their applications in ultrasensitive detection of pesticides, *Carbon* 104 (2016) 33–39.
- [59] X. Yan, H. Li, X. Wang, X. Su, A novel fluorescence probing strategy for the determination of parathion-methyl, *Talanta* 131 (2015) 88–94.
- [60] Health Canada, Guidelines for Canadian Drinking Water Quality—Summary Table, Water and Air Quality Bureau, Healthy Environments and Consumer Safety Branch, Health Canada, Ottawa, Ontario, 2014. Retrieved from, http://www.hc-sc.gc.ca/ewh-semt/pubs/water-eau/sum_guide-res_recom/index-eng.php.
- [61] Code of Federal Regulations, Tolerances and Exemptions for Pesticide Chemical Residues in Food, 2016.
- [62] C.L.L. Justino, A.C. Freitas, R. Pereira, A.C. Duarte, T.A.P. Rocha Santos, Recent developments in recognition elements for chemical sensors and biosensors, *TrAC Trends Anal. Chem.* 68 (2015) 2–17.
- [63] S. Walia, A. Acharya, Fluorescent cadmium sulfide nanoparticles for selective and sensitive detection of toxic pesticides in aqueous medium, *J. Nanopart. Res.* 16 (2014) 1–10.
- [64] Y. Lou, Y. Zhao, J. Chen, J.-J. Zhu, Metal ions optical sensing by semiconductor quantum dots, *J. Mater. Chem. C* 2 (2014) 595–613.
- [65] E. Mohamed Ali, Y. Zheng, H.-h. Yu, J.Y. Ying, Ultrasensitive Pb²⁺ detection by glutathione-capped quantum dots, *Anal. Chem.* 79 (2007) 9452–9458.
- [66] F.O. Silva, M.S. Carvalho, R. Mendonça, W.A. Macedo, K. Balzuweit, P. Reiss, M.A. Schiavon, Effect of surface ligands on the optical properties of aqueous soluble CdTe quantum dots, *Nanoscale Res. Lett.* 7 (2012) 1–10.
- [67] P. Wu, X.-P. Yan, Doped quantum dots for chemo/biosensing and bioimaging, *Chem. Soc. Rev.* 42 (2013) 5489–5521.
- [68] S. Cao, C. Li, L. Wang, M. Shang, G. Wei, J. Zheng, W. Yang, Long-lived and well-resolved Mn²⁺ ion emissions in CuInS-ZnS quantum dots, *Sci. Rep.* 4 (2014) 7510.
- [69] R. Subha, V. Nalla, J.H. Yu, S.W. Jun, K. Shin, T. Hyeon, C. Vijayan, W. Ji, Efficient photoluminescence of Mn²⁺-doped ZnS quantum dots excited by two-photon absorption in near-infrared window II, *J. Phys. Chem. C* 117 (2013) 20905–20911.
- [70] M. Yang, A. Han, J. Duan, Z. Li, Y. Lai, J. Zhan, Magnetic nanoparticles and quantum dots co-loaded imprinted matrix for pentachlorophenol, *J. Hazard. Mater.* 237–238 (2012) 63–70.
- [71] X. Ren, L. Chen, Quantum dots coated with molecularly imprinted polymer as fluorescence probe for detection of cyphenothrin, *Biosens. Bioelectron.* 64 (2015) 182–188.
- [72] B. Lin, Y. Yu, R. Li, Y. Cao, M. Guo, Turn-on sensor for quantification and imaging of acetamiprid residues based on quantum dots functionalized with aptamer, *Sens. Actuators B Chem.* 229 (2016) 100–109.
- [73] X. Gao, G. Tang, X. Su, Optical detection of organophosphorus compounds based on Mn-doped ZnSe d-dot enzymatic catalytic sensor, *Biosens. Bioelectron.* 36 (2012) 75–80.
- [74] X. Ren, L. Chen, Preparation of molecularly imprinted polymer coated quantum dots to detect nicosulfuron in water samples, *Anal. Bioanal. Chem.* 407 (2015) 8087–8095.
- [75] H. Li, Y. Li, J. Cheng, Molecularly imprinted silica nanospheres embedded CdSe quantum dots for highly selective and sensitive optosensing of pyrethroids, *Chem. Mater.* 22 (2010) 2451–2457.
- [76] H. Li, F. Qu, Synthesis of CdTe quantum dots in Sol–Gel-derived composite silica spheres coated with Calix[4]arene as luminescent probes for pesticides, *Chem. Mater.* 19 (2007) 4148–4154.
- [77] X. Yan, H. Li, X. Han, X. Su, A ratiometric fluorescent quantum dots based biosensor for organophosphorus pesticides detection by inner-filter effect, *Biosens. Bioelectron.* 74 (2015) 277–283.
- [78] C. Wang, Q. Ma, W. Dou, S. Kanwal, G. Wang, P. Yuan, X. Su, Synthesis of aqueous CdTe quantum dots embedded silica nanoparticles and their

- applications as fluorescence probes, *Talanta* 77 (2009) 1358–1364.
- [79] Y. Yang, L. Jing, X. Yu, D. Yan, M. Gao, Coating aqueous quantum dots with silica via reverse microemulsion Method: toward size-controllable and robust fluorescent nanoparticles, *Chem. Mater.* 19 (2007) 4123–4128.
- [80] V.V. Gofman, T. Aubert, D.V. Ginste, R. Van Deun, N.V. Beloglazova, Z. Hens, S. De Saeger, I.Y. Goryacheva, Synthesis, modification, bioconjugation of silica coated fluorescent quantum dots and their application for mycotoxin detection, *Biosens. Bioelectron.* 79 (2016) 476–481.
- [81] X. Wang, W. Li, B. Zhao, D. Zhang, K. Sun, X. An, Z. Zhang, Z. Shen, Highly fluorescent quantum dot@silica nanoparticles by a novel post-treatment for live cell imaging, *RSC Adv.* 3 (2013) 3553–3556.
- [82] M. Bottini, F. D'Annibale, A. Magrini, F. Cerignoli, Y. Arimura, M.I. Dawson, E. Bergamaschi, N. Rosato, A. Bergamaschi, T. Mustelin, Quantum dot-doped silica nanoparticles as probes for targeting of T-lymphocytes, *Int. J. Nanomed.* 2 (2007) 227–233.
- [83] Q. Ma, Y. Li, X. Su, Silica nanobead-based sensors for analytical and bio-analytical applications, *TrAC Trends Anal. Chem.* 74 (2015) 130–145.
- [84] X. Hu, X. Gao, Silica–Polymer dual layer-encapsulated quantum dots with Remarkable stability, *ACS Nano* 4 (2010) 6080–6086.
- [85] G. Bapat, C. Labade, A. Chaudhari, S. Zinjarde, Silica nanoparticle based techniques for extraction, detection, and degradation of pesticides, *Adv. Colloid Interface Sci.* (2016), <http://dx.doi.org/10.1016/j.cis.2016.06.001>.
- [86] S. Ge, J. Lu, L. Ge, M. Yan, J. Yu, Development of a novel deltamethrin sensor based on molecularly imprinted silica nanospheres embedded CdTe quantum dots, *Spectrochim. Acta Part A Mol. Biomol. Spectrosc.* 79 (2011) 1704–1709.
- [87] E. Zor, E. Morales-Narváez, A. Zamora-Gálvez, H. Bingol, M. Ersoz, A. Merkoçi, Graphene quantum dots-based photoluminescent sensor: a multifunctional composite for pesticide detection, *ACS Appl. Mater. Interfaces* 7 (2015) 20272–20279.
- [88] F. Qu, X. Zhou, J. Xu, H. Li, G. Xie, Luminescence switching of CdTe quantum dots in presence of p-sulfonatocalix[4]arene to detect pesticides in aqueous solution, *Talanta* 78 (2009) 1359–1363.
- [89] H.-J. Schneider, Limitations and extensions of the lock-and-key principle: differences between gas state, solution and solid state structures, *Int. J. Mol. Sci.* 16 (2015) 6694–6717.
- [90] Q. Chen, Y. Fung, Capillary electrophoresis with immobilized quantum dot fluorescence detection for rapid determination of organophosphorus pesticides in vegetables, *Electrophoresis* 31 (2010) 3107–3114.
- [91] K. Zhang, Q. Mei, G. Guan, B. Liu, S. Wang, Z. Zhang, Ligand Replacement-induced fluorescence switch of quantum dots for ultrasensitive detection of organophosphorothioate pesticides, *Anal. Chem.* 82 (2010) 9579–9586.
- [92] L. Wang, Y. Bi, J. Hou, H. Li, Y. Xu, B. Wang, H. Ding, L. Ding, Facile, green and clean one-step synthesis of carbon dots from wool: application as a sensor for glyphosate detection based on the inner filter effect, *Talanta* 160 (2016) 268–275.
- [93] J. Tang, L. Xiang, Development of a probe based on quantum dots embedded with molecularly imprinted polymers to detect parathion, *Pol. J. Environ. Stud.* 25 (2016) 787–793.
- [94] X. Wei, T. Hao, Y. Xu, K. Lu, H. Li, Y. Yan, Z. Zhou, Facile polymerizable surfactant inspired synthesis of fluorescent molecularly imprinted composite sensor via aqueous CdTe quantum dots for highly selective detection of λ -cyhalothrin, *Sens. Actuators B Chem.* 224 (2016) 315–324.
- [95] S. Li, J. Luo, G. Yin, Z. Xu, Y. Le, X. Wu, N. Wu, Q. Zhang, Selective determination of dimethoate via fluorescence resonance energy transfer between carbon dots and a dye-doped molecularly imprinted polymer, *Sens. Actuators B Chem.* 206 (2015) 14–21.
- [96] C. Zhang, H. Cui, J. Cai, Y. Duan, Y. Liu, Development of fluorescence sensing material based on CdSe/ZnS quantum dots and molecularly imprinted polymer for the detection of carbaryl in rice and Chinese cabbage, *J. Agric. Food. Chem.* 63 (2015) 4966–4972.
- [97] A. Sassolas, B. Prieto-Simón, J.-L. Marty, Biosensors for pesticide detection: new trends, *Am. J. Anal. Chem.* 3 (2012) 210–232.
- [98] J. Guo, Y. Li, L. Wang, J. Xu, Y. Huang, Y. Luo, F. Shen, C. Sun, R. Meng, Aptamer-based fluorescent screening assay for acetamiprid via inner filter effect of gold nanoparticles on the fluorescence of CdTe quantum dots, *Anal. Bioanal. Chem.* 408 (2016) 557–566.
- [99] N. Xia, Q. Wang, L. Liu, Nanomaterials-based optical techniques for the detection of acetylcholinesterase and pesticides, *Sensors (Basel, Switz.)* 15 (2015) 499–514.
- [100] L. Nan, W. Xuewan, C. Jie, S. Lei, C. Peng, Graphene quantum dots for ultrasensitive detection of acetylcholinesterase and its inhibitors, *2D Mater.* 2 (2015) 034018.
- [101] J. Dong, H. Zhao, F. Qiao, P. Liu, X. Wang, S. Ai, Quantum dot immobilized acetylcholinesterase for the determination of organophosphate pesticides using graphene-chitosan nanocomposite modified electrode, *Anal. Methods* 5 (2013) 2866–2872.
- [102] D. Du, W. Chen, W. Zhang, D. Liu, H. Li, Y. Lin, Covalent coupling of organophosphorus hydrolase loaded quantum dots to carbon nanotube/Au nanocomposite for enhanced detection of methyl parathion, *Biosens. Bioelectron.* 25 (2010) 1370–1375.
- [103] C.A. Constantine, K.M. Gattás-Asfura, S.V. Mello, G. Crespo, V. Rastogi, T.-C. Cheng, J.J. DeFrank, R.M. Leblanc, Layer-by-Layer films of chitosan, organophosphorus hydrolase and thioglycolic acid-capped CdSe quantum dots for the detection of paraoxon, *J. Phys. Chem. B* 107 (2003) 13762–13764.
- [104] X. Ji, J. Zheng, J. Xu, V.K. Rastogi, T.-C. Cheng, J.J. DeFrank, R.M. Leblanc, (CdSe) ZnS quantum dots and organophosphorus hydrolase bioconjugate as biosensors for detection of paraoxon, *J. Phys. Chem. B* 109 (2005) 3793–3799.
- [105] X. Yan, H. Li, Y. Yan, X. Su, Selective detection of parathion-methyl based on near-infrared CuInS₂ quantum dots, *Food Chem.* 173 (2015) 179–184.
- [106] X. Sun, B. Liu, K. Xia, A sensitive and regenerable biosensor for organophosphate pesticide based on self-assembled multilayer film with CdTe as fluorescence probe, *Luminescence* 26 (2011) 616–621.
- [107] Y. Dong, J. Cai, X. You, Y. Chi, Sensing applications of luminescent carbon based dots, *Analyst* 140 (2015) 7468–7486.
- [108] F.R. Baptista, S.A. Belhout, S. Giordani, S.J. Quinn, Recent developments in carbon nanomaterial sensors, *Chem. Soc. Rev.* 44 (2015) 4433–4453.
- [109] P. Roy, P.-C. Chen, A.P. Periasamy, Y.-N. Chen, H.-T. Chang, Photoluminescent carbon nanodots: synthesis, physicochemical properties and analytical applications, *Mater. Today* 18 (2015) 447–458.
- [110] S. Zhu, Y. Song, X. Zhao, J. Shao, J. Zhang, B. Yang, The photoluminescence mechanism in carbon dots (graphene quantum dots, carbon nanodots, and polymer dots): current state and future perspective, *Nano Res.* 8 (2015) 355–381.
- [111] J. Hou, J. Dong, H. Zhu, X. Teng, S. Ai, M. Mang, A simple and sensitive fluorescence sensor for methyl parathion based on l-tyrosine methyl ester functionalized carbon dots, *Biosens. Bioelectron.* 68 (2015) 20–26.
- [112] Y. Du, S. Guo, Chemically doped fluorescent carbon and graphene quantum dots for bioimaging, sensor, catalytic and photoelectronic applications, *Nanoscale* 8 (2016) 2532–2543.
- [113] J. Sun, S. Yang, Z. Wang, H. Shen, T. Xu, L. Sun, H. Li, W. Chen, X. Jiang, G. Ding, Z. Kang, X. Xie, M. Jiang, Ultra-high quantum yield of graphene quantum dots: aromatic-nitrogen doping and photoluminescence mechanism, *Part. Part. Syst. Charact.* 32 (2015) 434–440.
- [114] G. Garai-Ibabe, L. Saa, V. Pavlov, Thiocholine mediated stabilization of in situ produced CdS quantum dots: application for the detection of acetylcholinesterase activity and inhibitors, *Analyst* 139 (2014) 280–284.
- [115] N.N. Hai, V.D. Chinh, T.K. Chi, U.T.D. Thuy, N.X. Nghia, D.T. Cao, P.T. Nga, Optical detection of the pesticide by functionalized quantum dots as fluorescence-based biosensor, *Key Eng. Mater., Trans. Tech. Publ.* (2012) 314–318.
- [116] N.N. Hai, V.D. Chinh, U.T.D. Thuy, T.K. Chi, N.H. Yen, D.T. Cao, N.Q. Liem, P.T. Nga, Detection of the pesticide by functionalized quantum dots as fluorescence-based biosensor, *Int. J. Nanotechnol.* 10 (2013) 137–145.
- [117] T. Thi Kim Chi, V. Duc Chinh, U. Thi Dieu Thuy, N. Hai Yen, N. Ngoc Hai, D. Tran Cao, P. Thu Nga, N. Quang Liem, Fabrication of fluorescence-based biosensors from functionalized CdSe and CdTe quantum dots for pesticide detection, *Adv. Nat. Sci. Nanosci. Nanotechnol.* 3 (2012) 035008.
- [118] X. Meng, J. Wei, X. Ren, J. Ren, F. Tang, A simple and sensitive fluorescence biosensor for detection of organophosphorus pesticides using H2O2-sensitive quantum dots/bi-enzyme, *Biosens. Bioelectron.* 47 (2013) 402–407.
- [119] J. Hou, Z. Tian, H. Xie, Q. Tian, S. Ai, A fluorescence resonance energy transfer sensor based on quaternized carbon dots and Ellman's test for ultrasensitive detection of dichlorvos, *Sens. Actuators B Chem.* 232 (2016) 477–483.
- [120] A.C. Vinayaka, S. Basheer, M.S. Thakur, Bioconjugation of CdTe quantum dot for the detection of 2,4-dichlorophenoxyacetic acid by competitive fluoroimmunoassay based biosensor, *Biosens. Bioelectron.* 24 (2009) 1615–1620.
- [121] Y.P. Chen, B. Ning, N. Liu, Y. Feng, Z. Liu, X. Liu, Z.X. Gao, A rapid and sensitive fluoroimmunoassay based on quantum dot for the detection of chlorpyrifos residue in drinking water, *J. Environ. Sci. Health B* 45 (2010) 508–515.
- [122] D. Wang, B. Lin, Y. Cao, M. Guo, Y. Yu, A highly selective and sensitive fluorescence detection method of glyphosate based on an immune reaction strategy of carbon dot labeled antibody and antigen magnetic beads, *J. Agric. Food. Chem.* 64 (2016) 6042–6050.
- [123] D. Zhao, C. Chen, J. Sun, X. Yang, Carbon dots-assisted colorimetric and fluorometric dual-mode protocol for acetylcholinesterase activity and inhibitors screening based on the inner filter effect of silver nanoparticles, *Analyst* 141 (2016) 3280–3288.
- [124] J. Wang, Y. Yan, X. Yan, T. Hu, X. Tang, X. Su, Label-free fluorescent assay for high sensitivity and selectivity detection of acid phosphatase and inhibitor screening, *Sens. Actuators B Chem.* 234 (2016) 470–477.
- [125] P. ReddyPrasad, E.B. Naidoo, N.Y. Sreedhar, Electrochemical preparation of a novel type of C-dots/ZrO₂ nanocomposite onto glassy carbon electrode for detection of organophosphorus pesticide, *Arab. J. Chem.* (2015), <http://dx.doi.org/10.1016/j.arabj.2015.02.012>.
- [126] W. Guan, W. Zhou, J. Lu, C. Lu, Luminescent films for chemo- and biosensing, *Chem. Soc. Rev.* 44 (2015) 6981–7009.
- [127] C.A. Constantine, K.M. Gattás-Asfura, S.V. Mello, G. Crespo, V. Rastogi, T.-C. Cheng, J.J. DeFrank, R.M. Leblanc, Layer-by-Layer biosensor assembly incorporating functionalized quantum dots, *Langmuir* 19 (2003) 9863–9867.
- [128] A. Walcarious, A. Kuhn, Ordered porous thin films in electrochemical analysis, *TrAC Trends Anal. Chem.* 27 (2008) 593–603.
- [129] C. Odendaal, M.T. Seaman, G. Kemp, H.E. Patterton, H.-G. Patterton, An LC-MS/MS based survey of contaminants of emerging concern in drinking water in South Africa, *S. Afr. J. Sci.* 111 (2015) 01–06.



Sifiso Nsibande completed his BSc degree from the University of Swaziland in 2010. After working as a teacher for a year, he completed his BSc Honours and MSc degrees in chemistry at the University of Pretoria, South Africa. His MSc, which was awarded with distinction, focused on pesticide monitoring and dispersion modeling and won him various student awards. In 2016 he received funding from the Water Research Commission and the National Research Foundation of South Africa to proceed with a PhD degree in chemistry. His research focus is on developing sensors using nanomaterials for the detection of organic pollutants.



Patricia Forbes is an Associate Professor in Analytical Chemistry at the University of Pretoria, South Africa where she obtained her PhD (2010). She was previously Environmental Manager in the precious metals industry and Head of the Air Quality Research Laboratory of the CSIR. Her research focuses on the development of novel sampling and analytical methods for environmental pollutants, including denuder based sampling techniques; bio-monitors; and quantum dot based fluorescence sensors. She has served on the executive of the South African Chemical Institute and has received numerous awards.

CHAPTER 4 Advances in the application of nanomaterial-based sensors for detection PAHs in aquatic systems

This chapter consist of a review on the application of nanomaterials in designing a sensor for PAHs. A variety of detection techniques, including fluorescence, were reviewed. The work in this chapter has been published in Trends in Analytical Chemistry.

Paper

S.A. Nsibande, H. Montaseri, P.B.C. Forbes, Advances in the application of nanomaterial-based sensors for detection of polycyclic aromatic hydrocarbons in aquatic systems, *TrAC, Trends Anal. Chem.*, 115 (2019) 52 - 69.

DOI: <https://doi.org/10.1016/j.trac.2019.03.029>



Contents lists available at ScienceDirect

Trends in Analytical Chemistry

journal homepage: www.elsevier.com/locate/trac

Advances in the application of nanomaterial-based sensors for detection of polycyclic aromatic hydrocarbons in aquatic systems



S.A. Nsibandé, H. Montaseri, P.B.C. Forbes*

Chemistry Department, Faculty of Natural and Agricultural Sciences, University of Pretoria, South Africa

ARTICLE INFO

Article history:
Available online 5 April 2019

Keywords:
PAHs
Sensors
Nanomaterials
Fluorescence
SERS
Electrochemical

ABSTRACT

Polycyclic aromatic hydrocarbons (PAHs) are ubiquitous environmental pollutants which are of health concern. It is therefore not surprising that there has been significant research interest in developing sensitive and cost effective strategies for monitoring these compounds. Here we provide an update on applications of various nanomaterials and nanocomposites in the detection and quantification of PAHs in water. Advances in synthesis and tailoring of functional nanomaterials has allowed for their use in fluorescence spectrophotometry, surface-enhanced Raman spectrometry (SERS), and in electrochemical based sensor systems for different analytical applications. This can be attributed to their extensive tunability. Finally, we discuss future prospects on the role of nanoscience in PAH analysis and highlight the need to move towards the development of portable devices based on these nanomaterials for field analysis. This review thus gives an overview of a number of alternative methods to chromatography based analysis of PAHs.

© 2019 Elsevier B.V. All rights reserved.

1. Introduction

Polycyclic aromatic hydrocarbons (PAHs) are a class of organic compounds comprised of fused benzene rings which are of environmental concern because of their negative health effects. These compounds can be introduced into environmental water systems through various ways including industrial activities, biomass burning, and vehicular emissions – among other routes (Fig. 1). As a result, excellent reviews have been documented about their occurrence in air, food, water, sediments and various other matrices, for example [1].

Monitoring of these compounds continues to be of importance as a number of PAHs have been reported to be mutagenic and either carcinogenic or potentially carcinogenic [2,3]. The toxicity of some PAH compounds can further be enhanced by metabolic degradation and photooxidation into derivative compounds [4]. Moreover, in aquatic systems, where PAHs normally occur as mixtures of congeners, their toxicity has been shown to increase compared to that of the individual PAHs due to synergistic effects.

One of the analytical challenges with monitoring of PAHs is that they can occur at very low concentrations in the environment. For

example, a study on the global environmental distribution of PAHs showed that they can be found at concentrations as low as 0.11 ng m⁻³ in air, 0.06 ng L⁻¹ in water and 21 ng g⁻¹ in sediments [5]. Despite such low occurrence concentrations, continuous exposure to these levels can still potentially have adverse effects on organisms. Thus there is a need for the development of sensitive and selective methods for detecting these compounds. Gas chromatography coupled to mass spectrometry has been used as the “gold standard” for PAH analysis methods as reviewed by Bansal et al. [6]. However, chromatography-based methods can present cost challenges in some cases especially in the developing world.

Researchers have been working on using various nanomaterials as sensors and/or platforms as alternative approaches for the sensitive detection of PAHs. In addition, Fe-based magnetic nanoparticles have been widely used as sorbents for the pre-concentration of PAHs prior to chromatographic analysis. The different adsorbents used for isolation of PAHs from environmental samples has been reviewed by Ncube et al. [7]. These adsorbents include those based on silica, molecularly imprinted polymers and nanoparticles and they are therefore not discussed in this review.

Here we review studies where nanomaterials have been used as sensors or supports for the detection of PAH compounds in various matrices. A review on biological techniques for PAH analysis by Kumar et al. [8] highlighted the role of nanoparticles in PAH detection without going into details. Here we expand on this and

* Corresponding author.
E-mail address: patricia.forbes@up.ac.za (P.B.C. Forbes).

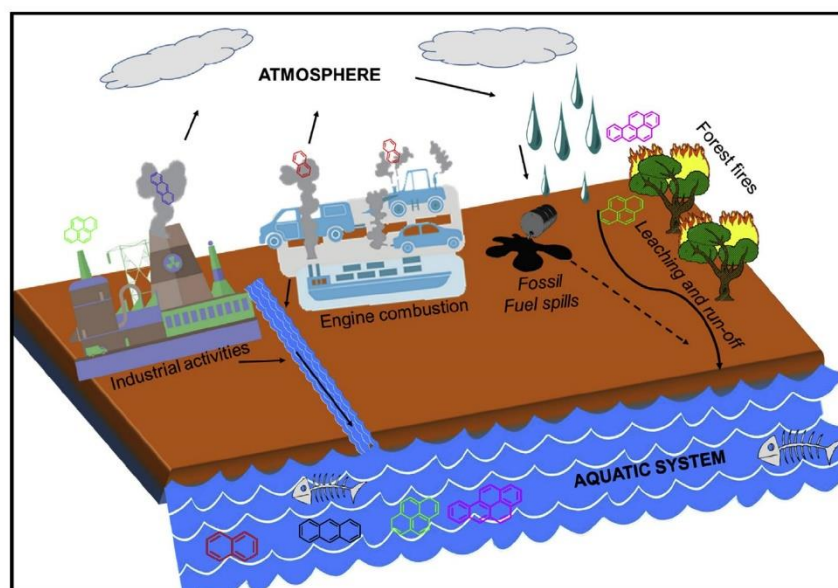


Fig. 1. Schematic illustration of the major sources of PAHs in the environment and their distribution and fate in the ecosystem.

showcase, in detail, the different analytical techniques where nanomaterials are used for PAH analysis. Specifically, our scope focuses on studies where nanomaterials are employed along with detection techniques including fluorescence spectrophotometry, electrochemistry, and Raman spectroscopy for quantification of PAHs in environmental water samples and their metabolites in biological matrices, whilst we exclude the traditional chromatography approaches.

2. Nanomaterials for the fluorescence detection of PAHs

Fluorescence spectrophotometry is a powerful analytical technique that has found many applications in the analysis and monitoring of PAHs due to their fluorescent properties. For example, fluorescence has been widely used in chromatographic systems to detect PAHs. Nanomaterials in fluorescence sensors can play the role of signal transducers and/or energy donors or selective pre-concentration substrates for the target analytes. The ability to modify nanomaterials has allowed for the development of PAH specific receptors, such as those based on macrocyclic molecules, graphene substrates, and molecularly imprinted polymers, leading to highly selective sensor systems. The use of fluorescent nanomaterials, particularly quantum dot-based materials, and their application in sensing of PAHs is discussed in this section and is summarized in Table 1.

2.1. Quantum dot-based PAH fluorescence sensors

Quantum dots (QDs) are crystalline nanomaterials with interesting optical and electronic properties which can be attributed mainly to quantum confinement effects [9]. These properties make them suitable for fluorescence sensing and they have consequently been utilized in various applications in this regard, including PAH detection. The versatile surface chemistry of QDs allows for modifications through various strategies, and has opened doors for encoring receptors which are tailored for specific target analytes [10]. QDs can therefore function as both signal transducers and

receptors in composite materials. The surface interaction of QDs with PAHs may result in energy transfer to or from the QDs thereby leading to a change in the fluorescence intensity of the QDs, allowing for PAH detection.

2.1.1. QD-macromolecule sensors

PAH-specific receptor macromolecules like cyclodextrins (CDs) and calixarenes (CAs) can be encored on QD surfaces to develop a sensor. CDs consist of cyclic oligosaccharides with 6(α -CD), 7(β -CD) or 8(γ -CD) glucose units linked to form a toroidal shape with a hydrophobic cavity and linked glucose units [11]. Thus the cavities can complex with PAHs easily through hydrophobic and guest-host interactions upon formation of inclusion complexes. Because the size of the CD cavity is fixed, only PAH compounds with appropriate molecular size and structure can form an inclusion complex, hence selectivity is attained. As a result, researchers have used CDs and CAs as receptors on QD surfaces for PAH detection.

For example, Li and Qu [12] used this strategy when they embedded CdTe QDs inside silica spheres and thereafter decorated the spheres with CAs to form CA[n]@SiO₂@CdTe nanoparticles for selective detection of PAHs. By using different sizes of CAs, the authors were able to selectively detect anthracene and pyrene using Ca[4]@SiO₂@CdTe and Ca[7]@SiO₂@CdTe, respectively, with corresponding detection limits of 2.45×10^{-8} mol L⁻¹ and 2.94×10^{-8} mol L⁻¹. Han and Li [13] used β -CD modified CdSe/ZnS QDs as a selective probe for anthracene detection down to 1.6×10^{-8} mol L⁻¹.

In a slightly different approach, β - and γ -CDs formed inclusion complexes with PAHs separately, then QDs were introduced to this solution for PAH detection (Fig. 2) [14]. The authors found that in the presence of β -CDs, only phenanthrene selectively quenched the QD fluorescence intensity while in the presence of γ -CDs both acenaphthene and 9,9-difluorofluorene, selectively quenched the fluorescence. This resulted in a linear decrease in fluorescence intensities and they reported detection limits of 0.53×10^{-6} mol L⁻¹ and 0.085×10^{-6} mol L⁻¹ for phenanthrene and acenaphthene respectively. More recently, 1,3-

Table 1

Research studies that use nanomaterials for fluorescence (PL) detection of PAHs in water samples (note: examples based on detection in solvents have been included as they have potential application to water samples).

Sensor	Analyte	Detection range (mol L ⁻¹)	LOD (mol L ⁻¹)	Medium	Ref
L-cys-CdSeTe/ZnSe/ZnS-GO	Phenanthrene	0–0.5 × 10 ⁻⁶	1.07 × 10 ⁻⁹	Millipore water	[23]
	Anthracene		1.46 × 10 ⁻⁹		
	Pyrene		1.29 × 10 ⁻⁹		
	Naphthalene		2.02 × 10 ⁻⁹		
L-cys-CdSeTeS/ZnS- GO	Phenanthrene	0.1–0.5 × 10 ⁻⁶	2.26 × 10 ⁻⁹	Millipore water	[20]
	Pyrene	60 × 10 ⁻⁹ –2 × 10 ⁻⁶	40.2 × 10 ⁻⁹	Water	[18]
GO-CdTe SWCNT–QDs	Pyrene	0.0004–0.05 × 10 ⁻⁶	0.1 × 10 ⁻⁹	River water, tap water, mineral water	[19]
	Benzo[a]pyrene	0.0007–0.05 × 10 ⁻⁶	0.2 × 10 ⁻⁹		
	Benzo[a]anthracene	0.002–0.1 × 10 ⁻⁶	0.7 × 10 ⁻⁶		
	Perylene	0.001–0.05 × 10 ⁻⁶	0.3 × 10 ⁻⁹		
CdSe/ZnS QDs @ sol-gel matrix	Anthracene	0.01–0.1 × 10 ⁻⁶	1.518 × 10 ⁻⁹	Water	[31]
	Phenanthrene	0.01–0.1 × 10 ⁻⁶	5.405 × 10 ⁻⁹		
	Pyrene	0.005–0.05 × 10 ⁻⁶	1.089 × 10 ⁻⁹		
CAD@CdSe	Fluorene	1–10 × 10 ⁻⁹	0.8 × 10 ⁻⁹	Chloroform	[15]
	Anthracene	0–10 × 10 ⁻⁶	16 × 10 ⁻⁹	–	[13]
β-CD-CdSe/ZnS β-CD-CdTe	Phenanthrene	0.5–75 × 10 ⁻⁶	0.53 × 10 ⁻⁶	–	[14]
	Acenaphthene	1.0–25 × 10 ⁻⁶	0.085 × 10 ⁻⁶		
CA[n]@SiO ₂ @CdTe NPs. (n = 4, 7)	Anthracene	0.1–50 × 10 ⁻⁶	24.5 × 10 ⁻⁹		[12]
	Pyrene		29.4 × 10 ⁻⁹		
CdTe-TiO ₂ nano tubes	Benzo[a]pyrene	400 × 10 ⁻⁹ –40 × 10 ⁻¹²	15 × 10 ⁻¹²	Tap water Spring water River water	[25]
Pyrene-Ag NPs- Hg	Pyrene	0.494–2.97 × 10 ⁻⁶	49.4 × 10 ⁻⁹	–	[32]
Pyrene-imprinted polythiophene thin film	Pyrene	0.01–1.0 × 10 ⁻⁶	0.01 × 10 ⁻⁶	–	[30]
MIP (Thymine based copolymers)	Benzo[a]pyrene	0.217–1.98 × 10 ⁻⁹	39.6 × 10 ⁻¹²	DMSO solvent	[27]
Fe ₃ O ₄ -MIPs	Pyrene	0.124–0.445 × 10 ⁻⁶	9.88 × 10 ⁻⁸	Water or acetonitrile/water mixture	[28]

CA = calixarene.

CAD = 1,3-bis(cyanomethoxy)-*tert*-butylcalix[4]arene.

GO = graphene oxide.

MIP = molecularly imprinted polymer.

SWCNT = single-walled carbon nanotubes.

β-CD = β-Cyclodextrin.

DMSO = Dimethyl sulfoxide.

bis(cyanomethoxy)calix [4]arene (CAD) on CdSe QDs were used to develop a probe for fluorene detection in chloroform down to 0.8 × 10⁻⁹ mol L⁻¹ [15].

Despite the promising advantages and application of macromolecule-based sensors, it should be born in mind that

their binding affinity to target analytes can be affected by factors like the binding mechanism, the pH of the medium, stereo-electronic effects, and allosteric effects [16]. Thus such probes could suffer from repeatability limitations in routine applications.

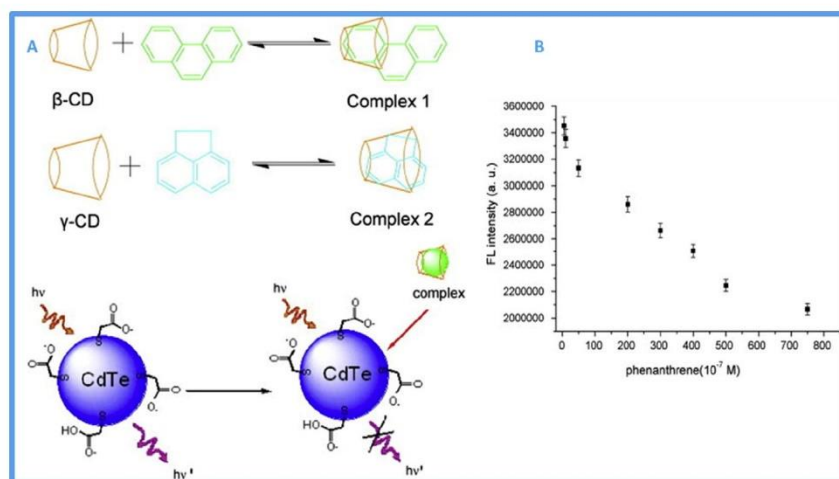


Fig. 2. (A) Illustration of the possible interaction of cyclodextrins with PAHs to form a complex with fluorescence quenching effect upon interaction with CdTe QDs. (B) Change in QD fluorescence intensity with change in phenanthrene concentration [14].

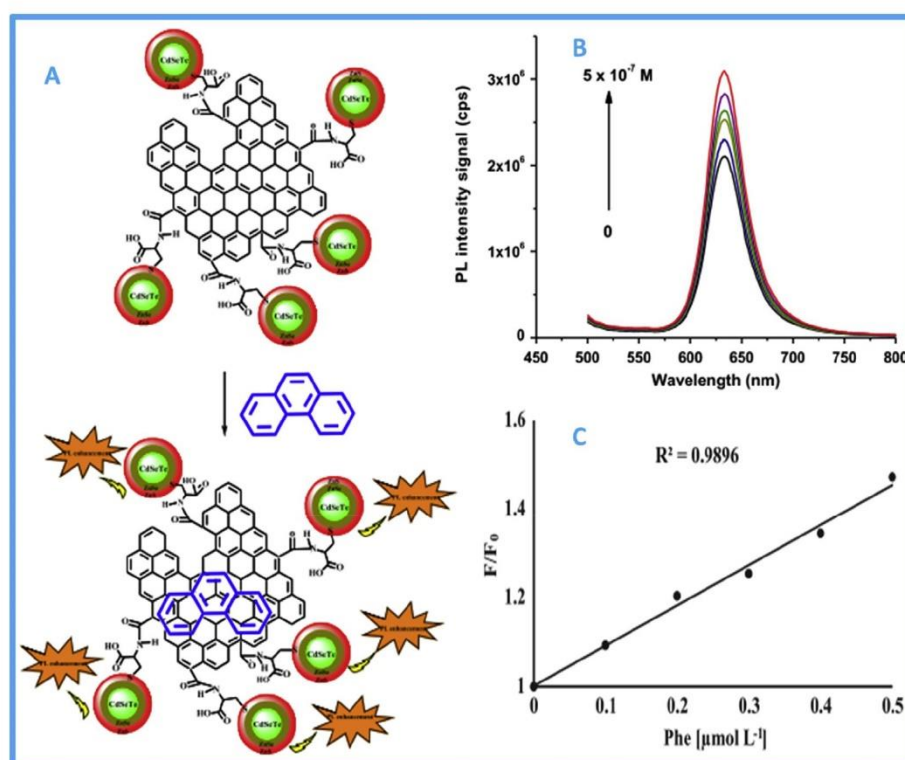


Fig. 3. (A) Schematic illustration of the phenanthrene detection mechanism upon interaction with GO. (B) Fluorescence response of the probe to phenanthrene. (C) Calibration curve showing a linear response of the QD-GO probe to increasing phenanthrene concentration. Adapted from Ref. [23].

2.1.2. QD-graphene nanocomposite sensors for PAH detection

Some researchers, including our group, have developed QD-graphene conjugate systems for fluorescence detection of PAHs [17,18,19,20]. These sensing systems make use of the unique properties of graphene which include a large surface area with delocalized π electrons which can adsorb and pre-concentrate the planar PAHs due to the fused benzene rings in their structure. PAHs have been shown to interact with graphene through physisorption and the adsorption energy increases with the number of rings [21,22].

Adegoke and Forbes [23] fabricated L-cysteine capped CdSeTe/ZnSe/ZnS QDs and conjugated them to graphene oxide (GO) to form a QD-GO nanocomposite for detection of PAHs in aqueous solutions (Fig. 3). The probe showed fluorescence enhancement with increasing concentration of PAHs and was used to detect ubiquitous PAHs including phenanthrene, anthracene, pyrene and naphthalene. Amongst the studied PAHs, phenanthrene showed the most significant fluorescence enhancement and could be detected down to $1.07 \times 10^{-9} \text{ mol L}^{-1}$. The success of the probe was attributed to strong π - π interactions of the PAH molecules with the graphene nano-sheets which brought them in close proximity to the QDs allowing for energy transfer to occur. A similar study was reported by Adegoke et al. [20] where CdSeTe/ZnS QDs were used instead, but the detection limit ($2.26 \times 10^{-9} \text{ mol L}^{-1}$ for phenanthrene) was slightly higher with this approach.

Another QD-graphene probe (Fig. 4) consisting of mercaptoacetic acid-capped CdTe QDs as signal transducers was reported by Wang et al. [18] for detection of pyrene. However, unlike the probe

reported by Adegoke and Forbes [23], they observed quenching of the fluorescence intensity with increasing pyrene concentration. This was attributed to photoinduced electron transfer (PET) whereby, upon excitation, the excited electrons of the QDs were transferred to pyrene through the π -conjugated system of graphene. Using this system they could detect pyrene down to $40.2 \times 10^{-9} \text{ mol L}^{-1}$. It is important to note that both studies demonstrated the affinity of graphene towards the planar structures of PAHs, making it useful as an adsorption surface for sensor development.

Other materials that have been used include single-walled carbon nanotubes [24] and titanium oxide (TiO_2) nanotubes [25] which also serve as adsorption surfaces to bring the PAHs closer to the QDs to improve energy transfer and allow for detection.

For all the systems, the main drawback is that they do not offer much selectivity since they rely on surface π - π interaction of the PAHs and graphene, which may also occur for other planar organic structures. Thus developing strategies to improve selectivity could lead to more practical use of these probes. On the upside however, these probes may be used for class identification or screening of samples for PAHs as a class of compounds prior to more selective analysis.

A drawback of the QD-based probes is that there is concern regarding the use of cadmium in the core which has the potential to leach and further pollute the environment after discarding the probes. Over-coating the cadmium core with less toxic shells has been seen to reduce this leaching risk [26]. Recently there has been a new drive towards non-cadmium based QDs like graphene

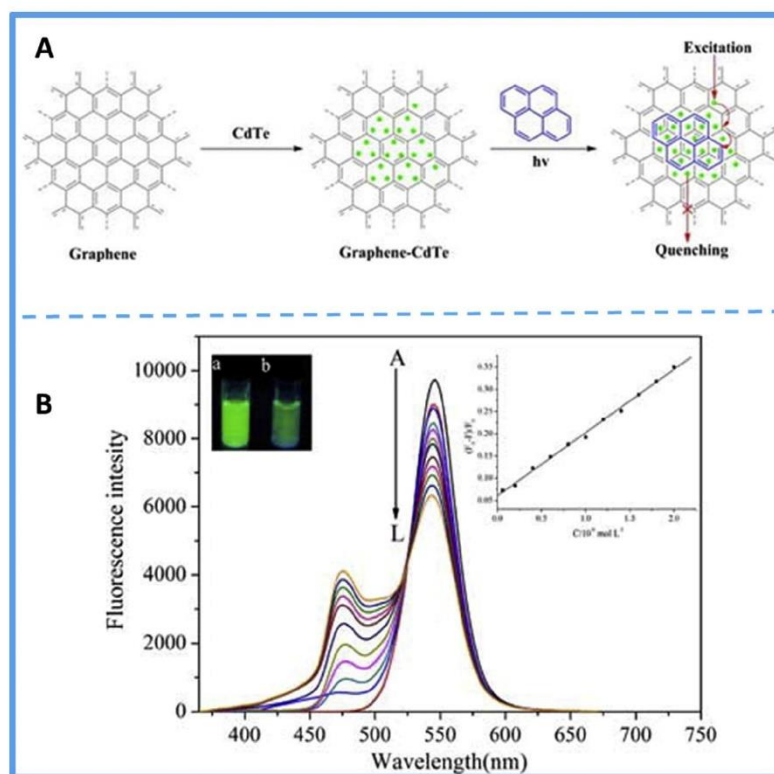


Fig. 4. (A) Schematic illustration of the pyrene detection mechanism. (B) Fluorescence quenching spectra of graphene–CdTe quantum dot nanocomposites upon addition of pyrene. Experimental conditions: graphene-cadmium telluride quantum dot nanocomposites, $2.0 \times 10^{-3} \text{ mol L}^{-1}$; pyrene (A–L; $0\text{--}2.0 \times 10^{-6} \text{ mol L}^{-1}$). Inset: fluorescence of graphene–cadmium telluride quantum dot nanocomposites in the (a) absence and (b) presence of pyrene. Adapted with permission from Ref. [18] Copyright (2015) Taylor & Francis.

quantum dots (GQDs) which could be better substitutes in developing PAH probes in future.

2.2. MIP-based fluorescence sensors for PAHs

Molecularly imprinted polymers (MIPs) are typically prepared by polymerization of compatible monomer units in the presence of template molecules, which in most cases is the analyte of interest. The template is thereafter removed from the resulting polymer, leaving recognition sites which can be used for selective re-binding of the target analyte during sensing. The interest in using MIPs as artificial receptors is mainly due to their low cost, ease of preparation, and their high mechanical and chemical stability. Some researchers use the MIPs in conjunction with nanoparticles for enhanced signal transduction. A number of fluorescent MIP-based sensors have been designed for selective detection of PAHs [27,28,29,30]. For example, Tiu et al. [30] fabricated a polythiophene MIP nanofilm on a gold surface for selective detection of pyrene (Fig. 5). The selectivity of the film was attributed to complementary binding sites and its ability to form π -donor and hydrogen bonding interactions with pyrene. Interaction of the nanofilm with pyrene produced a distinct fluorescence emission peak at 408 nm which was not observed in the non-imprinted polymer (NIP) nanofilms. The fluorescence response of the nanofilm to pyrene was linearly proportional to pyrene concentration within the $0.01\text{--}1.0 \times 10^{-6} \text{ mol L}^{-1}$ range, thus this sensor has promise for pyrene detection in environmental aquatic systems,

however the use of gold may have cost implications limiting its application.

Despite the success of MIP-based sensors, there are still challenges. For example, the process of effectively extracting the template molecules can be tedious and requires the use of large volumes of solvent, and could result in unintended fouling of the MIP, although progress is being made in overcoming these challenges. Furthermore, the long incubation time required for effective interaction can be disadvantageous when designing rapid sensing materials which are required in environmental monitoring.

3. Nanoparticles in SERS-based systems for detection of PAHs

Surface-enhanced Raman scattering (SERS), illustrated in Fig. 6, is becoming a popular analytical technique that is being employed for quantitative detection of PAHs in various media. The technique is based on the intrinsic vibrational modes of the analyte molecules, thus it can offer direct identification. But since this signal can be very weak in molecules such as PAHs, it can be enhanced or improved by making use of plasmonic nanostructures, or by using the extrinsic SERS signal from reporter molecules which only increases in the presence of the target analyte. SERS-based sensors have a number of unique advantages [33] that make the technique suitable for sensor development, including: (i) a unique spectral signature which allows for intrinsic molecular fingerprint information for target analytes identification (ii) ultrahigh sensitivity, down to single molecule levels (iii) the SERS substrate can be

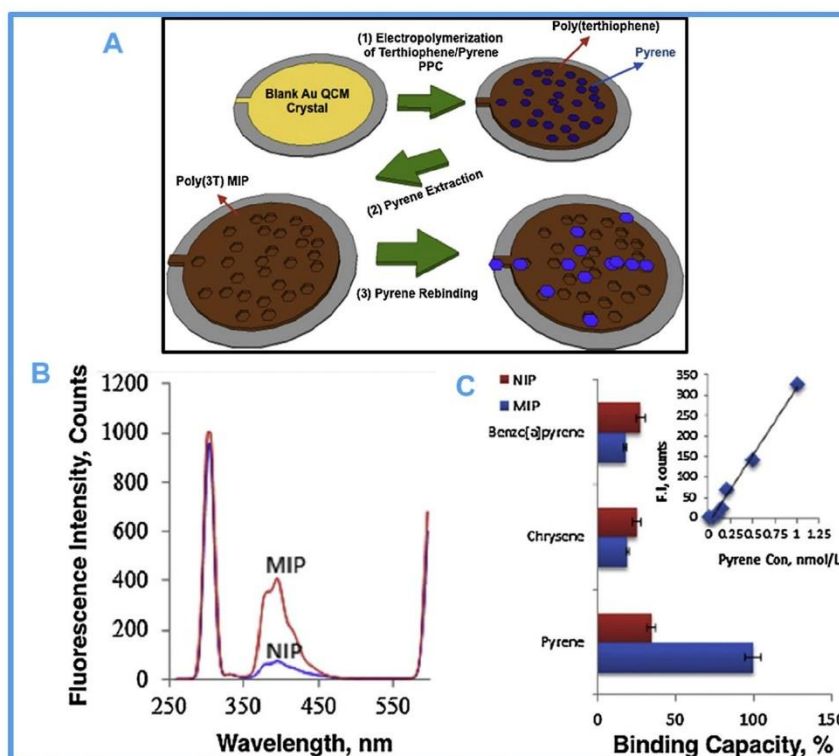


Fig. 5. (A) Schematic fabrication of pyrene-imprinted polyterthiophene (poly(3T)) thin film sensor (QCM = quartz crystal microbalance; PPC = pre-polymerization complex). (B) Fluorescence spectra showing the difference between MIP and NIP after pyrene binding. (C) MIP and NIP selective binding of pyrene. The inset shows the fluorescence response as a function of pyrene concentration. Adapted from Ref. [30].

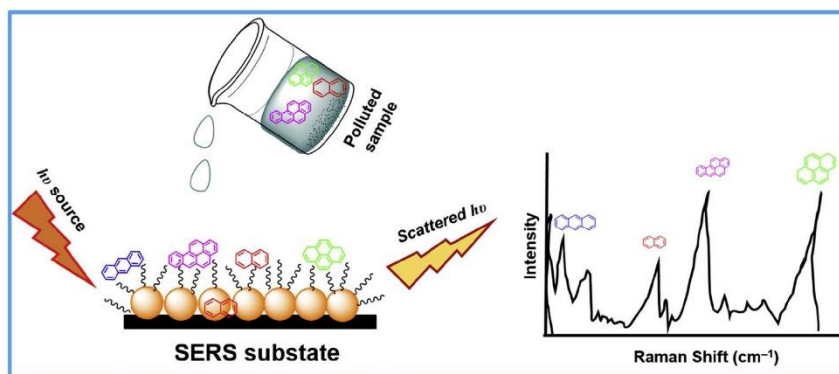


Fig. 6. Schematic illustration of SERS analysis and multiple analyte detection. SERS substrates can be modified via different strategies to facilitate adsorption of PAHs. The SERS spectrum is unique for each analyte.

modified by encoring size- and shape-specific plasmonic nanostructures for the desired sensing purpose (iv) SERS allows for multiple analytes to be detected simultaneously due to the narrow bandwidth of the spectra (v) the technique requires little or simple sample preparation and it is not affected by water.

Despite these attractive advantages, the SERS technique has some challenges which should be overcome for it to be used in sensor development. Firstly, strong contact between the analyte and the SERS substrate (usually silver/copper/gold substrates

which are roughened) must be established in order for the analyte's vibrational modes to be enhanced during measurements. Secondly, the continuous use and exposure of the SERS substrates to the incident laser beam can degrade the substrate and lead to a decrease in signal enhancement and, by extension, a decrease in sensitivity and poor repeatability and reproducibility. This needs serious consideration when designing re-useable sensor platforms. Thirdly, the substrates are by themselves not selective to target analytes and they therefore need to be chemically engineered or

Table 2

Summary of nanomaterials using different types of affinity agents for surface-enhanced Raman scattering (SERS) detection of polycyclic aromatic hydrocarbons (PAHs) in water samples (note: studies based on detection in solvents have been included as they have potential application to water samples).

Type of affinity agent	Sensor or substrate	Analyte	Linear range	LOD	Matrix/test solvent	Ref.
Macromolecule	β -CD dimer@Ag@SiO ₂ NPs	Perylene	$1 \times 10^{-6} - 10^{-2} \text{ mol L}^{-1}$	$0.1 \times 10^{-6} \text{ mol L}^{-1}$	DCM	[43]
		Anthracene	$1 \times 10^{-5} - 7.5 \times 10^{-3} \text{ mol L}^{-1}$	$10 \times 10^{-6} \text{ mol L}^{-1}$	Water	[41]
	β -CD-Ag NPs	Pyrene	$7.5 \times 10^{-6} - 5 \times 10^{-4} \text{ mol L}^{-1}$	$7.5 \times 10^{-6} \text{ mol L}^{-1}$		
		Anthracene	$1 \times 10^{-7} - 1 \times 10^{-4} \text{ mol L}^{-1}$	$0.1 \times 10^{-6} \text{ mol L}^{-1}$	–	[42]
	β -CD-Au NPs	Pyrene	$1 \times 10^{-8} - 1 \times 10^{-4} \text{ mol L}^{-1}$	$0.01 \times 10^{-6} \text{ mol L}^{-1}$		
		Anthracene	$2.5 - 10 \times 10^{-9} \text{ mol L}^{-1}$	$0.8 \times 10^{-9} \text{ mol L}^{-1}$	–	[47]
	β -CD-SH-AuNPs/PGMA- β -CD	Pyrene	$10 - 25 \times 10^{-9} \text{ mol L}^{-1}$	$2.4 \times 10^{-9} \text{ mol L}^{-1}$		
		Anthracene	$0 - 2 \times 10^{-9} \text{ mol L}^{-1}$	$2 \times 10^{-9} \text{ mol L}^{-1}$	Sea water	[46]
	GNPS-DSNB	Benzo[a]pyrene	$1 \times 10^{-9} - 1 \times 10^{-3} \text{ mol L}^{-1}$	$0.485 \times 10^{-9} \text{ mol L}^{-1}$	River water, spring water, tap water	[48]
	Au NPs- modified alginate gel network	Benzo[a]pyrene	$0.5 - 400 \times 10^9 \text{ mol L}^{-1}$	$0.5 \times 10^9 \text{ mol L}^{-1}$	Artificial sea water	[40]
Au NPs-DMCX	Pyrene	$0.5 - 80 \times 10^9 \text{ mol L}^{-1}$	$0.5 \times 10^9 \text{ mol L}^{-1}$			
Magnetic NPs	Fe ₃ O ₄ @Ag	Anthracene	$1 - 50 \text{ mg L}^{-1}$	$0.8 \times 10^6 \text{ mol L}^{-1}$	–	[38]
		Perylene	$1 - 50 \text{ mg L}^{-1}$	$0.8 \times 10^6 \text{ mol L}^{-1}$		
		Benzo[a]pyrene	$1 - 50 \text{ mg L}^{-1}$	$1 \times 10^{-6} \text{ mol L}^{-1}$		
		Pyrene	$1 - 50 \text{ mg L}^{-1}$	$5 \times 10^{-6} \text{ mol L}^{-1}$		
		Anthracene	$1 - 50 \text{ mg L}^{-1}$	$20 \times 10^{-6} \text{ mol L}^{-1}$		
	Fe ₃ O ₄ @AuNRs assemblies	Phenanthrene	$1 - 100 \text{ mg L}^{-1}$	$0.1 \times 10^{-9} \text{ mol L}^{-1}$	–	[49]
		PAHs (not specified)	$1 \times 10^{-10} - 1 \times 10^{-7} \text{ mol L}^{-1}$	$0.1 \times 10^{-9} \text{ mol L}^{-1}$	–	[39]
	Fe ₃ O ₄ @Au core-satellite MNPs	16 EPA priority PAHs	$2 - 1000 \times 10^{-9} \text{ mol L}^{-1}$	$100 - 5 \times 10^{-9} \text{ mol L}^{-1}$	–	[50]
	Au/PCTP on magnetic microparticles	Naphthalene	$1.5 - 16 \text{ } \mu\text{g mL}^{-1}$	$0.3 \text{ } \mu\text{g mL}^{-1}$	Water	[50]
	Other (or bare substrate)	Au NPs-SiO ₂	Naphthalene	$1.1 - 10 \text{ ppm}$	10 ppb	Artificial sea water
Pyrene		$1.2 - 0.1 \text{ ppm}$				
Polymers	Au-PS beads on SiO ₂ (quartz)	Naphthalene	$1 - 20 \text{ ppm}$	1 ppm	Distilled water	[52]
		Acenaphthene	$50 - 1000 \text{ ng mL}^{-1}$	$> 1000 \text{ } \mu\text{g mL}^{-1}$	MeOH solution	[36]
	AgNR (silver nanorod array substrates)	Acenaphthylene		$> 100 \text{ } \mu\text{g mL}^{-1}$		
		Anthracene		$50 \text{ } \mu\text{g mL}^{-1}$		
	N-TMDS-Ag NPs	Benz[a]anthracene		$100 \text{ } \mu\text{g mL}^{-1}$		
		Benzo[a]pyrene		$50 \text{ } \mu\text{g mL}^{-1}$		
	Hydrophobic gold nanostructures	Fluorene		$100 \text{ } \mu\text{g mL}^{-1}$		
		Pyrene		$10 \text{ } \mu\text{g mL}^{-1}$		
	AuNPs- GMA-EDMA	Pyrene		$100 \times 10^{-6} \text{ mol L}^{-1}$	Acetone solution	[53]
		Anthracene				
pNIPAM-Coated Nanostars	2,3-dihydroxy naphthalene					
	Fluoranthene	$0.02 - 200 \times 10^{-6} \text{ mol L}^{-1}$	$6.7 \times 10^{-9} \text{ mol L}^{-1}$	–	[54]	
AgNO ₃ - PVP dendrites	Anthracene	$1 \times 10^{-7} - 5 \times 10^{-5} \text{ mol L}^{-1}$	$0.93 \times 10^{-7} \text{ mol L}^{-1}$	Water	[55]	
	Phenanthrene	$5 \times 10^{-7} - 5 \times 10^{-5} \text{ mol L}^{-1}$	$4.5 \times 10^{-7} \text{ mol L}^{-1}$			
IP ₆ -Au NPs	Pyrene	$5 \times 10^{-7} - 5 \times 10^{-5} \text{ mol L}^{-1}$	$1.1 \times 10^{-7} \text{ mol L}^{-1}$			
	Pyrene			Gas phase	[56]	
Hydroxylamine reduced Ag NPs	Fluoranthene	$0.45 \times 10^9 - 1 \times 10^5 \text{ mol L}^{-1}$	$0.45 \times 10^9 \text{ mol L}^{-1}$	–	[57]	
	Benzo[a]pyrene	$1 \text{ g L}^{-1} - 1 \text{ } \mu\text{g L}^{-1}$	$1 \text{ } \mu\text{g L}^{-1}$	EtOH solution	[44]	
Citrate-Au NPs	Naphthalene	$1 \times 10^{-6} - 1 \times 10^{-12} \text{ mol L}^{-1}$	$1 \times 10^{-12} \text{ mol L}^{-1}$	Aqueous solutions	[58]	
	Phenanthrene	$1 \times 10^{-6} - 1 \times 10^{-9} \text{ mol L}^{-1}$	$0.1 \times 10^{-9} \text{ mol L}^{-1}$			
Ag NPs - LG	Naphthalene		$5 \times 10^{-6} \text{ mol L}^{-1}$	River water	[59]	
	Anthracene		$1 \times 10^{-6} \text{ mol L}^{-1}$			
Ag NPs - LG	Pyrene		$0.5 \times 10^{-6} \text{ mol L}^{-1}$			
	benzo[a]pyrene		$0.5 \times 10^{-6} \text{ mol L}^{-1}$			
Ag NPs - LG	Benzo[g,h,i]perylene		$0.25 \times 10^{-6} \text{ mol L}^{-1}$			
	Indeno[1,2,3-cd]pyrene		$0.25 \times 10^{-6} \text{ mol L}^{-1}$			
Ag NPs - LG	Anthracene	$1 - 100 \times 10^{-6} \text{ mol L}^{-1}$	$1 \times 10^6 \text{ mol L}^{-1}$	–	[60]	
	Pyrene		$1 \times 10^7 \text{ mol L}^{-1}$			
Ag NPs - LG	Benzo[c]phenanthrene		$1 \times 10^7 \text{ mol L}^{-1}$			
	Triphenylene		$1 \times 10^{-7} \text{ mol L}^{-1}$			
Ag NPs - LG	Chrysene		$1 \times 10^{-8} \text{ mol L}^{-1}$			

GNS-DS-C ₁₀ H ₂₁	Benzo[a]pyrene Fluoranthene	10 ⁻⁶ –10 ⁻³ g L ⁻¹	0.1 × 10 ⁻⁶ mol L ⁻¹ 0.32 × 10 ⁻⁶ mol L ⁻¹ Naphthalene	Water:MeOH (9:1 v/v)	[45]
31 × 10 ⁻⁶ mol L ⁻¹ HAs-Ag NPs	Anthracene Fluoranthene Pyrene 3,4-Benzopyrene	5.8 × 10 ⁻⁷ – 3.5 × 10 ⁻⁴ mol L ⁻¹ 8.3 × 10 ⁻⁷ – 2.5 × 10 ⁻⁴ mol L ⁻¹ 7.5 × 10 ⁻⁷ – 3.5 × 10 ⁻⁴ mol L ⁻¹ 8.5 × 10 ⁻⁸ – 1.5 × 10 ⁻⁵ mol L ⁻¹	4.8 × 10 ⁻⁷ mol L ⁻¹ 1.3 × 10 ⁻⁷ mol L ⁻¹ 5.5 × 10 ⁻⁷ mol L ⁻¹ 1.3 × 10 ⁻⁷ mol L ⁻¹	Acetone solution	[61]
Au film@C6-Au NPs	Benzo[b]fluoranthene Fluoranthene Benzo[a]anthracene Pyrene	10 ⁻³ – 1.2 × 10 ⁻⁸ mol L ⁻¹ 10 ⁻³ – 2.0 × 10 ⁻⁸ mol L ⁻¹ 10 ⁻³ – 5.5 × 10 ⁻⁸ mol L ⁻¹ 6.3 × 10 ⁻⁸ mol L ⁻¹	1.2 × 10 ⁻⁸ mol L ⁻¹ 2.0 × 10 ⁻⁸ mol L ⁻¹ 5.5 × 10 ⁻⁸ mol L ⁻¹ 6.3 × 10 ⁻⁸ mol L ⁻¹	MeOH solution	[62]

Ag NPs – LG = silver nanoparticles (NPs) functionalized with the molecular assembler bis-acridinium dication lucigenin (LG) AgNO₃ – PVP dendrites = polyvinylpyrrolidone.

AgNR = silver nanorod array substrates.

Au NPs = gold nanoparticles.

Au/PCTP = gold modified with pentachlorothiophenol

AuNPs - GMA-EDMA = gold nanoparticles - glycidyl methacrylate-ethylene dimethacrylate.

Au-PS = polystyrene beads coated with gold nanoparticles.

DMCX = 5, 27-dimercaptoacetic acid-26, 28-dihydroxy-4-terbutyl calix [4]arene.

GNS-DSNB = gold nanoparticles labeled with 5,5'-dithiobis(succinimidyl-2-nitrobenzoate).

GNS = gold nanostructures.

GNS-DS-C₁₀H₂₁ = gold nanostructures - 4-dodecyl benzenediazonium-tetrafluoroborate.

HAs-Ag NPs = Humic acid decorated silver nanoparticles.

IP₆-Au NPs = inositol hexaphosphate stabilized gold nanoparticles.

N-TMDS-Ag NPs = nitrogen doped transition metal dichalcogenides in silver nanoparticles.

pNIPAM = poly-N-isopropylacrylamide (pNIPAM).

PTH-Ag NPs = 1-propanethiol-modified silver nanoparticles.

β-CD-SH-AuNPs/PGMA-β-CD = per-6-deoxy-(6-thio)-β-cyclodextrin modified gold nanoparticles on β-cyclodextrin containing poly(glycidyl methacrylate).

β-CD = β-Cyclodextrin.

modified to enhance selectivity [34]. There are various strategies that researchers have used to overcome some of these challenges and these include the use of (i) reactions (ii) antigen-antibodies (iii) aptamers (iv) polymers (v) alkanethiols and (vi) cyclic macromolecules e.g. calixarenes [35]. The limitation that comes with modification of the SERS substrate is that it may lead to the so-called “first-layer effect” where a large portion of the signal is from the functionalized substrate and not the analyte itself. This may also complicate the spectrum leading to wrong assignment of analyte peaks [36].

A number of authors have exploited SERS techniques for detection of PAHs as summarized in Table 2 and some examples from these studies are discussed in the following sections.

3.1. Magnetic SERS sensors for PAHs

Magnetic nanoparticles (MNPs) have found application in SERS sensors where they can be coupled to plasmonic NPs for detection of PAHs. Some of the attractive properties of MNPs in SERS sensors include (i) enhancement of the vibrational signal (ii) their magnetic properties allow for extraction and enrichment of the target analyte thereby improving sensitivity (iii) they can be reused and (iv) biocompatibility allows for their conjugation to receptors like antibodies and aptamers for bio-sensing [37]. For example, Du and Jing [38] used Fe₃O₄ magnetic nanoparticles which they passivated with Ag NPs which were further functionalized with 1-pentanethiol for detection of benzo[a]pyrene, perylene, pyrene, phenanthrene and anthracene (Fig. 7). Upon interaction of the Fe₃O₄@Ag-thiol core-shell NPs with the PAH-containing solution, the PAHs were adsorbed and pre-concentrated. A magnetic field was then applied for isolation of the NPs followed by detection. Du et al. [39] used Fe₃O₄@Au core/shell NPs for on-site detection of 16 EPA priority PAHs in river water using a portable Raman spectrometer and achieved detection limits ranging from 5–100 × 10⁻⁹ mol L⁻¹.

3.2. Macromolecule-based SERS sensors for PAHs

As discussed in Section 2.1.1, macromolecules like cyclodextrins (CDs) and calixarenes (CAs) can be used to modify SERS nanoparticles for selective detection of target PAHs, mainly pyrene [40,41,42,43]. For example, Hahm et al. [43] used β-CD dimer-immobilized Ag assembly embedded on silica NPs (Fig. 8) for selective SERS detection of perylene. The β-CD dimer@Ag@SiO₂ sensor was sensitive and had a linear response between 1 × 10⁻⁷ and 1 × 10⁻² mol L⁻¹ and they found the LOD to be 1 × 10⁻⁸ mol L⁻¹.

Although the application of these sensors is promising, they suffer from the same limitations of using macrocycle receptors as discussed in Section 2.1.1.

3.3. Other receptor ligand modified SERS sensors

Various ligands and alkyl chains can be used to functionalize the nanoparticles in SERS substrates and play an important role in improving the affinity of the substrates towards the target analyte. For example, inositol hexaphosphate stabilized gold nanoparticles (IP₆-Au NPs) have been used for detection of benzo[a]pyrene in ethanol solutions [44]. The authors reported that the IP₆ increased the hydrophobic capacity of the gold substrate, thereby increasing its affinity for the PAH compounds in oil. Studies by Tijunelyte et al. [45] used 4-dodecyl benzenediazonium-tetrafluoroborate (DS-C₁₀H₂₁) to functionalize gold nanorods (Fig. 9) for detection of benzo[a]pyrene (LOD = 0.1 × 10⁻⁶ mol L⁻¹), fluoranthene (LOD = 0.32 × 10⁻⁶ mol L⁻¹) and naphthalene

(LOD = 31 × 10⁻⁶ mol L⁻¹). They showed that the DS-C₁₀H₂₁ layer could pre-concentrate the non-polar PAHs on the surface of the gold substrate and this they attributed to hydrophobic and/or π–π interactions. Since these interactions are weak, the authors showed that it was possible to regenerate the surface by simply washing the surface with methanol for 30 min. The variation after several wash and detection steps was found to be 11% which is promising for designing reusable sensors. Furthermore, they showed that the sensor was able to detect the three PAHs in a mixture using their characteristic Raman peaks, however, quantitation of the individual PAHs was a challenge due to spectral overlap.

3.4. Bio-modified SERS nanosensors

Biological receptors like antibodies can be immobilized on the various SERS nanoparticle substrates for sensitive detection of PAHs. The advantage of such sensing systems is that the antibodies can offer high specificity and sensitivity. For example, Dribek et al. [46] labeled gold nanoparticles (GNPs) with a Raman reporter, 5,5'-dithio-bis(succinimidyl-2-nitrobenzoate) (DSNB) which they then functionalized with monoclonal antibodies (*anti*-BaP) to develop a SERS immunoassay sensor for the detection of the benzo[a]pyrene in sea water (Fig. 10). The GNPs/DSNB/*anti*-BaP sensor was sensitive for benzo[a]pyrene allowing for detection down to 2 × 10⁻⁹ mol L⁻¹. Despite the success of this method, improvement in the reproducibility is needed in order to confirm effectiveness of the detection method, which could then be applied to other PAHs.

4. Nanomaterial-based electrochemical systems for PAH detection

The development of nanomaterial-based electrochemical sensors has found a number of applications in the analysis of PAHs (Table 3). The growing interest in electrochemical sensors can be attributed to the requirement of low cost instrumentation which uses low power and yet can be very sensitive to target analytes, and this has contributed to the success of this technique in PAH analysis. Moreover, the simple electronic setup of electrochemical systems opens prospects for designing portable devices for field monitoring of real samples.

In general, the measurable parameters in electrochemical sensors include (i) current (amperometry or voltammetry), (ii) potential difference (potentiometry) and (iii) impedance or electrochemical impedance spectroscopy (EIS). Amongst these techniques, voltammetry methods have found a lot of application as sensors for PAHs and these involve scanning the potential over a set range and monitoring the current response. The current results from the redox processes at the surface of the working electrodes and is therefore proportional to the analyte concentration. The different types of techniques include cyclic voltammetry (CV), differential pulse voltammetry (DPV), square-wave voltammetry (SWV) and linear sweep voltammetry (LSV).

The sensitivity and selectivity of electrochemical systems can be achieved through various modification strategies of the working electrodes, and nanomaterials have found application in this regard. By making use of nanomaterials one can achieve unique electrical and chemical properties and this can be exploited to offer improved response speed, sensitivity and selectivity for targeted PAHs in various matrices [63]. The synergistic effects of nanomaterials on the catalytic activity of electrodes can enhance signal transduction and therefore allow for the development of ultra-sensitive electrochemical systems [64]. Modification of electrodes with biological agents has also been used to design electrochemical biosensors and is discussed separately in Section 4.3.

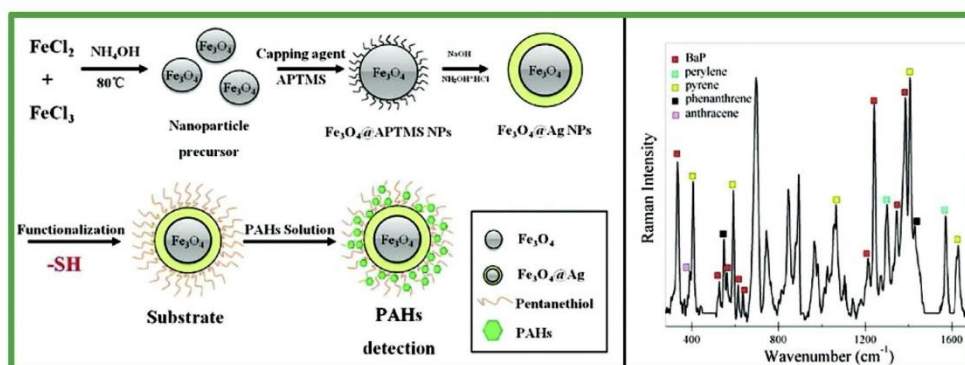


Fig. 7. Schematic representation of the procedure for SERS detection of PAHs. Reprinted with permission from Ref. [38]. Copyright (2011) American Chemical Society.

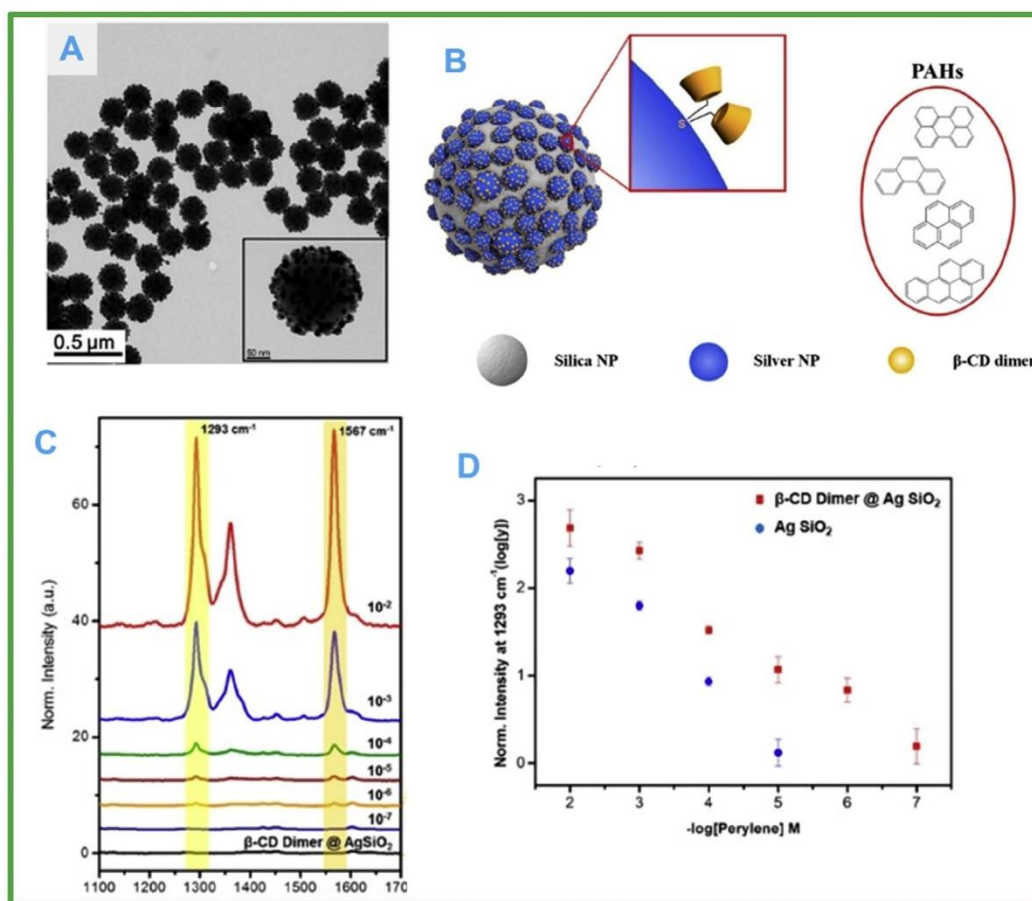


Fig. 8. (A) TEM images of single Ag@SiO₂ NPs and distribution of Ag@SiO₂ NPs in ethanol. (B) Schematic illustration of CD dimer-immobilized Ag assembly with embedded silica NPs for detection of PAHs. (C) SERS spectra of β-CD dimer@Ag@SiO₂ NPs at 1×10^{-2} mol L⁻¹ to 1×10^{-7} mol L⁻¹. (D) Normalized SERS intensities of β-CD dimer@Ag@SiO₂ and Ag@SiO₂ with perylene at 1293 cm⁻¹. Adapted from Ref. [43].

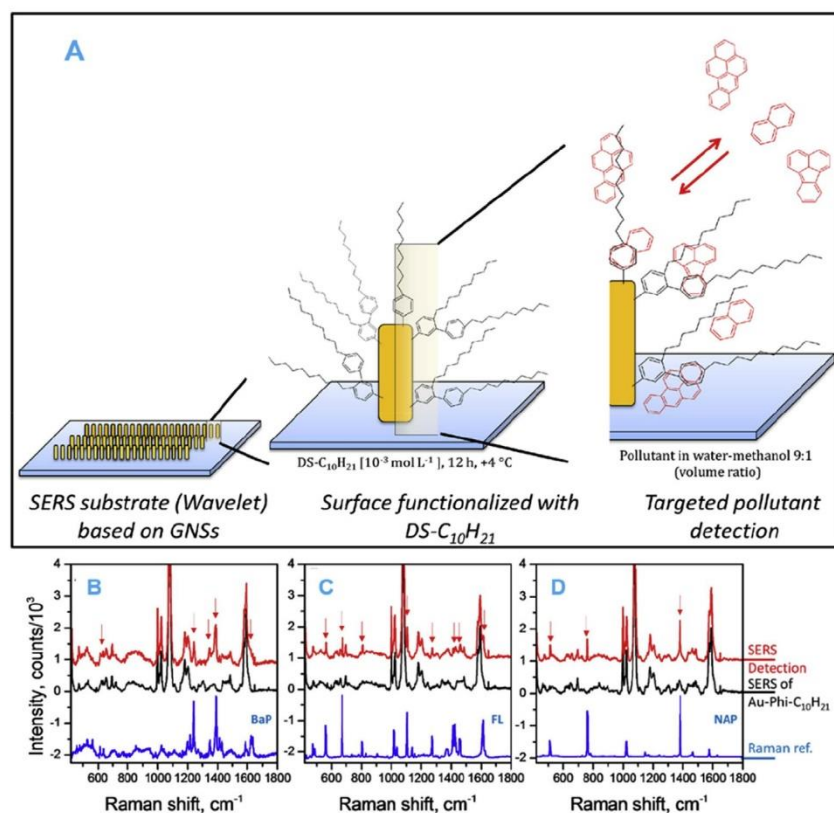


Fig. 9. (A) Schematic illustration of nanosensor surface functionalization and pre-concentration of the targeted compounds via weak interactions. Gold Nanostructures GNSs, DS-C₁₀H₂₁, 4-dodecyl benzenediazonium-tetrafluoroborate diazonium salt. (B – D) SERS detection of benzo[a]pyrene (BaP) at 0.75 mg L⁻¹, fluoranthene (FL) at 5 mg L⁻¹, and naphthalene (NAP) at 50 mg L⁻¹ (C) using gold nanostructures (GNSs) functionalized with diazonium salt (Au-Phi-C₁₀H₂₁). Adapted from Ref. [45].

A broad review on electrochemical devices for European Union (EU) priority pollutants was published by Díaz-González et al. [65] which focused on heavy metals, pesticides, hydrocarbons, halogenated hydrocarbons and alkyl phenols. Other reviews [63] on electrochemical detection of chemical contaminants focused on heavy metal ions, inorganic anions, pesticides, phenolic compounds, and chemical warfare agents – and did not include application to PAHs. Thus this section of our review is dedicated to applications of nanomaterial-based electrochemical sensors specifically for the detection of PAHs and these are summarized in Table 3.

4.1. Graphene-based electrochemical PAH sensors

Graphene nanomaterials have a number of attractive properties that make them suitable for application as electrochemical sensors, including inertness, large surface area, thermal stability, and high conductivity due to the delocalized π electrons. They also exhibit wide electrochemical potential windows and low resistance to charge-transfer. The electron transfer behavior in graphene shows that it has well-defined redox peaks and the redox processes are predominantly diffusion controlled [66]. Furthermore, graphene is a versatile material and can be modified with various catalytic NPs

to improve its redox activity and to enhance the voltammetric response in sensor systems. In PAH sensing systems, graphene can also serve as a pre-concentration substrate onto which the PAH can adsorb via π - π interactions as discussed in Section 2.1.2.

Therefore, a number of graphene-based composite nanomaterials have been fabricated for the detection of PAHs [67,68,69,70]. For example, Tovide et al. [68] fabricated a graphenated-polyaniline (GR-PANI) nanocomposite and used it to modify a glassy carbon electrode (GCE) for the detection of anthracene (LOD = 4.4×10^{-9} mol L⁻¹) using square-wave voltammetry (SWV) as shown in Fig. 11. In similar work, Tovide et al. [67] further modified the GR-PANI composite with tungsten oxide (WO₃) to form a graphenated polyaniline/tungsten oxide (PANI/WO₃/GR) nanocomposite which they used for detection of phenanthrene. They found that the incorporation of tungsten improved the sensitivity of the material due to its large surface-to-volume ratio and its ability to form different oxidation states. Thus they could detect phenanthrene down to 0.123×10^{-12} mol L⁻¹ in waste water, which is orders of magnitude below the 1.12×10^{-9} mol L⁻¹ limit as required by the World Health Organization (WHO) for phenanthrene. A drawback of such a sensor system, however, is the cost of the tungsten, thus cheaper metal oxides that could offer similar or better voltammetric enhancements may need to be investigated.

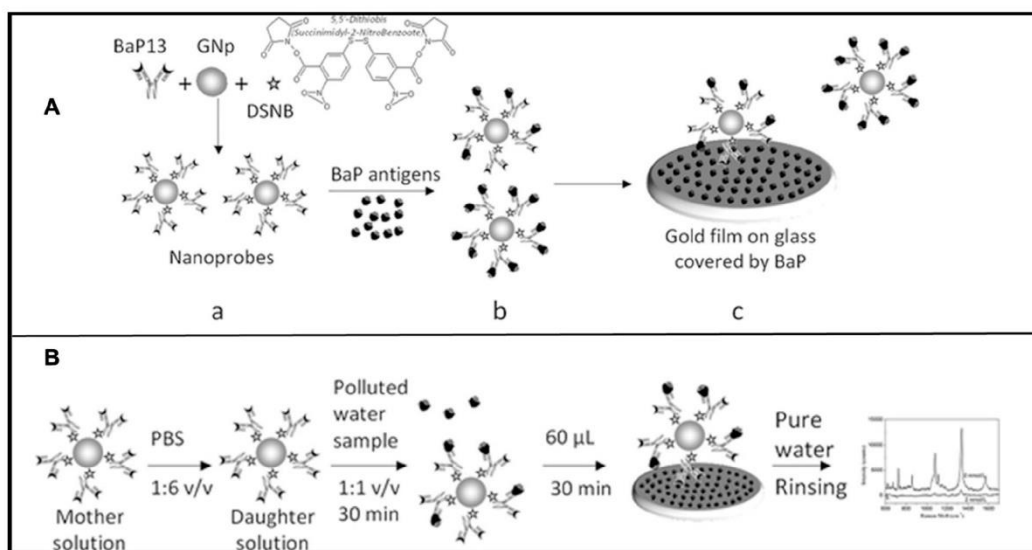


Fig. 10. (A) Complex assembling of gold nanoparticles and antibody *anti*-benzo[a]pyrene (BaP13) using 5,5'-dithiobis(succinimidyl-2-nitrobenzoate) (DSNB) as a coupling agent and Raman reporter and the interaction free antibody binding sites of the nanoprobe with grafted BaP on a gold coated quartz substrate. (B) Schematic illustration of the SERS sensing procedure for detection of BaP. Adapted with permission from Ref. [46] Copyright (2017) Springer.

Table 3

Examples of research studies that use nanomaterials for electrochemical detection of PAHs in water samples (note: studies based on detection in electrolyte solution have been included as they have potential application to water samples).

Sensor	Detection method	PAH Analyte	Linear range	LOD	Matrix	Ref.
Cd/Al-LDHs/GCE	DPV	Anthracene	$0.1\text{--}100.0 \times 10^{-12} \text{ mol L}^{-1}$	$0.5 \times 10^{-15} \text{ mol L}^{-1}$	Electrolyte solution	[79]
PPyox/Au–Ag NPs/GCE	CV	Pyrene	$0.1\text{--}1 \times 10^{-6} \text{ mol L}^{-1}$	$0.1 \times 10^{-6} \text{ mol L}^{-1}$	Electrolyte solution	[73]
Fe ₃ O ₄ -Calix [4]arene @ CdSe	SWV	Anthracene	$0.21\text{--}14 \times 10^{-6} \text{ mol L}^{-1}$	$0.11 \times 10^{-6} \text{ mol L}^{-1}$	Tap water	[80]
		Naphthalene	$1.5\text{--}25 \times 10^{-6} \text{ mol L}^{-1}$	$4.29 \times 10^{-8} \text{ mol L}^{-1}$		
ARS-SBA15/GCE	DPV	Anthracene	$1.0 \times 10^{-12} \text{--} 10.0 \times 10^{-9} \text{ mol L}^{-1}$	$0.5 \times 10^{-12} \text{ mol L}^{-1}$	Waste water	[81]
GCE-PANI-NiO	SWV	Phenanthrene	$7.6\text{--}14 \times 10^{-12} \text{ mol L}^{-1}$	$0.732 \times 10^{-12} \text{ mol L}^{-1}$	Electrolyte solution	[74]
GR-PANI-modified GCE	SWV	Anthracene	$0.012\text{--}1000 \times 10^{-6} \text{ mol L}^{-1}$	$4.4 \times 10^{-9} \text{ mol L}^{-1}$	Electrolyte solution	[68]
PANI/WO ₃ /GR/GCE	CV	Phenanthrene	$1.0\text{--}6.0 \times 10^{-12} \text{ mol L}^{-1}$	$0.123 \times 10^{-12} \text{ mol L}^{-1}$	Electrolyte solution	[67]
AQS/PDDA/ITO	CV	Phenanthrene	$1.0 \times 10^{-12} \text{--} 1.0 \times 10^{-9} \text{ mol L}^{-1}$	$0.50 \times 10^{-12} \text{ mol L}^{-1}$	Cloud water	[82]
					Rain water	
Au/G3PPT-co-P3HT	PSACV	Anthracene	$3.48\text{--}56.4 \times 10^{-9} \text{ mol L}^{-1}$	$2.62 \times 10^{-9} \text{ mol L}^{-1}$	Oil-polluted waste water	[76]
Au/G3PPT-co-P3HT	ACV	Phenanthrene	$2.78\text{--}37.65 \times 10^{-9} \text{ mol L}^{-1}$	$1.42 \times 10^{-9} \text{ mol L}^{-1}$	Oil-polluted waste water	[77]
Au/G3PPT-co-P3HT	CV	Phenanthrene	$13.35\text{--}35.86 \times 10^{-9} \text{ mol L}^{-1}$	$12.62 \times 10^{-9} \text{ mol L}^{-1}$	Tap water	[75]
	ACV		$5.46\text{--}42.57 \times 10^{-9} \text{ mol L}^{-1}$	$2.99 \times 10^{-9} \text{ mol L}^{-1}$		
	SWV		$10.34\text{--}40.56 \times 10^{-9} \text{ mol L}^{-1}$	$9.61 \times 10^{-9} \text{ mol L}^{-1}$		
PAA/GO/SPCE	SWV	Anthracene	$0.375\text{--}1.25 \times 10^{-6} \text{ mol L}^{-1}$	$6.7 \times 10^{-7} \text{ mol L}^{-1}$	Electrolyte solution	[69]
GO/SPCE			$0.375\text{--}1.0 \times 10^{-6} \text{ mol L}^{-1}$	$7.42 \times 10^{-7} \text{ mol L}^{-1}$		
ITO/PAA films	LSV	Anthracene	$5.15\text{--}21.5 \times 10^{-3} \text{ mol L}^{-1}$	$3.79 \times 10^{-6} \text{ mol L}^{-1}$	Electrolyte solution	[83]
Carbon-rich monolayer on ITO	EIS	Pyrene	1.75–7.00 ppt	1.75 ppt	Water	[84]

AQS/PDDA/ITO = anthraquinone sulfonate/poly diallyldimethylammonium chloride/indium–tin oxide.

ARS-SBA15/GCE = alizarin red S functionalized mesoporous silica material SBA15 onto glassy carbon electrode.

Au/G3PPT-co-P3HT = dendritic star-copolymer, generation 3 poly(propylene thiophenimine) (G3PPT)-co-poly(3-hexylthiophene) (P3HT) star co-polymer on gold electrode.

Cd/Al-LDHs/GCE = cadmium/aluminum layered double hydroxides on a glassy carbon electrode.

CV = cyclic voltammetry.

DPV = differential pulse voltammetry.

ECL = electrochemiluminescence.

EIS = electrochemical impedance spectroscopy.

GCE-PANI-NiO = glassy carbon electrode modified nickel oxide doped polyaniline nanofibers.

GO/SPCE = graphene oxide - screen printed carbon electrode.

GR-PANI = graphenated-polyaniline.

LSV = linear sweep voltammetry.

PAA/GO/SPCE = polyamic acid-graphene oxide - screen printed carbon electrode.

PPy = polypyrrole.

PSACV = phase selective alternating current voltammetry.

SWV = square-wave voltammetry.

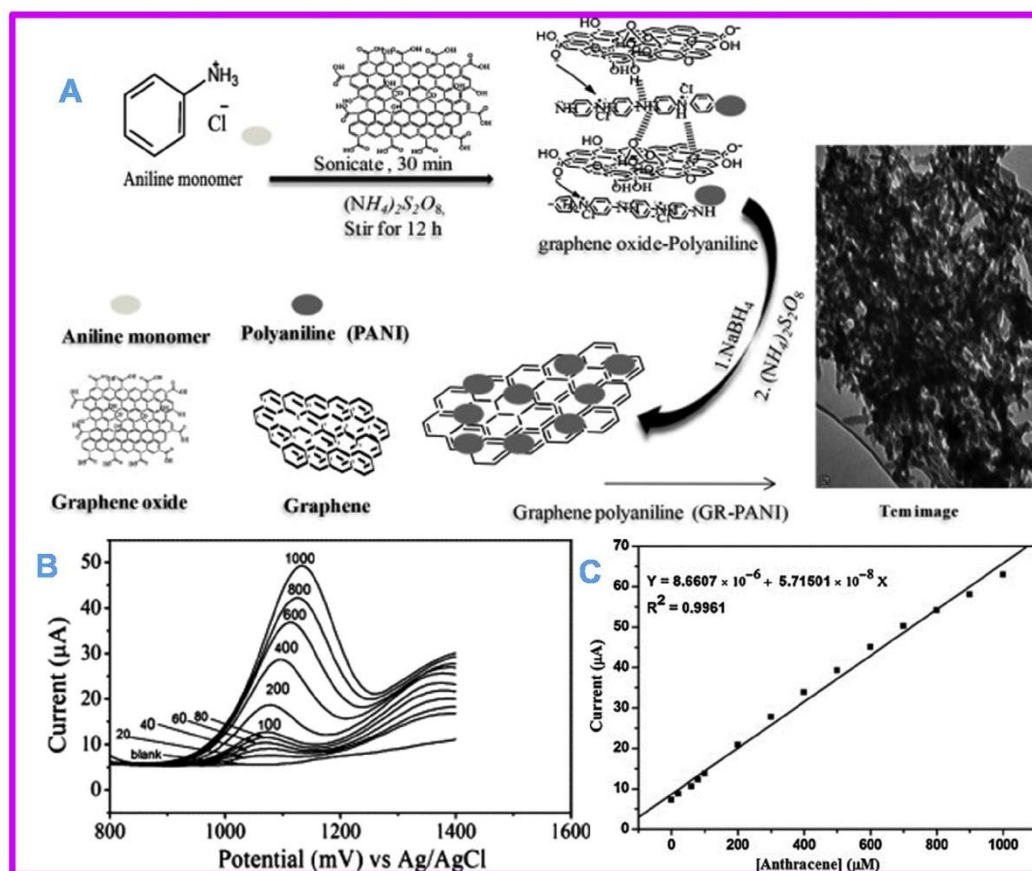


Fig. 11. (A) Schematic illustration of the synthesis of GR-PANI nanocomposite via in situ polymerization. (B) SWV responses of GR-PANI/GCE sensor for 20–1000 × 10⁻⁶ mol L⁻¹ anthracene. Experimental conditions: 0.1 mol L⁻¹ LiClO₄ in acetonitrile/water (80:20 v/v), (SW frequency = 5 Hz and SW amplitude = 25 mV). (C) A calibration plot of the GR-PANI/GCE sensor for 0.012–1000 × 10⁻⁶ mol L⁻¹ anthracene. Adapted from Ref. [68].

4.2. Polymer composite-based sensors for PAH detection

Polymers which have structural backbones consisting of delocalized π -bonds are able to facilitate electron transfer and have therefore found a number of applications in the design of electrochemical sensors due to their attractive optical and electrical properties. These materials are cheap, lightweight, resistant to corrosion, and contain functional groups which allow for their modification [71]. Examples of such polymers that have been used in designing PAH sensors include polyaniline (PANI), polypyrrole (PPy), polyamic acid (PAA), poly diallyldimethylammonium (PDDA) and poly(propylene thiophenoimine) (PPT). The drawbacks of these materials are their poor solubility and stability, but these are often overcome by modifications and blending to form functional polymer composite materials. Metal oxides can be used as dopants to improve photochemical stability, catalytic activity, surface area and adsorption capabilities of these materials [72]. However, the inherent disadvantage that comes with using these metals is that the metal precursors can be expensive which makes these sensors costly.

For example, a glassy carbon electrode was modified with oxidized PPy and further modified with Au-Ag in a 1:3 atomic

ratio for sensitive detection of pyrene [73]. The sensitivity of this sensor was found to increase by over 50% upon doping with the Au-Ag alloy and this was attributed to electro-catalytic activity towards oxidation of pyrene. Despite the sensitivity of the sensor, the authors acknowledged that using gold can be expensive and proposed switching to copper in future studies. PANI is another commonly used polymer in modified electrodes for sensitive detection of PAHs as it also facilitates their adsorption [67,68,74]. The study by Fayemi et al. [74] reported the use of nickel oxide-doped PANI to design a GCE-PANI-NiO sensor for detection phenanthrene. They showed that the NiO improved the electron transfer of the polymer and electrocatalytic activity towards phenanthrene allowing for a low detection limit of 0.732 × 10⁻¹² mol L⁻¹.

Dendritic star-copolymers based on generation of 3-poly(propylene thiophenoimine) (G3PPT)-co-poly(3-hexylthiophene) (P3HT) star co-polymer on a gold electrode (i.e., Au[G3PPT-co-P3HT]) have also been reported for detection of phenanthrene and anthracene in polluted water [75,76,77]. The success of this polymer was attributed to the reproducible adsorption of the PAHs on the polymer-modified electrodes. Using alternating current voltammetry (ACV) the authors were able to

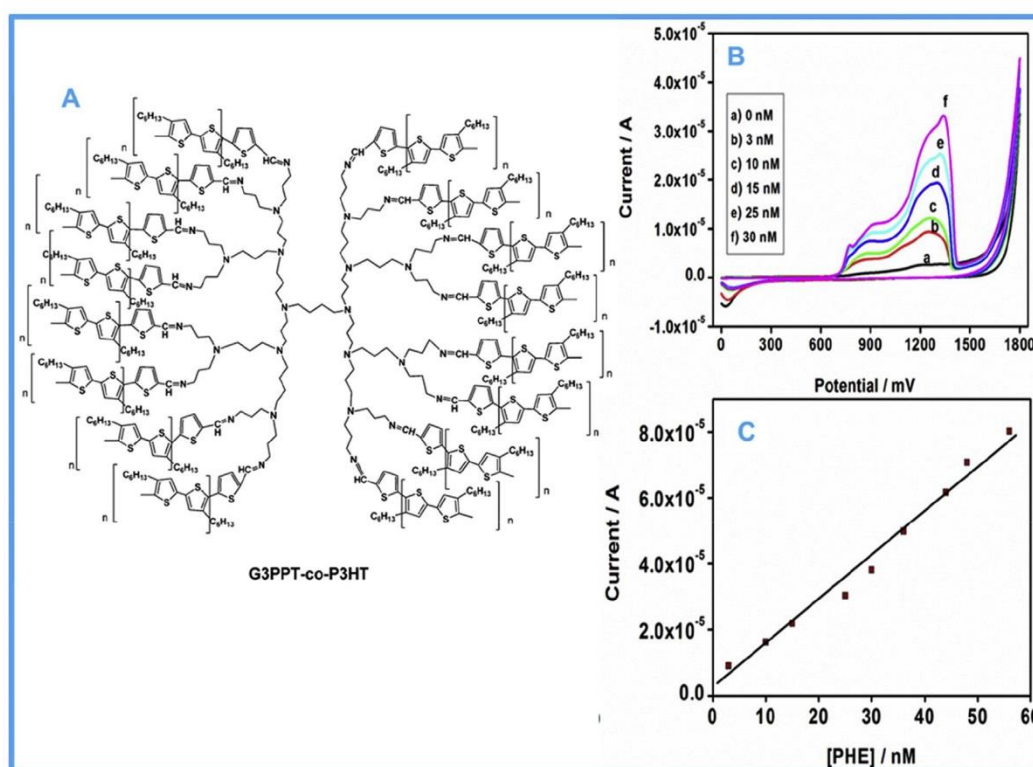


Fig. 12. (A) Structure of generation three poly(propylene thiophenimine) dendrimer (G3PPT-co-P3HT). (B) CV voltammograms of the Au|G3PPT-co-P3HT with different phenanthrene (PHE) concentrations. (C) The calibration plot of Au|G3PPT-co-P3HT sensor for PHE. Adapted from Ref. [75].

demonstrate that the sensor could distinguish between phenanthrene and anthracene due to different peak potentials (Fig. 12). The detection limits achieved were $1.42 \times 10^{-9} \text{ mol L}^{-1}$ for phenanthrene and $2.62 \times 10^{-9} \text{ mol L}^{-1}$ for anthracene. Thus dendritic star-copolymers hold great promise in designing selective sensors for other PAHs in future due to their large potential windows.

The advent of miniaturization technologies like microfluidics and sensor printing could open doors for the application of electrochemical sensors in the environmental field or for on-site monitoring applications [78]. The typical wide linear ranges of the reported sensors make them ideal as the occurrence levels of PAHs in the environment can widely vary. However, from the reviewed literature, this technology seems to have not yet found application in monitoring of PAHs. Thus more work can be done to adapt the various nanomaterial-based sensors in miniature electrochemical platforms for field application while maintaining their sensitivity.

4.3. Electrochemical biosensors

Bio-receptors like antigen-antibodies, hormone receptors, deoxyribonucleic acid (DNA) and aptamers have found a number of applications in nanomaterial-based sensors (Table 4). Apart from enzyme based sensors, the interaction between an analyte and these affinity type receptors is reversible and can be controlled by modifying the physico-chemical parameters such

as pH and ionic strength. Also, these interactions do not result in transformation of the analyte, but simply bind the target analyte selectively into close proximity with the nanomaterial for sensitive detection of occur [85].

Antigen-antibody bio-receptors have particularly been utilized in a number of applications in nanosensors for the detection of PAHs. For example a DNA/hemin/nafion-graphene biosensor (shown in Fig. 13) was fabricated on a glassy carbon electrode (GCE) through layer-by-layer deposition [70]. They used this sensor for indirect analysis of benzo[a]pyrene (BaP) using differential pulse voltammetry (DPV). They noted that after immersing the modified electrode in BaP and H₂O₂ there was an increase in the anodic peak around 1.0 V suggesting the BaP was oxidized by hemin to produce BaP-metabolites. The anodic peak increased linearly with BaP concentration within the $2.0\text{--}22.00 \times 10^{-8} \text{ mol L}^{-1}$ range and BaP could be detected down to $1.12 \times 10^{-8} \text{ mol L}^{-1}$ (see Table 4).

5. Nanosensors for PAH derivatives

PAHs often transform through various pathways into secondary metabolites or degradation products including oxygenated-PAHs, nitrated-PAHs, and azaarenes [91]. Some of the transformation pathways of PAHs in the environment may include photolysis, reaction with $\bullet\text{OH}$, NO_x or O₃, and biodegradation. The toxic effects of nitro-PAHs, for example, has been shown to be more pronounced than

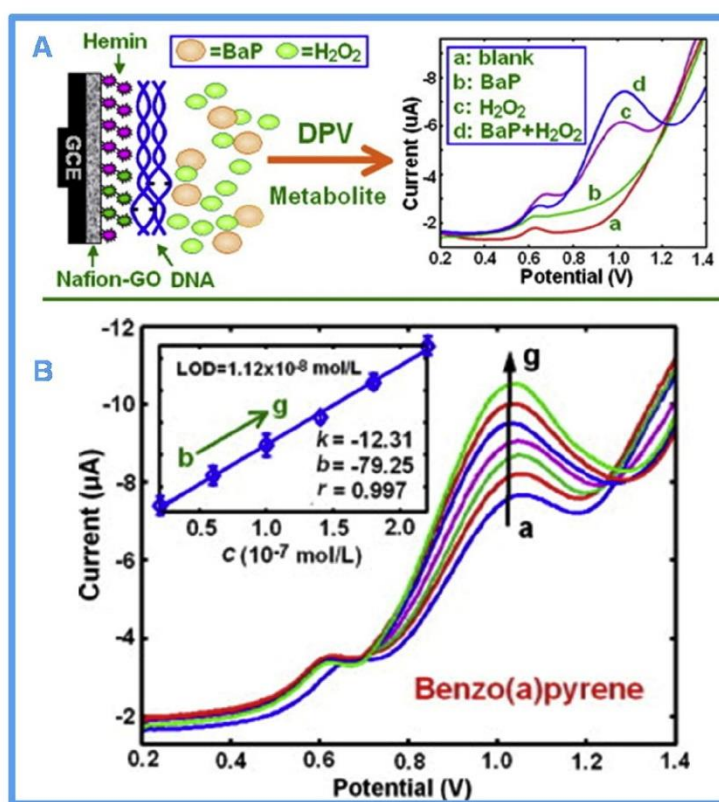


Fig. 13. (A) Schematic illustration of a benzo[a]pyrene biosensor. (B) DPV voltammograms of guanine obtained at the DNA/hemin/nafion-graphene/GCE at different concentrations of benzo[a]pyrene biosensor (a–g; $0\text{--}22 \times 10^{-8} \text{ mol L}^{-1}$). Adapted from Ref. [70].

Table 4

Summary of nanomaterial-based biosensor systems that use nanoparticles for PAH detection in water samples.

Sensor	Detection method	Analyte	Linear range	LOD	Matrix	Ref.
Dendritic SiO ₂ nanoparticles – HRP antibody	CV	Benzo[a]pyrene	$0.01\text{--}10 \times 10^{-6} \text{ mol L}^{-1}$	$8 \times 10^{-9} \text{ mol L}^{-1}$	Water	[86]
Fe ₃ O ₄ /PANI/Nafion-based immunosensor	CV	Benzo[a]pyrene	$8 \times 10^{-12} \text{--} 2 \times 10^{-9} \text{ mol L}^{-1}$	$4 \times 10^{-12} \text{ mol L}^{-1}$	Water	[87]
Multi-HRP-SiO ₂ Ab ₂ /Ab ₁ /BaP-Ag/PAMAM/PATT/Au	CV	Benzo[a]pyrene	$0.01\text{--}2.0 \text{ ng mL}^{-1}$	6 pg mL^{-1}	PBS solution	[88]
BaP-Ag/PAMAM/GS-CS/GCE immunosensor	CV	Benzo[a]pyrene	$5 \times 10^{-9} \text{--} 6 \times 10^{-6} \text{ mol L}^{-1}$	$3 \times 10^{-9} \text{ mol L}^{-1}$	Water	[89]
DNA/hemin/nafion-graphene/GCE	DPV	Benzo[a]pyrene	$2.0\text{--}22.00 \times 10^{-8} \text{ mol L}^{-1}$	$1.12 \times 10^{-8} \text{ mol L}^{-1}$	Aqueous solution	[70]
Anti-NA/NG/PB/GCE	CV	Naphthalene	$3.12\text{--}78 \times 10^{-8} \text{ mol L}^{-1}$	$4.68 \times 10^{-10} \text{ mol L}^{-1}$	River water	[90]

Anti-NA/NG/PB/GCE = Naphthalene antibody/nanometer-sized gold particles/Prussian blue/glassy carbon electrode.

EuNPs-Mab = Eu(III)-marked polystyrene nanoparticles (EuNPs) labeled with a monoclonal antibody (Mab).

MNPs-icCLEIA = Magnetic nanoparticle-phenanthrene hybrid conjugates (MNPs-Phe)-indirect competitive chemiluminescence enzyme immunoassay.

PBS = phosphate buffered saline.

those of parent PAHs [92], thus monitoring of these products is equally important, particularly in biological samples such as urine. Few studies have actually focused on monitoring of the PAH derivatives as they are often neglected. As shown in Table 5, electrochemical sensors are the most commonly applied sensor for the detection of PAH derivatives and this can be attributed to their redox activity. Table 5 presents a summary of sensors that have been developed for detection of some of the important PAH derivatives.

6. Conclusions and future outlook

The continuous release of PAHs into the environment through natural, biological, and anthropogenic activities implies that regulators will forever require monitoring of these compounds, especially given their potential toxic effects. Thus there is a need for continuous development of robust and highly sensitive analytical sensors to monitor their occurrence in the

Table 5
Examples of nano-sensors for PAH metabolites/degradation products.

Sensor	Detection method	Analyte	Linear range	LOD	Matrix	Ref
OTTLE	Spectroelectrochemical	1-hydroxypyrene	$0.01-1 \times 10^{-6} \text{ mol L}^{-1}$	$1 \times 10^{-8} \text{ mol L}^{-1}$	PBS and artificial urine	[93]
SnO ₂ /GCE	DPV	1-hydroxypyrene-glucuronide	$1 \times 10^{-9} - 1 \times 10^{-6} \text{ mol L}^{-1}$	$9 \times 10^{-11} \text{ mol L}^{-1}$	Water	[94]
GON/OA-POSS	DPV	1-hydroxypyrene	$0.1-12.55 \times 10^{-6} \text{ mol L}^{-1}$	$0.04 \times 10^{-6} \text{ mol L}^{-1}$	Methanol-water (50 vol%)	[95]
GR/GCE	DPV	1-hydroxypyrene	$5-300 \times 10^{-9} \text{ mol L}^{-1}$	$0.84 \times 10^{-9} \text{ mol L}^{-1}$	Urine	[96]
MIP TiO ₂ nanofilm	CV	1-hydroxypyrene	$1 \times 10^{-9} - 2 \times 10^{-7} \text{ mol L}^{-1}$	$3.353 \times 10^{-10} \text{ mol L}^{-1}$	Urine	[97]
β -CD-PTCA-SWCNTs	DPV	9-anthracenecarboxylic acid	$2.00-140.00 \times 10^{-9} \text{ mol L}^{-1}$	$0.65 \times 10^{-9} \text{ mol L}^{-1}$	Water	[98]
Nano-Au/Nafion composites - ELISA	EIS	1-pyrenebutyric acid	$0.1-150 \text{ ng mL}^{-1}$	0.03 ng mL^{-1}	Tap and river water	[99]

EIS = electrochemical impedance spectroscopy.

ELISA = Enzyme-linked immunosorbent assay.

GON/OA-POSS = graphene oxide nanoribbon/octa(3-aminopropyl)octasilane quinoxaline octahydrochloride

GR/GCE = graphene modified glassy carbon electrode.

MIP TiO₂ = molecular imprinted titanium dioxide gel matrix.

OTTLE = optically transparent thin layer electrode.

PBS = phosphate buffered saline.

Sn-In = Tin-doped indium optically transparent electrode coated with a Nafion thin-film.

β -CD-PTCA-SWCNTs = β -cyclodextrin non-covalently functionalized single-walled carbon nanotubes bridged by 3,4,9,10-perylene tetracarboxylic acid.

environment including water sources. The advent of nanotechnology has opened doors for developing a range of functional nanomaterials which have found application in various PAH sensors – from fluorescence, Raman, electrochemical and biologically based sensors, as we have demonstrated. In most cases, the nano-sensors were found to demonstrate very high sensitivity below the regulatory recommended limits.

Selectivity is achieved through modification with receptors like MIPs, macromolecules, and biological agents such as antigens or antibodies – thanks to the versatile surface chemistry of the materials. However, for application in real environmental water samples, sample preparation or pre-treatment is typically necessary and this is not highlighted in most of the studies. We recommend that this crucial step should be made explicit in future as it is pivotal when assessing the turnaround time of using the sensor. Some of the reported sensors were only applied in laboratory prepared standard solutions, where interferences potentially present in real water samples was not investigated. This, too, should be taken into consideration.

Future prospects include the following:

Portable sensor devices: Towards portable, sensitive and selective devices for real world application. Integration of quantum dot-based fluorescence sensors, for example, into microfluidic systems, could lead to the development of portable devices for on-site detection of PAHs. Current sensing systems are typically in solution form where aggregation of the nanomaterials upon long storage could be an issue for real application. This could be solved by designing compact sensing platforms, preferably in the form of immobilized NPs on solid supports (such as thin film materials), that are compatible with either portable fluorescence, SERS, or electrochemical devices such that systems are suitable for field application. The development of portable Raman instruments looks promising for SERS detection, as demonstrated by Du et al. [39]. However most of the nanoparticle-based substrates are not suitable for portable Raman instruments because of low reproducibility of Brownian movement and uncontrollable aggregation.

Multi analyte detection: One of the powerful strengths of chromatographic PAH analysis is its ability to identify multiple analytes in one run. Thus the ideal PAH sensor is one that can detect and quantify multiple PAHs, i.e. all or most of the 16 EPA priority PAHs in a single

analysis. The tunability of nanomaterials could lead to the realization of such sensors. SERS-based sensors are currently leading in terms of multiple PAH quantification since the technique relies on an analyte-specific signal. Electrochemical and fluorescence-based sensors, on the other hand, still typically detect one analyte at a time. The unique excitation-dependent fluorescence spectra of PAHs, we believe, could be explored for multiple PAH identification. Also, molecularly imprinted polymers (MIPs) with excellent binding affinities for the 16 priority PAHs have been synthesized [100]. Such MIPs could serve as suitable fluorescence or electrochemical signal reporters for simultaneous identification of PAHs.

Standardization: The discussed sensing methods will need standardization and validation if they are to be adopted by regulatory bodies for reliable routine monitoring. This, however, may still pose a serious challenge since the performance and indeed the detection limits of the various sensors are different for the different PAHs.

Sensing in gas phase: Finally, from the human health perspective, exposure to PAHs through inhalation remains a problem. Adapting nanomaterial systems for the detection and quantification of airborne PAHs would be a valuable future application. Thus designing nanomaterial platforms/substrates upon which gaseous PAHs can adsorb and pre-concentrate followed by direct detection should be explored. From the reviewed literature, only Mueller et al. [56] has used the SERS application in gas phase sensing of PAHs to date.

Acknowledgments

Funding from the Water Research Commission (WRC) (Grant K5/2438/1), the Photonics Initiative of South Africa (Grant PISA-15DIR-06) and the National Research Foundation of South Africa (postgraduate student bursary (SN) and funding grants 90720 and 93394 (PF)) is gratefully acknowledged.

References

- [1] V. Bansal, P. Kumar, E.E. Kwon, K.-H. Kim, Review of the quantification techniques for polycyclic aromatic hydrocarbons (PAHs) in food products, *Crit. Rev. Food Sci. Nutr.* 51 (2015) 3297–3397.
- [2] M. Rota, C. Bosetti, S. Boccia, P. Boffetta, C. La Vecchia, Occupational exposures to polycyclic aromatic hydrocarbons and respiratory and urinary tract

- cancers: an updated systematic review and a meta-analysis to 2014, *Arch. Toxicol.* 88 (2014) 1479–1490.
- [3] A.J. White, P.T. Bradshaw, A.H. Herring, S.L. Teitelbaum, J. Beyea, S.D. Stellman, S.E. Steck, I. Mordukhovich, S.M. Eng, L.S. Engel, K. Conway, M. Hatch, A.I. Neugut, R.M. Santella, M.D. Gammon, Exposure to multiple sources of polycyclic aromatic hydrocarbons and breast cancer incidence, *Environ. Int.* 89–90 (2016) 185–192.
 - [4] S. Marzocchi, D.M. Di Toro, A critical review of polycyclic aromatic hydrocarbon phototoxicity models, *Environ. Toxicol. Chem.* 36 (2017) 1138–1148.
 - [5] A. Ramesh, A.E. Archibong, D.B. Hood, Z. Guo, B.G. Loganathan, *Global Environmental Distribution and Human Health Effects of Polycyclic Aromatic Hydrocarbons*, CRC Press, Boca Raton, FL, USA, 2011, pp. 95–124.
 - [6] V. Bansal, P. Kumar, E.E. Kwon, K.-H. Kim, Review of the quantification techniques for polycyclic aromatic hydrocarbons (PAHs) in food products, *Crit. Rev. Food Sci. Nutr.* 57 (2017) 3297–3312.
 - [7] S. Ncube, L. Madikizela, E. Cukrowska, L. Chimuka, Recent advances in the adsorbents for isolation of polycyclic aromatic hydrocarbons (PAHs) from environmental sample solutions, *TrAC Trends Anal. Chem.* 99 (2018) 101–116.
 - [8] S. Kumar, S. Negi, P. Maiti, Biological and analytical techniques used for detection of polycyclic aromatic hydrocarbons, *Environ. Sci. Pollut. Res.* 24 (2017) 25810–25827.
 - [9] C.J. Murphy, Peer reviewed: optical sensing with quantum dots, *Anal. Chem.* 74 (2002) 520 A–526.
 - [10] R. Freeman, I. Willner, Optical molecular sensing with semiconductor quantum dots (QDs), *Chem. Soc. Rev.* 41 (2012) 4067–4085.
 - [11] J. Szejtli, Introduction and general overview of cyclodextrin chemistry, *Chem. Rev.* 98 (1998) 1743–1754.
 - [12] H. Li, F. Qu, Selective inclusion of polycyclic aromatic hydrocarbons (PAHs) on calixarene coated silica nanospheres englobed with CdTe nanocrystals, *J. Mater. Chem.* 17 (2007) 3536–3544.
 - [13] C.P. Han, H.B. Li, Novel β -cyclodextrin modified quantum dots as fluorescent probes for polycyclic aromatic hydrocarbons (PAHs), *Chin. Chem. Lett.* 19 (2008) 215–218.
 - [14] F. Qu, H. Li, Selective molecular recognition of polycyclic aromatic hydrocarbons using CdTe quantum dots with cyclodextrin as supramolecular nano-sensitizers in water, *Sens. Actuators B Chem.* 135 (2009) 499–505.
 - [15] R. Kumar, M. Arora, A.K. Jain, J.N. Babu, 1,3-Bis(cyanomethoxy)calix[4]arene capped CdSe quantum dots for the fluorogenic sensing of fluorene, *RSC Adv.* 7 (2017) 14015–14020.
 - [16] H.-J. Schneider, Limitations and extensions of the lock-and-key principle: differences between gas state, solution and solid state structures, *Int. J. Mol. Sci.* 16 (2015) 6694–6717.
 - [17] O. Adegoke, P.B.C. Forbes, I-Cysteine-capped core/shell/shell quantum dot–graphene oxide nanocomposite fluorescence probe for polycyclic aromatic hydrocarbon detection, *Talanta* 146 (2015) 780–788.
 - [18] L. Wang, Z. Huang, Q. Gao, Y. Liu, X. Kou, D. Xiao, A novel pyrene fluorescent sensor based on the π - π interaction between pyrene and graphene of graphene–cadmium telluride quantum dot nanocomposites, *Spectrosc. Lett.* 48 (2015) 748–756.
 - [19] C. Carrillo-Carrión, B.M. Simonet, M. Valcárcel, Carbon nanotube–quantum dot nanocomposites as new fluorescence nanoparticles for the determination of trace levels of PAHs in water, *Anal. Chim. Acta* 652 (2009) 278–284.
 - [20] O. Adegoke, H. Montaseri, S.A. Nsibande, P.B. Forbes, Alloyed quaternary/binary core/shell quantum dot–graphene oxide nanocomposite: preparation, characterization and application as a fluorescence “switch ON” probe for environmental pollutants, *J. Alloy. Comp.* 720 (2017) 70–78.
 - [21] B. Li, P. Ou, Y. Wei, X. Zhang, J. Song, Polycyclic aromatic hydrocarbons adsorption onto graphene: a DFT and AIMD study, *Materials* 11 (2018) 726.
 - [22] J. Wang, Z. Chen, B. Chen, Adsorption of polycyclic aromatic hydrocarbons by graphene and graphene oxide nanosheets, *Environ. Sci. Technol.* 48 (2014) 4817–4825.
 - [23] O. Adegoke, P.B.C. Forbes, I-Cysteine-capped core/shell/shell quantum dot–graphene oxide nanocomposite fluorescence probe for polycyclic aromatic hydrocarbon detection, *Talanta* 146 (2016) 780–788.
 - [24] C. Carrillo-Carrión, B.M. Simonet, M. Valcárcel, Carbon nanotube–quantum dot nanocomposites as new fluorescence nanoparticles for the determination of trace levels of PAHs in water, *Anal. Chim. Acta* 652 (2009) 278–284.
 - [25] L. Yang, B. Chen, S. Luo, J. Li, R. Liu, Q. Cai, Sensitive detection of polycyclic aromatic hydrocarbons using CdTe quantum dot-modified TiO₂ nanotube array through fluorescence resonance energy transfer, *Environ. Sci. Technol.* 44 (2010) 7884–7889.
 - [26] W. Kuzniak, O. Adegoke, K. Sekhosana, S. D’Souza, S.C. Tshangana, B. Hoffmann, E.A. Ermilov, T. Nyokong, M. Höpfer, Synthesis and characterization of quantum dots designed for biomedical use, *Int. J. Pharm.* 466 (2014) 382–389.
 - [27] J. Ledesma, P.L. Pisano, D.M. Martino, C.E. Boschetti, S.A. Bortolato, Thymine based copolymers: feasible sensors for the detection of persistent organic pollutants in water, *RSC Adv.* 7 (2017) 49066–49073.
 - [28] A.L. Medina-Castillo, G. Mistlberger, J.F. Fernandez-Sanchez, A. Segura-Cartero, I. Klimant, A. Fernandez-Gutierrez, Novel strategy to design magnetic, molecular imprinted polymers with well-controlled structure for the application in optical sensors, *Macromolecules* 43 (2010) 55–61.
 - [29] H. Li, L. Wang, Highly selective detection of polycyclic aromatic hydrocarbons using multifunctional magnetic–luminescent molecularly imprinted polymers, *ACS Appl. Mater. Interfaces* 5 (2013) 10502–10509.
 - [30] B.D.B. Tiu, R.J. Krupadam, R.C. Advincula, Pyrene-imprinted polythiophene sensors for detection of polycyclic aromatic hydrocarbons, *Sens. Actuators B Chem.* 228 (2016) 693–701.
 - [31] H.D. Duong, C.V.G. Reddy, J.I. Rhee, T. Vo-Dinh, Amplification of fluorescence emission of CdSe/ZnS QDs entrapped in a sol–gel matrix, a new approach for detection of trace level of PAHs, *Sens. Actuators B Chem.* 157 (2011) 139–145.
 - [32] L.S. Walekar, P. Hu, H. Vafaei Molamahmood, M. Long, FRET based integrated pyrene-AgNPs system for detection of Hg (II) and pyrene dimer: applications to environmental analysis, *Spectrochim. Acta A Mol. Biomol. Spectrosc.* 198 (2018) 168–176.
 - [33] C. Zong, M. Xu, L.-J. Xu, T. Wei, X. Ma, X.-S. Zheng, R. Hu, B. Ren, Surface-enhanced Raman spectroscopy for bioanalysis: reliability and challenges, *Chem. Rev.* 118 (2018) 4946–4980.
 - [34] P.A. Mosier-Boss, Review of SERS substrates for chemical sensing, *Nanomaterials* 7 (2017) 142.
 - [35] V.M. Szlag, R.S. Rodriguez, J. He, N.V. Hudson-Smith, H. Kang, N. Le, T.M. Reineke, C.L. Haynes, Molecular affinity agents for intrinsic surface-enhanced Raman scattering (SERS) sensors, *ACS Appl. Mater. Interfaces* 10 (2018) 31825–31844.
 - [36] J. Chen, Y.-W. Huang, Y. Zhao, Characterization of polycyclic aromatic hydrocarbons using Raman and surface-enhanced Raman spectroscopy, *J. Raman Spectrosc.* 46 (2015) 64–69.
 - [37] D. Song, R. Yang, F. Long, A. Zhu, Applications of magnetic nanoparticles in surface-enhanced Raman scattering (SERS) detection of environmental pollutants, *J. Environ. Sci.* (2018). <https://doi.org/10.1016/j.jes.2018.07.004>.
 - [38] J. Du, C. Jing, Preparation of thiol modified Fe₃O₄@Ag magnetic SERS probe for PAHs detection and identification, *J. Phys. Chem. C* 115 (2011) 17829–17835.
 - [39] J. Du, J. Xu, Z. Sun, C. Jing, Au nanoparticles grafted on Fe₃O₄ as effective SERS substrates for label-free detection of the 16 EPA priority polycyclic aromatic hydrocarbons, *Anal. Chim. Acta* 915 (2016) 81–89.
 - [40] X. Shi, Y.-H. Kwon, J. Ma, R. Zheng, C. Wang, H.-D. Kronfeldt, Trace analysis of polycyclic aromatic hydrocarbons using calixarene layered gold colloid film as substrates for surface-enhanced Raman scattering, *J. Raman Spectrosc.* 44 (2013) 41–46.
 - [41] Y. Xie, X. Wang, X. Han, X. Xue, W. Ji, Z. Qi, J. Liu, B. Zhao, Y. Ozaki, Sensing of polycyclic aromatic hydrocarbons with cyclodextrin inclusion complexes on silver nanoparticles by surface-enhanced Raman scattering, *Analyst* 135 (2010) 1389–1394.
 - [42] Y. Xie, X. Wang, X. Han, W. Song, W. Ruan, J. Liu, B. Zhao, Y. Ozaki, Selective SERS detection of each polycyclic aromatic hydrocarbon (PAH) in a mixture of five kinds of PAHs, *J. Raman Spectrosc.* 42 (2011) 945–950.
 - [43] E. Hahm, D. Jeong, M.G. Cha, J.M. Choi, X.-H. Pham, H.-M. Kim, H. Kim, Y.-S. Lee, D.H. Jeong, S. Jung, B.-H. Jun, β -CD dimer-immobilized Ag assembly embedded silica nanoparticles for sensitive detection of polycyclic aromatic hydrocarbons, *Sci. Rep.* 6 (2016) 26082.
 - [44] S. Fu, X. Guo, H. Wang, T. Yang, Y. Wen, H. Yang, Functionalized Au nanoparticles for label-free Raman determination of ppb level benzopyrene in edible oil, *Sens. Actuators B Chem.* 212 (2015) 200–206.
 - [45] I. Tijnunelyte, S. Betelu, J. Moreau, I. Ignatiadis, C. Berho, N. Lidgi-Guigui, E. Guénin, C. David, S. Vergnole, E. Rinnert, Diazonium salt-based surface-enhanced Raman spectroscopy nanosensor: detection and quantification of aromatic hydrocarbons in water samples, *Sensors* 17 (2017) 1198.
 - [46] M. Dribek, E. Rinnert, F. Colas, M.-P. Crassous, N. Thioune, C. David, M. De La Chapelle, C. Compère, Organometallic nanoprobe to enhance optical response on the polycyclic aromatic hydrocarbon benzo [a] pyrene immunoassay using SERS technology, *Environ. Sci. Pollut. Res.* 24 (2017) 27070–27076.
 - [47] A. Zengin, U. Tamer, T. Caykara, SERS detection of polyaromatic hydrocarbons on a β -cyclodextrin containing polymer brush, *J. Raman Spectrosc.* 49 (2018) 452–461.
 - [48] L. Bao, P. Sheng, J. Li, S. Wu, Q. Cai, S. Yao, Surface enhanced Raman spectroscopic detection of polycyclic aromatic hydrocarbons (PAHs) using a gold nanoparticles-modified alginate gel network, *Analyst* 137 (2012) 4010–4015.
 - [49] S. Tang, Y. Li, H. Huang, P. Li, Z. Guo, Q. Luo, Z. Wang, P.K. Chu, J. Li, X.-F. Yu, Efficient enrichment and self-assembly of hybrid nanoparticles into removable and magnetic SERS substrates for sensitive detection of environmental pollutants, *ACS Appl. Mater. Interfaces* 9 (2017) 7472–7480.
 - [50] P. Mosier-Boss, S. Lieberman, Surface-enhanced Raman spectroscopy substrate composed of chemically modified gold colloid particles immobilized on magnetic microparticles, *Anal. Chem.* 77 (2005) 1031–1037.
 - [51] O. Péron, E. Rinnert, M. Lehaitre, P. Crassous, C. Compère, Detection of polycyclic aromatic hydrocarbon (PAH) compounds in artificial sea-water using surface-enhanced Raman scattering (SERS), *Talanta* 79 (2009) 199–204.
 - [52] O. Péron, E. Rinnert, T. Toury, M.L. De La Chapelle, C. Compère, Quantitative SERS sensors for environmental analysis of naphthalene, *Analyst* 136 (2011) 1018–1022.
 - [53] M.A. Koklioti, C. Bittencourt, X. Noifalaise, I. Saucedo-Orozco, M. Quintana, N. Tagmatarchis, Nitrogen-doped silver-nanoparticle-decorated transition-metal dichalcogenides as surface-enhanced Raman scattering substrates for

- sensing polycyclic aromatic hydrocarbons, *ACS Appl. Nano Mater.* 1 (2018) 3625–3635.
- [54] L. Jing, Y.-e. Shi, J. Cui, X. Zhang, J. Zhan, Hydrophobic gold nanostructures via electrochemical deposition for sensitive SERS detection of persistent toxic substances, *RSC Adv.* 5 (2015) 13443–13450.
- [55] X. Wang, W. Hao, H. Zhang, Y. Pan, Y. Kang, X. Zhang, M. Zou, P. Tong, Y. Du, Analysis of polycyclic aromatic hydrocarbons in water with gold nanoparticles decorated hydrophobic porous polymer as surface-enhanced Raman spectroscopy substrate, *Spectrochim. Acta A Mol. Biomol. Spectrosc.* 139 (2015) 214–221.
- [56] M. Mueller, M. Tebbe, D.V. Andreeva, M. Karg, R.A. Alvarez Puebla, N. Pazos Perez, A. Fery, Large-area organization of pNIPAM-coated nanostars as SERS platforms for polycyclic aromatic hydrocarbons sensing in gas phase, *Langmuir* 28 (2012) 9168–9173.
- [57] H.-X. Gu, L. Xue, Y.-F. Zhang, D.-W. Li, Y.-T. Long, Facile fabrication of a silver dendrite-integrated chip for surface-enhanced Raman scattering, *ACS Appl. Mater. Interfaces* 7 (2015) 2931–2936.
- [58] K. Haruna, T.A. Saleh, M.K. Hossain, A.A. Al-Saadi, Hydroxylamine reduced silver colloid for naphthalene and phenanthrene detection using surface-enhanced Raman spectroscopy, *Chem. Eng. J.* 304 (2016) 141–148.
- [59] J. Xu, J. Du, C. Jing, Y. Zhang, J. Cui, Facile detection of polycyclic aromatic hydrocarbons by a surface-enhanced Raman scattering sensor based on the Au coffee ring effect, *ACS Appl. Mater. Interfaces* 6 (2014) 6891–6897.
- [60] I. López-Tocón, J.C. Otero, J.F. Arenas, J.V. García-Ramos, S. Sanchez-Cortes, Multicomponent direct detection of polycyclic aromatic hydrocarbons by surface-enhanced Raman spectroscopy using silver nanoparticles functionalized with the viologen host lucigenin, *Anal. Chem.* 83 (2011) 2518–2525.
- [61] L.-L. Qu, Y.-T. Li, D.-W. Li, J.-Q. Xue, J.S. Fossey, Y.-T. Long, Humic acids-based one-step fabrication of SERS substrates for detection of polycyclic aromatic hydrocarbons, *Analyst* 138 (2013) 1523–1528.
- [62] H.-X. Gu, K. Hu, D.-W. Li, Y.-T. Long, SERS detection of polycyclic aromatic hydrocarbons using a bare gold nanoparticles coupled film system, *Analyst* 141 (2016) 4359–4365.
- [63] C. Zhu, G. Yang, H. Li, D. Du, Y. Lin, Electrochemical sensors and biosensors based on nanomaterials and nanostructures, *Anal. Chem.* 87 (2015) 230–249.
- [64] Y. Zeng, Z. Zhu, D. Du, Y. Lin, Nanomaterial-based electrochemical biosensors for food safety, *J. Electroanal. Chem.* 781 (2016) 147–154.
- [65] M. Diaz-González, M. Gutiérrez-Capitán, P. Niu, A. Baldi, C. Jiménez-Jorquera, C. Fernández-Sánchez, Electrochemical devices for the detection of priority pollutants listed in the EU water framework directive, *TrAC Trends Anal. Chem.* 77 (2016) 186–202.
- [66] Y. Shao, J. Wang, H. Wu, J. Liu, I.A. Aksay, Y. Lin, Graphene based electrochemical sensors and biosensors: a Review, *Electroanalysis* 22 (2010) 1027–1036.
- [67] O. Tovide, N. Jaheed, N. Mohamed, E. Nxusani, C.E. Sunday, A. Tsegaye, R.F. Ajayi, N. Njomo, H. Makelane, M. Bilibana, P.G. Baker, A. Williams, S. Vilakazi, R. Tshikhudo, E.I. Iwuoha, Graphenated polyaniline-doped tungsten oxide nanocomposite sensor for real time determination of phenanthrene, *Electrochim. Acta* 128 (2014) 138–148.
- [68] O. Tovide, N. Jaheed, C.E. Sunday, K. Pokpas, R.F. Ajayi, H.R. Makelane, K.M. Molapo, S.V. John, P.G. Baker, E.I. Iwuoha, Electro-oxidation of anthracene on polyanilino-graphene composite electrode, *Sens. Actuators B Chem.* 205 (2014) 184–192.
- [69] S. Hamna, M. Ward, X.T. Ngema, E.I. Iwuoha, P.G.L. Baker, Development of graphenated polyamic acid sensors for electroanalytical detection of anthracene, *J. Nano Res.* 43 (2016) 11–22.
- [70] Y. Ni, P. Wang, H. Song, X. Lin, S. Kokot, Electrochemical detection of benzo(a)pyrene and related DNA damage using DNA/hemin/nafiion–graphene biosensor, *Anal. Chim. Acta* 821 (2014) 34–40.
- [71] M. El Rhazi, S. Majid, M. Elbasri, F.E. Salih, L. Oularbi, K. Lafdi, Recent progress in nanocomposites based on conducting polymer: application as electrochemical sensors, *Int. Nano Lett.* 8 (2018) 79–99.
- [72] X.-Y. Yu, Z.-G. Liu, X.-J. Huang, Nanostructured metal oxides/hydroxides-based electrochemical sensor for monitoring environmental micro-pollutants, *TrAC Trends Environ. Anal. Chem.* 3–4 (2014) 28–35.
- [73] A. Shah, S.B. Khan, A.M. Asiri, H. Hussain, C. Han, R. Qureshi, M.N. Ashiq, M.A. Zia, M. Ishaq, H.-B. Kraatz, Synthesis, characterization, and application of Au–Ag alloy nanoparticles for the sensing of an environmental toxin, pyrene, *J. Appl. Electrochem.* 45 (2015) 463–472.
- [74] O.E. Fayemi, A.S. Adekunle, E.E. Ebenso, Electrochemical detection of phenanthrene using nickel oxide doped PANI nanofiber based modified electrodes, *J. Nanomater.* 2016 (2016) 88.
- [75] H. Makelane, O. Tovide, C. Sunday, T. Waryo, E. Iwuoha, Electrochemical interrogation of G3-poly(propylene thiophenoimine) dendritic star polymer in phenanthrene sensing, *Sensors* 15 (2015) 22343.
- [76] H. Makelane, S.V. John, A.L.D. Yonkeu, T. Waryo, O. Tovide, E. Iwuoha, Phase selective alternating current voltammetric signalling protocol: application in dendritic co-polymer sensor for anthracene, *Electroanalysis* 29 (2017) 1887–1893.
- [77] H.R. Makelane, S.V. John, T.T. Waryo, A. Baleg, N. Mayedwa, C. Rassie, L. Wilson, P. Baker, E.I. Iwuoha, AC voltammetric transductions and sensor application of a novel dendritic poly(propylene thiophenoimine)-co-poly(3-hexylthiophene) star co-polymer, *Sens. Actuators B Chem.* 227 (2016) 320–327.
- [78] F. Arduini, S. Cinti, V. Scognamiglio, D. Moscone, G. Palleschi, How cutting-edge technologies impact the design of electrochemical (bio) sensors for environmental analysis. A review, *Anal. Chim. Acta* 959 (2017) 15–42.
- [79] X. Qiao, M. Wei, D. Tian, F. Xia, P. Chen, C. Zhou, One-step electrosynthesis of cadmium/aluminum layered double hydroxides composite as electrochemical probe for voltammetric detection of anthracene, *J. Electroanal. Chem.* 808 (2018) 35–40.
- [80] B. Sehatnia, R.E. Sabzi, F. Kheiri, A. Nikoo, Sensitive molecular determination of polycyclic aromatic hydrocarbons based on thiolated Calix[4]arene and CdSe quantum dots (QDs), *J. Appl. Electrochem.* 44 (2014) 727–733.
- [81] S. Liu, M. Wei, X. Zheng, S. Xu, F. Xia, C. Zhou, Alizarin red S functionalized mesoporous silica modified glassy carbon electrode for electrochemical determination of anthracene, *Electrochim. Acta* 160 (2015) 108–113.
- [82] M. Wei, S. Duan, S. Liu, X. Zheng, F. Xia, C. Zhou, Electrochemical determination of phenanthrene based on anthraquinone sulfonate and poly diallyldimethylammonium chloride modified indium–tin oxide electrode, *RSC Adv.* 5 (2015) 48811–48815.
- [83] X.T. Ngema, M. Ward, S. Hamna, P.G.L. Baker, E.I. Iwuoha, Spectro-electrochemical of detection anthracene at electrodeposited polyamic acid thin films, *J. Nano Res.* 44 (2016) 63–78.
- [84] J. Muñoz, N. Crivillers, M. Mas-Torrent, Carbon-rich monolayers on ITO as highly sensitive platforms for detecting polycyclic aromatic hydrocarbons in water: the case of pyrene, *Chem. Eur J.* 23 (2017) 15289–15293.
- [85] L. Rotariu, F. Lagarde, N. Jaffrezic-Renault, C. Bala, Electrochemical biosensors for fast detection of food contaminants – trends and perspective, *TrAC Trends Anal. Chem.* 79 (2016) 80–87.
- [86] C. Wang, M. Lin, Y. Liu, H. Lei, A dendritic nanosilica-functionalized electrochemical immunosensor with sensitive enhancement for the rapid screening of benzo[a]pyrene, *Electrochim. Acta* 56 (2011) 1988–1994.
- [87] M. Lin, Y. Liu, Z. Sun, S. Zhang, Z. Yang, C. Ni, Electrochemical immunoassay of benzo[a]pyrene based on dual amplification strategy of electron-accelerated Fe₃O₄/polyaniline platform and multi-enzyme-functionalized carbon sphere label, *Anal. Chim. Acta* 722 (2012) 100–106.
- [88] M. Lin, Y. Liu, C. Liu, Z. Yang, Y. Huang, Sensitive immunosensor for benzo[a]pyrene detection based on dual amplification strategy of PAMAM dendrimer and amino-modified methylene blue/SiO₂ core–shell nanoparticles, *Biosens. Bioelectron.* 26 (2011) 3761–3767.
- [89] M. Lin, Y. Liu, Z. Yang, Y. Huang, Z. Sun, Y. He, C. Ni, Construction of sensitive amperometric immunosensor based on poly (amidoamine) dendrimer and one-step ionic-liquid-assisted graphene/chitosan platform for benzo [a] pyrene detection, *Int. J. Electrochem. Sci.* 7 (2012) 965–978.
- [90] Y. Zhang, S. Wei, J. Xu, S. Chen, An electrochemical immune bioassay for naphthalene using Prussian blue and a nano-gold particle modified glass carbon electrode, *Anal. Meth.* 5 (2013) 6141–6146.
- [91] C. Wei, B.A.M. Bandowe, Y. Han, J. Cao, C. Zhan, W. Wilcke, Polycyclic aromatic hydrocarbons (PAHs) and their derivatives (alkyl-PAHs, oxygenated-PAHs, nitrated-PAHs and azarenes) in urban road dusts from Xi'an, Central China, *Chemosphere* 134 (2015) 512–520.
- [92] B.A.M. Bandowe, H. Meusel, Nitrated polycyclic aromatic hydrocarbons (nitro-PAHs) in the environment – a review, *Sci. Total Environ.* 581–582 (2017) 237–257.
- [93] R.A. Wilson, C.J. Seliskar, G. Talaska, W.R. Heineman, Spectroelectrochemical sensing of pyrene metabolites 1-hydroxypyrene and 1-Hydroxypyrene-glucuronide, *Anal. Chem.* 83 (2011) 3725–3729.
- [94] X. Huang, G. Zhao, M. Liu, F. Li, J. Qiao, S. Zhao, Highly sensitive electrochemical determination of 1-naphthol based on high-index facet SnO₂ modified electrode, *Electrochim. Acta* 83 (2012) 478–484.
- [95] X. Shen, Y. Cui, Y. Pang, H. Qian, Graphene oxide nanoribbon and polyhedral oligomeric silsesquioxane assembled composite frameworks for pre-concentrating and electrochemical sensing of 1-hydroxypyrene, *Electrochim. Acta* 59 (2012) 91–99.
- [96] Y. Pang, Y. Zhang, X. Sun, H. Ding, T. Ma, X. Shen, Synergistical accumulation for electrochemical sensing of 1-hydroxypyrene on electroreduced graphene oxide electrode, *Talanta* 192 (2019) 387–394.
- [97] D.-H. Yang, C.-S. Lee, B.-H. Jeon, S.M. Choi, Y.-D. Kim, J.S. Shin, H. Kim, An electrochemical nanofilm sensor for determination of 1-hydroxypyrene using molecularly imprinted receptors, *J. Ind. Eng. Chem.* 51 (2017) 106–112.
- [98] G. Zhu, X. Zhang, P. Gai, X. Zhang, J. Chen, β -Cyclodextrin non-covalently functionalized single-walled carbon nanotubes bridged by 3,4,9,10-perylene tetracarboxylic acid for ultrasensitive electrochemical sensing of 9-anthracenecarboxylic acid, *Nanoscale* 4 (2012) 5703–5709.
- [99] P. Yang, Q. Zheng, H. Xu, J. Liu, L. Jin, A highly sensitive electrochemical impedance spectroscopy immunosensor for determination of 1-pyronebutyric acid based on the bifunctionality of nafion/gold nanoparticles composite electrode, *Chin. J. Chem.* 30 (2012) 1155–1162.
- [100] S. Ncube, N. Tavengwa, A. Soqaka, E. Cukrowska, L. Chimuka, Development of a single format membrane assisted solvent extraction-molecularly imprinted polymer technique for extraction of polycyclic aromatic hydrocarbons in wastewater followed by gas chromatography mass spectrometry determination, *J. Chromatogr. A* 1569 (2018) 36–43.

CHAPTER 5 Development of a quantum dot molecularly imprinted polymer sensor for fluorescence detection of atrazine

This chapter deals with the development and application of a quantum dot-based sensor for detection of atrazine in water. The format is as published in Luminescence.

Paper

S.A. Nsibande, P.B.C. Forbes, Development of a quantum dot molecularly imprinted polymer sensor for fluorescence detection of atrazine, *Luminescence*, 34 (2019) 1 - 9.

DOI: <https://doi.org/10.1002/bio.3620>

Development of a quantum dot molecularly imprinted polymer sensor for fluorescence detection of atrazine

Sifiso A. Nsibande  | Patricia B.C. Forbes 

Department of Chemistry, Faculty of Natural & Agricultural Sciences, University of Pretoria, Pretoria, South Africa

Correspondence

Patricia B.C. Forbes, Department of Chemistry, Faculty of Natural & Agricultural Sciences, University of Pretoria, Pretoria, South Africa.
Email: patricia.forbes@up.ac.za

Funding information

National Research Foundation of South Africa; Photonics Initiative of South Africa, Grant/Award Number: PISA-15DIR-06; Water Research Commission (WRC), Grant/Award Numbers: K5/2752 and K5/2438/1

Abstract

Atrazine is a common agricultural pesticide which has been reported to occur widely in surface drinking water, making it an environmental pollutant of concern. In the quest for developing sensitive detection methods for pesticides, the use of quantum dots (QDs) as sensitive fluorescence probes has gained momentum in recent years. QDs have attractive and unique optical properties whilst coupling of QDs to molecularly imprinted polymers (MIPs) has been shown to offer excellent selectivity. Thus, the development of QD@MIPs based fluorescence sensors could provide an alternative for monitoring herbicides like atrazine in water. In this work, highly fluorescent CdSeTe/ZnS QDs were fabricated using the conventional organometallic synthesis approach and were then encapsulated with MIPs. The CdSeTe/ZnS@MIP sensor was characterized and applied for selective detection of atrazine. The sensor showed a fast response time (5 min) upon interaction with atrazine and the fluorescence intensity was linearly quenched within the 2–20 mol L⁻¹ atrazine range. The detection limit of 0.80 × 10⁻⁷ mol L⁻¹ is comparable to reported environmental levels. Lastly, the sensor was applied in real water samples and showed satisfactory recoveries (92–118%) in spiked samples, hence it is a promising candidate for use in water monitoring.

KEYWORDS

atrazine, fluorescence sensor, molecularly imprinted polymer, quantum dot

1 | INTRODUCTION

Atrazine is an extensively used herbicide in agriculture for controlling weeds and it may thus eventually contaminate water systems through leaching, runoff and spray drift. For example, it is widely used in South Africa particularly in maize and sorghum production areas and has been reported to occur in water systems.^[1,2] The high global use of atrazine, and pesticides in general, can be attributed to the ever increasing food demand and the need to ensure food security which consequently comes with the risk of environmental contamination. The potential toxic effects of atrazine on aquatic organisms and humans, including endocrine disruption, mutagenicity and potential carcinogenicity, have been well documented.^[3–5] Thus the continuous use and release of this pesticide in the environment warrants the development of simple, economical and yet sensitive analytical

methods which can be adapted for routine monitoring of this compound. Such methods thus serve as an alternative to conventional chromatographic methods which have relatively high running costs.

Fluorescence sensors, particularly quantum dot (QD) based probes, are being explored as an alternative analytical technique for sensitive detection of pesticides as shown in our previous review.^[6] Semiconductor QDs are attractive fluorescence signal reporters in sensing applications due to their unique optical properties which surpasses those of organic fluorophores, including high fluorescence quantum yields, broad absorption, narrow fluorescence emission, high photostability and resistance to photodegradation.^[7–9] They also have a versatile surface chemistry which can be exploited for tailoring probes with desired functionalities.

Molecularly imprinted polymers (MIPs) are popular synthetic receptors that are widely used in designing selective sensors for targeted

application.^[10–15] Some of the attractive advantages of using MIPs is that they are easy to prepare, cost effective, and have high mechanical and chemical stability, and can be tailored towards an analyte of interest. The ability of MIPs to effectively recognize target analytes is dependent on the choice of monomers. Among the commonly used acrylic monomers for atrazine MIPs, simulation studies have shown that methacrylic acid (MAA) is favored since it has better imprinting effects and allows for maximum hydrogen bonding with atrazine.^[16,17]

In this work, therefore, we report on the fabrication of L-cysteine capped CdSeTe/ZnS QDs functionalized with MIPs for the first time and demonstrate the potential application of this probe for atrazine detection. The choice of a ternary alloyed CdSeTe QD core was because they have been shown to have better chemical stability and increased conduction band edge compared to their binary counterparts (CdSe or CdTe).^[18] However, since this structure typically has a high density of surface defects possibly due to the susceptibility of tellurium (Te) to oxidation,^[19] it was necessary to overcoat the core with a ZnS shell. The core/shell QDs were further functionalized with MIPs using MAA as a monomer to enhance selectivity and the resulting CdSeTe/ZnS@MIP was characterized and applied for fluorescence detection of atrazine.

2 | MATERIALS AND METHODS

2.1 | Chemicals

Cadmium oxide (CdO), octadec-1-ene (ODE), tellurium powder (Te), zinc oxide (ZnO), sulfur (S), selenium powder (Se), trioctylphosphine oxide (TOPO), L-cysteine, oleic acid (OA), atrazine standard, (3-mercaptopropyl)trimethoxysilane (MPS), methacrylic acid (MAA),

ethylene glycol dimethacrylate (EGDMA), and 2,2'-azobisisobutyronitrile (AIBN) standard were purchased from Sigma-Aldrich (St Louis, MO, USA). Methanol, absolute ethanol, chloroform, acetone, and potassium hydroxide (KOH) were purchased from Associated Chemical Enterprises (ACE, Johannesburg, South Africa). Deionized water was from an in-house Milli-Q water system.

2.2 | Equipment

Fluorescence emission measurements were recorded on a Horiba Jobin Yvon Fluoromax-4 spectrofluorometer (Horiba Instruments Inc., Edison, NJ, USA). UV-visible absorption spectra were recorded on a Cary Eclipse spectrophotometer (Varian Pty Ltd, Australia). Transmission electron microscopy (TEM) images were taken using a JEOL JEM 2100F (JOEL Ltd, Tokyo, Japan) operated at 200 kV. Powder X-ray diffraction (XRD) patterns were obtained using a Bruker, D2 Phaser (Bruker AXS GmbH, Karlsruhe, Germany), Cu (K α) radiation ($\lambda = 1.54184 \text{ \AA}$). FTIR spectra were measured using a Bruker Alpha-T spectrometer (Bruker Optik GmbH, Ettlingen, Germany).

2.3 | Synthesis of CdSeTe/ZnS QDs

The synthesis of CdSeTe/ZnS QDs was carried out based on a reported procedure for the synthesis of core/shell QDs by our group^[20] with some modifications. A schematic illustration of the synthesis process is shown in Figure 1. Briefly, CdO was added into a solution of 50 mL of ODE and 30 mL of OA and the solution was vigorously stirred in a three-necked flask under argon atmosphere to a temperature of $\sim 260^\circ\text{C}$ in order to form a colorless Cd-OA complex. Once the colorless complex solution was formed, a premixed TOPTe solution

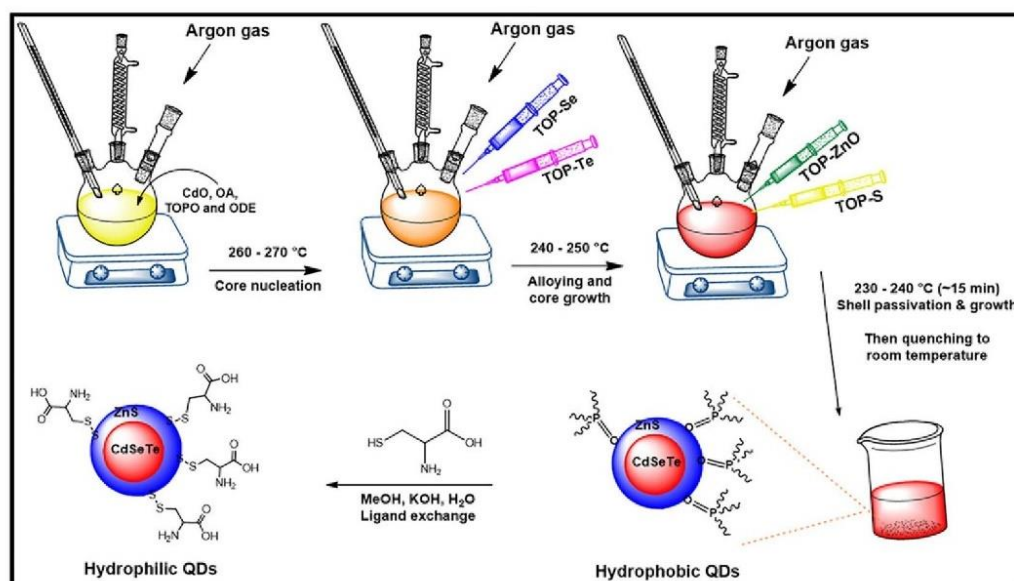


FIGURE 1 Schematic illustration of the synthesis of hydrophobic CdSeTe/ZnS QDs through stepwise hot injection of organometallic precursors. The reaction was continuously purged with argon while monitoring time and temperature. Water soluble QDs were obtained after ligand exchange with L-cysteine

containing 0.48 g of Te and 1.93 g of TOPO in 25 mL of ODE was added into the solution and this was followed swiftly by the addition of a TOPSe solution containing 0.30 g of Se and 1.93 g of TOPO in 25 mL of ODE. Nucleation and growth of the alloyed core QDs was allowed to proceed for about 15 min after which a ZnO solution containing 0.41 g of ZnO dissolved in 20 mL of OA and 30 mL of ODE was injected into the growth solution and this was followed immediately by the addition of the S precursor which consisted of 0.17 g of S in 30 mL ODE and 20 mL OA. The CdSeTe/ZnS QDs were allowed to react for around 40 min with continuous monitoring of the shell growth. Purification of the hydrophobic QDs was carried out using methanol followed by acetone.

The obtained QDs were then surface modified with L-cysteine through ligand exchange in order to make them water soluble (Figure 1). Briefly, the ligand exchange reaction was performed as follows: a KOH-methanolic-L-cysteine solution was prepared by dissolving 3.0 g of KOH in 40 mL of methanol and 2.0 g of L-cysteine was then dissolved in the solution via ultrasonication. The hydrophobic CdSeTe/ZnS QD solution was then added into the KOH-methanolic-L-cysteine solution followed by the addition of Millipore water. This resulted in the separation of the organic phase from the water soluble phase. The solution was stirred for 15 min and was then purified by successive washing with acetone, chloroform, water-chloroform-acetone, and finally with acetone. This rigorous purification step was necessary in order to remove unreacted organic layers embedded on the surface of the QDs.

2.4 | Synthesis of CdSeTe/ZnS@MIP

The strategy that was used to prepare CdSeTe/ZnS@MIP involved firstly the functionalization of the L-cysteine capped QDs with MPS through active condensation of the hydroxyl groups in order to introduce polymerizable vinyl groups on the QD surface,^[21] as shown in Figure 2. To achieve this, 10 mL of MPS was mixed with 5 mL of methanol at room temperature for a few minutes to hydrolyze the alkoxy groups in MPS to form silanol groups. Then 10 mL of aqueous QD solution was added and the mixture was stirred vigorously for about 10 min before heating to 60°C to allow for silanization through condensation of the silanol groups with hydroxy groups on the QD surface. Afterwards the mixture was quenched with methanol and

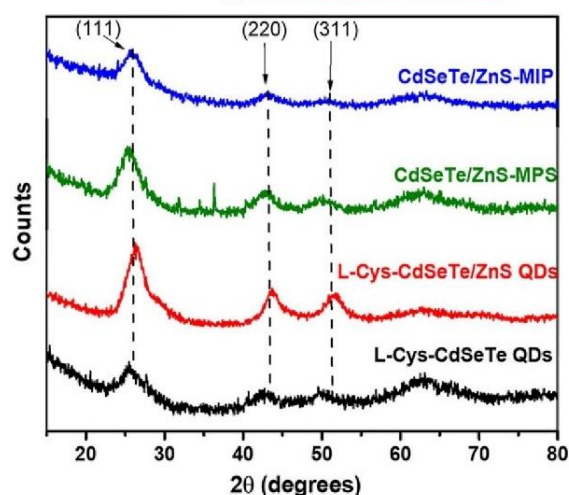


FIGURE 3 Powder X-ray diffraction patterns for CdSeTe QDs, CdSeTe/ZnS QDs, CdSeTe/ZnS-MPS and CdSeTe/ZnS@MIP showing the characteristic zinc-blende crystal structure which was retained after polymerization

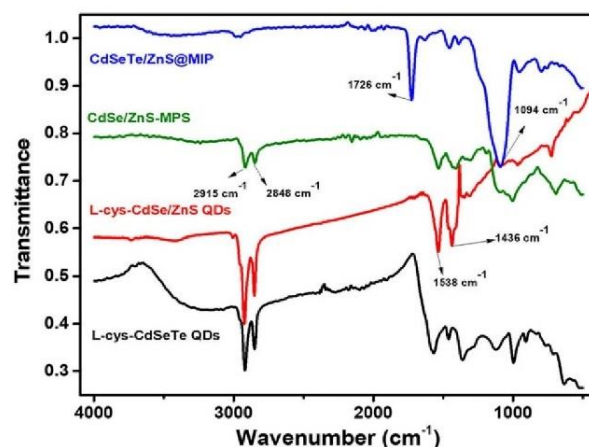


FIGURE 4 FTIR spectra of CdSeTe QDs, CdSeTe/ZnS QDs, CdSeTe/ZnS-MPS and CdSeTe/ZnS@MIP nanoparticles

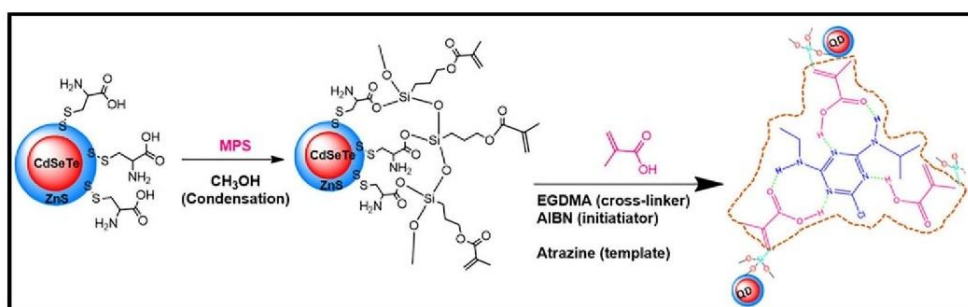


FIGURE 2 Schematic representation of the simultaneous silica encapsulation and vinyl modification of the CdSeTe/ZnS QDs. The MPS caps on the hydroxyl groups of L-cysteine through active condensation, leaving the vinyl groups free for polymerization

the MPS capped QDs were obtained by precipitation with acetone and stored for further use and characterization.

To prepare the QD@MIP, a previously reported method was adapted with modification.^[22] Firstly, in a 250 mL flask, 0.01 mmol atrazine (template) was mixed with 0.4 mmol MAA in ethanol and stirred for about 2 h at room temperature to allow for pre-polymerization self-assembly. Then, 100 mg of the MPS capped QDs was added to the mixture followed by addition of 2 mmol EGDMA crosslinker and 0.06 mmol AIBN which served as a free radical initiator. The mixture that was obtained was purged with nitrogen for about 10 min before it was sealed and heated to 60°C for 24 h to allow for polymerization to occur. The next day the obtained polymer was washed with a 9:1 (v/v) mixture of methanol and acetic acid several times to remove the template, and was dried for further characterization and sensing application. For control, non-molecularly

imprinted CdSeTe/ZnS@NIPs were prepared by following the same procedure but without atrazine template.

2.5 | Determination of fluorescence quantum yield and band gap energies

The fluorescence quantum yield (Φ) was calculated using Equation 1 which compares the integrated fluorescence intensities of the QDs (F_x) to a reference standard, Rhodamine 6G in ethanol (F_{std}) and the respective absorbance of A_x and A_{std} . The refractive indices of solvents used for the sample and standard are represented by n_x and n_{std} respectively, and Φ_{std} represents the fluorescence quantum yield of Rhodamine 6G.^[23] For all measurements, the absorbance at the excitation wavelength was kept below 0.05 in order to avoid inner filter effects.

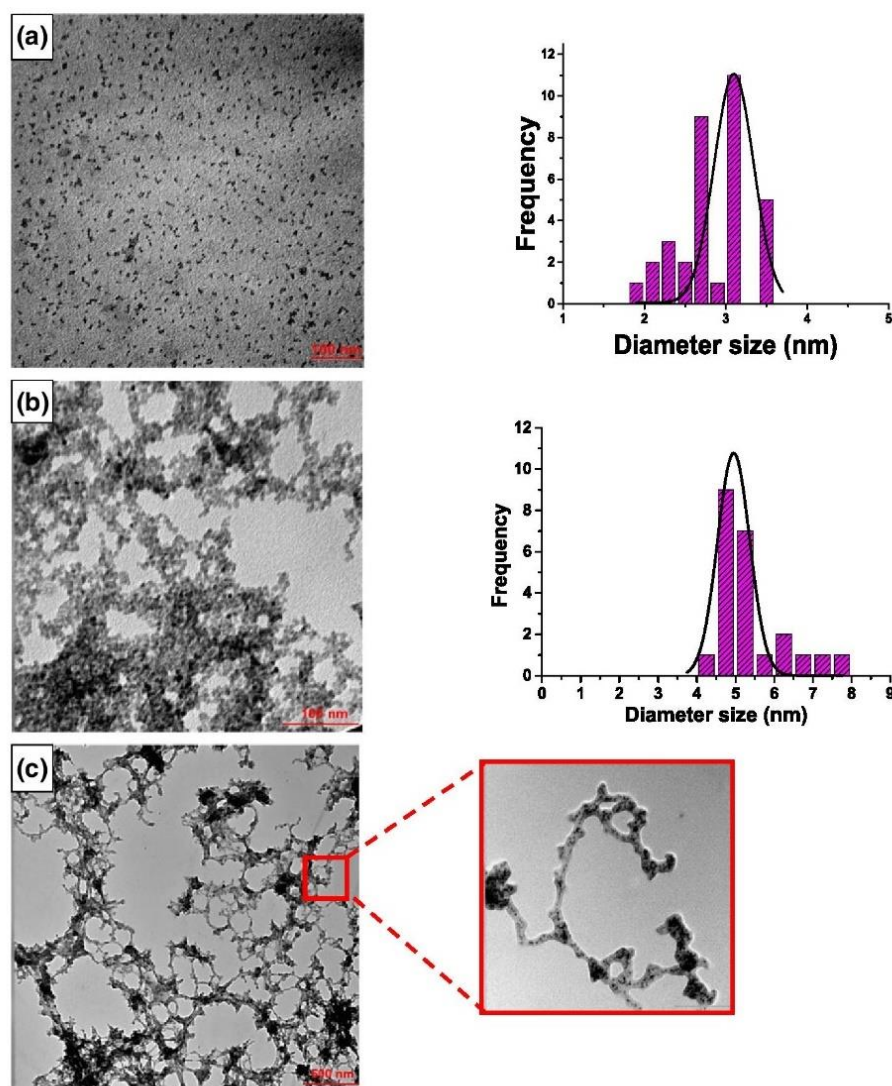


FIGURE 5 Transmission electron microscopy (TEM) images showing spherically shaped CdSeTe QDs (a) and CdSeTe/ZnS QDs (b) dispersed in water. The insets show statistical size distributions with Gaussian fits (black curves). The average particle size for the core was 3.1 ± 0.1 nm while the core/shell was 5.0 ± 0.5 nm. Images in (c) show the CdSeTe/ZnS@MIP material with the QDs imbedded inside the polymer's fiber-like network

$$\phi = \phi_{\text{std}} \frac{F_x A_{\text{std}}}{F_{\text{std}} A_x} \left(\frac{n_x}{n_{\text{std}}} \right)^2 \quad (1)$$

The band gap energy (E) of the different materials was estimated using both absorption data by means of Tauc plots (see Supporting Information Figure S1) and from emission data using Equation 2. Where h is Planck's constant (in J s), c is the speed of light (in m s^{-1}) and λ is the cutoff emission wavelength (in meters).

$$E = \frac{hc}{\lambda} \quad (2)$$

2.6 | Procedure for fluorescence sensing of atrazine

The sensor solution was prepared by dissolving the CdSeTe/ZnS@MIP in ethanol and sonicating for several minutes to allow dispersion of the QD@MIP. The concentration of the QD@MIP was optimized by dilution to 0.05 mg L^{-1} to avoid self-quenching during sensing. Also, the pH of the sensing solution was adjusted to pH 8 using phosphate-buffered saline (PBS) solution, as this was determined to be the optimum. To $500 \mu\text{L}$ of the buffered sensing solution, $100 \mu\text{L}$ of each of a range of atrazine standard solutions ($2\text{--}20 \times 10^{-7} \text{ mol L}^{-1}$) was spiked and an incubation period of 5 min was allowed before taking fluorescence measurements. This was to allow binding of atrazine to the cavities of the polymer. For all fluorescence measurements, 365 nm excitation wavelength was used and both the excitation and emission slit widths were set to 5 nm .

To test the performance of the sensor in real water samples, these were collected from a local tap and from a lake at the University of Pretoria's Sports Campus. After collection, the samples were placed in a cooler box and taken for storage in a refrigerator (at 4°C). Before analysis, the water was centrifuged at 4000 rpm and filtered to remove excess humic matter and particulate suspensions.

3 | RESULTS AND DISCUSSION

3.1 | Powder X-ray analysis

The diffraction patterns showed the characteristic zinc-blende crystal structure for CdSeTe and CdSeTe/ZnS QDs as indexed at the (111), (220) and (311) lattice planes (Figure 3). These confirm epitaxial growth and formation of the ZnS shell around the CdSeTe core whose crystalline form is retained during the synthesis.^[24] These peaks were also retained after functionalization of the QDs with MPS and MIPs which shows that the surface chemistry that was carried out on the core/shell QDs had no effect on the crystal structure.

3.2 | FTIR analysis

FTIR spectra of L-cysteine, core and core/shell QDs are shown in Figure 4. The stretching bands for C=O and C-O were observed at 1537 cm^{-1} and 1434 cm^{-1} , respectively. The bands at $2924\text{--}2850 \text{ cm}^{-1}$ were attributed to N-H. A broad band $\sim 3500 \text{ cm}^{-1}$ was attributed to O-H stretching. This FTIR data, together with

disappearance of the S-H band at 2077 cm^{-1} indicated successful functionalization of the QD surface.

3.3 | TEM analysis

TEM analysis was carried out to investigate the particle size and distribution of the different nanoparticles. As shown in Figure 5, the L-cysteine capped CdSeTe core was mono dispersed in water and had an average particle size of $3.1 \pm 0.1 \text{ nm}$, while the CdSeTe/ZnS

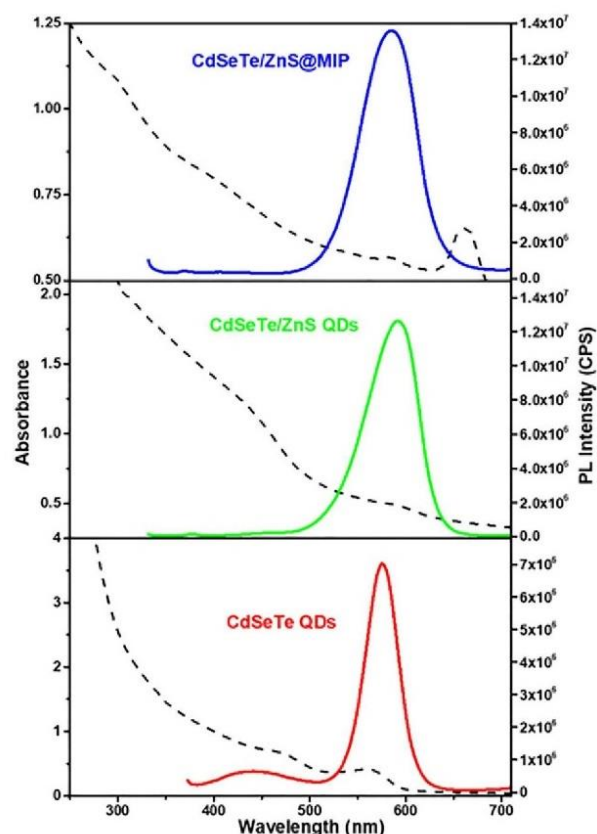


FIGURE 6 Fluorescence emission spectra (solid lines) of CdSeTe QDs at 575 nm , CdSeTe/ZnS QDs at 605 nm , and CdSeTe/ZnS@MIP at 599 nm . The excitation wavelength was 365 nm for all measurements. Absorption spectra (dotted lines) are included with the corresponding emission spectra

TABLE 1 Summary of the photo physical properties CdSeTe QDs, CdSeTe/ZnS QDs and CdSeTe/ZnS@MIP

	CdSeTe QDs	CdSeTe/ZnS QDs	CdSeTe/ZnS @MIP
λ_{em} (nm)	575	605	599
FWHM (nm)	40	57	60
E_g (eV)	2.2	2.0	2.1
ϕ (%)	14.8	72.2	37.3

Note: λ_{em} , wavelength at maximum emission; FWHM, full width at half maximum; E_g , band gap energy; ϕ , fluorescence quantum yield.

QDs had an average size of 5.0 ± 0.5 nm, confirming coating of the core with the ZnS shell (≈ 1 nm thickness).

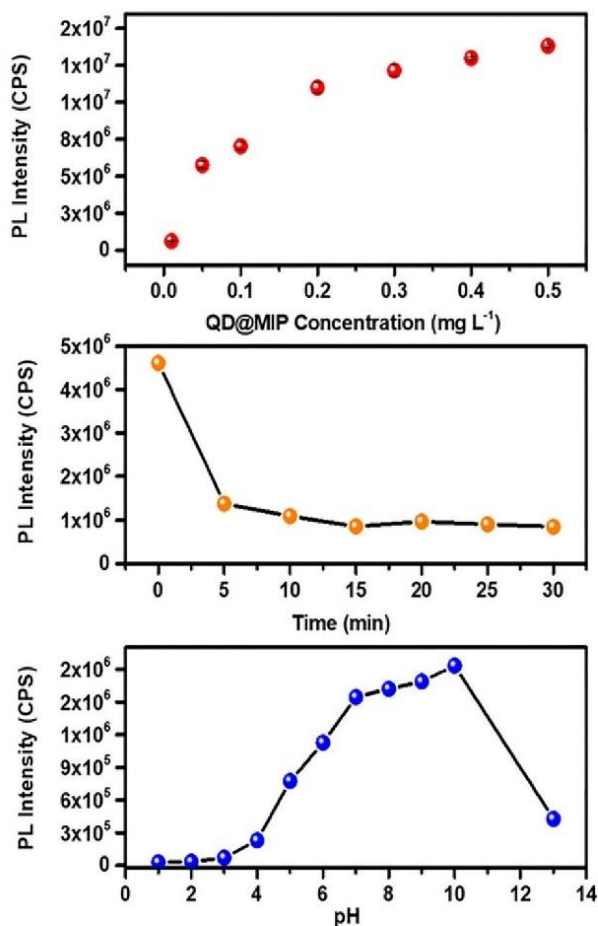


FIGURE 7 (a) The effect of concentration on the fluorescence intensity of the CdSeTe@MIP sensor. (b) The effect of incubation time on the quenching of sensor solution $100 \mu\text{L}$ of $6 \times 10^{-7} \text{ mol L}^{-1}$ concentration. (c) Effect of pH on the fluorescence intensity of the sensor

3.4 | Absorption and fluorescence properties

The normalized fluorescence spectra of core QDs, core/shell QDs and QD@MIP are shown in Figure 6. During synthesis, the core QDs were allowed to grow until the fluorescence emission peak was at 575 nm before adding the ZnS which allowed the QDs to grow further resulting in a shift in emission of 30 nm to 605 nm. It was observed that following the polymerization process, the emission of the QD slightly blue shifted to 599 nm. The characteristic broad absorption spectra are shown in Figure 6 with the corresponding emission spectra. A summary of the optical properties is provided in Table 1.

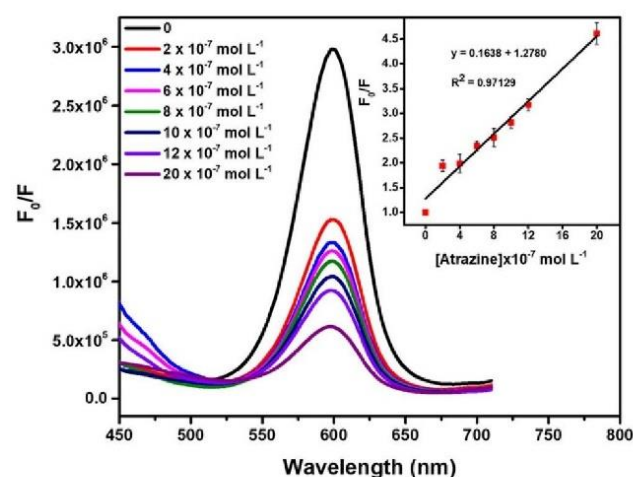


FIGURE 9 The fluorescence spectra of L-cys-CdSeTe/ZnS@MIP in the presence of different concentrations of atrazine (2 – $20 \times 10^{-7} \text{ mol L}^{-1}$). The inset shows the linear response of F_0/F versus atrazine concentration where F_0 is the fluorescence intensity of CdSeTe/ZnS@MIP without atrazine and F is the fluorescence intensity after interaction with atrazine ($n = 3$)

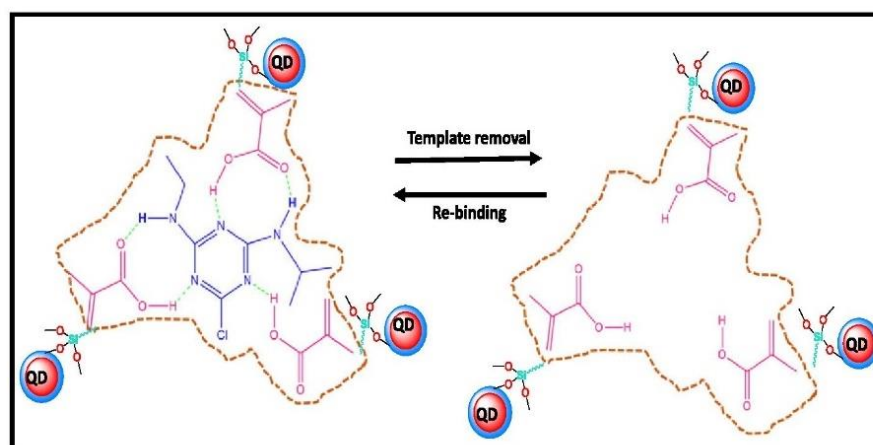


FIGURE 8 Schematic illustration of the binding of atrazine (template) carboxyl groups on methacrylic acid (MAA) through hydrogen bonding on the molecularly imprinted polymer (MIP) matrix and the specific site cavities left after removal of the template

3.5 | Sensor optimization

The effects of concentration, incubation time and pH were investigated in order to determine the optimal working conditions of the CdSeTe/ZnS@MIP sensor. The QD@MIP concentration range was varied from 0.01 to 0.5 mg L⁻¹. As shown in Figure 7(a), detector saturation was approached when the concentration was higher than 0.3 mg L⁻¹ while the fluorescence signal was too weak below 0.01 mg L⁻¹. Therefore, the QD@MIP sensor solution was diluted to 0.05 mg L⁻¹ for application. In any case, low sensor concentrations are ideal to avoid self-quenching during sensing and are also more cost effective.

The effect of incubation time was investigated by mixing 500 μ L of the sensor solution with 100 μ L of 6×10^{-7} mol L⁻¹ of atrazine standard solution. As shown in Figure 7(b) the sensor had a fast response time as interaction with atrazine led to significant fluorescence quenching after 5 min. There was no appreciable quenching beyond

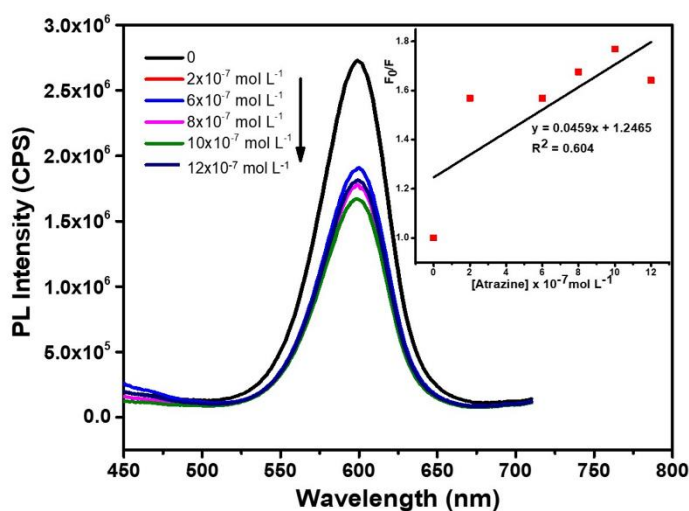


FIGURE 10 The fluorescence spectra of L-cys-CdSeTe/ZnS@NIP in the presence of different concentrations of atrazine (2 – 12×10^{-7} mol L⁻¹). The inset shows a plot of F_0/F versus atrazine concentration where F_0 is the fluorescence intensity of CdSeTe/ZnS@NIP without atrazine and F is the fluorescence intensity after interaction with atrazine

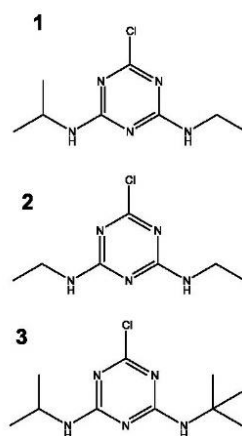


FIGURE 11 Quenching effect of (1) atrazine, (2) simazine and (3) terbutylazine on CdSeTe/ZnS@MIP sensor solution. A 100 μ L of 6×10^{-7} mol L⁻¹ for each compound was used ($n = 3$)

that, hence 5 min incubation time was applied for subsequent sensing applications.

Since the interaction between atrazine and the MIP is dependent on hydrogen bonding, it was also important to investigate the effect of pH by employing buffer solutions. Figure 7(c) shows that the fluorescence intensity is almost completely quenched at extreme pH values and is optimal between pH 7–10. Under very acidic conditions,

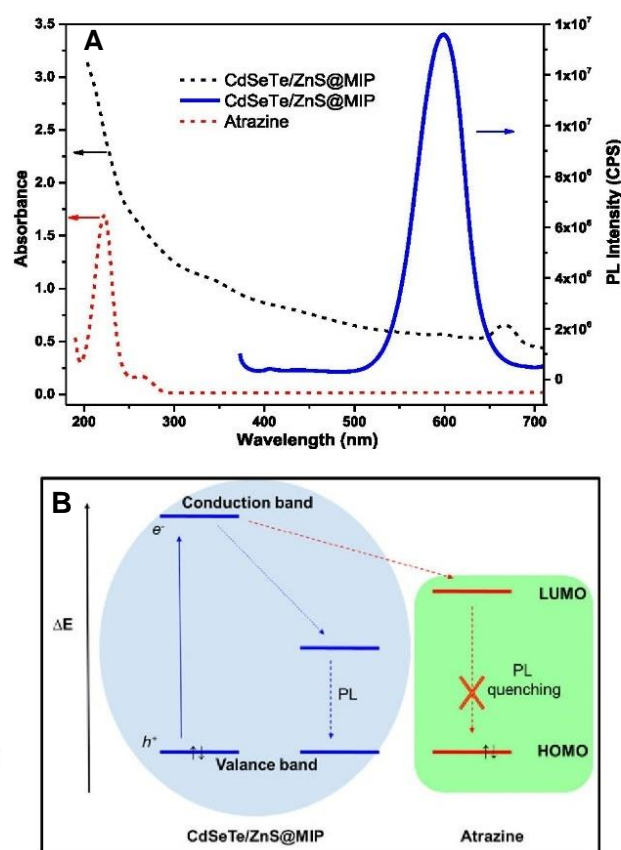
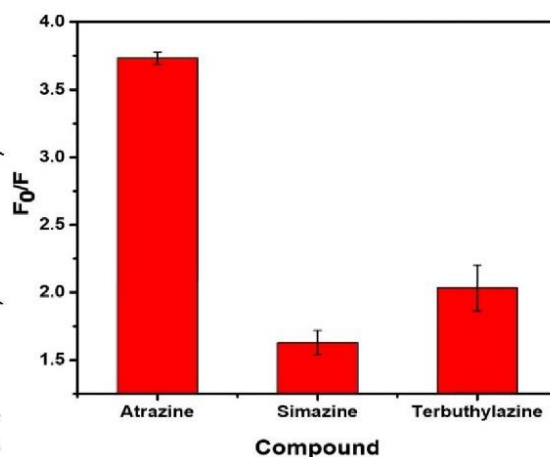


FIGURE 12 (a) UV-visible absorption spectra of atrazine, CdSeTe/ZnS@MIP and emission spectrum of CdSeTe/ZnS@MIP. (b) Schematic illustration of the proposed fluorescence quenching mechanism based on molecular orbital theory



hydrogen bonding would be disrupted and under very basic conditions degradation of the MIP occurs.^[25,26] For subsequent sensing pH 8 was thus chosen as the optimal pH value.

3.6 | Sensing application

The interaction between atrazine with MAA based polymers has been shown to be mainly through hydrogen bonding between the –COOH groups of the MAA monomer^[16] and this is illustrated in Figure 8. Thus, after adding atrazine to the prepared QD@MIP sensor solution, the fluorescence intensity was quenched linearly within the $2\text{--}20 \times 10^{-7} \text{ mol L}^{-1}$ range as shown in Figure 9. For comparison, a similar experiment was done using non-imprinted QD@NIPs and the quenching response linearity was poor compared to QD@MIPs (Figure 10). This can be attributed to the lack of complementary binding cavities for atrazine on the QD@NIP surface.

The limit of detection (LOD) and limit of quantification (LOQ) were calculated for the QD@MIPs using the equations $3\delta/K$ and $10\delta/K$, respectively. Where δ is the standard deviation of blank measurements ($n = 9$) and K is the slope of the calibration curve. Thus, the LOD was found to be $0.80 \times 10^{-7} \text{ mol L}^{-1}$ while the LOQ was $2.7 \times 10^{-7} \text{ mol L}^{-1}$.

3.7 | Specificity of the sensor

The selectivity of the QD@MIP sensor was investigated using atrazine structural analogues, namely terbuthylazine and simazine (Figure 11). These herbicides have similar use to atrazine and therefore it is not

TABLE 2 Recovery tests of atrazine spiked in tap water and lake water at three different concentrations ($n = 3$)

Water sample	Spiked atrazine (mol L^{-1})	Detected atrazine (mean \pm RSD; $n = 3$, mol L^{-1})	Recovery (%)
Tap water	2.0×10^{-7}	2.4 ± 0.2	118.8
	6.0×10^{-7}	6.1 ± 0.1	100.9
	12.0×10^{-7}	11.0 ± 0.04	92.0
Lake water	2.0×10^{-7}	2.2 ± 0.1	111.0
	6.0×10^{-7}	6.2 ± 0.2	103.2
	12.0×10^{-7}	11.6 ± 0.2	97.0

TABLE 3 Comparison of the proposed CdSeTe/ZnS@MIP sensor with other reported sensor systems

Sensor material	Detection method	Matrix	Linear range (mol L^{-1})	LOD (mol L^{-1})	Reference
MICP on platinum electrode	CV	–	$10^{-9}\text{--}1.5 \times 10^{-2}$	1.0×10^{-7}	[27]
MIP film using o-PD	DPV	–	$0.05\text{--}1.4 \times 10^{-7}$	0.001×10^{-6}	[28]
Ag/AgCl electrode @MIP	CV	–	$1\text{--}10 \times 10^{-6}$	1×10^{-6}	[29]
Platinum NPs/C ₃ N ₄ NTs	SWV	–	$10^{-12}\text{--}10^{-10}$	0.15×10^{-12}	[30]
Fe ₃ O ₄ -chitosan@MIP	Fluorescence	Water	$2.32\text{--}185.4 \times 10^{-6}$	0.86×10^{-6}	[31]
SiO ₂ @Zn protoporphyrin – MIP (core-shell)	Fluorescence	Deionized water and lake water	$0\text{--}1 \times 10^{-4}$	1.8×10^{-6}	[32]
L-cys-CdSeTe/ZnS@MIP	Fluorescence	PBS buffer solution	$2\text{--}20 \times 10^{-7} \text{ M}$	0.80×10^{-7}	This work

Note: CV, cyclic voltammetry; DPV, differential pulse voltammetry; LOD, limit of detection; MIP, molecularly imprinted polymer; MICP, molecularly imprinted conducting polymer, i.e. poly(3,4-ethylenedioxythiophene-co-thiophene-acetic acid); NPs, nanoparticles; NTs, nanotubes; o-PD, o-phenylenediamine; PBS, phosphate-buffered saline; SWV, square wave voltammetry.

uncommon that they tend to occur simultaneously with atrazine in water systems. To $500 \mu\text{L}$ (pH 8) of the sensor solution, $100 \mu\text{L}$ $6 \times 10^{-7} \text{ mol L}^{-1}$ of each compound was added followed by a 5 min incubation time before taking photoluminescence measurements. As can be seen in Figure 11, the fluorescence intensity was quenched more in the case of atrazine than for terbuthylazine and simazine, respectively.

3.8 | Proposed sensing mechanism

In order to elucidate the fluorescence quenching mechanism of the sensor, the absorption spectra of atrazine and CdSeTe/ZnS@MIP were overlaid with the emission spectrum of CdSeTe/ZnS@MIP and no overlap was evident (Figure 12a). Thus, the fluorescence quenching that was observed during sensing could likely be attributed to electron transfer between atrazine and the CdSeTe/ZnS@MIP nanoparticle. The fluorescence quenching can further be explained using molecular orbital theory, as shown in Figure 12(b). Upon formation of the strong hydrogen bond between atrazine and CdSeTe/ZnS@MIP, the excited electron could instead of returning to the ground state, be captured into the lowest unoccupied molecular orbital (LUMO) of atrazine thereby leading to fluorescence quenching.

3.9 | Application to real water samples

Water samples were collected from a local tap and from a lake at the University of Pretoria's Sports Campus. After confirmation by ultra-high performance liquid chromatography coupled with tandem mass spectrometry (UPLC-MS/MS) that no atrazine was present in these samples, they were spiked at three different concentrations within the linear range of the calibration curve. Thus, $100 \mu\text{L}$ of each spiked sample was mixed with $500 \mu\text{L}$ of buffered CdSeTe/ZnS@MIP sensor solution and an incubation period of 5 min was allowed before taking fluorescence measurements. Table 2 shows the recoveries and these were found to be satisfactory ranging from 92 to 118%, indicating that the performance of the sensor was not significantly affected by potential interfering compounds that could be present in environmental water.

Finally, the analytical performance of our proposed sensor was compared to that of other atrazine sensors that have been reported as shown in Table 3. The reported electrochemical methods generally

have lower detection limits and wider linear ranges, but their drawback is the use of expensive materials like platinum. However, when the CdSeTe/ZnS@MIP sensor is compared to other reported fluorescence methods, it shows an improved detection limit and this could be due to our choice of fluorescence signal reporter (the QDs) which are more sensitive and have superior optical properties than other fluorophores.

4 | CONCLUSION

The continuous use of atrazine in agriculture sometimes leads to unintended contamination of water resources and this warrants the development of simple and sensitive analytical methods that can be used for monitoring this herbicide in water. In this work we synthesized and characterized the morphological and optical properties of CdSeTe/ZnS@MIP using TEM, powder XRD, FTIR, UV-visible and fluorescence spectrophotometry. We then demonstrated its potential application as a selective fluorescence sensor for sensitive detection of atrazine in buffer solutions. The sensor showed linear fluorescence quenching upon interaction with atrazine in the $2\text{--}20 \times 10^{-7} \text{ mol L}^{-1}$ range with a LOD of $0.80 \times 10^{-7} \text{ mol L}^{-1}$. The World Health Organization (WHO) guideline limit for atrazine in water is 0.1 mg L^{-1} ($4.6 \times 10^{-7} \text{ mol L}^{-1}$) hence the sensor has potential in regulatory applications. The performance was further tested in tap and lake water samples and showed satisfactory recoveries ranging from 92 to 118%.

ACKNOWLEDGEMENTS

Funding from the Water Research Commission (WRC) (Grant K5/2438/1 and K5/2752), the Photonics Initiative of South Africa (Grant PISA-15DIR-06) and the National Research Foundation of South Africa (postgraduate student bursary to SN) is gratefully acknowledged. The authors thank the Microscopy and Microanalysis Laboratory of the University of Pretoria, for their assistance with microscopy measurements and Dr Melanie Rademeyer for assistance with XRD measurements.

ORCID

Sifiso A. Nsibande  <https://orcid.org/0000-0001-7371-9356>

Patricia B.C. Forbes  <https://orcid.org/0000-0003-3453-9162>

REFERENCES

- [1] J. M. Dabrowski, J. M. Shadung, V. Wepener, *Environ. Intern.* **2014**, *62*, 31.
- [2] L. H. Du Preez, P. J. Jansen van Rensburg, A. M. Jooste, J. A. Carr, J. P. Giesy, T. S. Gross, R. J. Kendall, E. E. Smith, G. Van Der Kraak, K. R. Solomon, *Environ. Pollut.* **2005**, *135*(1), 131.
- [3] A. C. Bejarano, G. T. Chandler, *Environ. Toxicol. Chem.* **2003**, *22*(12), 3009.
- [4] S. K. Nair, S. M. Bartell, R. A. Brain, *Environ. Toxicol. Chem.* **2015**, *34*(11), 2590.
- [5] R. J. Wood, S. M. Mitrovic, R. P. Lim, B. J. Kefford, *Aquat. Toxicol.* **2017**, *189*, 200.
- [6] S. A. Nsibande, P. B. C. Forbes, *Anal. Chim. Acta* **2016**, *945*, 9.
- [7] L. Cui, X.-P. He, G.-R. Chen, *RSC Adv.* **2015**, *5*(34), 26644.
- [8] R. Freeman, I. Willner, *Chem. Soc. Rev.* **2012**, *41*(10), 4067.
- [9] L. Lin, M. Rong, F. Luo, D. Chen, Y. Wang, X. Chen, *TrAC, Trends Anal. Chem.* **2014**, *54*, 83.
- [10] L. Chen, X. Wang, W. Lu, X. Wu, J. Li, *Chem. Soc. Rev.* **2016**, *45*(8), 2137.
- [11] G. Ertürk, B. Mattiasson, *Sensors* **2017**, *17*(2), 288.
- [12] J. Li, J. Fu, Q. Yang, L. Wang, X. Wang, L. Chen, *Analyst* **2018**, *143*(15), 3570.
- [13] X. Wang, J. Yu, X. Wu, J. Fu, Q. Kang, D. Shen, J. Li, L. Chen, *Biosens. Bioelectron.* **2016**, *81*, 438.
- [14] Q. Yang, J. Li, X. Wang, H. Peng, H. Xiong, L. Chen, *Biosens. Bioelectron.* **2018**, *112*, 54.
- [15] Z. Zhang, J. Li, X. Wang, D. Shen, L. Chen, *ACS Appl. Mater. Interfaces* **2015**, *7*(17), 9118.
- [16] Y. Han, L. Gu, M. Zhang, Z. Li, W. Yang, X. Tang, G. Xie, *Comput. Theor. Chem.* **2017**, *1121*, 29.
- [17] D. Lakshmi, M. Akbulut, P. K. Ivanova-Mitseva, M. J. Whitcombe, E. V. Piletska, K. Karim, O. Güven, S. A. Piletsky, *Ind. Eng. Chem. Res.* **2013**, *52*(39), 13910.
- [18] Z. Pan, K. Zhao, J. Wang, H. Zhang, Y. Feng, X. Zhong, *ACS Nano* **2013**, *7*(6), 5215.
- [19] J. Yang, J. Wang, K. Zhao, T. Izuishi, Y. Li, Q. Shen, X. Zhong, *J. Phys. Chem. C* **2015**, *119*(52), 28800.
- [20] O. Adegoke, P. B. C. Forbes, *Talanta* **2016**, *146*, 780.
- [21] C. Bressy, V. G. Ngo, F. Ziarelli, A. Margailan, *Langmuir* **2012**, *28*(6), 3290.
- [22] Z. Zhou, T. Li, W. Xu, W. Huang, N. Wang, W. Yang, *Sens. Actuators, B* **2017**, *240*, 1114.
- [23] D. Magde, R. Wong, P. G. Seybold, *Photochem. Photobiol.* **2002**, *75*(4), 327.
- [24] G. X. Liang, L. L. Li, H. Y. Liu, J. R. Zhang, C. Burda, J. J. Zhu, *Chem. Commun.* **2010**, *46*(17), 2974.
- [25] C. Wang, Q. Ma, W. Dou, S. Kanwal, G. Wang, P. Yuan, X. Su, *Talanta* **2009**, *77*(4), 1358.
- [26] J. Yu, X. Wang, Q. Kang, J. Li, D. Shen, L. Chen, *Environ. Sci.: Nano* **2017**, *4*(2), 493.
- [27] E. Pardieu, H. Cheap, C. Vedrine, M. Lazerges, Y. Lattach, F. Garnier, S. Remita, C. Pernelle, *Anal. Chim. Acta* **2009**, *649*(2), 236.
- [28] X. Li, Y. He, F. Zhao, W. Zhang, Z. Ye, *RSC Adv.* **2015**, *5*(70), 56534.
- [29] R. Shoji, T. Takeuchi, I. Kubo, *Anal. Chem.* **2003**, *75*(18), 4882.
- [30] M. L. Yola, N. Atar, *Ind. Eng. Chem. Res.* **2017**, *56*(27), 7631.
- [31] G. Liu, T. Li, X. Yang, Y. She, M. Wang, J. Wang, M. Zhang, S. Wang, F. Jin, M. Jin, H. Shao, Z. Jiang, H. Yu, *Carbohydr. Polym.* **2016**, *137*, 75.
- [32] R. Liu, G. Guan, S. Wang, Z. Zhang, *Analyst* **2011**, *136*(1), 184.

SUPPORTING INFORMATION

Additional supporting information may be found online in the Supporting Information section at the end of the article.

How to cite this article: Nsibande SA, Forbes PBC. Development of a quantum dot molecularly imprinted polymer sensor for fluorescence detection of atrazine. *Luminescence*. 2019;1–9. <https://doi.org/10.1002/bio.3620>

Supporting information

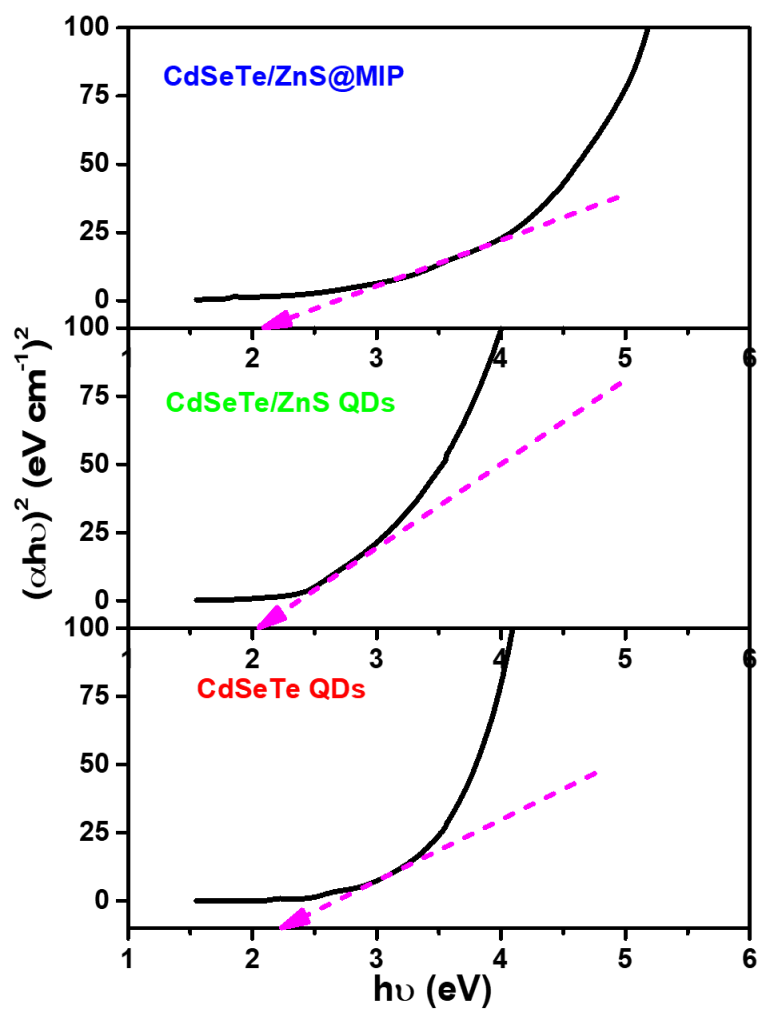


Figure S4 Tauc plots used for estimating the band gap (eV) of CdSeTe QDs, CdSeTe/ZnS QDs and CdSeTe/ZnS@MIP.

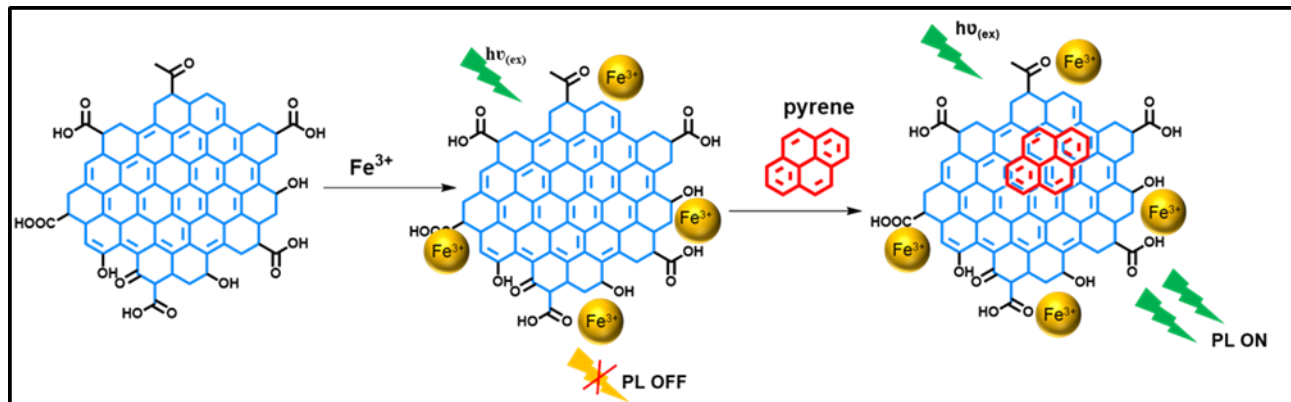
CHAPTER 6 Development of a turn-on graphene quantum dot-based fluorescence probe for sensing of pyrene in water

In this chapter a detection strategy that uses GQDs and ferric ions was developed for detection of pyrene in water samples. The format is as published in RSC Advances.

Paper

S.A. Nsibande, P.B.C. Forbes, Development of a turn-on graphene quantum dot-based fluorescence probe for sensing of pyrene in water, RSC Advances, 10 (2020)12119 – 12128.

DOI: <https://doi.org/10.1039/c9ra10153e>



PAPER

Cite this: *RSC Adv.*, 2020, 10, 12119

Development of a turn-on graphene quantum dot-based fluorescent probe for sensing of pyrene in water†

Nsibande S. A.  and Forbes P. B. C. *

Polycyclic aromatic hydrocarbons (PAHs) are potentially harmful pollutants that are emitted into the environment from a range of sources largely due to incomplete combustion. The potential toxicity and carcinogenic effects of these compounds warrants the development of rapid and cost-effective methods for their detection. This work reports on the synthesis and use of graphene quantum dots (GQDs) as rapid fluorescence sensors for detecting PAHs in water. The GQDs were prepared from two sources, *i.e.* graphene oxide (GO) and citric acid (CA) – denoted GO-GQDs and CA-GQDs, respectively. Structural and optical properties of the GQDs were studied using TEM, Raman, and fluorescence and UV-vis spectroscopy. The GQDs were then applied for detection of pyrene in environmental water samples based on a “turn-off-on” mechanism where ferric ions were used for turn-off and pyrene for turn-on of fluorescence emission. The fluorescence intensity of both GQDs was switched on linearly within the $2\text{--}10 \times 10^{-6} \text{ mol L}^{-1}$ range and the limits of detection were found to be $0.325 \times 10^{-6} \text{ mol L}^{-1}$ and $0.242 \times 10^{-6} \text{ mol L}^{-1}$ for GO-GQDs and CA-GQDs, respectively. Finally, the potential application of the sensor for environmental water samples was investigated using lake water and satisfactory recoveries (97–107%) were obtained. The promising results from this work demonstrate the feasibility of pursuing cheaper and greener environmental monitoring techniques.

Received 4th December 2019
Accepted 19th March 2020

DOI: 10.1039/c9ra10153e

rsc.li/rsc-advances

1. Introduction

Polycyclic aromatic hydrocarbons (PAHs) are a class of organic compounds with fused benzene rings which are of environmental concern. These compounds can be introduced into environmental compartments (water, soil, sediments and air) through various pathways including industrial activities, biomass burning, and vehicular emissions, amongst others. A number of comprehensive studies have documented the occurrence of PAHs in a variety of matrices, including water.^{1–7}

The environmental monitoring of these compounds continues to be of importance due to their potential negative health effects, as some PAHs have been reported to be either carcinogenic or potentially carcinogenic.^{8–10} The toxicity of a number of PAH compounds can further be enhanced upon their metabolism and photooxidation into derivative compounds.^{4,11} Moreover, in aquatic systems, where PAHs normally occur as mixtures, they can have increased toxicity compared to individual PAHs due to synergistic effects.¹²

The low solubility of PAHs in water means that they typically occur at low concentrations in environmental samples, thus

sensitive analytical techniques are required for monitoring of these compounds. Traditionally, chromatographic techniques are used as ‘gold standards’ for monitoring and quantification of PAHs. However, these techniques can be expensive especially where routine monitoring is required. As an alternative to chromatographic techniques, researchers have been investigating the use of various nanomaterials as sensors and/or platforms for sensitive detection of PAHs, as recently reviewed.¹³

Graphene materials have been widely explored in developing sensors for PAHs. We previously demonstrated the potential use of semiconductor quantum dots coupled to graphene oxide to form conjugate platforms for fluorescence detection of PAHs,^{14,15} for example. The success of such sensors was attributed to the excellent fluorescence properties QDs (including high quantum yields and photostability) and the ability to modify their surfaces with desired functionalities, such as the formation of a nanocomposite with graphene oxide to enhance interaction with PAHs. However, the major drawback of these sensors is the use of heavy metals like cadmium which have the potential to leach from the sensor material and raise environmental and health concerns.

In recent years, graphene quantum dots (GQDs) have emerged as a possible alternative to semiconductor QDs. GQDs can be regarded as extremely small, zero-dimensional pieces of graphene which have quantum confinement and edge effect properties similar to carbon dots.¹⁶ The fluorescence properties

Chemistry Department, Faculty of Natural and Agricultural Sciences, University of Pretoria, South Africa. E-mail: patricia.forbes@up.ac.za

† Electronic supplementary information (ESI) available. See DOI: 10.1039/c9ra10153e

of GQDs arise from the radiative recombination of electron-hole (e-h) pairs in sp^2 aromatic carbon sites. This is because graphene has infinitely large Bohr diameters (distance between electron and hole) and therefore its fragments, *i.e.* GQDs, of any size exhibit quantum confinement effects.¹⁷

These GQDs have certain advantageous properties over semiconductor QDs, including higher photostability, biocompatibility, large surface area, better surface grafting using π - π conjugation and surface groups, and they have lower toxicity^{18–20} which has allowed for their use in biological applications.²¹ Thus GQDs have recently found extensive application in the design of sensing probes.^{18,22–24} Moreover, GQDs can be easily prepared using various synthesis routes, which can be categorized into two main categories; namely the “top-down” approach or the “bottom-up” approach. The top-down approach involves the breaking of bulk macroscopic carbon materials (like graphite, carbon fibers, graphene oxide, metal-organic frameworks, *etc.*) usually through harsh oxidation treatments or lithography techniques. The bottom-up approach involves growing GQDs from small molecular precursors (like citric acid, glucose, PAHs, *etc.*) through controlled reactions to obtain desired GQDs nano-sizes.^{18,23,25} These two approaches have been widely used by researchers and they each have pros and cons depending on the intended application and availability of raw materials.

To this end, the analytical application of GQDs has mostly been towards metal ions sensing²⁶ with few studies reporting their use for organic pollutant detection like pentachlorophenol,²⁷ trinitrotoluene²⁸ and the pesticide tributyltin.²⁹

In this work therefore, we report on the use of GQDs with associated ferric ions for fluorescence detection of PAHs in environmental water samples. Two GQD synthetic approaches were explored for comparison, where those made from citric acid are denoted CA-GQDs, and those prepared from graphene oxide are denoted GO-GQDs. The GQDs were then applied to the detection of pyrene, a four-ring PAH, in environmental water samples for the first time. A fluorescence “turn-off-on” detection strategy was used where ferric ions were used to turn off the fluorescence of the GQDs and subsequent contact with pyrene switched the fluorescence back on.

2. Materials and methods

2.1 Equipment and reagents

Fluorescence emission spectra were recorded on a Horiba Jobin Yvon Fluoromax-4 Spectrofluorometer (Horiba Instruments Inc., Edison, NJ, USA). UV-vis absorption spectra were recorded on a Cary Eclipse spectrophotometer (Varian Pty Ltd, Australia).

FTIR spectra were measured using a Bruker Alpha-T spectrometer (Bruker Optik GmbH, Ettlingen, Germany). Transmission electron microscopy (TEM) images were taken using a JEOL JEM 2100F (JOEL Ltd, Tokyo, Japan) operated at 200 kV. The ImageJ software was used to analyse particle size distribution. Raman spectra were recorded with a Horiba T64000 spectrometer (Horiba Jobin Yvon, France) using a 514 nm laser source operated at 0.020 W. SnakeSkin™ dialysis tubing (3.5 kDa MCOW) was purchased from Thermo Fisher Scientific. Polytetrafluoroethylene micro-filters (0.22 μm and 0.45 μm) were purchased from Stargate Scientific.

Citric acid (CA), sodium hydroxide (NaOH), hydrochloric acid (HCl), iron III chloride (FeCl_3), potassium permanganate (KMnO_4), sodium nitrate (NaNO_3), sulphuric acid (H_2SO_4) and hydrogen peroxide (H_2O_2) were all purchased from Sigma-Aldrich. Deionized (DI) water for all experiments was obtained from a Millipore Direct-Q® 3 UV system (Molsheim, France).

The fluorescence quantum yield for all GQDs was calculated by comparing the fluorescence integrated intensities of the GQDs in water to that of a reference standard, namely pyrene, in ethanol.³⁰

$$\Phi_x = \Phi_{\text{std}} \left(\frac{m_x}{m_{\text{std}}} \right) \left(\frac{n_x^2}{n_{\text{std}}^2} \right)$$

where Φ_x is the quantum yield of GQDs, Φ_{std} is the quantum yield of the reference standard, (0.65 in this case), m_x and m_{std} are gradients for the plot of integrated fluorescence intensities *vs.* absorbances for GQDs and standard, respectively, and n refers to the refractive indices of the solvents.

2.2 Bottom-up synthesis of CA-GQDs

GQDs were prepared from citric acid (CA) *via* direct pyrolysis³¹ as illustrated in Fig. 1. Briefly, about 2 g of CA was placed in a beaker and heated to ~ 200 °C on a hot plate. After about 5 min the CA turned into a transparent solution and after a further 15 min of heating it turned pale yellow, suggesting formation of GQDs. The reaction was then stopped followed by slow addition of NaOH (0.25 mol L^{-1}) while stirring vigorously at 300 rpm with a magnetic stirrer. The pH was then adjusted to pH 7 using NaOH and HCl as required, and the resulting pale-yellow solution was purified through dialysis tubing for 2 days to remove unreacted citric acid and excess Na^+ and Cl^- ions. The obtained solution was stored in the refrigerator for further use and analysis.

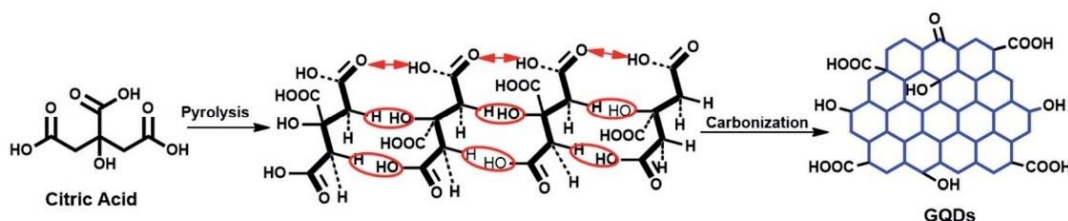


Fig. 1 Schematic illustration of the synthesis of fluorescent GQDs from citric acid through pyrolysis and carbonization.

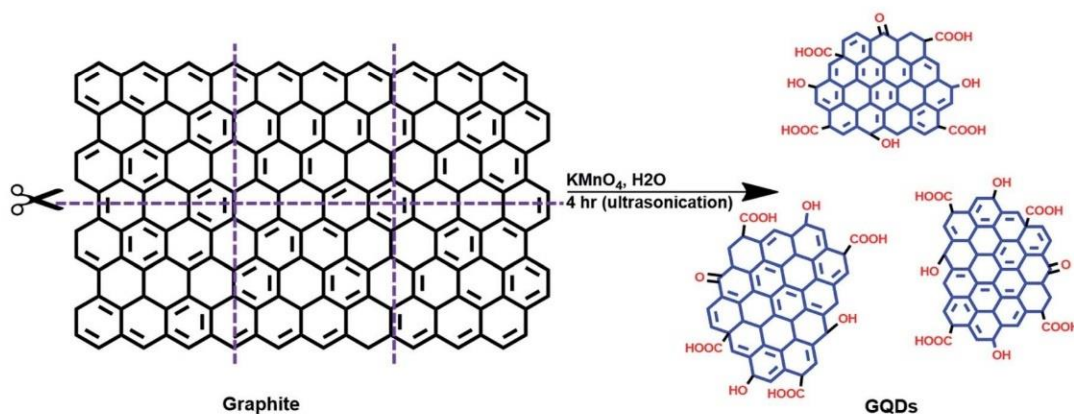


Fig. 2 Schematic illustration of the top-down preparation of QGDs through oxidation of graphene oxide.

2.3 Top-down synthesis of GO-QGDs

Graphene oxide (GO) was first prepared from graphite powder using a modified Hummers' method.³² In a 250 mL round-bottom flask which was placed in an ice bath, 60 mL of H₂SO₄ was added followed by 2.5 g of graphite powder and 1.25 g of NaNO₃. This mixture was stirred vigorously to allow for

dispersion of the graphite. Then 7.5 g of KMnO₄ was added and after stirring for a few hours the ice bath was removed and the mixture was stirred at room temperature overnight resulting in formation of a brownish mixture. 75 mL of DI water was gradually added to this mixture, which was then allowed to stir overnight. The following day, 25 mL of 30% H₂O₂ was added

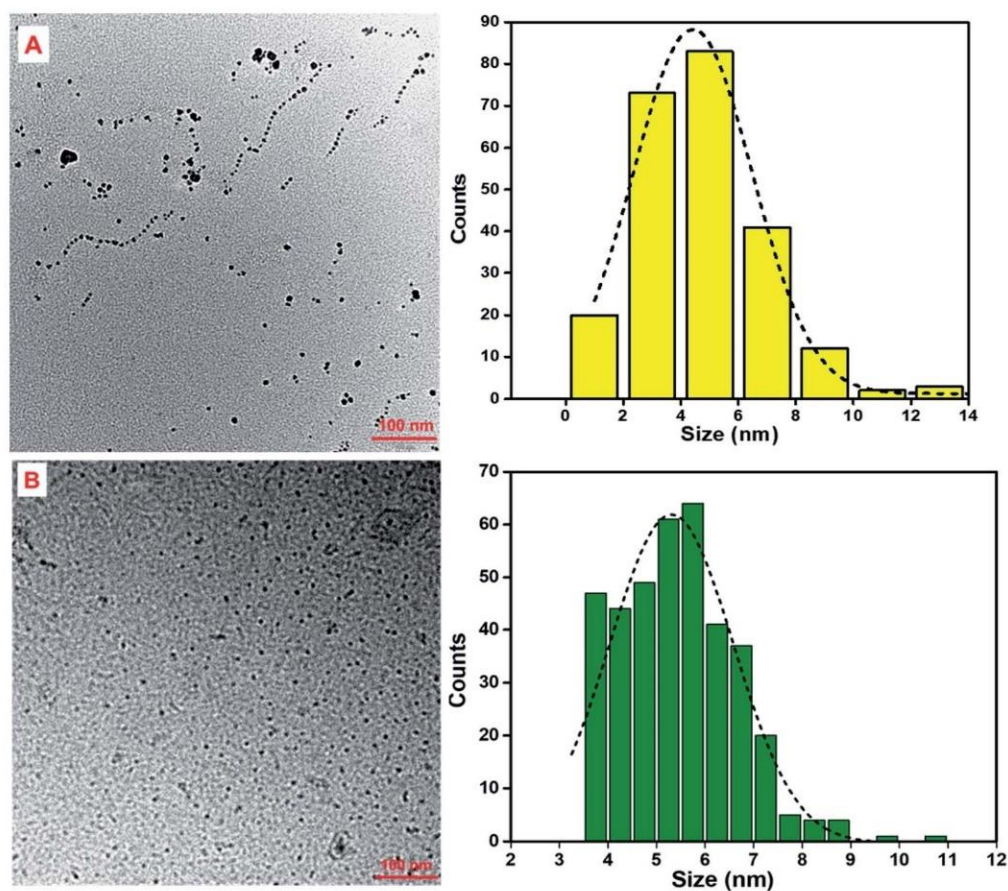


Fig. 3 (a) TEM images of (A) CA-QGDs and (B) GO-QGDs with corresponding particle size distributions (right). The average size for CA-QGDs was 4.8 ± 0.1 nm and 5.5 ± 0.3 nm for GO-QGDs.

and the mixture was then centrifuged and washed first with 5% HCl then with DI water to remove excess unreacted reactant metal ions. The obtained GO powder was dried in an oven at 65 °C and subsequently used to prepare QGDs.

The synthesis of QGDs from GO was carried out using previously reported methods with some modifications³³ and is schematically shown in Fig. 2. Briefly, in a round-bottom flask, 0.050 g of graphene oxide (GO) was mixed with 0.050 g KMnO_4 followed by addition of 100 mL of water to form a homogenous mixture. This mixture was then sonicated for 4 h to ensure complete oxidation. Then the mixture was centrifuged at 500 rpm for 10 min to remove large unreacted GO. The supernatant was then filtered first with a 0.45 μm filter PTFE then with a 0.22 μm filter to obtain the QGD solution (Fig. S1†). The solution was further purified by dialysis against deionized water using a 3.5 kDa membrane to remove excess salts and was stored in the refrigerator (at ~ 4 °C) for further use and

characterization. The QGDs prepared through this method are denoted by GO-QGDs.

2.4 Fluorescence detection of pyrene

QGDs have been widely used as sensors for selective detection of Fe^{3+} ions.^{34–36} The ability of Fe^{3+} to induce fluorescence quenching has been attributed to coordination of the ferric ions with surface hydroxyl groups of QGDs to form aggregates like iron hydroxides.³⁷ In this work, the quenched QGDs–Fe aggregates were then used for fluorescence turn-on detection of pyrene. A fixed amount of Fe^{3+} solution (50 μL of 30 $\mu\text{g L}^{-1}$) was introduced to 400 μL of QGD solution (~ 0.5 mg mL^{-1}) and 1 min time interval was allowed for interaction. Thereafter 200 μL of different pyrene concentrations ($2\text{--}10 \times 10^{-6}$ mol L^{-1}) were individually added and an incubation time of 5 min was allowed before fluorescence measurements were recorded. For

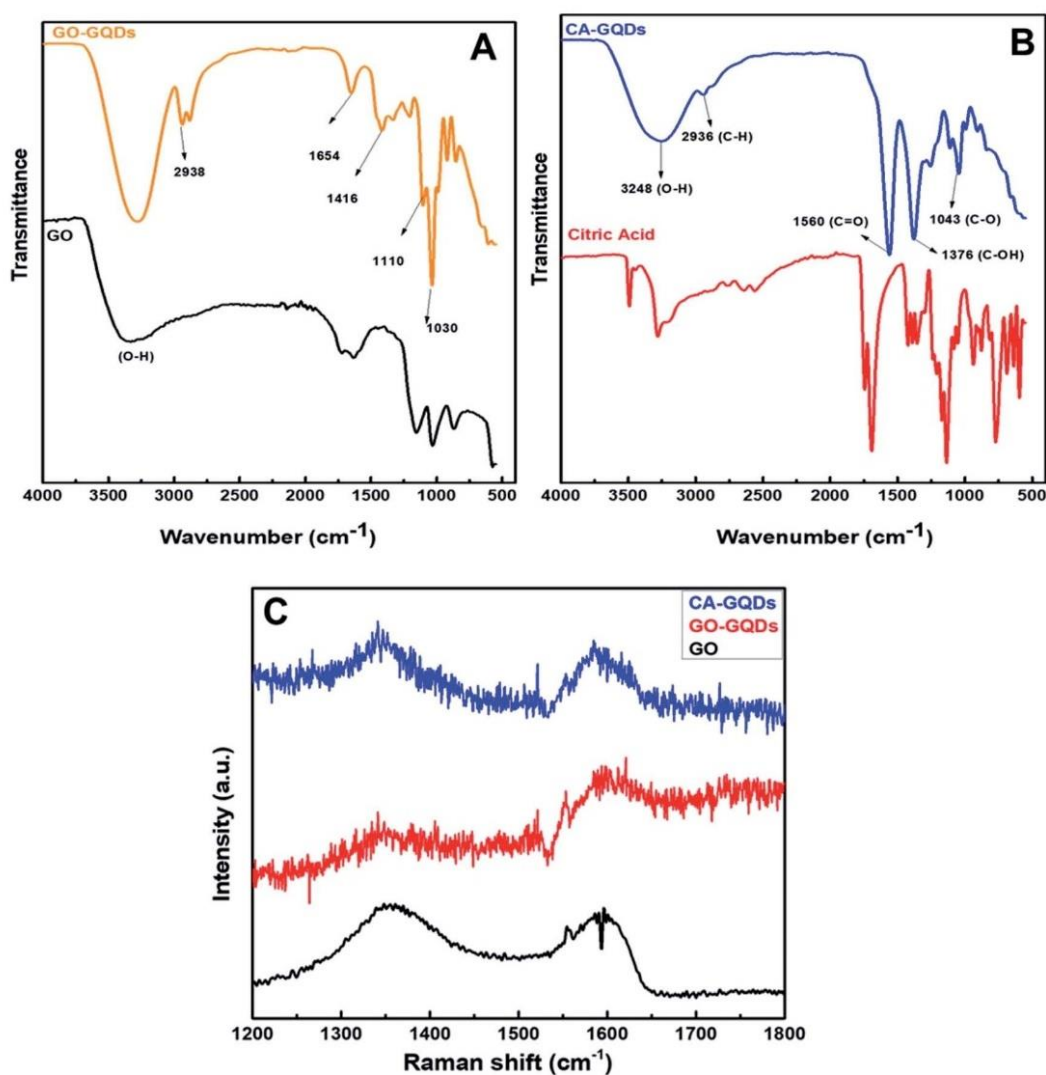


Fig. 4 FTIR spectra of both GO-QGDs (A) and CA-QGDs (B) and their respective precursors. (C) Raman spectra of graphene oxide (GO), CA-QGDs and GO-QGDs.

all PL measurements, the excitation wavelength was 320 nm and both the excitation and emission slit widths were set at 5 nm. The performance of the sensor was tested for real environmental water samples using water from a small lake within the University of Pretoria's Sports Campus. The samples were filtered through a 0.45 μm filter to remove any entrained sediments or suspended material, and aliquots were then spiked at three different concentrations ($3, 6$ and 10×10^{-6} mol L $^{-1}$) within the calibration curve and were then analyzed in the same manner as standard solutions.

3. Results and discussion

3.1 TEM analysis

Transmission electron microscopy (TEM) analysis was conducted to investigate the particle shape, size and distribution. As can be seen in Fig. 3, both types of GQDs have various polygon-like shapes which indicate formation of thin graphene-like structures during synthesis. The particles were also well dispersed in water and this can be attributed to the presence of $-\text{COOH}$ groups on the edges thereof. The average particle size was found to be 4.8 ± 0.1 nm and 5.5 ± 0.3 nm for CA-GQDs and GO-GQDs, respectively.

3.2 FTIR analysis

FTIR analysis was carried out to characterize the type of functional groups that were present in the QDs as shown in Fig. 4A and B, where the characteristic vibrational modes of citric acid are also shown for comparison. The broad band around 3248 cm^{-1} can be attributed to hydroxyl groups, and the 2936 cm^{-1} bands are due to both sp^2 and sp^3 C-H stretching modes. The bands at $1560, 1376$ and 3248 cm^{-1} indicate the presence of C=O and C-O groups. The observed bands correspond to those reported in previous studies on GQDs prepared from citric acid.³⁸ It should also be noted that there was no detected C-O-C stretching vibration which confirms that the carbonization process was terminated before the formation of graphene oxide.

3.3 Raman analysis

It must be noted that the fluorescent emission from the GQDs can mask the Raman signal resulting in a poor signal-to-noise ratio. In this case, a 514 nm laser was used, and to minimize the effect of fluorescence on the Raman peaks the laser power was reduced. The Raman spectra of the GQDs (Fig. 4C) show the characteristic D and G bands at 1349 cm^{-1} and 1590 cm^{-1} , respectively. The D-band can be attributed to disordered sp^3 carbons and the G-band is due to in-plane stretching vibrations of crystalline graphite carbons. The ratio of the intensities of the D and G bands (I_D/I_G) can be used to infer information about the degree of crystallinity and abundance of core carbon and surface carbon atoms. For CA-GQDs and GO-GQDs the I_D/I_G ratio was 1.02 and 0.95, respectively. This high ratio confirms the presence of defects in the structure of the GQDs and a partially disordered crystal structure from the small sp^2 cluster sizes.

3.4 Absorption and fluorescence properties

The absorption and fluorescence emission spectra of both GO-GQDs and CA-GQDs are presented in Fig. 5. As can be seen, both sets of GQDs show the typical broad absorption in the UV region with a tail that extends to the visible range. The GO-GQDs show two shoulder peaks at 230 and 300 nm. The CA-GQDs on the other hand show a distinct peak around 250 nm followed by a broad shoulder at 350 nm. In both cases, the absorption peaks at lower wavelengths can be attributed to $\pi-\pi$ electronic transitions of the aromatic C-C bonds in their structure. The absorption shoulder peaks at higher wavelengths can be attributed to the functional groups on their edges, specifically $\pi^*-\text{n}$ transitions of the C=O bonds.^{17,39}

The GQDs showed strong fluorescence emission peaks at 500 nm and 460 nm for GO-GQDs and CA-GQDs, respectively. The width of the emission peaks is related to the size distribution of GQDs which is in turn related to the synthesis method. The emission wavelength on the other hand is attributed to the functional groups on the edges of GQDs.¹⁷ A distinctive feature between GO-GQDs and CA-GQDs is the dependence of the emission on excitation wavelength as shown in Fig. 6. GO-GQDs show an initial red-shift as the excitation wavelength is changed from 340–360 nm, after which the emission wavelength remains unchanged (Fig. 6A). The excitation dependence can be attributed to wider size distribution of the GO-GQDs which is a consequence of the synthesis route. In

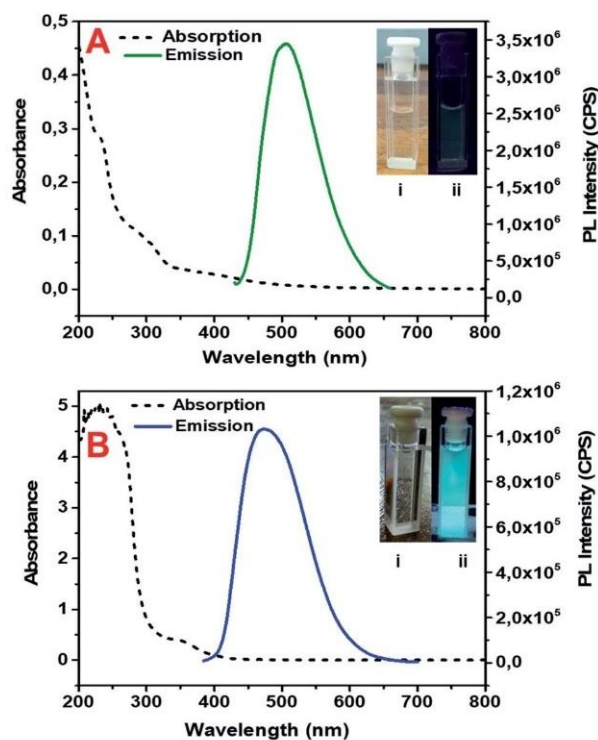


Fig. 5 Absorption and emission spectra of GO-GQDs (A) and CA-GQDs (B). The inset shows the GQDs solution under visible light (i) and under 365 nm UV light (ii).

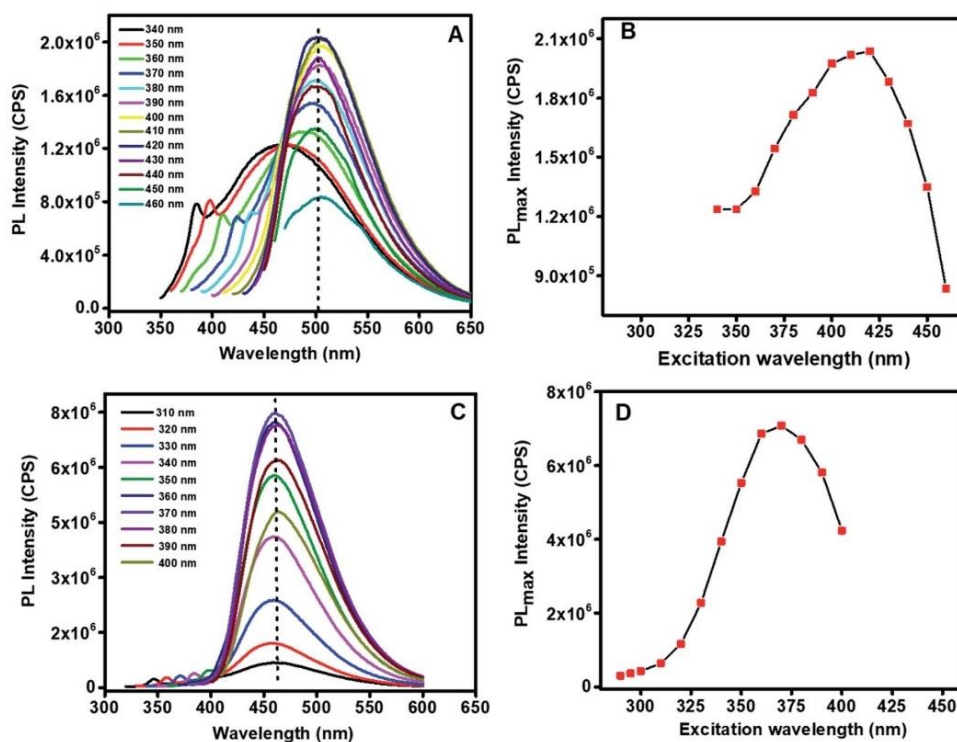


Fig. 6 The effect of excitation wavelength on the emission spectra of (A) GO-GQDs and (C) CA-GQDs. (B) and (D) show the effect of excitation wavelength on the maximum PL intensity (PL_{max}) in each case.

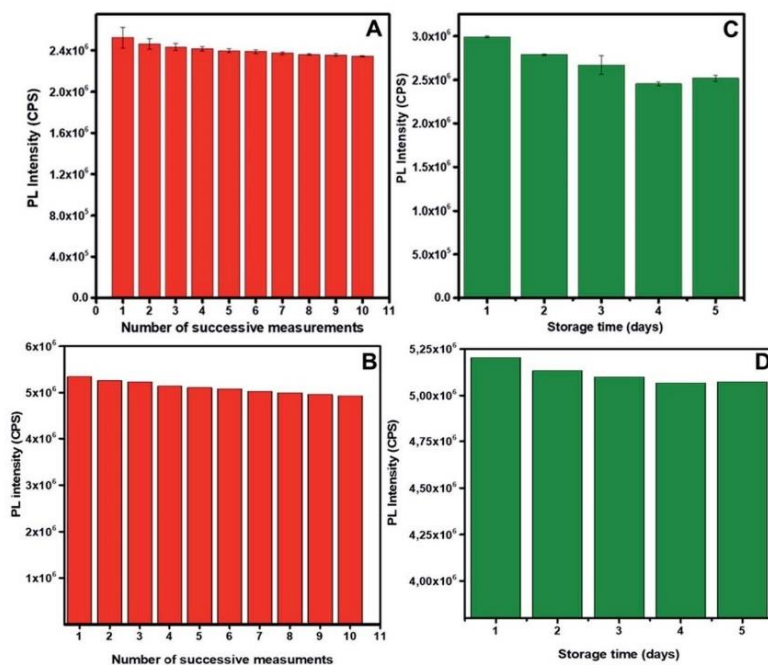


Fig. 7 The effect of successive irradiations at the excitation wavelength for GO-CQDs (A) and CA-GQDs (B). The effect of storage at 4 °C on the stability of the GO-GQDs (B) and CA-GQDs (C).

contrast, CA-GQDs show excitation independent emission (Fig. 6C) which is typical for GQDs made from bottom-up approaches. This can be attributed to uniform size and surface states of the sp^2 clusters present.³¹ The fluorescence quantum yields for CA-GQDs and GO-GQDs were found to be 10.2% and 12.2%, respectively.

Both GO-GQDs and CA-GQDs were shown to be photo-stable, as shown in Fig. 7. After ten successive irradiations at the respective excitation wavelengths, the decrease in PL intensity was about 7.1% for GO-GQDs and about 7.6% for CA-GQDs. The effect of storage on the photoluminescence of GQDs is also a critical parameter in their application as sensors. Generally, the photoluminescence of GQDs decreases with storage, and storage at low temperatures has been shown to preserve them. As seen in Fig. 7, storage at 4 °C for both GQDs resulted in minimal decrease in PL intensity (18% for GO-GQDs and 2.3% for CA-GQDs) over a 5 day period, after which they stabilized. This indicates the storage and stabilization period which should at least be allowed before using the GQDs for sensing after synthesis in order to ensure repeatability.

3.5 Fluorescence sensing

The GQDs were applied in detection of the PAH pyrene, as shown in Fig. 9. For both CA-GQDs and GO-GQDs, following the initial treatment with ferric ions as explained in section 2.4, fluorescence enhancement was observed upon addition of increasing concentrations of pyrene. The fluorescence enhancement was linear within the $2\text{--}10 \times 10^{-6} \text{ mol L}^{-1}$ range. The limit of detection (LOD) and limit of quantitation (LOQ) were determined using the equations $3\delta/K$ and $10\delta/K$, respectively. Where δ is the standard deviation of blank measurements ($n = 10$) and K is the slope of the linear calibration curve. For GO-GQDs the LOD was found to be $0.325 \times 10^{-6} \text{ mol L}^{-1}$ and the LOQ was $1.08 \times 10^{-6} \text{ mol L}^{-1}$. For CA-GQDs the LOD was $0.242 \times 10^{-6} \text{ mol L}^{-1}$ and the LOQ was $0.807 \times 10^{-6} \text{ mol L}^{-1}$. The CA-GQDs showed better linearity (Fig. 8) and slightly higher sensitivity compared to GO-GQDs which could be attributed to their uniform size distribution as shown in the TEM analysis (Fig. 3) which itself is a consequence of the synthesis approach.

3.6 Sensing mechanism

A schematic illustration of the interaction of PAHs and the GQDs treated with Fe is shown in Fig. 9. The fluorescence quenching that was observed upon addition of Fe^{3+} ions could be due to their ability to coordinate with the phenolic hydroxyl groups on the GQD surface, leading to formation of aggregates with neighboring GQDs.³⁷ The introduction of pyrene weakens these aggregates as it binds with the GQDs through $\pi\text{--}\pi$ stacking, leading to fluorescence enhancement.

3.7 Application to PAH sensing in real water samples

Water samples obtained from a lake at the University of Pretoria Sports Campus were spiked with different concentrations of pyrene standard solutions within the calibration curve ($2\text{--}10 \times 10^{-6} \text{ mol L}^{-1}$). The elemental ion composition of the unspiked water sample was also determined using ICP-MS

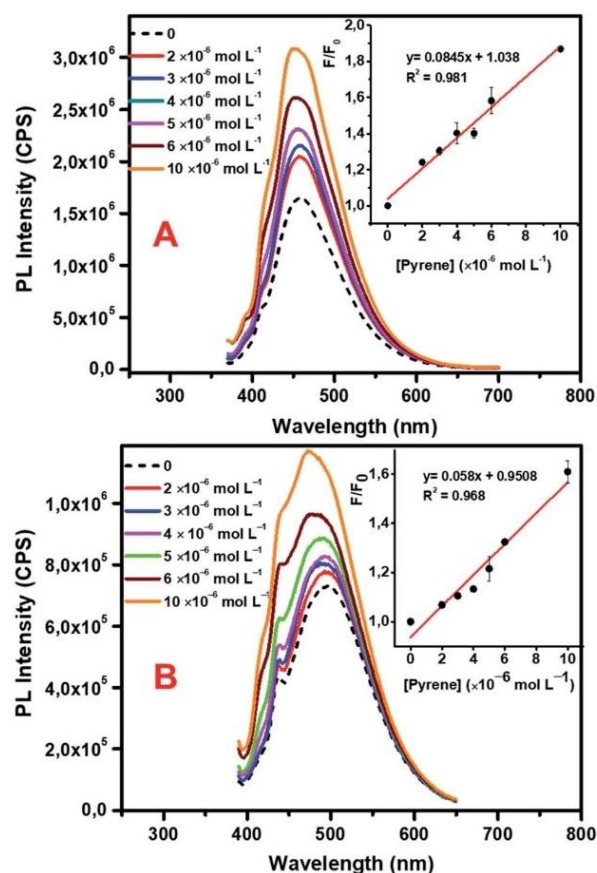


Fig. 8 Fluorescence detection of pyrene using CA-GQDs (A) and GO-GQDs (B). The concentration of pyrene ranged from $2\text{--}10 \times 10^{-6} \text{ mol L}^{-1}$. The inset shows a linear response of F/F_0 versus concentration where F_0 is the fluorescence intensity of GQDs- Fe^{3+} in the absence of pyrene and F is the fluorescence intensity after interaction with pyrene ($n = 3$).

screening analysis, and the results are shown in Table S1.† Fluorescence detection of the spiked water samples was then carried out following a similar protocol as with standard solutions. The sensor demonstrated satisfactory recoveries ranging from 97–107% (Table 1). This demonstrates that additional metal ions, humic matter, and other matrix components had no effect on the performance of the sensor. Thus, this sensing strategy has excellent potential for application in environmental water samples.

Fluorescence sensing of PAHs by means of other graphene based materials has previously been explored^{14,15,40,41} and good sensitivity thereof has been reported. However, their application may be limited due to the inclusion of toxic metals, such as in the case of cadmium based QDs as signal transducers. The levels of pyrene in drinking water are reported to range between $14.3 \times 10^{-12}\text{--}5.62 \times 10^{-6} \text{ mol L}^{-1}$ and between $94.4 \times 10^{-12}\text{--}5.87 \times 10^{-6} \text{ mol L}^{-1}$ in river water.⁷ The proposed sensor developed in this work, despite having a somewhat higher detection limit than other reported methods, uses GQDs of low toxicity for both pre-concentration and signal transduction

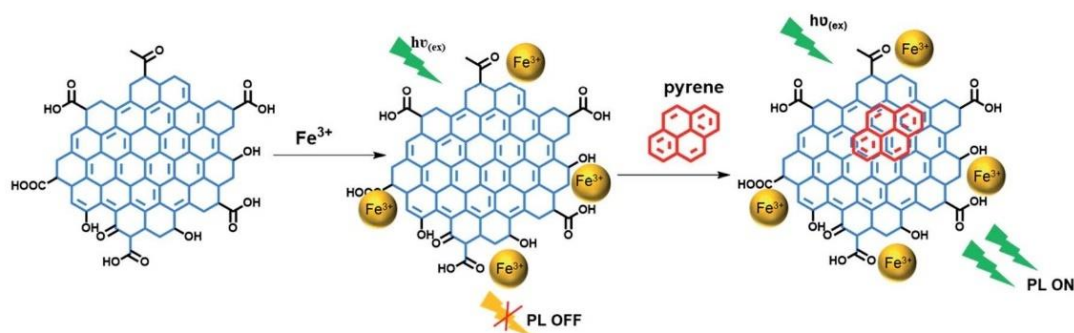


Fig. 9 Schematic illustration of the interaction of GQDs with Fe^{3+} which results in fluorescence quenching. Upon interaction with pyrene the fluorescence is turned on.

Table 1 Recovery tests of pyrene spiked lake water at three different concentrations

Sensing solution	Spiked pyrene concentration ($\times 10^{-6} \text{ mol L}^{-1}$)	Detected concentration (mean \pm SD*, $n = 3$; $\times 10^{-6} \text{ mol L}^{-1}$)	Recovery (%)
GO-GQDs	4.0	4.1 ± 0.28	102
	6.0	6.2 ± 0.19	103
	10.0	10.0 ± 0.64	107
CA-GQDs	3.0	3.04 ± 0.08	101
	6.0	5.87 ± 0.51	98
	10.0	9.73 ± 0.28	97

(detection) of PAHs. This detection strategy offers promising prospects towards the development of 'green' sensors for environmental PAH monitoring considering that the LODs are within the range of reported concentrations in water.

4. Conclusion

In conclusion, simple synthesis approaches were used to successfully prepare graphene quantum dots, denoted GO-GQDs and CA-GQDs. We further demonstrate the potential application of these GQDs in the detection of pyrene, a common PAH compound in environmental water samples. The interaction of the GQDs with ferric ions led to fluorescence quenching due to aggregation, but subsequent interaction with pyrene through π - π stacking switched on the fluorescence. The detection of pyrene was therefore realized and the detection limits were $0.351 \times 10^{-6} \text{ mol L}^{-1}$ and $0.242 \times 10^{-6} \text{ mol L}^{-1}$ for GO-GQDs and CA-GQDs, respectively. GQDs have been known to be environmentally friendly, low-cost, and easier to prepare compared to semi-conductor QDs, thus this work paves the way for greener fluorescence monitoring of PAHs. Future work will focus on improving the sensitivity of these sensors and, ultimately to also investigate their reusability and incorporation into portable devices.

Conflicts of interest

We declare are no conflicts of interest.

Acknowledgements

Funding from the University of Pretoria, Water Research Commission (WRC) (Grant K5/2752 and K5/2438), the Photonics Initiative of South Africa (Grant PISA-15DIR-06) and the National Research Foundation of South Africa (post-graduate student bursary (SN) and funding grants 90720 and 93394 (PF)) is gratefully acknowledged. We thank the Microscopy and Microanalysis Laboratory of the University of Pretoria, for their assistance with microscopy measurements.

References

- 1 L. Van der Wat and P. B. C. Forbes, Lichens as biomonitors for organic air pollutants, *TrAC, Trends Anal. Chem.*, 2015, **64**, 165–172.
- 2 Z. Zelinkova and T. Wenzl, The occurrence of 16 EPA PAHs in food – a review, *Polycyclic Aromat. Compd.*, 2015, **35**, 248–284.
- 3 L. Chimuka, P. Sibiyi, R. Amdany, E. Cukrowska and P. B. C. Forbes, Status of PAHs in environmental compartments of South Africa: a country report, *Polycyclic Aromat. Compd.*, 2016, **36**, 1–19.
- 4 H. I. Abdel-Shafy and M. S. M. Mansour, A review on polycyclic aromatic hydrocarbons: source, environmental impact, effect on human health and remediation, *Egypt. J. Pet.*, 2016, **25**, 107–123.
- 5 P. B. C. Forbes and E. R. Rohwer, Investigations into a novel method for atmospheric polycyclic aromatic hydrocarbon monitoring, *Environ. Pollut.*, 2009, **157**, 2529–2535.

- 6 V. Bansal, P. Kumar, E. E. Kwon and K.-H. Kim, Review of the quantification techniques for polycyclic aromatic hydrocarbons (PAHs) in food products, *Crit. Rev. Food Sci. Nutr.*, 2015, **51**, 3297–3397.
- 7 A. Mojiri, J. L. Zhou, A. Ohashi, N. Ozaki and T. Kindaichi, Comprehensive review of polycyclic aromatic hydrocarbons in water sources, their effects and treatments, *Sci. Total Environ.*, 2019, **696**, 133971.
- 8 ATSDR, *Case studies in environmental medicine toxicity of polycyclic aromatic hydrocarbons (PAHs)*, Agency for Toxic Substances and Disease Registry, 2012.
- 9 M. Rota, C. Bosetti, S. Boccia, P. Boffetta and C. La Vecchia, Occupational exposures to polycyclic aromatic hydrocarbons and respiratory and urinary tract cancers: an updated systematic review and a meta-analysis to 2014, *Arch. Toxicol.*, 2014, **88**, 1479–1490.
- 10 A. J. White, P. T. Bradshaw, A. H. Herring, S. L. Teitelbaum, J. Beyea, S. D. Stellman, S. E. Steck, I. Mordukhovich, S. M. Eng, L. S. Engel, K. Conway, M. Hatch, A. I. Neugut, R. M. Santella and M. D. Gammon, Exposure to multiple sources of polycyclic aromatic hydrocarbons and breast cancer incidence, *Environ. Int.*, 2016, **89–90**, 185–192.
- 11 S. Marzocchi and D. M. Di Toro, A critical review of polycyclic aromatic hydrocarbon phototoxicity models, *Environ. Toxicol. Chem.*, 2017, **36**, 1138–1148.
- 12 M. Engraff, C. Solere, K. E. C. Smith, P. Mayer and I. Dahllöf, Aquatic toxicity of PAHs and PAH mixtures at saturation to benthic amphipods: linking toxic effects to chemical activity, *Aquat. Toxicol.*, 2011, **102**, 142–149.
- 13 S. A. Nsibandé, H. Montaseri and P. B. C. Forbes, Advances in the application of nanomaterial-based sensors for detection of polycyclic aromatic hydrocarbons in aquatic systems, *TrAC, Trends Anal. Chem.*, 2019, **115**, 52–69.
- 14 O. Adegoke and P. B. C. Forbes, L-Cysteine-capped core/shell/shell quantum dot-graphene oxide nanocomposite fluorescence probe for polycyclic aromatic hydrocarbon detection, *Talanta*, 2016, **146**, 780–788.
- 15 O. Adegoke, H. Montaseri, S. A. Nsibandé and P. B. Forbes, Alloyed quaternary/binary core/shell quantum dot-graphene oxide nanocomposite: preparation, characterization and application as a fluorescence “switch ON” probe for environmental pollutants, *J. Alloys Compd.*, 2017, **720**, 70–78.
- 16 L. Li, G. Wu, G. Yang, J. Peng, J. Zhao and J.-J. Zhu, Focusing on luminescent graphene quantum dots: current status and future perspectives, *Nanoscale*, 2013, **5**, 4015–4039.
- 17 S. Zhu, Y. Song, X. Zhao, J. Shao, J. Zhang and B. Yang, The photoluminescence mechanism in carbon dots (graphene quantum dots, carbon nanodots, and polymer dots): current state and future perspective, *Nano Res.*, 2015, **8**, 355–381.
- 18 J. Shen, Y. Zhu, X. Yang and C. Li, Graphene quantum dots: emergent nanolights for bioimaging, sensors, catalysis and photovoltaic devices, *Chem. Commun.*, 2012, **48**, 3686–3699.
- 19 Y. Chong, Y. Ma, H. Shen, X. Tu, X. Zhou, J. Xu, J. Dai, S. Fan and Z. Zhang, The in vitro and in vivo toxicity of graphene quantum dots, *Biomaterials*, 2014, **35**, 5041–5048.
- 20 S. Wang, I. S. Cole and Q. Li, The toxicity of graphene quantum dots, *RSC Adv.*, 2016, **6**, 89867–89878.
- 21 X. T. Zheng, A. Ananthanarayanan, K. Q. Luo and P. Chen, Glowing graphene quantum dots and carbon dots: properties, syntheses, and biological applications, *Small*, 2015, **11**, 1620–1636.
- 22 H. Sun, L. Wu, W. Wei and X. Qu, Recent advances in graphene quantum dots for sensing, *Mater. Today*, 2013, **16**, 433–442.
- 23 S. Benítez-Martínez and M. Valcárcel, Graphene quantum dots in analytical science, *TrAC, Trends Anal. Chem.*, 2015, **72**, 93–113.
- 24 L. Lin, M. Rong, F. Luo, D. Chen, Y. Wang and X. Chen, Luminescent graphene quantum dots as new fluorescent materials for environmental and biological applications, *TrAC, Trends Anal. Chem.*, 2014, **54**, 83–102.
- 25 P. Tian, L. Tang, K. S. Teng and S. P. Lau, Graphene quantum dots from chemistry to applications, *Mater. Today Chem.*, 2018, **10**, 221–258.
- 26 J. Ju and W. Chen, Graphene quantum dots as fluorescence probes for sensing metal ions: synthesis and applications, *Curr. Org. Chem.*, 2015, **19**, 1150–1162.
- 27 Q. Liu, K. Wang, J. Huan, G. Zhu, J. Qian, H. Mao and J. Cai, Graphene quantum dots enhanced electrochemiluminescence of cadmium sulfide nanocrystals for ultrasensitive determination of pentachlorophenol, *Analyst*, 2014, **139**, 2912–2918.
- 28 L. Fan, Y. Hu, X. Wang, L. Zhang, F. Li, D. Han, Z. Li, Q. Zhang, Z. Wang and L. Niu, Fluorescence resonance energy transfer quenching at the surface of graphene quantum dots for ultrasensitive detection of TNT, *Talanta*, 2012, **101**, 192–197.
- 29 E. Zor, E. Morales-Narváez, A. Zamora-Gálvez, H. Bingöl, M. Ersoz and A. Merkoçi, Graphene quantum dots-based photoluminescent sensor: a multifunctional composite for pesticide detection, *ACS Appl. Mater. Interfaces*, 2015, **7**, 20272–20279.
- 30 G. A. Crosby and J. N. Demas, Measurement of photoluminescence quantum yields. Review, *J. Phys. Chem.*, 1971, **75**, 991–1024.
- 31 Y. Dong, J. Shao, C. Chen, H. Li, R. Wang, Y. Chi, X. Lin and G. Chen, Blue luminescent graphene quantum dots and graphene oxide prepared by tuning the carbonization degree of citric acid, *Carbon*, 2012, **50**, 4738–4743.
- 32 W. S. Hummers and R. E. Offeman, Preparation of graphitic oxide, *J. Am. Chem. Soc.*, 1958, **80**, 1339.
- 33 Y. Zhu, G. Wang, H. Jiang, L. Chen and X. Zhang, One-step ultrasonic synthesis of graphene quantum dots with high quantum yield and their application in sensing alkaline phosphatase, *Chem. Commun.*, 2015, **51**, 948–951.
- 34 T. V. Tam, N. B. Trung, H. R. Kim, J. S. Chung and W. M. Choi, One-pot synthesis of N-doped graphene quantum dots as a fluorescent sensing platform for Fe³⁺ ions detection, *Sens. Actuators, B*, 2014, **202**, 568–573.
- 35 A. Ananthanarayanan, X. Wang, P. Routh, B. Sana, S. Lim, D.-H. Kim, K.-H. Lim, J. Li and P. Chen, Facile synthesis of graphene quantum dots from 3D graphene and their

- application for Fe³⁺ sensing, *Adv. Funct. Mater.*, 2014, **24**, 3021–3026.
- 36 Y.-L. Zhang, L. Wang, H.-C. Zhang, Y. Liu, H.-Y. Wang, Z.-H. Kang and S.-T. Lee, Graphitic carbon quantum dots as a fluorescent sensing platform for highly efficient detection of Fe³⁺ ions, *RSC Adv.*, 2013, **3**, 3733–3738.
- 37 X. Zhu, Z. Zhang, Z. Xue, C. Huang, Y. Shan, C. Liu, X. Qin, W. Yang, X. Chen and T. Wang, Understanding the selective detection of Fe³⁺ based on graphene quantum dots as fluorescent probes: The Ksp of a metal hydroxide-assisted mechanism, *Anal. Chem.*, 2017, **89**, 12054–12058.
- 38 R. Álvarez-Diduk, J. Orozco and A. Merkoçi, Paper strip-embedded graphene quantum dots: a screening device with a smartphone readout, *Sci. Rep.*, 2017, **7**, 976.
- 39 Y. Wang, S. Kalytchuk, Y. Zhang, H. Shi, S. V. Kershaw and A. L. Rogach, Thickness-dependent full-color emission tunability in a flexible carbon dot ionogel, *J. Phys. Chem. Lett.*, 2014, **5**, 1412–1420.
- 40 L. Wang, Z. Huang, Q. Gao, Y. Liu, X. Kou and D. Xiao, A novel pyrene fluorescent sensor based on the π - π Interaction between pyrene and graphene of graphene-cadmium telluride quantum dot nanocomposites, *Spectrosc. Lett.*, 2015, **48**, 748–756.
- 41 C. Carrillo-Carrión, B. M. Simonet and M. Valcárcel, Carbon nanotube-quantum dot nanocomposites as new fluorescence nanoparticles for the determination of trace levels of PAHs in water, *Anal. Chim. Acta*, 2009, **652**, 278–284.

Supplementary information

Purification of GQDs:

Following the oxidation of GO through ultra-sonication in with MnO_4 , a brown mixture was obtained indicating complete oxidation (**Figure S1 A**). This mixture was then filtered using a $0.45\ \mu\text{m}$ PTFE filter (**Figure S1 B**) and the filtrate was further filtered using a $0.22\ \mu\text{m}$ PTFE filter to obtain a pale yellow GQDs solution (**Figure S1 C**). Using the $0.22\ \mu\text{m}$ PTFE was shown to improve the PL by up to 20% as shown in **Figure S2**.

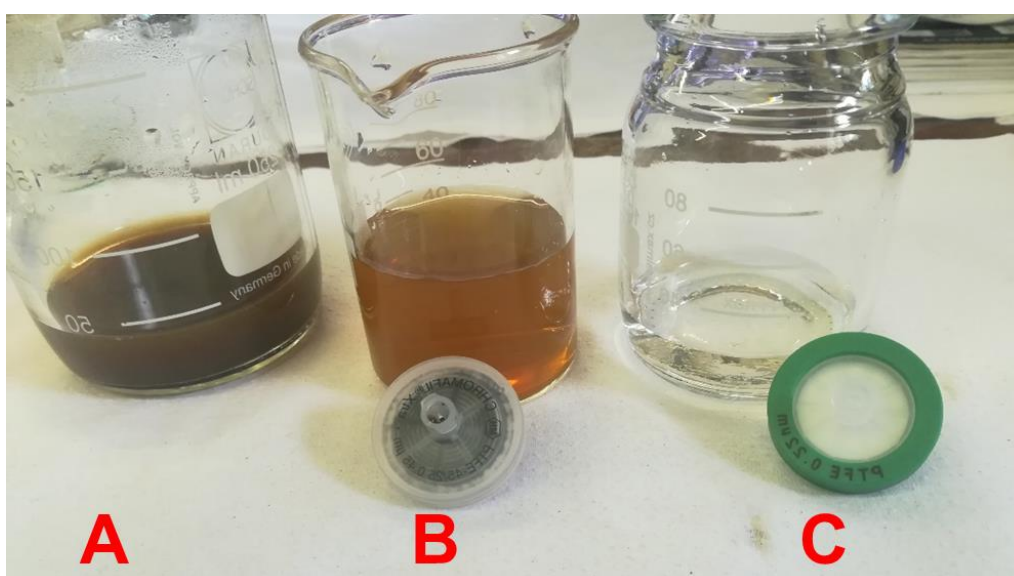


Figure S1 (A) raw unfiltered GQDs after oxidation of GO. (B) Orange-yellowish GQDs solution after filtering through $0.45\ \mu\text{m}$ PTFE filter, (C) pale yellow GQDs solution after filtering through a $0.22\ \mu\text{m}$ PTFE filter.

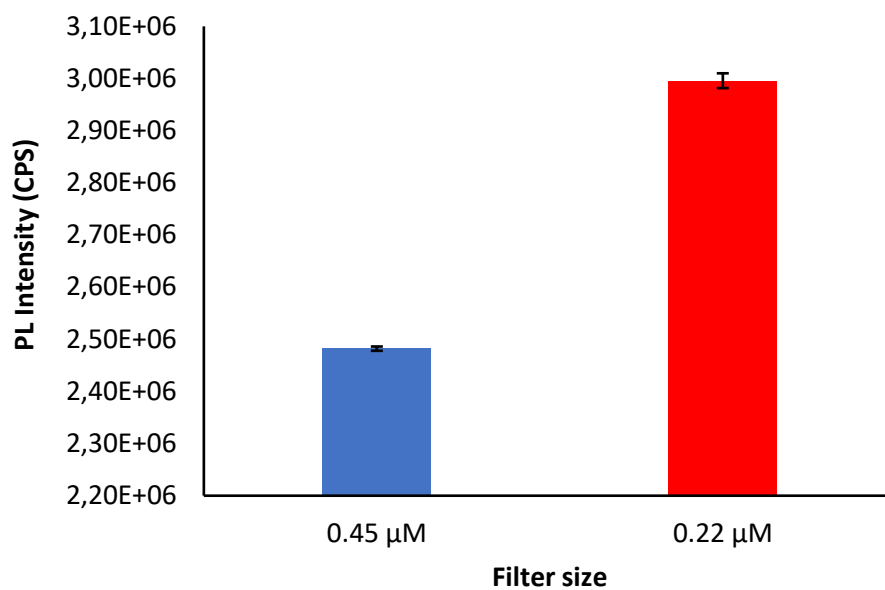


Figure S5 Effect of filtering on the PL intensity during the purification step.

HRSEM of graphite and graphene oxide:

High resolution scanning electron microscopy (HRSEM) was used to study the morphology of the graphene oxide from exfoliation of graphite precursors. The HRSEM images show that the graphite had characteristic flat carbon sheets stacked into layers (**Figure S3-A**) and after exfoliation to graphene oxide the sheets become folded into crumpled silk waves (**Figure S3-B**). This transformation is due to the harsh oxidation conditions which the graphite was subjected to in order to produce graphene oxide.

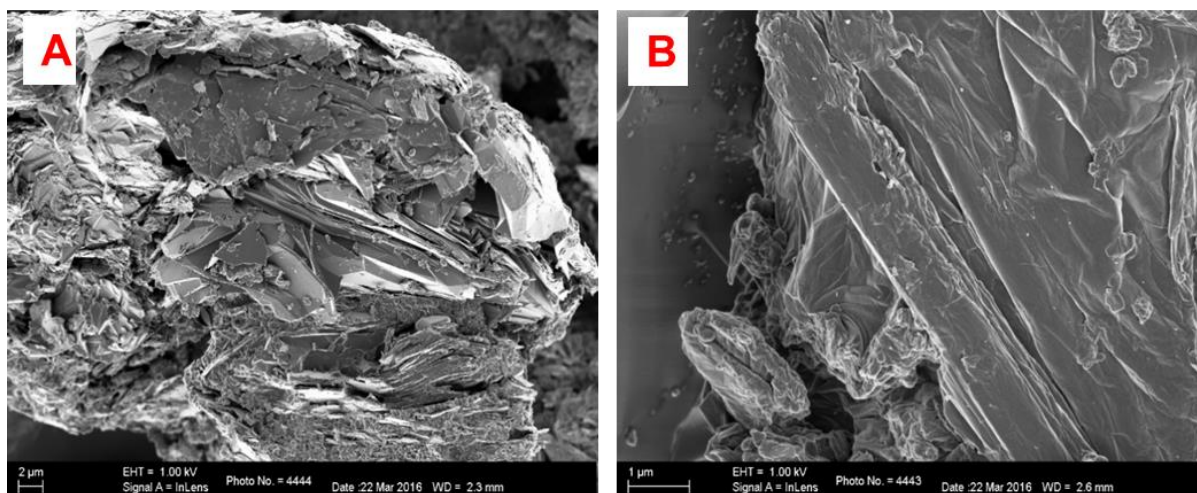


Figure S3 (A) HRSEM image of graphite showing flat shiny carbon sheets staked in layers. (B) Graphene oxide sheets folded into crumpled silk waves following oxidation.

Table S1 ICP scan results showing background elemental composition (mg L⁻¹) of the lake water sample.

Ag	Al	As	Au	B	Ba	Be	Bi	Ca	Cd	Ce	Co
< 0.010	< 0.100	< 0.010	< 0.010	0,095	0,066	< 0.010	< 0.010	28	< 0.010	< 0.010	< 0.010
Cr	Cs	Cu	Dy	Er	Eu	Fe	Ga	Gd	Ge	Hf	Hg
< 0.010	< 0.010	< 0.010	< 0.010	< 0.010	< 0.010	0,070	0,010	< 0.010	< 0.010	< 0.010	< 0.010
In	Ir	K	La	Li	Lu	Mg	Mn	Mo	Na	Nb	Nd
< 0.010	< 0.010	6,1	< 0.010	< 0.010	< 0.010	10	< 0.025	< 0.010	13	< 0.010	< 0.010
Ni	Os	P	Pb	Pd	Pr	Pt	Rb	Rh	Ru	Sb	Sc
< 0.010	< 0.010	0,047	< 0.010	< 0.010	< 0.010	< 0.010	< 0.010	< 0.010	< 0.010	< 0.010	< 0.010
Se	Si	Sm	Sn	Sr	Ta	Tb	Te	Th	Ti	Tl	Tm
< 0.010	0,3	< 0.010	< 0.010	0,040	< 0.010	< 0.010	< 0.010	< 0.010	0,011	< 0.010	< 0.010
U	V	W	Y	Yb	Zn	Zr					
< 0.010	< 0.010	< 0.010	< 0.010	< 0.010	0,030	< 0.010					

CHAPTER 7 Conclusions and future work

This chapter summarizes the whole project and presents some proposals that can be considered for future work.

7.1 Conclusions

Pesticides and polycyclic aromatic hydrocarbons (PAHs) are environmental pollutants that continue to be of great concern due to their potential toxic effects for both humans and aquatic organisms. Prolonged exposure to these pollutants has been linked with serious endocrine disruption and carcinogenic effects. Human activities play a significant role in the release of these compounds into the environment. Their occurrence at low concentrations and the need for their ongoing monitoring presents a challenge to the environmental analytical chemist. Sensitive analytical techniques that can selectively detect these compounds without being affected by the environmental matrix are required.

This work therefore sought to address this challenge by using nanotechnology to design sensitive quantum dot (QD) fluorescence probes for the detection of pesticides and PAHs in water. As such, extensive reviews were first conducted on the current application of QDs and nanoparticles in designing probes for the detection of these analytes. Quantum dot-based fluorescence probes were then designed for targeted detection of the pesticide atrazine and PAHs in environmental water samples.

CdSeTe/ZnS QDs were fabricated via a one-pot organometallic hot injection approach and were functionalized with molecularly imprinted polymers (MIPs) for selective fluorescence detection of atrazine. Various techniques were used to characterize and confirm the optical and structural properties of the QD@MIP sensor material. The QD@MIP sensor demonstrated excellent selectivity due to the size and shape specificity of the molecularly imprinted polymers as a

receptor. The developed sensor showed excellent sensitivity and could detect atrazine down to $0.80 \times 10^{-7} \text{ mol L}^{-1}$ which is below the World Health Organization (WHO) guideline for atrazine in water ($4.6 \times 10^{-7} \text{ mol L}^{-1}$). The developed sensor has potential application in real environmental water samples with minimal sample preparation. It was able to detect atrazine in spiked environmental water samples and provided recoveries of 92–118%. This shows that it was selective enough not to be affected by the sample matrix and this was attributed to both the intrinsic excellent optical properties of the QDs and the analyte specificity provided by the MIPs. The sensor had a quick detection response time (5 min), making it suitable for routine high throughput analysis of environmental samples.

Graphene quantum dots (GQDs) were explored for the detection of pyrene in water samples. GQDs were attractive because of their ability to pre-concentrate planar molecules like PAHs on their surface and offered a safer alternative to the cadmium based QDs. As such, GQDs were synthesized using bottom-up and top-down approaches to produce GQDs from citric acid (CA-GQDs) and from graphene oxide (GO-GQDs), respectively. A fluorescence “turn-off-on” strategy that incorporated ferric ions into the GQD sensor solution was developed for rapid detection of pyrene in water. The ferric ions quenched the fluorescence intensity of the GQDs and when increasing concentrations of pyrene were added, the fluorescence was switched back on. The sensor had a linear response to pyrene concentrations within the $2 - 10 \times 10^{-6} \text{ mol L}^{-1}$ range. Using this approach, pyrene could be detected down to $0.325 \times 10^{-6} \text{ mol L}^{-1}$ and $0.242 \times 10^{-6} \text{ mol L}^{-1}$ for GO-GQDs and CA-GQDs, respectively. The potential application of the developed probe was tested using real environmental water samples spiked with known pyrene concentration, and recoveries between 97 – 107% were obtained. This part of the thesis demonstrated, for the first time, the promising application of GQDs for environmental monitoring of PAHs in water.

In conclusion, this work has demonstrated QD fluorescence probes offer a viable alternative to conventional analytical methods for detection and monitoring of emerging chemical pollutants like

pesticides and PAHs in environmental water samples. The sensitivity of these sensor materials was found to be relevant for the typical environmental concentrations of these compounds. Furthermore, the fast response times makes them suitable candidates for routine environmental monitoring campaigns and for semi-quantitative screening of pollutants.

7.2 Future work

- The QD@MIP-based sensor that was developed in this work showed excellent sensitivity, selectivity and a quick response time, making it a potential candidate for field monitoring of atrazine in water samples. Therefore, future work needs to focus on the immobilization of the nanomaterials on solid support materials that could be used with portable spectrometers. Since MIPs are theoretically re-usable, immobilizing this sensor on a support material could allow for re-usability of the sensor.
- The GQD sensor for the detection of PAHs showed promising applications for compound class screening of PAHs in water. Future work can still be done to further optimize the sensor for targeted PAHs and to improve its sensitivity. For example, modifying the GQDs through doping heteroatoms like nitrogen, phosphorus, or boron could be investigated to improve the photoluminescence of the GQDs and thereby their sensitivity. Strategies to immobilize the GQDs on solid support materials can also be investigated with the view of developing portable reusable sensing devices for field screening of PAHs.
- The detection of multiple analytes with QD fluorescence sensors is a research niche that still needs to be explored. This is important because an environmental chemist often has to monitor more than one pollutant. While chromatographic methods are well established in this regard, there is a need for alternative methods for multiple analyte screening. For example, QDs could be functionalized with MIPs containing various target analyte cavities and such materials could be potential candidates for this purpose.

- Lastly, reproducible synthetic methods for developing QD fluorescence sensors needs to be investigated in order provide better standardization. From a regulatory perspective, this is important in order to come up with standard screening protocols that could be used for enforcement of pollutant regulatory limits. This would open doors for the development of commercial fluorescence sensing devices that could be used in routine environmental monitoring, particularly in developing countries where conventional techniques are not affordable.

APPENDICES

Co-authored paper 1: Fluorescence sensor for PAHs detection

O. Adegoke, H. Montaseri, S.A. Nsibande*, P.B. Forbes, Alloyed quaternary/binary core/shell quantum dot-graphene oxide nanocomposite: Preparation, characterization and application as a fluorescence “switch ON” probe for environmental pollutants, *Journal of Alloys and Compounds*, 720 (2017) 70 - 78. DOI: <https://doi.org/10.1016/j.jallcom.2017.05.242>

*Contributions by S.A. Nsibande:

- Conjugation of CdSeTe/ZnS QDs to graphene oxide (Section 2.5)
- Sensor optimization, specifically, investigating the effects of incubation time and nanocomposite concentration (Section 3.9)
- Manuscript review



Contents lists available at ScienceDirect

Journal of Alloys and Compounds

journal homepage: <http://www.elsevier.com/locate/jalcom>

Alloyed quaternary/binary core/shell quantum dot-graphene oxide nanocomposite: Preparation, characterization and application as a fluorescence “switch ON” probe for environmental pollutants



Oluwasesan Adegoke*, Hanieh Montaseri, Sifiso A. Nsiband, Patricia B.C. Forbes**

Department of Chemistry, Faculty of Natural and Agricultural Sciences, University of Pretoria, Lynnwood Road, Pretoria, 0002, South Africa

ARTICLE INFO

Article history:

Received 2 March 2017

Received in revised form

15 May 2017

Accepted 23 May 2017

Available online 24 May 2017

Keywords:

Graphene oxide

Quantum dots

Polycyclic aromatic hydrocarbon

Photoluminescence

Fluorescence probe

ABSTRACT

Alloyed L-cysteine-capped CdSeTeS/ZnS quantum dots (QDs) have been covalently linked to graphene oxide (GO) to form a new QD-GO nanocomposite material. Transmission electron microscopy, scanning electron microscopy, Raman, energy dispersive X-ray spectroscopy, X-ray diffraction, FT-IR, UV/vis and fluorescence spectrophotometry were used to characterize the nanocomposite material. Covalent binding of GO to the QDs quenched the fluorescence (“switch OFF”) of the QDs. The planar structure of GO and its π electron rich surface enables the adsorption of π rich aromatic analytes. Environmental pollutants, belonging to the class of polycyclic aromatic hydrocarbons (PAHs) were used as model analytes to test their affinity to adsorb onto GO via π - π interaction and trigger fluorescence transduction changes (“switch ON”) in the conjugated QDs. Our investigation showed that the affinity of the four PAH analytes tested to switch on the fluorescence of the nanocomposite probe followed the order phenanthrene > anthracene > naphthalene > pyrene.

© 2017 Elsevier B.V. All rights reserved.

1. Introduction

Nanocomposites, composed of hierarchically-structured composite materials with one or more components of a nanostructured domain, have the potential to pave the way for the next-generation of device materials for sensor nanotechnologies. Selection of the appropriate nanostructured materials as building blocks, and the development of methods to assemble these materials to meet targeted applications, is a requisite to produce nanocomposite materials with unique optical, electronic and mechanical properties [1].

Graphene is a nanomaterial which is characterized by sp^2 hybridized carbon atoms which are covalently bonded to three other atoms and has a monolayer thickness of ~ 0.34 nm [2–5]. The carbon atoms are assembled in a honeycomb-like crystal lattice and exhibit a unique array of unparalleled electrical, mechanical and structural properties [6–10]. Other carbon-based materials such as graphite, fullerene and carbon nanotubes are known to derive their basic structure from graphene [11–13]. With respect to nanodevice

applications, many technological and scientific breakthroughs have been reported using graphene, the most common being in the development of chemical sensors and biosensors [14–16]. A limitation of graphene is its tendency to aggregate when used in bulk quantities during adsorption reactions as well as its susceptibility to restack to graphite. To improve chemisorption, graphene needs to be functionalized or bonded with other materials of interest [17,18]. The presence of oxygen functional groups in the basal edges and planes renders graphene oxide (GO) highly soluble in water when compared to reduced graphene. It is known that the degree of oxidation of GO influences the assembly of oxide functional groups as well as their identity while the structural atomic nature should mostly resemble that of a 2D amorphous sheet of carbon atoms with partially bonded oxygen atoms, rather than an exact graphene sheet with oxidized surface [19]. For direct conjugation to other materials and for biocompatibility, single layer GO nanosheets are highly desirable.

Fluorescent semiconductor quantum dot (QDs) nanocrystals have in the last two decades generated enormous interest due to their unique optical properties which are far superior to fluorescent organic dyes. Their broad absorption and narrow fluorescence emission, large extinction coefficient, brightness, high resistance to photodegradation, excellent photostability and multiplex detection

* Corresponding author.

** Corresponding author.

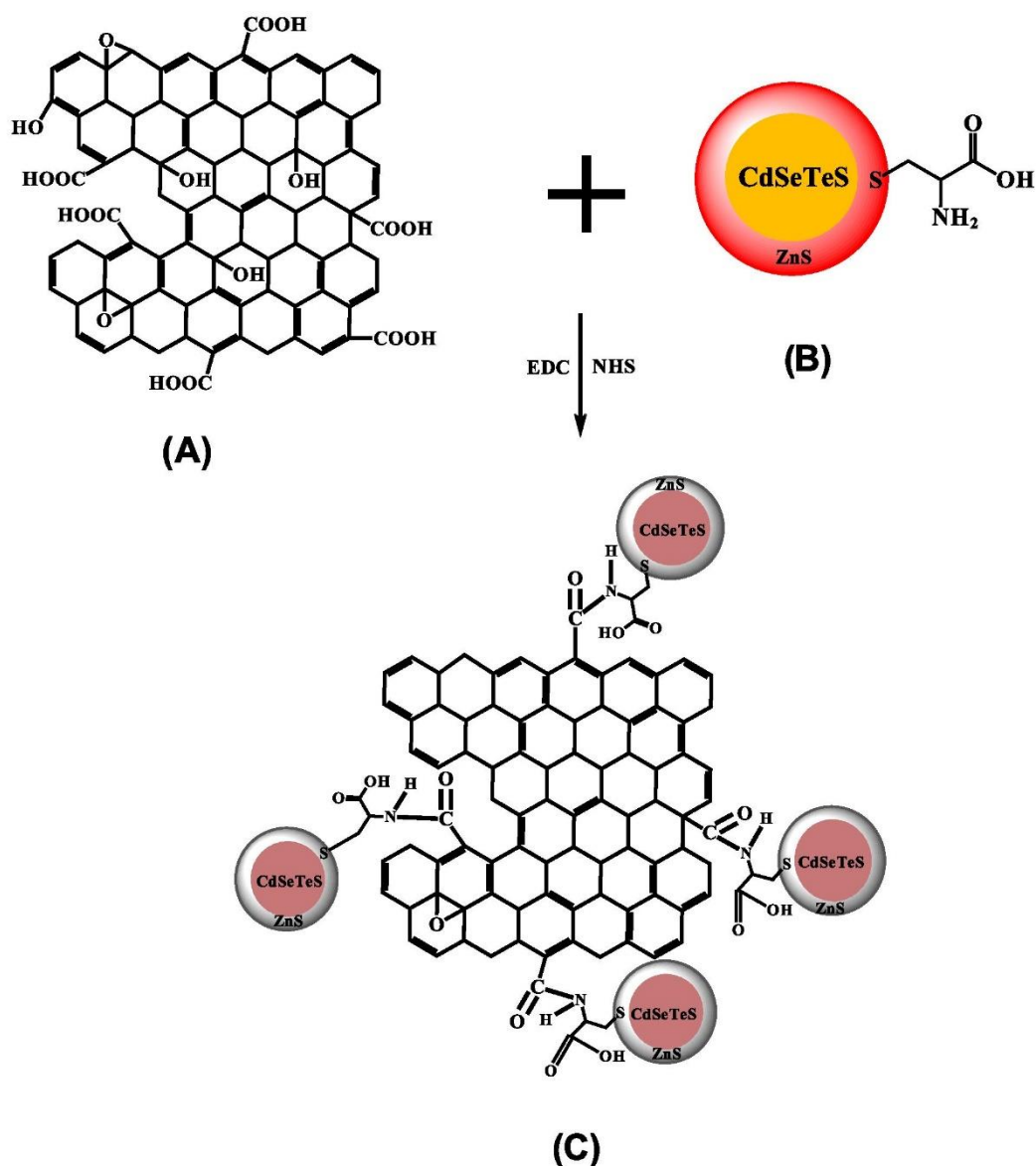
E-mail addresses: adegoke.sesan@mailbox.co.za (O. Adegoke), patricia.forbes@up.ac.za (P.B.C. Forbes).<http://dx.doi.org/10.1016/j.jallcom.2017.05.242>

0925-8388/© 2017 Elsevier B.V. All rights reserved.

capabilities have made them a powerful tool as nanodevices in biology, chemistry and physics applications [20–22]. QDs represent an excellent choice of nanocrystalline material for bonding to GO due to their surface biocompatibility, stability and unique optical properties. To meet the demand for highly sensitive detection in sensor design, the choice of QDs is crucial. Following recent developments in bandgap engineering of QDs, alloyed QDs composed of two or more semiconductor metals have been reported to generate improved sensitivity for analyte sensing than conventional QDs systems [23,24]. This makes their use as fluorescence reporters interesting.

In this work, we report on the preparation, characterization and

chemical sensing application of a L-cysteine-capped alloyed CdSeTeS/ZnS quaternary/binary core/shell QD-GO nanocomposite. A non-toxic ZnS shell was passivated onto the cadmium-based alloyed QD core to reduce leaching of Cd from the core and thereby render the nanocrystals environmentally safe. Alloyed L-cysteine-capped CdSeTeS/ZnS QDs and GO were synthesized, characterized and chemically bonded via covalent coupling chemistry. The structural and optical properties of the new QD-GO nanocomposite were studied and thereafter applied as a fluorescent probe for environmental water pollutants belonging to the class of polycyclic aromatic hydrocarbons (PAHs). PAHs are ubiquitous environmental pollutants, known to be persistent in the



Scheme 1. Conjugation of GO (A) to alloyed L-cysteine-capped CdSeTeS/ZnS QDs (B) to form the QD-GO nanocomposite (C).

environment and are released into the environment during the incomplete combustion of organic substances [25]. Many of the PAH molecules are known to be mutagenic and carcinogenic [26], hence there is a need to develop efficient probes to detect them.

Our approach exploits the unique adsorption properties of GO. The π electron rich surface of GO allows π - π interactions with organic compounds containing benzene rings or C=C bonds such as PAHs. Our detection principle is based on the quenching of the fluorescence of the QDs by GO ("switch OFF") due to their strong binding effect whilst the subsequent adsorption of PAH on the GO surface, triggers the fluorescence recovery ("switch ON") process of the QDs in a concentration-dependent manner. Our work is the first to exploit a QD-GO as an OFF/ON sensor for PAHs.

2. Experimental

2.1. Materials

Cadmium oxide, trioctylphosphine oxide, N-Hydroxysuccinimide, N-(3-dimethylaminopropyl)-N'-ethylcarbodiimide hydrochloride, sulphur, octadecene, tellurium powder, oleic acid, L-cysteine and PAH standards consisting of anthracene (Ant), naphthalene (Naph), phenanthrene (Phe) and pyrene (Py) were purchased from Sigma Aldrich. Sulphuric acid, hydrogen peroxide, methanol, zinc powder, absolute ethanol, sodium nitrate, acetone, chloroform, selenium powder, hydrochloric acid, potassium hydroxide, potassium permanganate and graphite powder were purchased from Merck. Water dispensed from an ultrapure Milli-Q Water System was used as the measurement medium.

2.2. Apparatus

Fluorescence emission measurements were performed using a Horiba Jobin Yvon Fluoromax-4 spectrofluorometer. UV-vis absorption spectra were performed using a Cary Eclipse (Varian) spectrophotometer. Powder X-ray diffraction (PXRD) analyses were performed using a PANalytical X'Pert Pro powder diffractometer in θ - θ configuration with an X'Celerator detector, variable divergence and receiving slits with Fe filtered Co-K α radiation ($\lambda = 1.789 \text{ \AA}$). Transmission electron microscopy (TEM) images were taken using a JEOL JEM 2100F operated at 200 kV. Raman analyses were performed using a T64000 micro-Raman spectrometer (HORIBA Scientific Jobin Yvon Technology) equipped with a triple monochromator system to eliminate contributions from the Rayleigh line. Scanning electron microscopy (SEM) measurements were performed using a JEOL JSM-5800LV operated at 20 kV, whilst high resolution scanning electron microscopy (HRSEM) measurements were obtained using an FE-SEM Zeiss Ultra Plus. A RX system from Perkin Elmer was used for FT-IR analyses. Energy dispersive X-ray spectroscopy (EDS) analysis was carried out using a SEM integrated EDS Zeiss Crossbeam 540 with software AZtech version 3 by Oxford Instruments.

2.3. Synthesis of L-cysteine-capped CdSeTeS/ZnS alloyed QDs

The synthesis of L-cysteine-capped CdSeTeS/ZnS alloyed QDs has previously been reported by our group [27] and here we provide a brief description. Firstly, hydrophobic alloyed CdSeTeS/ZnS QDs were synthesized via the hot organometallic route. To a solution of cadmium oxide (1.3 g) in 30 mL oleic acid and 50 mL octadecene at $\sim 280 \text{ }^\circ\text{C}$, precursor solutions of selenium (0.3 g selenium + 1.93 g trioctylphosphine oxide + 25 mL octadecene), tellurium (0.48 g tellurium + 1.93 g trioctylphosphine oxide + 25 mL octadecene) and sulphur (0.16 g sulphur + 20 mL oleic acid + 30 mL octadecene) were added to grow the quaternary alloyed CdSeTeS QDs. After

satisfactory growth of the core QDs, ZnS shell precursor solution consisting of zinc ($\sim 0.4 \text{ g}$ zinc + 20 mL oleic acid + 30 mL octadecene) and sulphur (as used in the growth of the core QDs) were added. The hydrophobic CdSeTeS/ZnS QDs were allowed to grow with time and harvested thereafter. Purification was performed using methanol and acetone.

Conversion of the hydrophobic CdSeTeS/ZnS QDs to water-soluble QDs was performed by a ligand exchange reaction utilising a potassium hydroxide-methanolic-L-cysteine-water solution. This separated the organic-phase soluble QDs from the water-soluble QDs. The latter were purified by acetone and chloroform.

2.4. Synthesis of GO nanosheets

The synthesis of GO nanosheets has previously been reported by our group [28] and here we provide a brief description. GO was synthesized via a modified Hummer's method [29]. Briefly, 7.5 g of potassium permanganate was used to oxidize an acidic solution of 2.5 g graphite and 1.25 g sodium nitrate in 60 mL of sulphuric acid. The solution was kept under ice for few hours and stirred until the following day. A pasty light brown solution was formed to which 75 mL of ultrapure deionized water was added and the solution was stirred at $60 \text{ }^\circ\text{C}$ overnight. A solution of 30% hydrogen peroxide (25 mL) was added into the reaction mixture which was then centrifuged using 5% hydrogen chloride and ultrapure deionized water. This produced graphene oxide with a yield of 4.0 g after drying at $65 \text{ }^\circ\text{C}$. Graphite oxide (0.8 g), dissolved in ultrapure deionized water was exfoliated to GO nanosheets by ultrasonication for 3 h followed by purification using 5% hydrogen chloride. After drying at $65 \text{ }^\circ\text{C}$, the yield of GO was 0.4 g.

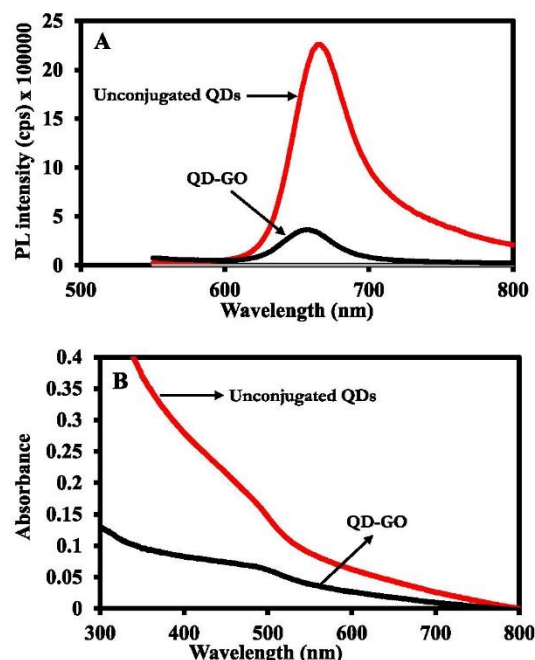


Fig. 1. PL emission (A) and UV/vis absorption spectra (B) of unconjugated L-cysteine-capped CdSeTeS/ZnS QDs and the QD-GO nanocomposite.

2.5. Preparation of CdSeTeS/ZnS QD-GO nanocomposite

The descriptive preparation of the QD-GO nanocomposite is shown in Scheme 1. A 5 mL solution of 0.1 M EDC was used to activate the carboxylic groups of GO (Scheme 1A) (20 mg in 5 mL of ultrapure deionized water) for ~30 min. A 5 mL solution of the QDs (Scheme 1B) (20 mg) was then added followed by 5 mL of 0.1 M NHS to stabilize the amide bond. The reaction was stirred at ambient temperature for ~24 h. The QD-GO (Scheme 1C) nanocomposite was purified by centrifugation with acetone.

2.6. Procedure for the fluorescence “switch ON” detection of PAHs

Four PAHs (Py, Naph, Ant and Phe) which are in the list of the

sixteen priority PAHs documented by the US Environmental Protection Agency [30] were tested in this work. The four selected PAHs are commonly detected in water systems [31,32]. PAH standards ($1 \times 10^{-7} - 5 \times 10^{-7}$ M) were prepared in an ethanol:water (1:2) mixture and were added into the QD-GO nanocomposite solution (~0.7 mg/mL) and allowed to equilibrate for ~5 min. The probe solution was excited at 470 nm and the fluorescence emission measuring range was 480–800 nm.

3. Results and discussion

3.1. Fluorescence quenching effect of GO on the QDs

Structurally, GO has several oxygen containing functional

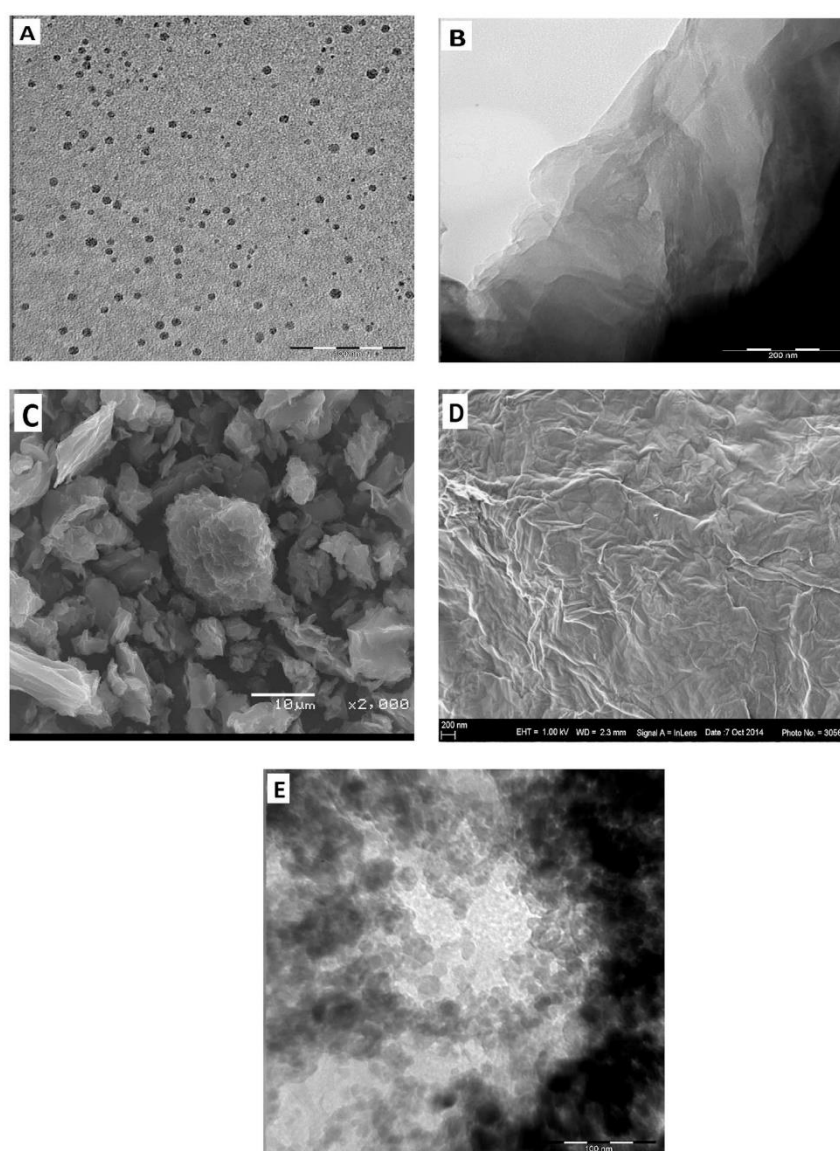


Fig. 2. TEM images of (A) l-cysteine CdSeTeS/ZnS QDs and (B) GO. (C) SEM image of GO and (D) HRSEM image of GO. (E) TEM image of the QD-GO nanocomposite.

groups on its carbon surface such as hydroxyl, epoxy and carboxylic groups. It is believed that the exact structure and composition of GO is difficult to ascertain as this depends on the synthetic method used [33]. In our work, we employed the modified Hummer's method, hence GO should exhibit hydroxyl/epoxy functional groups on the basal plane and carboxylic functional groups at the edges of its planer structure (Scheme 1A). The Hummer's method is applicable for producing high yield water-soluble GO nanosheets.

The fluorescence quenching effect of the QDs after covalent binding to GO is shown in Fig. 1A whilst the corresponding UV/vis absorption spectra are shown in Fig. 1B. The fluorescence emission maximum of the QDs before conjugation was 666 nm and upon binding to GO a slight blue shift to 658 nm was observed. The blue shift reflects a possible increase in the QDs band gap and the lack of agglomerated nanocrystals upon binding to GO. Changes in the absorption spectrum of the nanocomposite also reflects the binding effect of the QDs to GO. There are three possible mechanisms associated with the quenching effect as proposed in the literature [34]; (i) nano-metal surface energy transfer (NSET), (ii) Förster resonance energy transfer (FRET) and (iii) a charge transfer or electron-donor-acceptor mechanism. With respect to the three possible mechanisms, the QDs act as the donor and GO acts as the acceptor. For the charge transfer mechanism, the distance between the QD fluorophore and the GO quencher induces electronic charge transfer from the donor to the acceptor whilst in the case of FRET, energy transfer from the QDs to GO induces the quenching effect which is also made possible by the distance (d) that separates the QDs donor from the GO acceptor. This energy transfer efficiency is inversely proportional to the separation distance ($1/d^6$) for FRET and $1/d^4$ for NSET [35,36]. It has been reported that the higher the separation distance of the donor from the acceptor, the lower the energy transfer efficiency, with the degree of energy transfer efficiency being greater for NSET-based processes than FRET-based processes when a nanoparticle is the acceptor [35].

GO exhibits a weak absorption in the UV region [33], hence making the possibility of charge or energy transfer mechanisms difficult. Li and co-workers [34] proposed that the NSET mechanism dominates the quenching of CdSe/ZnS QDs by GO and this theory has also been supported by another group [37]. However, based on the poor absorption of GO as evidenced from the UV/vis spectrum measured in this work (data not shown), we believe that bonding of GO to CdSeTeS/ZnS QDs may have introduced surface defect states to the QDs fluorescence, hence resulting in the observed quenching.

3.2. Morphology of the QDs, GO and QD-GO nanocomposite

A TEM image of ι -cysteine CdSeTeS/ZnS QDs shown in Fig. 2A reveal a mono-dispersed particle size distribution averaging 5.5 nm. The morphology of GO as characterized by TEM (Fig. 2B), shows layers of GO nanosheets interlocking with each other, and rolled into connected networks of sheets. The SEM image in Fig. 2C, showed that the surfaces of GO were wrinkled into curling edges, with connected networks of interlocking flakes, which will enable strong interaction with other conjugated entities. The corresponding HRSEM image (Fig. 2D) also showed the rolling up of GO into interconnected sheets. The TEM image of the QD-GO displays the binding effect of the QDs onto the GO. It is difficult to see individual QDs anchored onto the GO due to the strong inter-connecting layers of GO. The coarse nature of the image showed its difference from the TEM images of GO and the QDs and thus indicate the bonding of QDs to GO via covalent interaction.

3.3. Crystal structure of the QDs, GO and QD-GO nanocomposite

Fig. 3 shows the XRD patterns for GO, the QDs and QD-GO

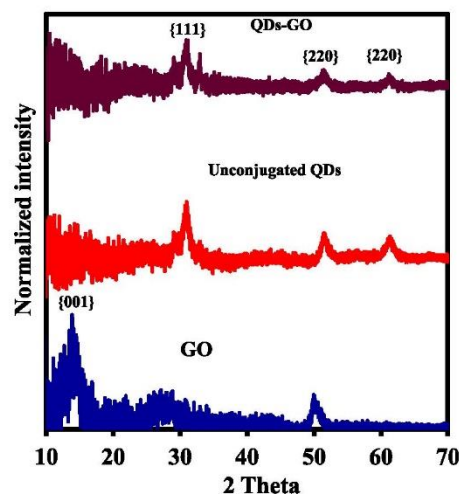


Fig. 3. PXRD spectra of GO, unconjugated QDs and the QD-GO nanocomposite.

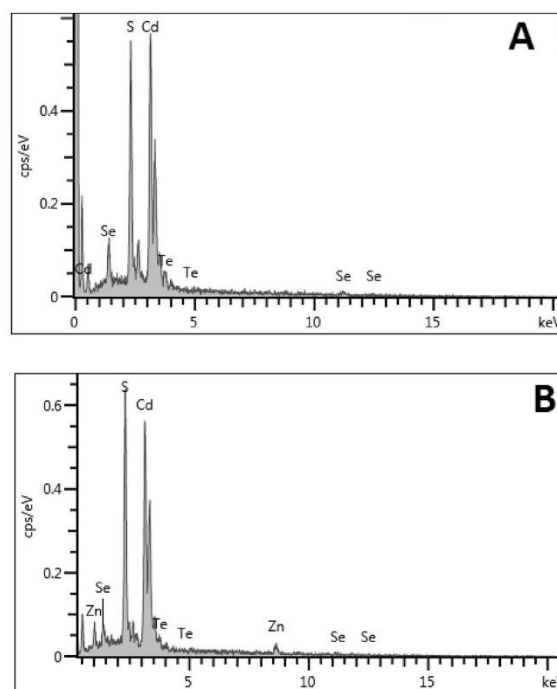


Fig. 4. EDS spectra of (A) CdSeTeS core and (B) CdSeTeS/ZnS QDs.

nanocomposite. GO displayed a typical peak at $2\theta = 13.83^\circ$ [28]. For the QDs, the diffraction pattern fits to a typical zinc-blende crystal structure with the three notable peaks at planes {111}, {220} and {311}, thus corresponding to the JCPDS Card No. 19–0191 for CdSe QDs. The three peaks were displayed at $2\theta = 30.97^\circ$, $2\theta = 51.53^\circ$ and $2\theta = 61.39^\circ$. For the XRD pattern of the QD-GO nanocomposite, we could observe that the zinc-blende crystal structure of the QDs prevailed but with weaker diffraction peaks in

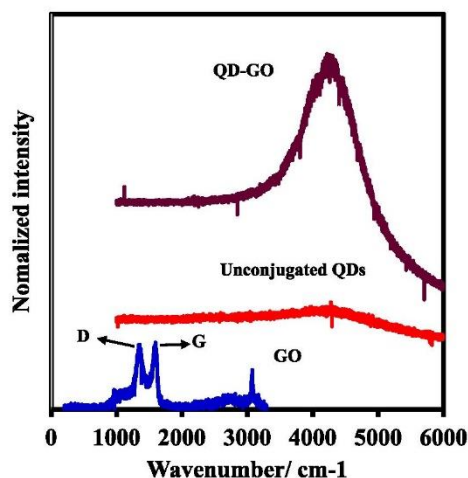


Fig. 5. Raman spectra of GO, unconjugated QDs and the QD-GO nanocomposite.

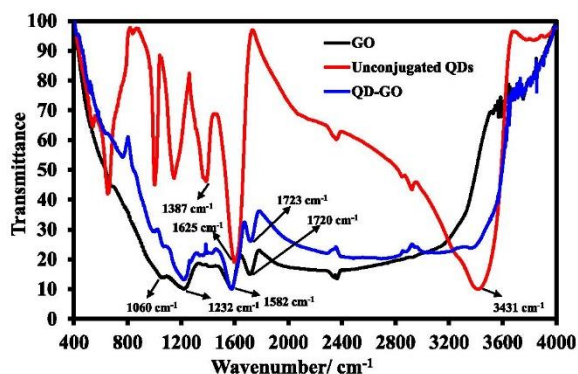


Fig. 6. FT-IR spectra of GO, unconjugated QDs and the QD-GO nanocomposite.

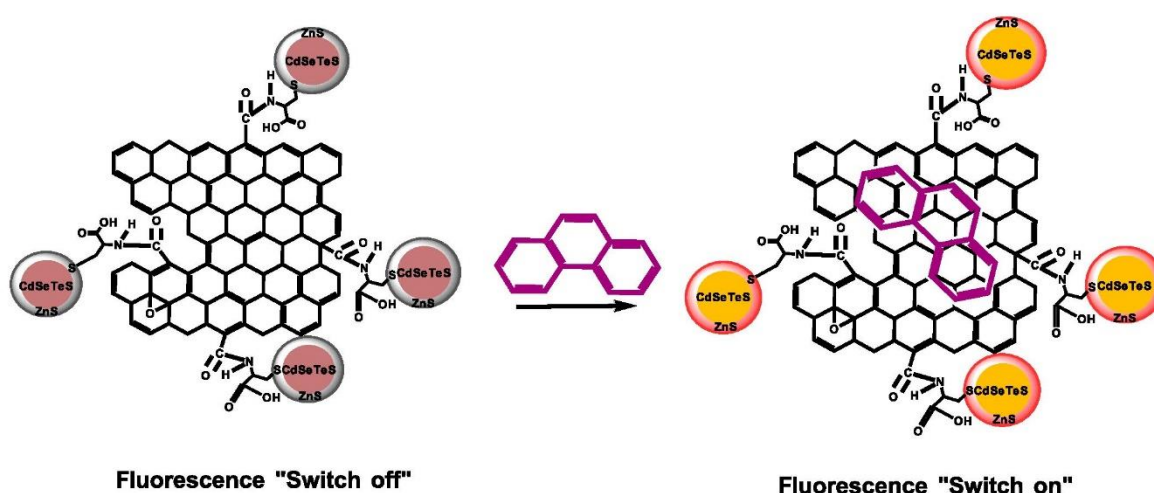
comparison to those of the unconjugated QDs. It is difficult to see the peak of GO in the diffraction pattern of the nanocomposite probably due to the weak intensity thereof. The diffraction peaks of the nanocomposite were displayed at $2\theta = 31.17^\circ$, $2\theta = 51.43^\circ$ and $2\theta = 61.16^\circ$. Comparing the diffraction peak position of the unconjugated QDs with the QD-GO nanocomposite, we observed no significant peak shift. This suggests that the binding of GO to the QDs did not alter the structural nature of the QDs.

3.4. EDS analysis of the QDs

EDS analysis was carried out to semi-quantitatively determine the semiconductor metal components present in the CdSeTeS core and CdSeTeS/ZnS core/shell structures (Fig. 4A and B). The presence of Cd, Se, Te and S were effectively identified in both the core and core/shell spectra while the additional Zn metal component in the core/shell structure was evident. The approximate elemental composition for the CdSeTeS core was Cd (69%), Se (7%), Te (5%) and S (19%) and that for the CdSeTeS/ZnS core/shell was Cd (66.43%), Se (3.37%), Te (3.05%), Zn (5.67%) and S (21.48%). An increase in the Zn and S content and decrease in the Cd content of the core/shell QDs relative to the core QDs was a direct evidence of the effects of shell layering.

3.5. Raman analysis of the QDs, GO and QD-GO nanocomposite

The Raman spectrum of GO [28] shown in Fig. 5 displayed the characteristic D and G band at 1350 cm^{-1} and 1596 cm^{-1} respectively. The D band is generally assigned to vibration of sp^3 hybridized carbon atoms of defects which can break the selection rule and symmetry, while the G band is ascribed to the sp^2 hybridized carbon domain entailed with E_{2g} mode [38]. For the Raman spectrum of the QDs, a broad and weak peak around the region of $4000\text{--}4600\text{ cm}^{-1}$ was observed. The Raman spectrum of the QDs is typical for fluorescent-emitting nanocrystals [28]. For the QD-GO nanocomposite, we observed that the QDs dominated the Raman spectrum. The interesting feature is that the Raman spectrum of the nanocomposite was stronger and more refined than the unconjugated QDs. This is strongly induced by the binding effect of GO.



Scheme 2. Schematic representation of the π - π induced PAH adsorption on GO which triggers the fluorescence enhancement of the conjugated QDs.

3.6. FT-IR spectra of the QDs, GO and QD-GO nanocomposite

The FT-IR spectrum of GO (Fig. 6) exhibited characteristic bands at $\nu_{C-O} = 1060 \text{ cm}^{-1}$ (alkoxy), $\nu_{C-O} = 1232 \text{ cm}^{-1}$ (epoxy), $\nu_{C-O} = 1582 \text{ cm}^{-1}$ (aromatic), $\nu_{C-O} = 1720 \text{ cm}^{-1}$ (carbonyl and carboxylic) and $\nu_{O-H} = 3000 - 3050 \text{ cm}^{-1}$ (hydroxyl) [28]. For the unconjugated QDs, the symmetric and asymmetric carboxylic bands appeared at $\nu_{C-O} = 1387$ and 1625 cm^{-1} while the hydroxyl functional group appeared at $\nu_{O-H} = 3431 \text{ cm}^{-1}$. A careful assessment of the FT-IR spectrum of the QD-GO nanocomposite indicated a slight resemblance to GO. This is due to the strong binding effect of GO to the QDs. The formation of the amide linkage between GO and the QDs is difficult to ascertain from the FT-IR spectrum due to remaining unconjugated moieties on the GO, however the band at 1723 cm^{-1} is in the region for CO-NH formation.

3.7. Fluorescence detection principle

Studies have shown that drugs, pesticides, phenolic compounds, humic acids and PAHs [12,28,33] can adsorb onto graphene-related materials. There are five possible mechanistic pathways by which aromatic-based analytes can interact with the surface of carbon-based materials, namely (i) π - π interactions, (ii) hydrophobic effects, (iii) electrostatic interactions, (iv) covalent interactions and (v) hydrogen bonds [33]. For graphene-based materials, most studies have found π - π interaction to play the dominant role for adsorption [12,33], although hydrophobic effects may also play a role when considering interactions with non-polar organic species in water. Scheme 2 shows the proposed mechanism for the detection of the targeted PAHs by the QD-GO nanocomposite (Scheme 2A), using Phe as an example. Upon binding of GO to the QDs, the fluorescence of the QDs is quenched ("switched OFF"), whilst interaction of the targeted PAH analytes with the QD-GO probe switched on the fluorescence of the conjugated QDs. The PAH analytes were able to adsorb onto graphene via π - π interactions of their aromatic ring system with the π electron rich carbon system of GO (Scheme 2B). The adsorption process then remediates the surface defect states on the QD-GO surface leading to fluorescence enhancement.

3.8. Relative fluorescence enhancement effects of different PAHs on the QD-GO nanocomposite

The affinity of Py, Naph, Ant and Phe to switch on the fluorescence of the QD-GO nanocomposite probe was investigated. It is expected that each of the PAH compounds can adsorb onto GO and trigger fluorescence transduction changes in the conjugated QDs. However, the degree of fluorescence enhancement may vary amongst the PAH analytes due to structural differences. Fig. 7A shows the enhancement effects of the PAH analytes (at a fixed concentration) on the fluorescence of the nanocomposite probe. Each of the tested PAH analytes showed affinity for the nanocomposite probe. The variation in affinity based on the relative % fluorescence enhancement followed the order $\text{Py} < \text{Naph} < \text{Ant} < \text{Phe}$.

3.9. Effect of incubation time and nanocomposite concentration

The effect of incubation time on the PL intensity of the QD-GO nanocomposite probe was studied. Fig. 7B shows the time-dependent (5–40 min) fluorescence intensity change for the detection of a fixed concentration of Phe ($5 \times 10^{-7} \text{ M}$). The data obtained shows that the fluorescence enhancement, and thereby nanocomposite/analyte interactions, were greatest after 5 min incubation and thereafter a steady decrease in the fluorescence

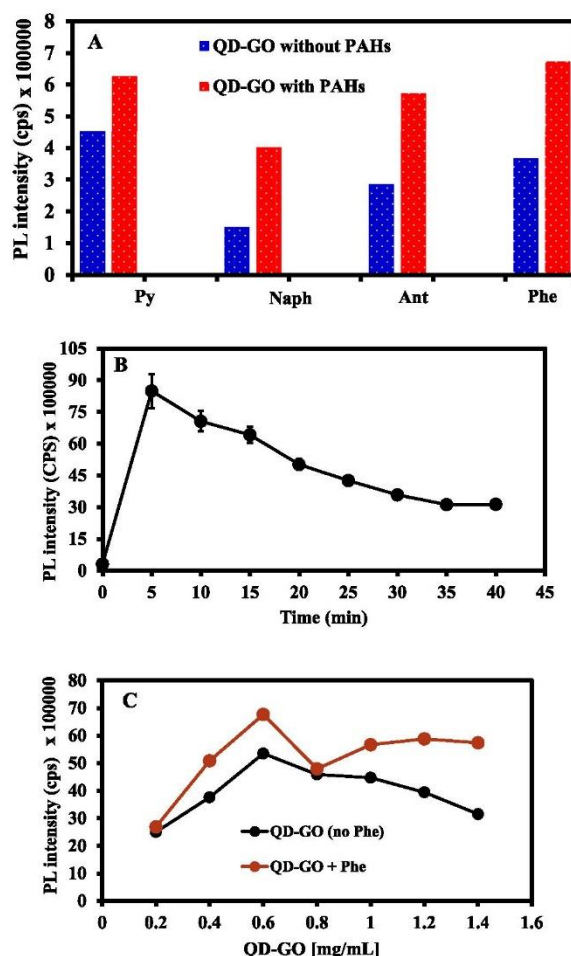


Fig. 7. Effects of PAHs on the PL emission of QD-GO nanocomposite. [PAH] = $5 \times 10^{-7} \text{ M}$. Effect of incubation time (0–40 min) (B) and concentration (C) on the PL emission of the QD-GO nanocomposite in the presence of $5 \times 10^{-7} \text{ M}$ Phe target. Error bars represent standard deviation of 3 successive measurements.

intensity occurred from 10 min to 40 min. The results indicate that Phe can be detected between 5 and 40 min of incubation time but shorter incubation time is more favourable due to the greater enhancement in fluorescence signal. The effect of the QD-GO concentration on the detection of a fixed concentration of Phe is shown in Fig. 7C. With the exception of 0.2 mg/mL and 0.8 mg/mL (which may be considered an outlier) concentration of the QD-GO which exhibited low fluorescence signal enhancement, the rest of the concentrations showed appreciable fluorescence signal enhancement. It appears that there is an increase in PL intensity up to a concentration of 0.6 mg/mL of nanocomposite, indicating an increased interaction of the analyte with the nanocomposite as more of the latter is available in solution. Thereafter, it appears that the nanocomposite is in excess, as there was no further increase in PL intensity with additional increase in concentration of the nanocomposite. In fact, it appears that some degree of self-quenching or agglomeration may have occurred at the higher nanocomposite concentrations due to the slight decrease in PL intensity.

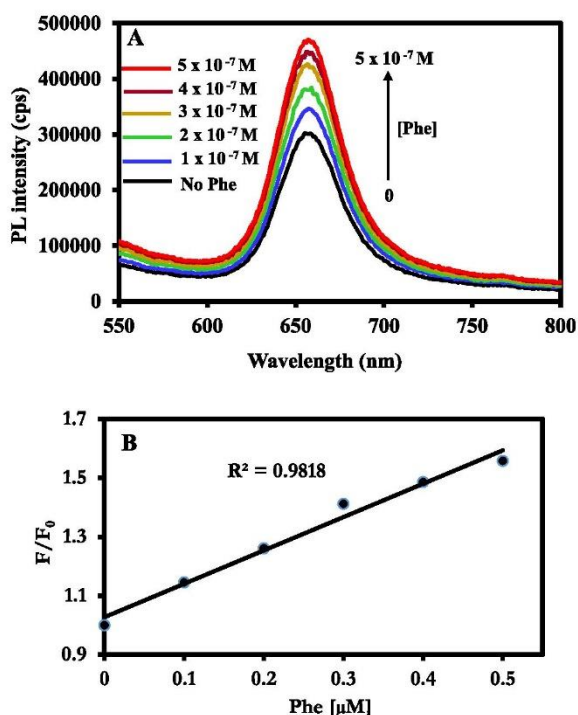


Fig. 8. (A) PL “switch ON” emission spectra for the detection of Phe using the QD-GO nanocomposite for a range of phenanthrene concentrations and (B) corresponding fluorescence signal calibration curve.

3.10. Fluorescence “switch ON” detection of phenanthrene

Phe, used as a typical test PAH analyte, was detected by the nanocomposite probe at different concentrations. Fig. 8A shows the fluorescence detection of Phe by the nanocomposite probe. At increasing concentration of Phe, the fluorescence of the conjugated QDs was switched on. No noticeable peak shift was observed as the target Phe was detected. This implies that the fluorescence of the QD-GO nanocomposite remained stable during the detection process. The corresponding fluorescence calibration curve is shown in Fig. 8B and the limit of detection (LOD) was estimated as three times the standard deviation of blank measurements ($n = 9$) divided by the slope of the linear calibration curve. The LOD of Phe was 2.26×10^{-9} M or 0.4 $\mu\text{g/L}$. The nanocomposite developed in this work is not only suitable for the detection of PAHs but will be sensitive to analytes having fused benzene rings in which their electron rich system can result in adsorption onto the surface of graphene and trigger fluorescence changes in the bonded fluorophore. We believe our detection system is simple, cheap and sensitive.

4. Conclusions

A new nanocomposite material involving the conjugation of L-cysteine-capped CdSeTeS/ZnS QDs to GO has been developed. Characterization of the nanocomposite has been performed using transmission electron microscopy, scanning electron microscopy, Raman, X-ray diffraction, FT-IR, UV/vis and fluorescence spectrophotometry. We have taken advantage of the π electron rich system of GO and its planar structure as a mechanism for the adsorption of

the π electron rich aromatic system of PAHs. The affinity of four different PAH analytes to switch on the fluorescence of the conjugated QDs based on π - π interaction with the surface of GO followed the order Phe > Ant > Naph > Py and the LOD for Phe was 2.26×10^{-9} M.

Acknowledgements

A postdoctoral fellowship offered by the University of Pretoria is gratefully appreciated by O. Adegoke. This work is based on research supported in part by the National Research Foundation of South Africa, Grant Numbers: 90720 and 93394 (P. Forbes), as well as the Department of Science and Technology (DST) through the Photonics Initiative of South Africa (PISA Grant PISA-15-DIR-06), and the Water Research Commission (WRC Grant K5/2438/1). Wirsam Scientific, South Africa is thanked for their support of this research. We thank the Laboratory for Microscopy and Microanalysis of the University of Pretoria (UP), for assistance with the microscopy measurements and Wiebke Grote of UP for the XRD analyses.

References

- [1] J. Kao, K. Thorkelsson, P. Bai, B.J. Rancatore, T. Xu, Toward functional nanocomposites: taking the best of nanoparticles, polymers, and small molecules, *Chem. Soc. Rev.* 42 (2013) 2654–2678.
- [2] K.S. Novoselov, A.K. Geim, S.V. Morozov, D. Jiang, Y. Zhang, S.V. Dubonos, I.V. Grigorieva, A.A. Firsov, Electric field effect in atomically thin carbon films, *Science* 306 (2004) 666–669.
- [3] T.P. Kaloni, Y.C. Cheng, R. Faccio, U. Schwingenschlöggl, Oxidation of monovacancies in graphene by oxygen molecules, *J. Mater. Chem.* 21 (2011) 18284–18288.
- [4] Y.C. Cheng, T.P. Kaloni, Z.Y. Zhu, U. Schwingenschlöggl, Oxidation of graphene in ozone under ultraviolet light, *Appl. Phys. Lett.* 101 (2012) 073110.
- [5] T.P. Kaloni, M. Upadhyay Kahaly, R. Faccio, U. Schwingenschlöggl, Modelling magnetism of C at O and B monovacancies in graphene, *Carbon* 64 (2013) 281–287.
- [6] W. Choi, I. Lahiri, R. Seelaboyina, Y.S. Kang, Synthesis of graphene and its applications: a review, *Crit. Rev. Solid State* 35 (2010) 52–71.
- [7] Y. Si, E.T. Samulski, Synthesis of water soluble graphene, *Nano Lett.* 8 (2008) 1679–1682.
- [8] E.W. Hill, A. Vijayaraghavan, K. Novoselov, Graphene sensors, *IEEE Sens. J.* 11 (2011) 3161–3170.
- [9] V. Singh, D. Joung, L. Zhai, S. Das, S.I. Khondaker, S. Seal, Graphene based materials: past, present and future, *Prog. Mater. Sci.* 56 (2011) 1178–1271.
- [10] L. Gomez De Arco, Y. Zhang, C.W. Schlenker, K. Ryu, M.E. Thompson, C. Zhou, Continuous, highly flexible, and transparent graphene films by chemical vapor deposition for organic photovoltaics, *ACS Nano* 4 (2010) 2865–2873.
- [11] M.J. Allen, V.C. Tung, L. Gomez De Arco, Z. Xu, L.M. Chen, K.S. Nelson, C. Zhou, R.B. Kaner, Y. Yang, Soft transfer printing of chemically converted graphene, *Adv. Mater.* 21 (2009) 2098–2102.
- [12] S. Basua, P. Bhattacharyya, Recent developments on graphene and graphene oxide based solid state gas sensors, *Sens. Actuat. B-Chem.* 173 (2012) 1–21.
- [13] Y. Zhang, Y.W. Tan, H.L. Stormer, P. Kim, Experimental observation of the quantum Hall effect and Berry's phase in graphene, *Nature* 438 (2005) 201–204.
- [14] T. Kuila, S. Bose, P. Khanra, A.K. Mishra, N.H. Kim, J.H. Lee, Recent advances in graphene-based biosensors, *Biosens. Bioelectron.* 26 (2011) 4637–4648.
- [15] N. Tombros, C. Jozsa, M. Popinciuc, H. Jonkman, B. van Wees, Electronic spin transport and spin precession in single graphene layers at room temperature, *Nature* 448 (2007) 571–574.
- [16] T.J. Booth, P. Blake, R.R. Nair, D. Jiang, E.W. Hill, U. Bangert, A. Bleloch, M. Gass, K.S. Novoselov, M.I. Katsnelson, A.K. Geim, Macroscopic graphene membranes and their extraordinary stiffness, *Nano Lett.* 8 (2008) 2442–2446.
- [17] B. Lang, A LEED study of the deposition of carbon on platinum crystal surfaces, *Surf. Sci.* 53 (1975) 317–329.
- [18] M. Pumera, A. Ambrosi, A. Bonanni, E.L.K. Chng, H.L. Poh, Graphene for electrochemical sensing and biosensing, *Trac-Trend Anal. Chem.* 29 (2010) 954–965.
- [19] R.M. Singh, R. Kumar, D.P. Singh, Graphene oxide: strategies for synthesis, reduction and frontier applications, *RSC Adv.* 6 (2016) 64993–65011.
- [20] M. Han, X. Gao, J.Z. Su, S. Nie, Quantum-dot-tagged microbeads for multiplexed optical coding of biomolecules, *Nat. Biotechnol.* 19 (2001) 631–635.
- [21] A.P. Alivisatos, The use of nanocrystals in biological detection, *Nat. Biotechnol.* 22 (2004) 47–52.
- [22] N.L. Rosi, C.A. Mirkin, Nanostructures in biodiagnostics, *Chem. Rev.* 105 (2005) 1547–1562.
- [23] O. Adegoke, T. Kato, E.Y. Park, An ultrasensitive alloyed near-infrared

- quinternary quantum dot-molecular beacon nanodiagnostic bioprobe for influenza virus RNA, *Biosens. Bioelectron.* 80 (2016) 483–490.
- [24] O. Adegoke, M.-W. Seo, T. Kato, S. Kawahito, E.Y. Park, Gradient band gap engineered alloyed quaternary/ternary CdZnSeS/ZnSeS quantum dots: an ultrasensitive fluorescence reporter in a conjugated molecular beacon system for the biosensing of influenza virus RNA, *J. Mater. Chem. B* 4 (2016) 1489–1498.
- [25] H. Richter, J.B. Howard, Formation of polycyclic aromatic hydrocarbons and their growth to soot—a review of chemical reaction pathways, *Prog. Energ. Combust.* 26 (2000) 565–608.
- [26] G. Falco, J.L. Domingo, J.M. Llobet, A. Teixido, C. Casas, L. Muller, Polycyclic aromatic hydrocarbons in foods: human exposure through the diet in Catalonia, Spain, *J. Food. Prot.* 66 (2003) 2325–2331.
- [27] O. Adegoke, T. Nyokong, P.B.C. Forbes, Structural and optical properties of alloyed quaternary CdSeTeS core and CdSeTeS/ZnS core–shell quantum dots, *J. Alloy Compd.* 645 (2015) 443–449.
- [28] O. Adegoke, P.B.C. Forbes, L-cysteine-capped core/shell/shell quantum dot-graphene oxide nanocomposite fluorescence probe for polycyclic aromatic hydrocarbon detection, *Talanta* 146 (2016) 780–788.
- [29] W.S. Hummers Jr., R.E. Offeman, Preparation of graphitic oxide, *J. Am. Chem. Soc.* 80 (1958) 1339.
- [30] US Environmental Protection Agency, Guidelines Establishing Test Procedures for the Analysis of Pollutants, Proposed Regulations, Federal Register, vol. 49, no. 209, USEPA, Washington, DC.
- [31] L. Chimuka, P. Sibiyi, R. Amdany, E. Cukrowska, P.B.C. Forbes, Status of PAHs in environmental compartments of South Africa: a country report, *Polycycl. Aromat. Comp.* 36 (2015) 376–394.
- [32] E. Martinez, M. Gros, S. Lacorte, D. Barceló, Simplified procedures for the analysis of polycyclic aromatic hydrocarbons in water, sediments and mussels, *J. Chrom. A* 1047 (2004) 181–188.
- [33] S. Wang, H. Sun, H.M. Ang, M.O. Tadé, Adsorptive remediation of environmental pollutants using novel graphene-based nanomaterials, *Chem. Eng. J.* 226 (2013) 336–347.
- [34] M. Li, X. Zhou, S. Guo, N. Wu, Detection of lead (II) with a “turn-on” fluorescent biosensor based on energy transfer from CdSe/ZnS quantum dots to graphene oxide, *Biosens. Bioelectron.* 43 (2013) 69–74.
- [35] H. Tao, X. Liao, M. Xu, X. Xie, F. Zhong, Z. Yi, Detection of immunoglobulin G based on nanoparticle surface energy transfers from fluorescein isothiocyanate to gold nanoparticles, *Anal. Methods* 6 (2014) 2560–2565.
- [36] X. Huang, I.H. El-Sayed, W. Qian, M.A. El-Sayed, Cancer cells assemble and align gold nanorods conjugated to antibodies to produce highly enhanced, sharp, and polarized surface Raman spectra: a potential cancer diagnostic marker, *Nano Lett.* 7 (2007) 1591–1597.
- [37] S. Jander, A. Kornowski, H. Weller, Energy transfer from CdSe/CdS nanorods to amorphous carbon, *Nano Lett.* 11 (2011) 5179–5183.
- [38] X.-j. Hu, Y.-g. Liu, H. Wang, A.-w. Chen, G.-m. Zeng, S.-m. Liu, Y.-m. Guo, X. Hu, T.-t. Li, Y.-q. Wang, L. Zhou, S.-h. Liu, Removal of Cu(II) ions from aqueous solution using sulfonated magnetic graphene oxide composite, *Sep. Purif. Technol.* 108 (2013) 189–195.

Co-authored paper 2: Synthesis & characterization of CdS/AgZnSe QDs

O. Adegoke, H. Montaseri, S.A. Nsibande*, P.B.C. Forbes, Passivating effect of ternary alloyed AgZnSe shell layer on the structural and luminescent properties of CdS quantum dots, *Materials Science in Semiconductor Processing*, 90 (2019) 162-170.

DOI: <https://doi.org/10.1016/j.mssp.2018.10.025>

*Contributions by S.A. Nsibande:

- Assisted the main author in the synthesis of CdS/AgZnSe QDs (Section 2.4 and 2.5)
- TEM characterization (Section 3.2.1)
- XRD characterization (Section 3.2.2)
- Manuscript review



Contents lists available at ScienceDirect

Materials Science in Semiconductor Processing

journal homepage: www.elsevier.com/locate/mssp

Passivating effect of ternary alloyed AgZnSe shell layer on the structural and luminescent properties of CdS quantum dots



Oluwasesan Adegoke^{*}, Hanieh Montaseri, Sifiso A. Nsiband, Patricia B.C. Forbes^{*}

Department of Chemistry, Faculty of Natural and Agricultural Sciences, University of Pretoria, Lynnwood Road, Pretoria 0002, South Africa

ARTICLE INFO

Keywords:

Quantum dots
Surface defects
Photoluminescence
Quantum yield
Alloyed

ABSTRACT

The surface passivation of luminescent CdS quantum dots (QDs) via epitaxial overgrowth of new alloyed ternary AgZnSe shell layer is reported here. Two synthetic fabrication strategies were used to tune the optical properties of CdS/AgZnSe core/alloyed shell QDs across the visible region. Transmission electron microscopy, powder X-ray diffraction, Raman, UV/vis and fluorescence spectrophotometric techniques were used to characterize the nanocrystals. Analysis of the internal structure of the QDs revealed that homogeneity of the particle reduced as the size increased, thus indicating that the QDs growth transitioned from an interfacial epitaxial homogenous state to a heterogeneous state. The crystal structure of the QDs revealed a distinct zinc-blende diffraction pattern for CdS while CdS/AgZnSe core/alloyed shell QDs kinetically favoured a phase change process from the zinc-blende phase to a wurtzite phase. Analysis of the photophysical properties revealed varying degrees of interfacial defect state suppression in CdS/AgZnSe QDs which was dependent on the QDs size. Specifically, the fluorescence quantum yield (QY) of CdS/AgZnSe QDs was at most ~5-fold higher than the CdS core and varied from 35% to 73%. We found that band gap modulation via the synthetic fabrication strategy employed, influenced the optical properties of the core/alloyed shell QDs. The CdS/AgZnSe QDs produced in this work hold great promise in light-emitting optoelectronic applications.

1. Introduction

The wide electro-luminescent applications of colloidal semiconductor quantum dot (QD) nanocrystals in various fields of chemistry, biology and physics, stem from their unique optoelectronic properties [1,2]. Particularly, the size-dependent optical and electronic properties of QDs which are governed by the associated quantum confinement feature, allows tuning of the photoluminescence (PL) emission from the ultraviolet/visible (UV/vis) region to the far infra-red region [3–6]. In contrast to bulk semiconductors in which the surface represents a tiny fraction of the bulk material, colloidal QDs have their size typically in the range of 2–10 nm. This unique characteristic enables a large number of atoms to be embedded on the QD surface [7].

The QD surface represents a highly sensitive region that is exposed to its surrounding environment (matrices, solvents and various other species in solution) and it is typically coordinated by chemical ligands, surfactants or stabilizers that influence the QD optoelectronic properties [7]. The synergistic effects of precursor material which create low numbers of coordinated surface atoms may lead to highly reactive or localized electronic sites that are susceptible to redox and chemical processes. Thus, it is very likely for midgap, shallow or deep surface

defect states to be formed and induce the pathway for poor PL properties. The characteristic phenomenon is nonradiative recombination exciton (electron and hole) states associated with low PL quantum yield (QY) [8,9]. One of the widely used strategies to eliminate surface traps is to passivate the QD core surface with a wider band gap shell material [10–13]. This strategy shifts the surface defects to the outer domain of the shell layer, thus improving the PL QY [4]. The electron and hole being localized in the core, represents a signature process associated with the low probability of the outer surface state being subjected to trapped photogenerated charge carriers [14,15].

Over the past two decades, the most studied class of semiconductor QDs are the group II-VI metal chalcogenides with CdSe-based QDs being the most popular for fabricating new synthetic routes [16], shell passivation [17], ligand dynamics [18] and alloying [19]. On the other hand, CdS nanocrystals are probably the second most studied QD system [20–23], exhibiting an exciton Bohr radius of 3.0 nm [24] and a bulk band gap of 2.48 eV [25]. Its characteristic PL emission is known to be highly prone to surface defects which results in low PL QY [26]. Nonetheless, it is widely used as a shell layer to overcoat the surface of CdSe-based QDs. The well-known strategy to isolate the exciton wave function from the surface of the core QDs with embedded surface

^{*} Corresponding authors.

E-mail addresses: adegoke.sesan@mailbox.co.za (O. Adegoke), patricia.forbes@up.ac.za (P.B.C. Forbes).

<https://doi.org/10.1016/j.mssp.2018.10.025>

Received 6 October 2018; Received in revised form 21 October 2018; Accepted 24 October 2018
1369-8001/ © 2018 Elsevier Ltd. All rights reserved.

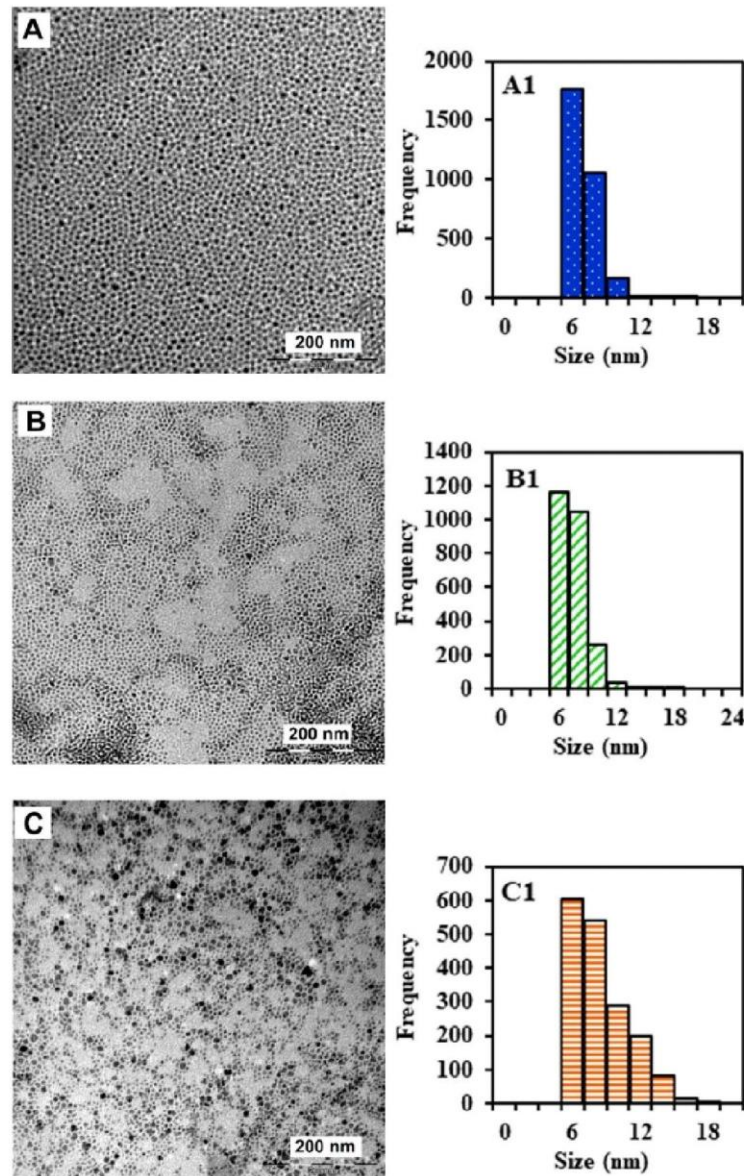


Fig. 1. TEM images (A, B and C) and average particle size distribution (A1, B1 and C1) of CdS core QDs.

defects and dangling bonds is to coat with a shell layer of a wide band gap [27]. However, it is important to note that lattice mismatch between the core and binary shell material at the interface can also induce surface defects that degrade the luminescence of the core/shell QDs, thus lowering the PL QY [28].

Another strategy which has drawn significant interest in improving the PL QY of binary core QDs is to coat the surface with an alloyed ternary shell layer. Alloyed QDs (AB_xC_{1-x}) have become important in mainstream nanoscale optical engineering due to the added degree of freedom in tuning the exciton energy for either extended PL emission range or improved optical properties [29–32]. The coating of an alloyed ternary shell around binary core QDs to improve the PL efficiency has mostly been reported for CdSe-based QDs [33,34] with rare reports for

CdS-based QDs [13]. It is noteworthy that apart from the formation of a smooth gradient band gap, the lattice strain of the core/shell QDs can be relaxed due to alloying [35]. Furthermore, it has been demonstrated that shell alloying suppressed Auger exciton recombination in core/alloyed shell/shell QDs, thus increasing the PL QY [36].

Overcoating a shell layer around the CdS core to improve the PL QY of QDs has rarely been studied. Thus, in this paper, we report on a new strategy to suppress the surface defect states of CdS QDs by coating with a new ternary alloyed shell layer. CdS QDs, characterized by low PL QY due to embedded surface defects were synthesized in this work via the organometallic synthetic route. We have demonstrated for the first time that improved PL QY in CdS QDs can be achieved via passivation with a ternary alloyed AgZnSe shell layer. To the best of our knowledge, our

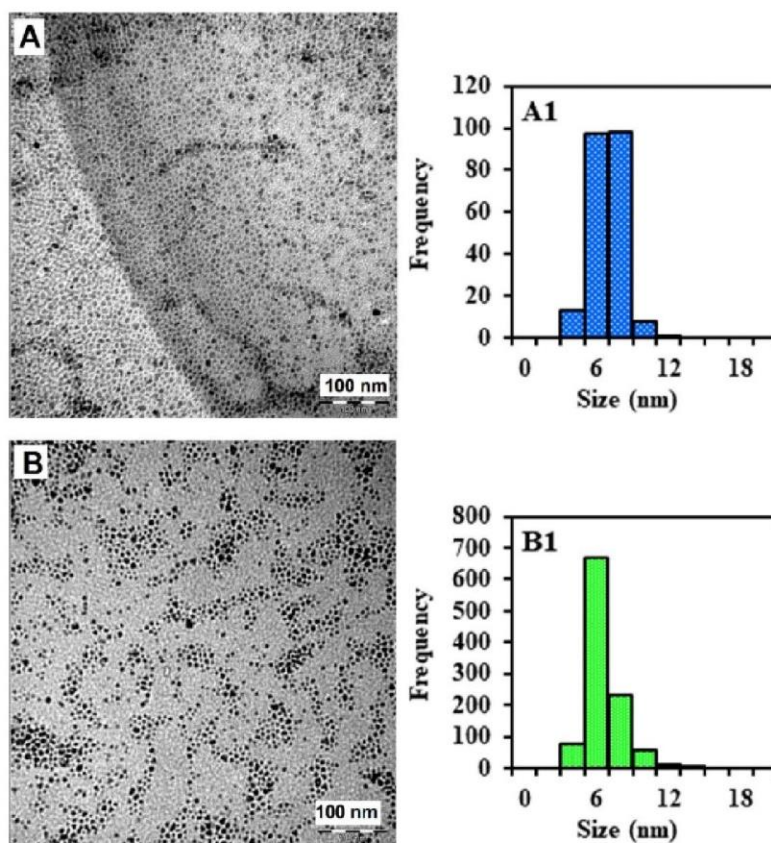


Fig. 2. TEM images (A, B, C and D) and average particle size distribution (A1, B1, C1 and D1) of CdS/AgZnSe core/alloved shell QDs synthesized via method 1.

work is the first to overcoat a AgZnSe shell around CdS core QDs with the sole aim of suppressing interfacial defect states in the core QDs. The organic-phase CdS/AgZnSe core/alloved shell QDs produced in this work hold great promise in light-emitting optoelectronic applications.

2. Experimental section

2.1. Materials

Cadmium oxide (CdO), myristic acid, trioctylphosphine oxide (TOPO), hexadecylamine (HDA), trioctylphosphine (TOP), octadecene (ODE), oleic acid, sulphur (S), γ -cysteine, diethylzinc (Et₂Zn) and zinc oxide (ZnO) were purchased from Sigma Aldrich. Silver nitrate (AgNO₃) was purchased from Saarchem. Selenium (Se) was purchased from Merck. Methanol, acetone, hexane and chloroform were purchased from ACE Chemicals.

2.2. Characterization

UV/vis absorption spectra were obtained using a Cary Eclipse (Varian) spectrophotometer. PL emission measurements were carried out using a Horiba Jobin Yvon Fluoromax-4 spectrofluorometer. Powder X-ray diffraction (PXRD) measurements were determined using a Cu(K α) radiation ($\lambda = 1.54184 \text{ \AA}$) on a Bruker D2 Phaser. Transmission electron microscopy (TEM) images were produced using a JEOL JEM 2100 F operated at 200 kV. Raman spectra were recorded using a WITec Alpha 300 micro-Raman imaging system with a 488 nm excitation laser and CCD detector at ambient temperature with the laser power below 2 mW in order to reduce heating effects.

2.3. Preparation of the precursors

2.3.1. TOPSe

To prepare the Se precursor, 0.12 g Se was dissolved in 5 mL TOP and sonicated until complete dissolution of Se, thus resulting in a clear solution. The solution was then stirred at room temperature prior to use and was stable for 3 days.

2.3.2. TOPZn

To prepare the Zn precursor from Et₂Zn, 1.93 g TOPO was firstly dissolved in 10 mL ODE and 5 mL of oleic acid. The solution was then heated up until the complete dissolution of TOPO surfactant, thus resulting in a clear solution. Thereafter, 2 mL Et₂Zn and 1 mL TOP were added and the solution was stirred at room temperature before use.

To prepare the Zn precursor from ZnO, 0.4 g ZnO was added to a mixture of 15 mL ODE and 10 mL oleic acid and sonicated for a few minutes. Thereafter, the precursor solution was stirred at room temperature prior to use.

2.3.3. TOPAg

Ag precursor was prepared by mixing 0.5 g AgNO₃ with 5 mL TOP. The solution was then heated up until complete dissolution of the AgNO₃ which was evident by the change in colour from colourless to brownish black.

2.3.4. TOPS

To prepare the TOPS precursor used in method 1 synthesis of CdS/AgZnSe QDs (refer to Section 2.4), 1.93 g TOPO was first dissolved in 15 mL ODE and 10 mL oleic acid followed by the addition of 0.16 g S

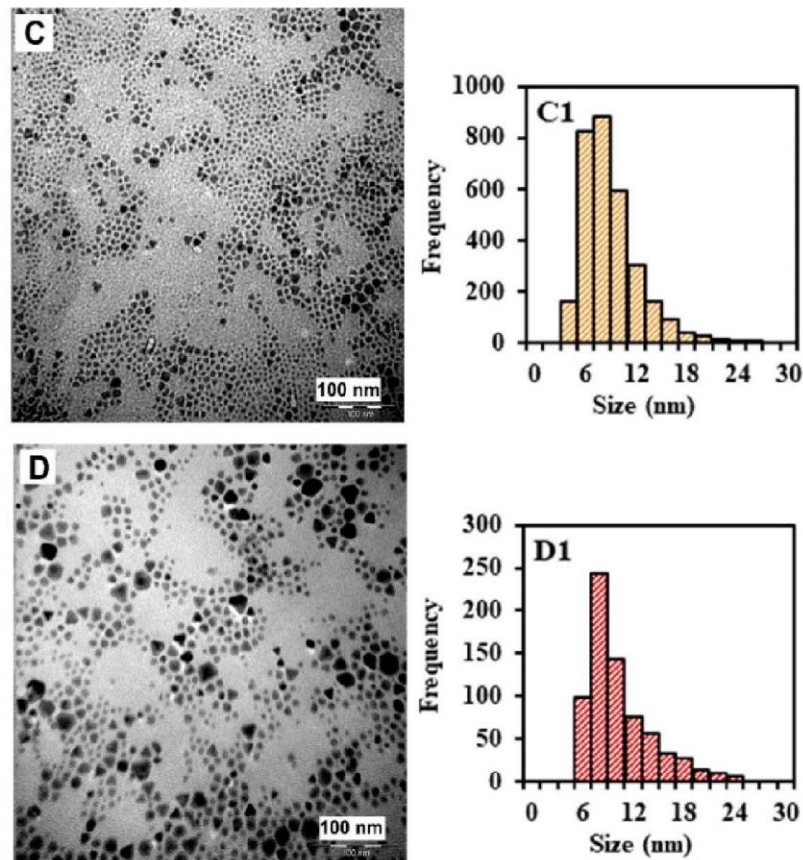


Fig. 2. (continued)

and 1 mL TOP. For method 2 synthesis of CdS/AgZnSe QDs (Section 2.5), 1.93 g TOPO was dissolved in 10 mL ODE and 5 mL oleic acid, then 0.08 g S and 1 mL TOP was added thereafter. The solutions were sonicated and heated up to aid complete dissolution of the S and thereafter stirred at room temperature prior to use.

2.4. Synthesis of CdS/AgZnSe core/alloyed shell QDs (method 1)

The synthesis of CdS/AgZnSe core/alloyed shell QDs was carried out via the organometallic one-pot synthetic route but with modifications [37]. Complexation between the Cd ion, surfactants and capping ligands was formed by mixing 1.3 g CdO, 1.2 g myristic acid, 1.93 g TOPO and 1.2 g HDA with 50 mL ODE and 30 mL of oleic acid. The solution was bubbled with Ar gas and heated up until complete dissolution of the Cd ion which was evident by a change in colour of the solution from pale brown to colourless. At $\sim 220^\circ\text{C}$, TOPS solution was added into the Cd precursor solution to form the CdS core QDs. Once satisfactory growth of the QD core was achieved, a fraction of the growth solution was injected into a beaker. To form the core/alloyed shell QDs, 1 mL of TOPSe solution was added into the CdS growth solution followed swiftly by the addition of 1 mL TOPAg and TOPZn (using ZnO). Portions of the core/shell QDs were taken out at different time intervals.

2.5. Synthesis of CdS/AgZnSe QDs (method 2)

Method 2 synthesis was carried out according to the fabrication steps detailed in method 1 but with slight modifications of the precursor concentrations. For the complexation of Cd ion with the precursor materials, 2 mL TOP, 0.4 g CdO, 0.6 g HDA and 0.6 g myristic acid were

mixed with 20 mL ODE and 15 mL oleic acid. The synthetic process of method 1 was thereafter followed by adding TOPS (prepared specifically for method 2) to form the CdS QDs. Formation of the core/alloyed shell QDs was followed according to method 1 except that TOPZn prepared from Et_2Zn was used.

3. Results and discussion

3.1. Fabrication of the QDs

One-pot organometallic synthesis of metal precursors in the presence of surfactants, organic-capping ligands and a non-coordinating solvent (ODE) was used to engineer the structure of the QDs. It is well known that the growth kinetics influences the PL emission and absorption evolution of the QDs [38]. The nature of the precursor material with respect to the concentration, quantity, time of injection, temperature and the interplay between them are reaction conditions that influence the growth of the QDs. We have therefore exploited these reaction conditions to engineer the optical properties of CdS/AgZnSe core/alloyed shell QDs.

In method 1 synthesis, higher quantities of the Cd metal precursor, surfactants, organic ligands and the non-coordinating solvent were used to aid the Cd-precursor complexation for the subsequent nucleation and growth of CdS QDs. Conversely, lower concentrations of the Cd precursor, surfactants and ligands were employed in method 2 synthesis of the QDs. Before adding the TOPS precursor, the Cd precursor solution was heated up to $> 200^\circ\text{C}$ to aid complete dissolution and complexation of the Cd precursor. The change in colour of the solution from brown to colourless confirmed the complexation process which was accompanied by injection of the TOPS precursor. As the CdS core QDs

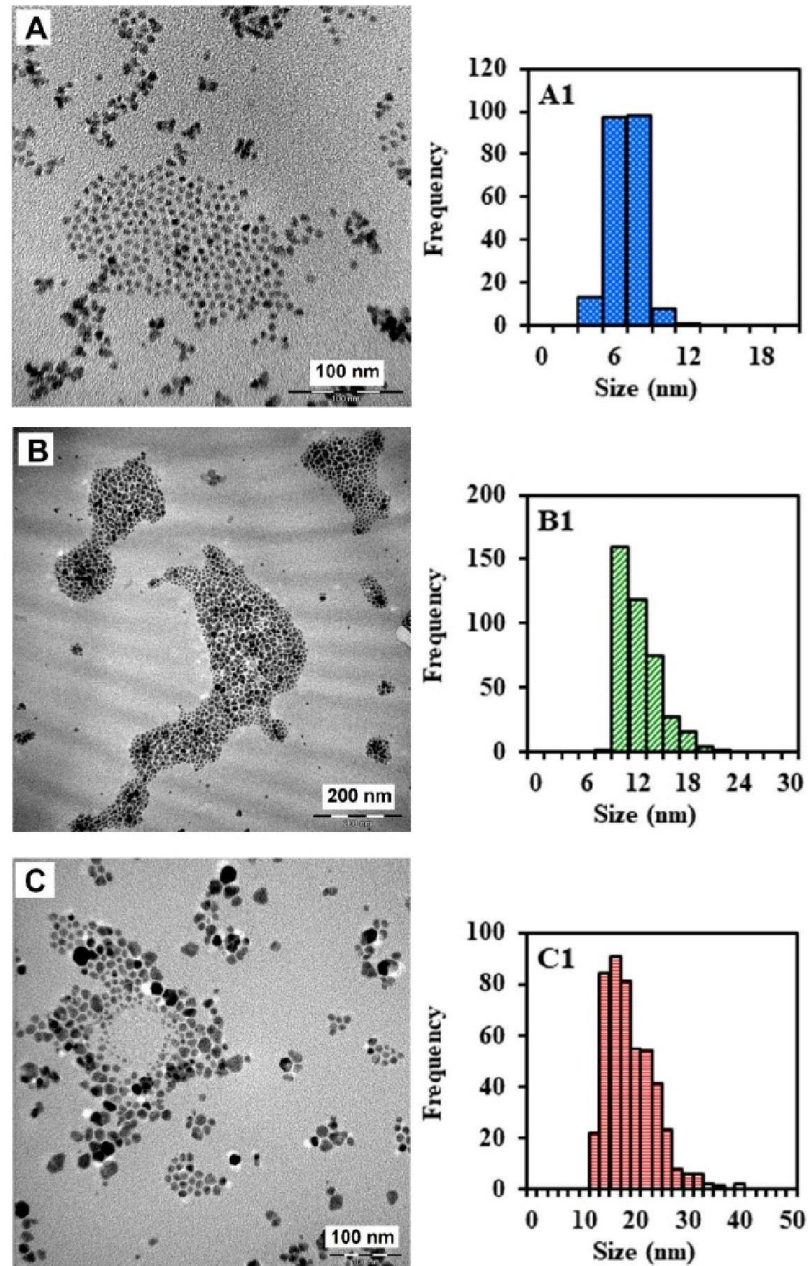


Fig. 3. TEM images (A, B and C) and average particle size distribution (A1, B1 and C1) of CdS/AgZnSe core/alloved shell QDs synthesized via method 2.

nucleated, the temperature of the growth solution increased steadily and was accompanied by a concomitant change in the colour. During this period, a fraction of the CdS core QDs was removed in order to probe the structural and optical properties thereof in comparison to the core/alloved shell QDs.

The temperature at which the AgZnSe alloved shell was overcoated on the CdS core surface is very crucial to the overall optical properties of the CdS/AgZnSe core/alloved shell QDs. At higher temperature and longer reaction time, CdS QDs size distribution is expected to deteriorate and lead to broadening of the spectral line widths. On the other hand, overcoating the shell layer at relatively low temperature could either reduce the crystallinity of CdS/AgZnSe core/alloved shell QDs or lead to incomplete decomposition of the precursor materials [39].

Therefore, an appropriate temperature was determined independently for each method used to fabricate the core/alloved shell QDs. The concentration and rate at which the AgZnSe shell precursor is added is also crucial in influencing the optical properties of the QDs. Slow addition of the precursor shell materials prevents homogenous nucleation and induces most of the AgZnSe shell to grow heterogeneously on the CdS nuclei. Hence, the precursor solutions for the shell layering were injected into the CdS growth solution in swift succession. Addition of TOPSe, TOPZn and TOPAg precursors to the CdS growth solution triggered a progressive change in the colour of the solution from orange to red and to dark brown. Different sizes of the CdS/AgZnSe QDs were thereafter harvested at different time intervals whilst the QDs were purified with acetone, chloroform/acetone and chloroform/acetone/

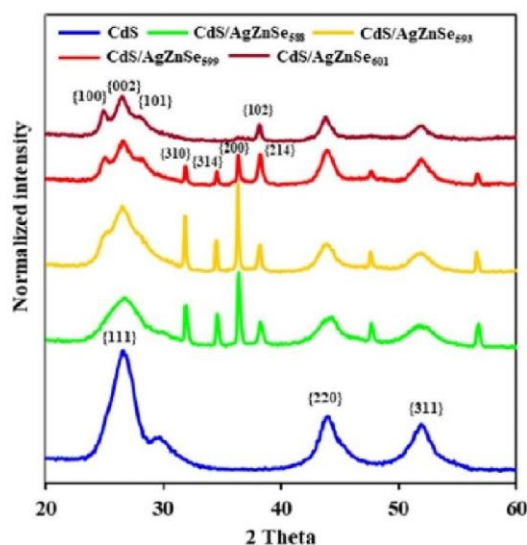


Fig. 4. XRD plots of CdS, CdS/AgZnSe₅₈₈, CdS/AgZnSe₅₉₃, CdS/AgZnSe₅₉₉ and CdS/AgZnSe₆₀₁ QDs.

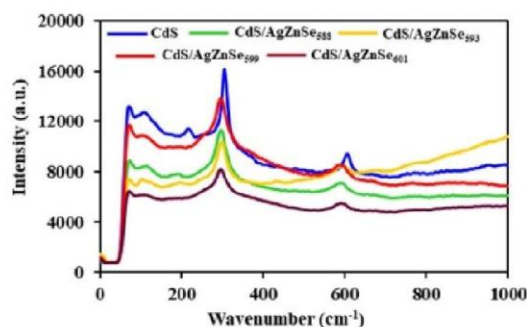


Fig. 5. Raman spectra of CdS, CdS/AgZnSe₅₈₈, CdS/AgZnSe₅₉₃, CdS/AgZnSe₅₉₉ and CdS/AgZnSe₆₀₁ QDs.

ethanol mixture.

3.2. Structural properties

3.2.1. Surface morphology

TEM analysis was used to qualitatively probe the internal structure of the QDs with respect to the shape, size distribution, and shell coverage. Fig. 1A–C shows the TEM images of three different-sized CdS QDs with average sizes of 6.0 ± 0.5 , 6.5 ± 0.5 and 7.5 ± 1.2 nm respectively. Our aim was to synthesize uniform-sized CdS QDs in order to effectively understand the structural effects of shell layering. Looking closely at each TEM micrograph, a uniform size distribution, embedded with a mixture of spherical and quasi-spherical shapes was observed. Thus, the monodispersed particle size distribution provides direct indication of homogenous nucleation and growth of the core QDs.

Alloyed semiconductor QD nanocrystals can be grouped as having either a gradient internal structure derived from varying the alloy composition or a uniform internal structure ascribed to homogenous alloying. In our work, a fixed composition of the shell precursor was used to engineer the structure of the core/alloyed shell QDs. Fig. 2A–D shows the representative TEM images of CdS/AgZnSe core/alloyed shell QDs synthesized via method 1 with average particle sizes of 5.1 ± 0.6 , 5.5 ± 0.7 , 7.9 ± 1.6 and 9.1 ± 1.9 nm respectively. The striking feature was the decrease in the core/alloyed shell QDs particle size

relative to the core which is an unusual phenomenon as the size of the core/shell QDs is expected to increase after shell passivation. Since shell passivation of the 7.5 nm CdS QDs led to rapid nucleation and growth of the different sized CdS/AgZnSe QDs, it is imperative to suggest that either CdS was buried within the shell domain or an intermediate formation of CdS/CdSe occurred before the growth of CdS/AgZnSe QDs.

As the CdS/AgZnSe QDs grew, a steady transformation in the particle morphology with respect to the size distribution was observed. The homogeneity of the particle reduced as the size increased, thus indicating that the QDs growth transitioned from an interfacial epitaxial homogenous state to a heterogeneous state. During the period of harvesting each of the different-sized QDs, the temperature of the solution increased from ~ 240 – 310 °C and this should tentatively influence the nucleation and growth of the QDs. It is also noteworthy to emphasize that the transition in homogeneity of the QDs correlated significantly to the shape engineering of the particle. Looking closely at the TEM monograph of 7.9 nm and 9.1 nm-sized CdS/AgZnSe QDs (Figs. 2C and 2D), the emergence of trigonal-shaped particles was observed. Tentatively, we could attribute the shape engineering of the QDs to the passivating effect of AgZnSe shell, thus implying that the electronic structure of CdS/AgZnSe QDs led to different confinement levels for electron and hole. The hole may be strongly confined to the CdS core while the electron may be delocalised into the shell layer [40].

Three different sizes of CdS/AgZnSe QDs were harvested using method 2 synthetic route. The corresponding TEM images and particle size histograms are shown in Fig. 3. The particle size distribution revealed a prolate heterogeneous particle morphology, resembling an anisotropic-like growth pattern. The anisotropic growth pattern can be understood in terms of the reaction conditions used in the synthesis as it applies to low reactivity precursors and low volume of coordinating solvent. Under these reaction conditions, CdS/AgZnSe heteroepitaxial growth is kinetically controlled (i.e., AgZnSe formation at the surface is the rate-limiting step, rather than the precursor diffusion) and slow. Thus, the high reactivity of the Ag, Zn and Se of the AgZnSe shell layer will favour anisotropic-type growth [41].

Generally, the mechanism of nucleation and growth of CdS/AgZnSe QDs can be understood in terms of Ostwald ripening. At relatively low temperature (220–240 °C), Ostwald ripening dominated as a result of dissolution and surface energy of small particles which redissolve to allow subsequent growth of larger particles. At higher temperature (> 260 °C), Brownian motion will increase in the synthetic system due to higher thermal energy. Hence it is more likely that the increase in motion will allow the particles to interact at the exact crystallographic orientation, leading to orientated attachment [42].

3.2.2. Crystal phase analysis

The crystal structure of CdS core and CdS/AgZnSe QDs was studied using XRD. From the diffraction pattern of the CdS core (Fig. 4), a pure zinc-blende crystal structure with three prominent peaks at planes {111}, {220} and {311} was observed. The three planes exhibited Bragg angles at 26.5° , 43.9° and 51.9° respectively. Comparison of the diffraction pattern of CdS/AgZnSe core/alloyed shell QDs with CdS QDs reveal notable differences. Firstly, the three-notable peaks (associated with zinc-blende crystal structure) present in CdS were observed in CdS/AgZnSe₅₈₈. However, the appearance of four additional peaks between 30° and 40° and two additional peaks at higher Bragg angle (47.6° and 56.8°) provides direct evidence that the shell alloying process induced crystal phase changes in the QDs. Since the CdS/AgZnSe QDs size was tuned by fixed shell alloying, it is interesting to note the phase transition changes in the core/alloyed shell QDs. As the size of CdS/AgZnSe QDs increased, a steady transformation in the diffraction pattern as it relates to changes in the diffraction peaks was observed. A close assessment of the diffraction pattern of CdS/AgZnSe₅₉₃, revealed detailed formation of a duplet peak at low Bragg angle which can be attributed to the steady phase transition from a zinc-blende diffraction pattern to a wurtzite diffraction pattern. Further growth of the core/

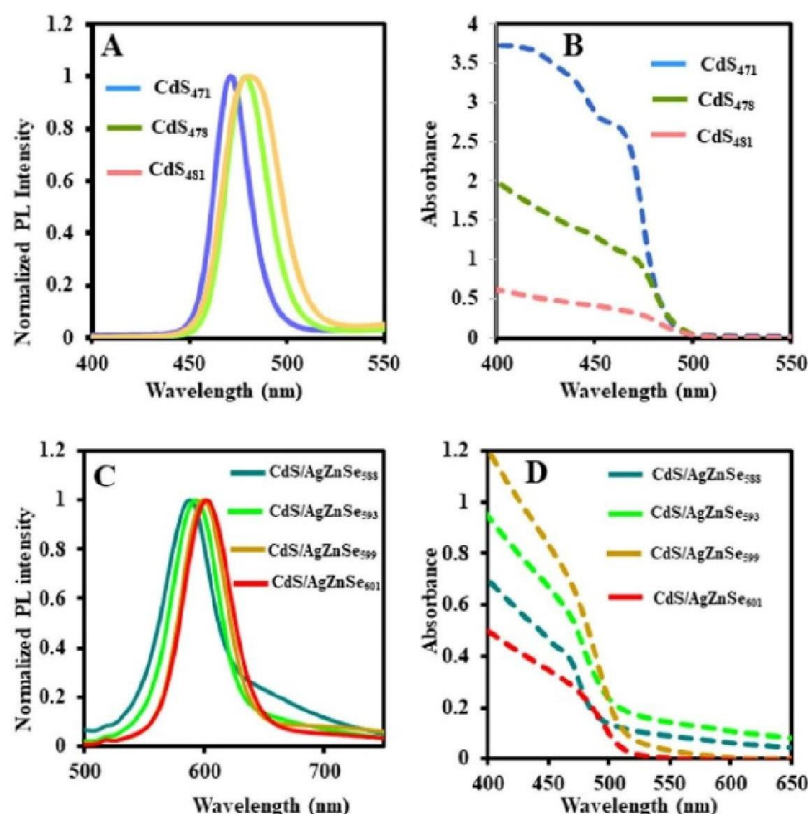


Fig. 6. PL and UV/vis absorption spectra of the different sized CdS (A and B) and CdS/AgZnSe core/alloys shell QDs (C and D) synthesized via method 1.

Table 1

Summary of the photophysical properties of the different-sized CdS core and CdS/AgZnSe QDs.

QDs- λ_{Emi} (nm)	λ_{Abs} (nm)	FWHM (nm)	Band gap (eV)	PL QY (%)
CdS ₄₇₁	458	20	2.64	16
CdS ₄₇₈	471	26	2.60	4
CdS ₄₈₁	476	33	2.58	8
^a CdS/AgZnSe ₅₈₈	464	41	2.11	48
^b CdS/AgZnSe ₅₉₁	449	34	2.10	73
^a CdS/AgZnSe ₅₉₃	468	42	~2.10	50
^a CdS/AgZnSe ₅₉₉	473	40	2.07	49
^a CdS/AgZnSe ₆₀₁	477	45	~2.07	51
^b CdS/AgZnSe ₆₀₂	473	39	2.06	35
^b CdS/AgZnSe ₆₁₂	481	40	2.03	42

^a Method 1 synthesis.

^b Method 2 synthesis.

alloys shell QDs led to the formation of a triplet peak at low angle as observed from the diffraction pattern of CdS/AgZnSe₅₉₉. Further assessment of the diffraction pattern of CdS/AgZnSe₆₀₁ revealed the formation of a pure wurtzite diffraction pattern. Thus it can be concluded that CdS core QDs favoured a zinc-blende crystal structure while the CdS/AgZnSe core-alloyed QDs kinetically favoured a phase change from a zinc-blende diffraction pattern to a wurtzite diffraction pattern.

3.2.3. Raman analysis

Core/shell QDs have been proven to reduce Auger recombination rates, which is important in multiexciton recombination and OFF/ON blinking process [43]. It is also believed that the core/shell interfacial alloying region is associated with a graded interface [44]. Hence, the potential of Raman to probe the internal structure of the core/alloys shell QDs interface was investigated. Fig. 5 shows the Raman spectra for

CdS core and the different-sized CdS/AgZnSe QDs. The similarities with reference to the peak position of CdS longitudinal optical phonon (LO) bulk frequency at $\sim 300 \text{ cm}^{-1}$ and CdS overtone at $\sim 600 \text{ cm}^{-1}$ with those of CdS/AgZnSe₅₈₈ and CdS/AgZnSe₅₉₃, provides strong indication of the homogenous growth of the core/alloys shell QDs. For CdS/AgZnSe₅₉₉ and CdS/AgZnSe₆₀₁, we observed significant changes in the peak position when compared to the CdS core. Specifically, the peak position of CdS/AgZnSe₅₉₉ exhibited similar frequency to CdS LO frequency but the peak at the CdS overtone region was more blue-shifted in frequency. Conversely, the peak frequencies of CdS/AgZnSe₅₉₉ relative to CdS LO and the overtone region were more red-shifted in comparison to the CdS core. The degree of frequency shift in CdS/AgZnSe₅₉₉ and CdS/AgZnSe₆₀₁ peak position relative to CdS can be understood in terms of the growth morphology and the degree of interfacial defect states in the QDs. Thus, the frequency shift and strain relaxation in the core/alloys shell interface will differ due to the QDs size and shell thickness. The relatively less-pronounced peaks below 220 cm^{-1} for the core/alloys shell QDs can be ascribed to a surface optical phonon feature which is inherent in finite sized crystals and also from the varying degree of alloying at the interface between CdS core and AgZnSe shell [45,46]. The variation in the intensity of the modes below 220 cm^{-1} could probably also account for the differences in alloying efficiency of the AgZnSe shell relative to the CdS core.

3.3. Optical properties

The QDs surface is influenced by the nature and chemical reaction of the synthetic constituents (surfactants, capping ligands and solvents) used in fabricating its structure. The atomistic effects of these constituents form the basis for assessing the quality of the QDs surface as it relates to the optical properties, such as the PL stability, spectral

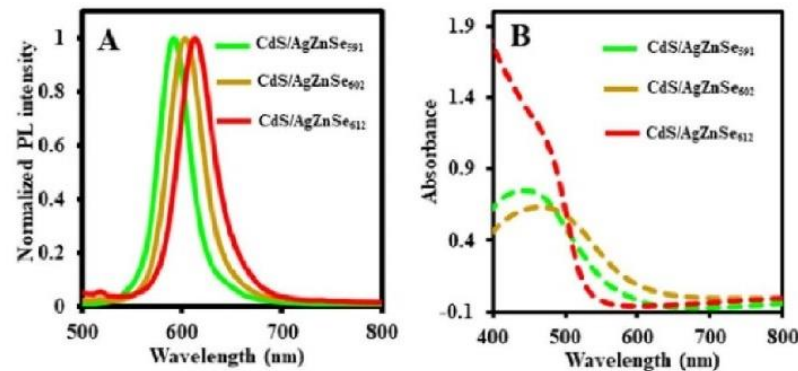


Fig. 7. PL (A) and UV/vis absorption (B) spectra of the different sized and CdS/AgZnSe core/alloyed shell QDs synthesized via method 2.

features and PL QY. The formation of midgap, deep and shallow states as surface traps provides the basis to which nonradiative electron-hole recombination degrades the QDs fluorescence. The suppression or total elimination of surface trap states in core QDs via coating of a shell layer is useful for light-associated applications and it provides a platform for better understanding of synthetic fabrication strategies required to construct high-quality QD nanocrystals. Our objective is to investigate the influence of a new shell layer (AgZnSe) on the luminescent properties of colloidal CdS QDs. We have utilized the shell alloying process to unravel how the QDs band gap and synthetic fabrication strategy influences the PL properties of CdS/AgZnSe core/alloyed shell QDs. The PL QY was determined according to the equation:

$$\Phi_F^{QD} = \Phi_F^{Std} \frac{F_{QDs} \cdot OD_{Std}(\lambda_{exc}) \cdot n_{water}^2}{F_{Std} \cdot OD_{QD}(\lambda_{exc}) \cdot n_{ethanol}^2} \quad (1)$$

where Φ_F^{Std} is the PL quantum yield of rhodamine 6G standard in ethanol ($\Phi = 0.95$); F_{Std} and F_{QDs} are the integrated sum of the fluorescence intensity of the standard and QDs; $OD_{QD}(\lambda_{exc})$ and $OD_{Std}(\lambda_{exc})$ are the optical densities of the QDs and standard while $n_{ethanol}^2$ and n_{water}^2 are the refractive indices of ethanol and water used to prepare the standard and QDs respectively.

Fig. 6A and B shows the evolution of the PL emission and absorption spectra of three different-sized CdS core QDs and Table 1 summarizes the corresponding photophysical properties as they relate to the absorption wavelength maximum, full width at half maximum (FWHM), band gap and PL QY. We harvested three-sized CdS core QDs with the sole aim of assessing their optical properties in comparison to the different-sized CdS/AgZnSe core/alloyed shell QDs. A small red shift in PL emission was observed for the harvested different-sized CdS core QDs with the absorption wavelength maximum and FWHM increasing in relation to the core size. The striking feature is the low PL QY which was increasingly tuned from 4% to 16% and also dependent on each core size. We observed that CdS₄₇₁ produced the highest PL QY of 16% while the lowest PL QY value of 4% was exhibited by CdS₄₇₈. Based on the relatively low PL QY, CdS core QDs suffers significantly from interfacial surface defects and residual strain in which the degree of defect states depends on the core size.

To effectively understand the effect of ternary AgZnSe shell alloying on the PL properties of CdS QDs, we employed two synthetic fabrication strategies. The most obvious and direct evidence of shell alloying comes from the PL emission and absorption spectra shown in Fig. 6C. The evolution of the PL emission of CdS/AgZnSe QDs synthesized via method 1 was tuned from 588 to 601 nm while the absorption spectra (Fig. 6D) was tuned from 464 nm to 477 nm. AgZnSe shell precursors used in method 1 synthesis of CdS/AgZnSe QDs was added into the growth solution after harvesting fraction of CdS₄₈₁ core QDs. The striking feature is the blue-shifted absorption wavelength and corresponding red shift in PL emission of CdS/AgZnSe₅₈₈ relative to CdS₄₈₁

QDs. The shift reveals that the shell alloying strategy, induced band gap modulation of the QDs in the visible region of the electromagnetic spectrum. For CdS/AgZnSe QDs synthesized via method 2, the PL emission spectra was tuned from 591 to 612 nm (Fig. 7A) while the absorption spectra were tuned from 449 to 481 nm (Fig. 7B). Despite the PL emission being more red-shifted relative to the CdS core, the absorption spectrum of CdS/AgZnSe₅₉₁ was significantly blue-shifted. From Table 1, the efficiency of band gap modulation of CdS/AgZnSe QDs was observed to vary narrowly from 2.07 to 2.11 eV for method 1 synthesis and from 2.03 to 2.10 eV for method 2 synthesis of the QDs.

To determine if the band gap modulation of CdS/AgZnSe QDs originated from the intrinsic optical properties of the core/alloyed nanostructures, a deeper assessment of the PL QY values (Table 1) was performed. The most striking observation is the variation in the PL QY of CdS/AgZnSe QDs synthesized via method 1 and 2 and the remarkable increase in comparison to the values obtained for CdS core. Via method 1 synthesis, the PL QY of CdS/AgZnSe QDs was tuned from 48% to 51% but via method 2 synthesis the PL QY was tuned from 35% to 73%. It is noteworthy that shell alloying of CdS QDs suppressed interfacial defect states in the core/alloyed shell nanocrystals due to the remarkable increase in the PL QY. However, it is important to emphasize that the defect state suppression efficiency varied amongst the QDs size and was dependent on the quality of the fabrication method.

Examining closely how the shell alloying process influenced the optical properties of the QDs, we have probed the correlation between the band gap modulation and the PL QY. It is a well-established phenomenon that a semiconductor band gap can be reduced by residual strain, thus leading to deformed potential [47,48]. Therefore, the low PL QY reveals that CdS core QDs suffer from residual strain due to surface traps embedded within the nanocrystals. The narrow band gap (2.07–2.11 eV) exhibited by the different-sized CdS/AgZnSe QDs (synthesized via method 1), correlated precisely to the small difference in PL QY (48–51%). This suggests that suppression of surface defect states in CdS QDs was with a very small margin across the core/alloyed shell QDs size. However, a wider margin in defect state suppression was observed for CdS/AgZnSe QDs synthesized via method 2, due to the wider difference in PL QY from 35% to 73%. Two important features are the maximum PL QY of 73% and the precise correlation in the margin of difference between the band gap and the PL QY. It is also noteworthy that the high PL QY implies much of the surface defects were suppressed by the shell alloying process while the variation in PL QY correlated precisely to the efficiency of surface defect suppression.

4. Conclusions

The passivation of CdS QDs with a new ternary alloyed AgZnSe shell layer was obtained via the organometallic synthetic route. The band gap of CdS/AgZnSe core/alloyed shell QDs was tuned across the visible

region with the nanocrystals exhibiting varying PL QYs. We observed a precise correlation in the margin of difference between the band gap of the QDs and the PL QY. The effect of shell alloying was observed in the QDs growth morphology in which the QDs growth transitioned from a homogeneous state to a heterogeneous state. Transition in the phase structure of the QDs from a zinc blende diffraction pattern to a wurtzite diffraction pattern was also observed. Generally, we have established that AgZnSe shell passivation on luminescent CdS QDs suppressed interfacial defect states in the CdS core QDs with the degree of suppression dependent on the size of the QDs derived from the finely-tuned synthetic fabrication strategy.

Acknowledgement

Financial support from the Water Research Council (WRC) project K5/2752, South Africa and the University of Pretoria is gratefully acknowledged.

References

- [1] T.V. Duncan, M.A. Mendez Polanco, Y. Kim, S.-J. Park, Improving the quantum yields of semiconductor quantum dots through photoenhancement assisted by reducing agents, *J. Phys. Chem. C* 11 (2009) 7561–7566.
- [2] A. Hassinen, I. Moreels, K. De Nolf, P.F. Smet, J.C. Martins, Z. Hens, Short-chain alcohols strip X-type ligands and quench the luminescence of PbSe and CdSe Quantum dots, acetonitrile does not, *J. Am. Chem. Soc.* 134 (2012) 20705–20712.
- [3] M. Nasilowski, P. Spinicelli, G. Patriarcho, B. Dubertret, Gradient CdSe/CdS quantum dots with room temperature biexciton unity quantum yield, *Nano Lett.* 15 (2015) 3953–3958.
- [4] P. Reiss, M. Potiere, L. Li, Core/shell semiconductor nanocrystals, *Small* 5 (2009) 154–168.
- [5] D.V. Talapin, J.-S. Lee, M.V. Kovalenko, E.V. Shevchenko, Prospects of colloidal nanocrystals for electronic and optoelectronic applications, *Chem. Rev.* 110 (2010) 389–458.
- [6] O. Chen, J. Zhao, V.P. Chauhan, J. Cui, C. Wong, D.K. Harris, H. Wei, H.-S. Han, D. Fukumura, R.K. Jain, M.G. Bawendi, Compact high-quality CdSe–CdS core–shell nanocrystals with narrow emission linewidths and suppressed blinking, *Nat. Mater.* 12 (2013) 445–451.
- [7] C. Giansante, I. Infante, Surface traps in colloidal quantum dots: a combined experimental and theoretical perspective, *J. Phys. Chem. Lett.* 8 (2017) 5209–5215.
- [8] M. Nirmal, B.O. Dabbousi, M.G. Bawendi, J.J. Macklin, J.K. Trautman, T.D. Harris, L.E. Brus, Fluorescence intermittency in single cadmium selenide nanocrystals, *Nature* 383 (1996) 802–804.
- [9] A. Efros, M. Rosen, Random telegraph signal in the photoluminescence intensity of a single quantum dot, *Phys. Rev. Lett.* 78 (1997) 1110–1113.
- [10] Y. Altintas, M.Y. Talpur, F. Mutlugün, Highly efficient cd-free alloyed core/shell quantum dots with optimized precursor concentrations, *J. Phys. Chem. C* 120 (2016) 7885–7892.
- [11] J. Bang, J. Park, J.H. Lee, N. Won, J. Nam, J. Lim, B.Y. Chang, H.J. Lee, B. Vhon, J. Shin, J.B. Park, H. Choi, K. Cho, S.M. Park, T. Joo, S. Kim, ZnTe/ZnSe (core/shell) type-II quantum dots: their optical and photovoltaic properties, *Chem. Mater.* 22 (2010) 233–240.
- [12] M.D. Tessier, D. Dupont, K. De Nolf, J. De Roo, Z. Hens, Economic and Size-tunable synthesis of InP/ZnE (E = S, Se) colloidal quantum dots, *Chem. Mater.* 27 (2015) 4893–4898.
- [13] W. Jiang, A. Singhal, J. Zheng, C. Wang, W.C.W. Chan, Optimizing the synthesis of red- to near-ir-emitting CdS-capped CdTe_{1-x}Se_x alloyed quantum dots for biomedical imaging, *Chem. Mater.* 18 (2006) 4845–4854.
- [14] P. Tyagi, P. Kambampati, Independent control of electron and hole localization in core/barrier/shell nanostructures, *J. Phys. Chem. C* 116 (2012) 8154–8160.
- [15] M. Nasilowski, P. Spinicelli, G. Patriarcho, B. Dubertret, Gradient CdSe/CdS quantum dots with room temperature biexciton unity quantum yield, *Nano Lett.* 15 (2015) 3953–3958.
- [16] M. Wang, M. Zhang, J. Qian, F. Zhao, L. Shen, G.D. Scholes, M.A. Winnik, Enhancing the photoluminescence of polymer-stabilized CdSe/CdS/ZnS core/shell/shell and CdSe/ZnS core/shell quantum dots in water through a chemical-activation approach, *Langmuir* 25 (2009) 11732–11740.
- [17] W. Liu, H. Soo Choi, J.P. Zimmer, E. Tanaka, J.V. Frangioni, M. Bawendi, Compact cysteine-coated CdSe(ZnCdS) quantum dots for in vivo applications, *J. Am. Chem. Soc.* 129 (2007) 14530–14531.
- [18] K. Yu, S. Singh, N. Patrito, V. Chu, Effect of reaction media on the growth and photoluminescence of colloidal CdSe nanocrystals, *Langmuir* 20 (2004) 11161–11168.
- [19] R.E. Bailey, S. Nie, Alloyed semiconductor quantum dots: tuning the optical properties without changing the particle size, *J. Am. Chem. Soc.* 125 (2003) 7100–7106.
- [20] J. Quyang, C.I. Ratcliffe, D. Kingston, B. Wilkinson, J. Kuijper, X. Wu, J.A. Ripmeester, K. Yu, Gradiently alloyed Zn_xCd_{1-x}S colloidal photoluminescent quantum dots synthesized via a noninjection one-pot approach, *J. Phys. Chem. C* 112 (2008) 4908–4919.
- [21] R. Gui, A. Wan, H. Jin, H. Li, C. Zhou, Acetyl acetate-stabilized Mn²⁺:cds quantum dots: aqueous synthesis and reversible fluorescence tuned by redox reaction, *Mater. Lett.* 98 (2013) 190–193.
- [22] R. Gui, X. An, H. Su, W. Shen, Z. Chen, X. Wang, A near-infrared-emitting CdTe/CdS core/shell quantum dots-based OFF–ON fluorescence sensor for highly selective and sensitive detection of Cd²⁺, *Talanta* 94 (2012) 257–262.
- [23] R. Gui, X. An, Layer-by-layer aqueous synthesis, characterization and fluorescence properties of type-II CdTe/CdS core/shell quantum dots with near-infrared emission, *RSC Adv.* 3 (2013) 20959–20969.
- [24] M.V. Rama Krishna, R.A. Friesner, Quantum confinement effects in semiconductor clusters, *J. Chem. Phys.* 95 (1991) 8309–8322.
- [25] I. Hernandez-Calderon, II-VI semiconductor materials and their applications, in: M.C. Tamargo, M.O. Manasreh (Eds.), *Optoelectronic Properties of Semiconductors and Superlattices*, 12 Taylor & Francis Inc, New York, 2002, pp. 136–138.
- [26] A.I. Ekimov, I.A. Kudryavtsev, M.G. Ivanov, A.L. Efros, Spectra and decay kinetics of radiative recombination in CdS microcrystals, *J. Lumin.* 46 (1990) 83–95.
- [27] K. Gong, D.F. Kelley, Lattice strain limit for uniform shell deposition in zincblende CdSe/CdS quantum dots, *J. Phys. Chem. Lett.* 6 (2015) 1559–1562.
- [28] C.-C. Hung, S.-J. Ho, C.-W. Yeh, G.-H. Chen, J.-H. Huang, H.-S. Chen, Highly luminescent dual-color-emitting alloyed [Zn_xCd_{1-x}Se_{1-y}] quantum dots: investigation of bimodal growth and application to lighting, *J. Phys. Chem. C* 121 (2017) 28373–28384.
- [29] L.A. Swafford, L.A. Weigand, M.J. Bowers, J.R. McBride, J.L. Rapaport, T.L. Watt, S.K. Dixit, L.C. Feldman, S.J. Rosenthal, Homogeneously alloyed CdS_{1-x}Se_x nanocrystals: synthesis, characterization, and composition/size-dependent band gap, *J. Am. Chem. Soc.* 128 (2006) 12299.
- [30] Z. Pan, K. Zhao, J. Wang, H. Zhang, Y.Y. Feng, X. Zhong, Near infrared absorption of CdSe_{1-x}Te_x alloyed quantum dot sensitized solar cells with more than 6% efficiency and high stability, *ACS Nano* 7 (2013) 5215–5222.
- [31] A. Kigel, M. Brumer, A. Sashchuk, L. Amirav, E. Lifshitz, PbSe/PbSe_xS_{1-x} core-alloyed shell nanocrystals, *Mater. Sci. Eng., C* 25 (2005) 604–608.
- [32] H. Jin, R. Gui, Z. Wang, J. Xia, M. Yang, F. Zhang, S. Bi, Facile fabrication of water-dispersible AgInS₂ quantum dots and mesoporous AgInS₂ nanospheres with visible photoluminescence, *RSC Adv.* 5 (2015) 68287–68292.
- [33] P. Yang, M. Ando, N. Murase, Highly luminescent CdSe/Cd_{1-x}Zn_xS quantum dots coated with thickness-controlled SiO₂ shell through silanization, *Langmuir* 27 (2011) 9535–9540.
- [34] K. Boldt, N. Kirkwood, G.A. Beane, P. Mulvaney, Synthesis of highly luminescent and photo-stable, graded shell CdSe/Cd_{1-x}Zn_xS nanoparticles by in situ alloying, *Chem. Mater.* 25 (2013) 4731–4738.
- [35] S.M. Fairclough, E.J. Tyrrell, D.M. Graham, P.J.B. Lunt, S.J.O. Hardman, A. Pietzsch, F. Hennies, J. Moghal, W.R. Flavell, A.A.R. Watt, J.M.J. Smith, Growth and characterization of strained and alloyed Type-II ZnTe/ZnSe core–shell nanocrystals, *Phys. Chem. C* 16 (2012) 26898–26907.
- [36] W.K. Bae, L.A. Padilha, Y.-S. Park, H. McDaniel, I. Robel, J.M. Pietryga, V.I. Klimov, Controlled alloying of the core-shell interface in CdSe/CdS quantum dots for suppression of Auger recombination, *ACS Nano* 7 (2013) 3411–3419.
- [37] O. Adegoke, K. Takemura, E.Y. Park, Plasmonic oleylamine-capped gold and silver nanoparticle-assisted synthesis of luminescent alloyed CdZnSe quantum dots, *ACS Omega* 3 (2018) 135–136.
- [38] J. Quyang, C.I. Ratcliffe, D. Kingston, B. Wilkinson, J. Kuijper, X. Wu, J.A. Ripmeester, K. Yu, Gradiently alloyed Zn_xCd_{1-x}S colloidal photoluminescent quantum dots synthesized via a noninjection one-pot approach, *J. Phys. Chem. C* 112 (2008) 4908–4919.
- [39] B.O. Dabbousi, Rodriguez-Viejo, F.V. Mikulec, J.R. Heine, H. Mattoussi, R. Ober, K.F. Jensen, M.G. Bawendi, (CdSe)ZnS core-shell quantum dots: synthesis and characterization of a size series of highly luminescent nanocrystallites, *J. Phys. Chem. B* 101 (1997) 9463–9475.
- [40] D.V. Talapin, I. Mekis, S. Götzinger, A. Kornowski, O. Benson, H. Weller, CdSe/CdS/ZnS and CdSe/ZnSe/ZnS core-shell-shell nanocrystals, *J. Phys. Chem. B* 108 (2004) 18826–18831.
- [41] P.T.K. Chin, C. de Mello Donega, S.S. van Bavel, S.C.J. Meskers, N.A.J.M. Sommerdijk, R.A.J. Janssen, Highly luminescent CdTe/CdSe colloidal heteronanocrystals with temperature-dependent emission color, *J. Am. Chem. Soc.* 129 (2007) 14880–14886.
- [42] N.T.K. Thanh, N. Maclean, S. Mahiddine, Mechanisms of nucleation and growth of nanoparticles in solution, *Chem. Rev.* 114 (2014) 7610–7630.
- [43] F. Garcia-Santamaría, S. Brovelli, R. Viswanatha, J.A. Hollingsworth, H. Htoon, S.A. Crooker, V.I. Klimov, Breakdown of volume scaling in Auger recombination in CdSe/CdS heteronanocrystals: the role of the core-shell interface, *Nano Lett.* 11 (2011) 687–693.
- [44] G.E. Cragg, A.L. Efros, Suppression of auger processes in confined structures, *Nano Lett.* 10 (2009) 313–317.
- [45] F. Comas, N. Studart, G.E. Marques, Optical phonons in semiconductor quantum rods, *Solid State Commun.* 130 (2004) 477–480.
- [46] H. Lange, M. Artemyev, U. Woggon, C. Thomsen, Geometry dependence of the phonon modes in CdSe nanorods, *Nanotechnology* 20 (2009) 045705.
- [47] J. Kim, M.V. Fischetti, Electronic band structure calculations for biaxially strained Si, Ge, and III-V Semiconductors, *J. Appl. Phys.* 108 (2010) 013710.
- [48] J. Kim, M.V. Fischetti, S. Aboud, Structural, electronic, and transport properties of silicene nanoribbons, *Phys. Rev. B* 86 (2012) 205323.